

McMule

QED Corrections for Low-Energy Experiments

Dissertation

zur

Erlangung der naturwissenschaftlichen Doktorwürde
(Dr. sc. nat.)

vorgelegt der

Mathematisch-naturwissenschaftlichen Fakultät

der

Universität Zürich

von

Yannick Ulrich

aus

Deutschland

Promotionskommission

Prof. Dr. Adrian Signer (Vorsitz)

Prof. Dr. Stefano Pozzorini

PD Dr. Michael Spira

Zürich, 2020

Abstract

We present MCMULE, a unified framework for the calculation of NLO and NNLO corrections to many processes in QED with massive fermions. This easily extendable program allows users to calculate an arbitrary observable for any of the processes implemented. These include various lepton decays as well as certain low-energy scattering experiments such as $e\mu \rightarrow e\mu$ and $\ell p \rightarrow \ell p$ that can be measured to high enough a precision to warrant QED corrections.

As part of our discussion, we will present a pedagogical introduction to how these calculations are performed, focusing on technical aspects supplemented with examples. Our goal is to provide a useful introduction for those entering the field, covering all aspects relevant for the practitioner.

Acknowledgement

First things first: Adrian, I wish to express all my gratitude to you for suggesting and supervising this wonderful project. I'm grateful for your support and your supervision but also for letting me pursue pet projects such as **handyG** and for involving me in supervisions. Thank you for letting my take care of our pet mule!

The next Thank-You goes to my collaborators on and around MCMULE, Pulak Banerjee, Tim Engel, Christoph Gnendiger, Marco Pruna, and Adrian Signer. Thank you for working with me and for your many great ideas that can be found somewhere in these pages. This project would not have been possible without you.

Relatedly, I'd like to thank my predecessor, Andrea Visconti, for patiently explaining the art of two-loop calculations to me and for sharing his notes with me, even long after he has left academia.

Next, there are those whose supervision I was allowed to actively join. Thank you, Tim Engel, Nicolas Schalch, Luca Naterop, and Andrea Gurgone for indulging me during your various projects.

While talking collaborators, I'd like to thank the MUonE theorists and experimentalists for letting us join your ranks and for your ideas. In particular, I'd like to thank Massimo Passera for mentioning the experiment to us over lunch during the PSI 2016 conference, once again proving that lunch and coffee breaks are the most important parts of conferences.

Next, I'd like to express my gratitude to my experimental colleagues who patiently explained to me the many subtleties of experimental analysis, unwittingly helping to improve MCMULE. In alphabetical order, you are Niklaus Berger, Lukas Gerritzen, Carren Kresse, Alberto Lusiani, Umberto Marconi, Clara Matteuzzi, Angela Papa, Ann-Kathrin Perrevoort, Dinko Pocanic, Giada Rutar, Patrick Schwendimann, and Graziano Venanzoni.

Moving on, I must thank the present and former bachelor, master, and PhD students of the theory group at PSI for many helpful discussions and, more importantly, the morning tea breaks. Thank you (in chronological order) Seraina Glaus, Dario Müller, Tim Engel, Lukas Fritz, Nicolas Schalch, Luca Naterop, David Urwyler, Johannes Lade, Fiona Kirk, Claudio Manzari, Andrea Gurgone, and Natalie Schär.

I'm extremely happy to have joined such a wonderful group at PSI. Thank you for many great lunch and coffee breaks and extracurricular activities. I'm indebted to Adrian Signer and Michael Spira for running this amazing group as well as the group's other members, past and present, for creating such a wonderful working atmosphere. In addition to our group's students: Emanuele Bagnaschi, Pulak Banerjee Antonio Coutinho, Andrea Crivellin, Margherita Ghezzi, Chrisoph Gnendiger, Marco Pruna, Johannes Schlenk, Marc Montull, and Max Zoller.

Leaving academia and entering the real world, I'd like to thank the members of the albrechtstrings orchestra, especially Brigitte, Juliane, Magnus, Patrick, Stephanie, Ursula, and Sandra.

Last but not least, I'm grateful to my family, both in Northern and Southern Germany, and of course to my Amazing Group of friends outside PSI: Nadya, Daniel, and Marko. Finally, I'd like to thank John for putting up with me for the last few years. Thanks, mate!

Declaration

This thesis is based on the following works to which the author contributed to directly:

- [1] G. M. Pruna, A. Signer and Y. Ulrich, *Fully differential NLO predictions for the rare muon decay*, *Phys. Lett.* **B765** (2017) 280 [[1611.03617](#)].
- [2] C. Gnendiger et al., *To d, or not to d: recent developments and comparisons of regularization schemes*, *Eur. Phys. J.* **C77** (2017) 471 [[1705.01827](#)].
- [3] G. M. Pruna, A. Signer and Y. Ulrich, *Fully differential NLO predictions for the radiative decay of muons and taus*, *Phys. Lett.* **B772** (2017) 452 [[1705.03782](#)].
- [4] Y. Ulrich, *Fully differential NLO predictions for rare and radiative lepton decays*, *PoS NuFact2017* (2018) 124 [[1712.05633](#)].
- [5] T. Engel, C. Gnendiger, A. Signer and Y. Ulrich, *Small-mass effects in heavy-to-light form factors*, *JHEP* **02** (2018) 118 [[1811.06461](#)].
- [6] T. Engel, A. Signer and Y. Ulrich, *A subtraction scheme for massive QED*, *JHEP* **01** (2020) 085 [[1909.10244](#)].
- [7] P. Banerjee, T. Engel, A. Signer and Y. Ulrich, *QED at NNLO with McMule*, [2007.01654](#).

Hence, text may be copied in verbatim without direct reference. Further, because the author was closely involved in the supervision of

- [8] T. Engel, *“Two-loop corrections to the muon decay”*, Master’s thesis, Swiss Federal Institute of Technology in Zurich, 2018.

Sections [5.3](#) and [5.4](#) follow the resulting master thesis very closely.

Contents

1	Relevance of QED	1
1.1	Relevant experiments	1
1.2	Processes at Leading order	3
1.3	Processes at next-to-leading order	3
1.4	Processes at next-to-next-to-leading order	4
1.5	Processes at next-to-next-to-next-to-leading order	4
2	Introduction to QED	5
2.1	Renormalisation	6
2.1.1	Renormalisation schemes	7
2.1.2	Practical renormalisation	10
2.2	Effective theories and the muon decay	11
2.3	Infrared safety	12
2.4	Infrared prediction	13
3	Regularisation schemes	17
3.1	Formal aspects	18
3.2	γ_5 in dimensional schemes	19
3.3	The muon decay in all schemes	20
3.3.1	Neutrino average	21
3.3.2	Conventional dimensional regularisation (CDR)	22
3.3.3	The original scheme (HV)	23
3.3.4	The four-dimensional helicity scheme (FDH)	25
3.3.5	Four-dimensional formulation of FDH (FDF)	28
3.4	Regularisation-scheme dependence and IR prediction	30
4	The FKS² scheme	33
4.1	FKS for soft singularities at NLO	33
4.2	FKS ² : NNLO extension	36
4.2.1	Real-virtual correction	36
4.2.2	Double-real correction	38
4.2.3	Combination	39
4.3	Beyond NNLO	40
4.3.1	FKS ³ : extension to N ³ LO	40
4.3.2	FKS ^ℓ : extension to N ^ℓ LO	41
4.4	Comments on and properties of FKS ^ℓ	42
4.4.1	Regularisation-scheme and scale dependence	42
4.4.2	Ingredients required at NNLO	42
4.4.3	Phase-space parametrisation	43

5	Two-loop calculation	45
5.1	Gauge-invariant splitting of amplitudes	46
5.2	Scalar integrals	47
5.3	Integration-by-parts reduction	48
5.4	Calculation of master integrals	50
5.4.1	Feynman parametrisation	51
5.4.2	Method of regions	53
5.4.3	Light-cone coordinates and momentum regions	55
5.5	Massification	56
5.5.1	The soft function for $t \rightarrow W^\pm b$	57
5.5.2	Collinear contribution for $t \rightarrow W^\pm b$	58
5.5.3	The soft function for $\gamma^* \rightarrow qq$	59
5.5.4	Comparison with the heavy-quark form factor	59
5.5.5	Summary	60
6	The Monte Carlo code MCMULE	61
6.1	Structure of MCMULE	61
6.2	Running MCMULE: an example	65
6.2.1	Preparations	65
6.2.2	Running and analysing	69
6.3	General aspects of using MCMULE	75
6.3.1	Statistics	75
6.3.2	Analysis	76
6.4	Technical aspects of MCMULE	77
6.4.1	Phase-space generation	77
6.4.2	Implementation of FKS schemes	79
6.4.3	Random number generation	79
6.4.4	Differential distributions and intermediary state files	83
6.5	Implementing new processes in MCMULE	84
6.5.1	Study of ξ_c dependence	87
6.5.2	Example calculations in Mathematica	89
6.5.3	Coding style and best practice	91
7	Phenomenology	93
7.1	MUonE ($\mu^- e^- \rightarrow \mu^- e^-$)	93
7.2	MUSE ($ep \rightarrow ep$)	98
7.3	MEG and MEG II	99
7.3.1	Single radiative muon decay ($\mu \rightarrow \nu \bar{\nu} e \gamma$)	100
7.3.2	Double radiative muon decay ($\mu \rightarrow \nu \bar{\nu} e \gamma \gamma$)	101
7.4	BABAR ($\tau \rightarrow \nu \bar{\nu} e \gamma$)	101
7.5	Michel decay ($\mu \rightarrow \nu \bar{\nu} e$)	104
7.5.1	Results for the decay rate	104
7.5.2	The electron energy spectrum	105
7.5.3	Michel decay as a background in MEG	106
7.6	Mu3e	108
8	Outlook	111
A	Conventions	113

B	Constants in FDH	115
B.1	Renormalisation constants	115
B.2	Infrared prediction in QCD	117
B.3	Massification	119
B.4	Conclusion	120
C	Eikonal integrals $\hat{\mathcal{E}}$	121
D	Explicit derivation of FKS³	123
D.1	Real-virtual-virtual contribution	123
D.2	Real-real-virtual contribution	124
D.3	Triple-real contributions	124
D.4	Combination	125
	Index	127

Chapter 1

Relevance of QED

A naive estimate of the size of radiative corrections in any theory is generally driven by the size of its coupling. For quantum electrodynamics (QED) this is $\alpha \simeq 1/137$, implying that QED corrections can often be safely ignored and are only ever relevant for experiments with the highest precision. However, this naive estimate overlooks two aspects.

- QED corrections can easily become as large as ten percent if they include large logarithms of widely different masses and kinematic cuts.
- The other aspect has to do with the experimental precision that the theory has to ultimately match or even exceed. Current and future experiments will be able to push the precision of event rates – famously far more challenging to measure than shapes – to well below the percent level, mandating next-to-leading order (NLO) or even next-to-next-to-leading order (NNLO) calculations for many processes in QED.

To facilitate the implementation of many QED calculations (10 and counting up to NNLO at the time of this writing) we have developed a unified framework called MCMULE (**M**onte **c**arlo for **M**uons and other **l**eptons). With it, new processes can be added with relative ease, making MCMULE the defining aspect of the thesis.

In what follows, we list some experiments that in some way or form are relevant for MCMULE even though not all measure processes that can be calculated with MCMULE. Next, we will discuss the implemented processes sorted by order in perturbation theory.

The thesis-proper begins in Chapter 2 with a brief but mostly standard introduction to QED, defining some terminology that we refer to later. Next, in Chapter 3, we will discuss different dimensional regularisation schemes with the practitioner in mind, providing detailed examples. As a next big step, we will discuss in Chapter 4 the infrared (IR) subtraction schemes used by MCMULE, the development of which was a corner stone of this project. We will discuss practical aspects of a two-loop calculation in Chapter 5. For the technically inclined reader, we will discuss aspects of MCMULE’s implementation in Chapter 6. Most of this will not be relevant for users of MCMULE but serves as a guide on how MCMULE could be extended. Finally, we will review some results obtained by MCMULE in Chapter 7 before finally discussing future developments in Chapter 8.

1.1 Relevant experiments

As mentioned above, experimental progress requires more and more theory support. While this is of course also true for the LHC experiments that certainly drove the development of technology, we will focus exclusively on QED here. Still, even though many experiments have

driven this development, an exhaustive list would not be rewarding here. Instead, we will list some examples, mostly but not exclusively, focussing on muonic physics that benefit from fully-differential calculations:

- Bhabha scattering has been used at various lepton colliders as a standard candle for luminosity measurement. Hence, much theoretical effort has been devoted to this process. Presently, NNLO corrections, including leading electron mass effects, are known and matched to *parton shower* (PS). For a review of the state of Bhabha scattering, see for example [9].
- The $g - 2$ experiment [10] at Brookhaven, its successor at Fermilab [11] as well as a novel experiment planned at J-PARC [12] are precisely measuring the anomalous magnetic moment of the muon. This observable is thought to be – due to its high precision – very sensitive to BSM and indeed there is a tantalising discrepancy between the measurement and the SM prediction (for example cf. [13]). The theoretical prediction is plagued by uncertainties in the *hadronic vacuum polarisation* (HVP) and the hadronic light-by-light scattering.

However, as the QED corrections to this process are known to the five-loop level [14] and $g - 2$ is an intrinsically inclusive observable, there is nothing further for MCMULE to directly add to the QED calculation of $g - 2$. Hence, we will refrain from further commenting on the determination of the QED corrections to $g - 2$.

- The proposed MUonE experiment [15–17] plans to measure muon-electron scattering to high precision in order to independently determine the HVP contribution to the muon $g - 2$ through a novel approach. For this to be competitive with the orthodox methodology the relative systematic error needs to be under control below 10^{-5} . Aside from the obvious experimental challenges connected to this, the QED contributions should be known to at least the NNLO, level including mass effects and matched to PS.
- The P2 [18], PRad [19], and MUSE [20] experiments are measuring elastic electron-proton and muon-proton scattering, respectively. These measurements help to determine the proton radius. However, PRad uses Møller scattering ($ee \rightarrow ee$) for normalisation purposes, the theory uncertainties of which are a leading systematic.
- The MOLLER experiment [21] and the QWeak experiment [22] measure the Weinberg angle at low Q^2 in electron-electron and electron-proton scattering, respectively.
- The MuLan experiment at the Paul Scherrer Institute (PSI) has measured the muon lifetime to 1 ppm [23]. This measurement was then, in combination with theoretical calculations [24, 25], used to extract the Fermi constant G_F .
- The MEG experiment at PSI [26] and its successor MEG II [27] are searching for the lepton-flavour violating (LFV) decay $\mu \rightarrow e\gamma$ which is predicted by many BSM scenarios. As any observation of the LFV decay channel would constitute clear evidence of BSM physics, there is no pressing need for NLO corrections to this decay mode yet. However, $\mu \rightarrow e\gamma$ becomes indistinguishable from the *radiative muon decay* $\mu \rightarrow e\nu\bar{\nu} + \gamma$ for small neutrino energies. Hence, MEG is searching for a peak on a steeply falling background. It is now unsurprising that precise knowledge of this background is extremely helpful.
- The Mu3e experiment at PSI [28, 29] is searching for the LFV decay $\mu \rightarrow eee$. This is again difficult to disentangle from the *rare muon decay* $\mu \rightarrow e\nu\bar{\nu} + ee$ for small neutrino energies. Further, Mu3e is sensitive to light but weakly coupled BSM physics. These potential particles might not appear as a clear bump over the falling background but

as minute modifications to certain differential observables. For these types of analyses, radiative correction are essential.

- The PADME experiment at the INFN National Laboratory of Frascati [30] is searching for annihilation of e^+e^- pairs into a photon and a so-called dark photon. As such the Standard Model process $ee \rightarrow \gamma\gamma$ is of interest for PADME.

The high experimental accuracy obtained or planned by these experiments also requires a focussed theory support to make the best use of their data. This means that from the theoretical side all relevant processes need to be calculated

- to the highest order in perturbation theory possible,
- to be fully-differential, i.e. not just predicting inclusive cross section but to instead being able to model the experimental situation as closely as possible,
- to include polarisation effects, should these matter experimentally,
- to include all necessary mass effects wherever possible, and
- to include resummation where large logarithms are expected.

In the following sections we will comment on some of the processes in MCMULE, noticing some practical exceptions to the first point.

Even though MCMULE focusses on muonic processes, in some cases tauonic (eg. $\tau \rightarrow e\nu\bar{\nu}\gamma$) or hadronic (eg. $\ell p \rightarrow \ell p$) processes can be included with only minor changes.

1.2 Processes at Leading order

While leading order (LO) calculations are mostly trivial, that does not necessarily make them futile. In fact, the polarised rare muon decay $\mu \rightarrow e\nu\bar{\nu} + ee$ was first calculated and made available to the Mu3e collaboration in a predecessor of the MCMULE framework [31]. This was required by Mu3e to accurately simulate their background including polarisation effects which heavily influence angular distributions. While this was later superseded by a NLO calculation [1, 32], it was and still is very helpful for the planning of the Mu3e experiment.

Additionally to their searches for $\mu \rightarrow e\gamma$, the MEG collaboration also looks for the LFV decay of a muon into an electron and a Majoron J , a Goldstone boson associated with a hypothetical spontaneous breaking of lepton number [33, 34] (for a review of the Majoron in the context of MEG see [35, 36], and reference therein). This particle may decay promptly into $J \rightarrow \gamma\gamma$ [37] resulting in a $\mu \rightarrow e\gamma\gamma$ signature. This becomes indistinguishable from the double-radiative muon decay $\mu \rightarrow e\nu\bar{\nu} + \gamma\gamma$ if the neutrinos carry little energy. However, because the process is heavily suppressed, a LO study in MCMULE was sufficient to model the relevant background.

1.3 Processes at next-to-leading order

For many background processes, a NLO study is sufficient to meet the experimental requirements. Notable examples in MCMULE are the radiative ($\mu \rightarrow e\nu\bar{\nu} + \gamma$) and rare ($\mu \rightarrow e\nu\bar{\nu} + ee$) muon decays. These processes serve as backgrounds to MEG's and Mu3e's searches for LFV decays. As such, especially the region of low neutrino energy is of particular interest.

NLO studies conducted in MCMULE [1, 3] and elsewhere [32, 38] found relatively large corrections, reaching up to ten percent in the relevant regimes. In both cases, the NLO correction

was driven through large logarithms that somewhat spoil the perturbative expansion. As we will see, this is a recurring theme in perturbative calculations in general and MCMULE in particular. However, as in this case the corrections are largely negative, the SM background was generally overestimated. Naturally this is preferable as it slightly increases the actual efficiency.

From a theoretical point of view, an extension to the radiative tau decay $\tau \rightarrow \ell \nu \bar{\nu} \gamma$ seems natural. This was measured by BABAR [39, 40]. In the electronic case ($\ell = e$) the measured *branching ratio* (BR) was found to be significantly above the SM prediction [38]. Using MCMULE we were able to study this discrepancy and found hints towards a solution [3, 4].

With the high statistics of Belle and its successor, the rare τ decays $\tau \rightarrow \nu \bar{\nu} \ell \ell$ become accessible [41]. A NLO study that merges [32] with MCMULE [1] is forthcoming [42].

Finally, we should mention the NLO calculation of muon-electron scattering [43, 44] which was revisited later in the context of the MUonE experiment [45] (shortly thereafter confirmed independently by MCMULE [46] and [47]) as this allowed the first detailed study of the situation that will be faced by the MUonE experiment.

1.4 Processes at next-to-next-to-leading order

Even though NLO is enough for many background studies, precision measurements such as the measurement of the Fermi constant G_F [23], the extraction of the Michel parameters by TWIST [48], or the planned HVP fit by MUonE require yet higher precision. In these cases we need to turn to NNLO. While NLO corrections are essentially solved for processes involving not too many particles (and no loops at LO), we are far from accomplishing the same feat for NNLO. This is mostly, but not exclusively, due to the lack of two-loop integrals. Further complication arises from our wish to include mass effects wherever possible as analytic solutions to integrals with multiple masses quickly become impossible. In Chapter 5 we will comment on this issue and potential shortcuts.

Currently, MCMULE implements the conventional muon decay or *Michel decay* $\mu \rightarrow \nu \bar{\nu} e$ [6] and $ee \rightarrow \nu \bar{\nu}$ (which served as a test case) at NNLO. Further, μ - e scattering can be split into gauge invariant subsets by categorising which fermion radiates (cf. Section 5.1). Due to the lightness of the electron, corrections associated to it are expected to be dominant. These simpler contributions to μ - e scattering are already implemented in MCMULE at NNLO [7]. The NNLO leptonic corrections to lepton-proton scattering, too, is implemented because it can be obtained by tweaking μ - e scattering.

1.5 Processes at next-to-next-to-next-to-leading order

While many observables were calculated at NNLO for the LHC, only recently a select group of quantities reached N³LO accuracy. Of these, only one – deep inelastic jet production [49] – is fully-differential requiring a subtraction scheme (cf. Chapter 4).

The dominant contributions to muon-electron scattering would seem like an ideal candidate to join this select group. It would also be the first N³LO calculation involving massive particles in initial and final states as well as loops. While this calculation is not yet part of MCMULE, progress is made towards its addition.

Chapter 2

Introduction to QED

Quantum Field Theories (QFT) have proven to be immensely powerful tools to obtain evermore precise theoretical predictions for the physics at the smallest scale. Usually this is understood in the framework of the Standard Model (SM) of electroweak and strong interactions. However, we will not be discussing the full SM with its strengths and weaknesses, suffice it to say that, while very successful, we know that physics beyond the SM (BSM) must exist from a variety of evidence. When searching for BSM experimentally, it is crucial to have a precise understanding of the background due to known physics – be that the SM or one of its subsets.

For all processes under consideration here, the background is dominated by QED, a particularly simple part of the SM. This QFT is defined through its Lagrangian¹

$$\mathcal{L} = \sum_i \bar{\psi}_i (i\gamma^\mu D^\mu - m_i) \psi_i - \frac{1}{4} F^{\mu\nu} F^{\mu\nu} \quad (2.1a)$$

$$= \underbrace{\sum_i \bar{\psi}_i (i\cancel{\partial} - m_i) \psi_i}_{\text{free theory}} - \frac{1}{4} (F^{\mu\nu})^2 - e \sum_i \bar{\psi}_i \cancel{A} \psi_i, \quad (2.1b)$$

where ψ_i are the spinor fields of the leptons and $F^{\mu\nu}$ the electromagnetic field tensor. In the second step we have introduced some abbreviated notation, most notably the Feynman slash notation for $\gamma^\mu a^\mu = \cancel{a}$. $D^\mu = \partial^\mu + ieA^\mu$ is called the gauge covariant derivative and is a compact way to describe the interactions of leptons and photons.

Unfortunately, QED – like all phenomenologically relevant QFTs – is not exactly solvable. However, the free theory, i.e. the first two terms of (2.1b) are solvable. Hence, we use perturbation theory to expand in the electromagnetic coupling

$$\alpha = \frac{e^2}{4\pi} \approx \frac{1}{137}. \quad (2.2)$$

This coupling is small enough to serve as an excellent expansion parameter. Physical quantities like cross sections or decay rates are now written as

$$\sigma = \sigma^{(0)} + \left(\frac{\alpha}{\pi}\right)^1 \sigma^{(1)} + \left(\frac{\alpha}{\pi}\right)^2 \sigma^{(2)} + \left(\frac{\alpha}{\pi}\right)^3 \sigma^{(3)} + \mathcal{O}(\alpha^4), \quad (2.3)$$

where we refer to leading order (LO, $\sigma^{(0)}$), next-to-leading order (NLO, $\sigma^{(1)}$) etc. contributions.

¹Through this work, we will use upper Lorentz indices regardless of whether an object is co- or contravariant. The summation is still always implicit.

When calculating the contributions $\sigma^{(i)}$ we need to draw all connected and amputated Feynman diagrams contributing to the same observable including some fixed number of couplings. Here we distinguish *tree-level diagrams* and *loop diagrams*.

Obtaining the LO contribution $\sigma^{(0)}$ (which itself can contain further factors of α) is in most cases relatively straightforward. Note that $\sigma^{(0)}$ could already contain loops, i.e. a *loop-induced* process. We do not consider this case here. Instead, we assume that the first order is always given through a number of tree-level diagrams. Hence, we can use the number of loops and the order in perturbation theory interchangeably.

Once we have the matrix element, we need to integrate over the phase space to obtain a cross section or decay rate. At this stage, experimental subtleties enter. Modelling these as closely as possible may require us to include complicated cuts, making analytic integration over the phase space quickly infeasible. Hence, we will do the integration numerically. To facilitate the cuts, we define the so-called *measurement function* [50]. This function takes as arguments the four-momenta of all particles involved in the reaction and returns the experimentally measured quantity. The measurement function has to fulfil certain criteria. We will comment below on properties it has to fulfil beyond LO. But even at LO, an example for an invalid function would be to ask for a number of photons without also specifying the minimum energy of these photons. We call a calculation that can implement any measurement function without renewed effort *fully differential*.

We encounter our first loop diagram in $\sigma^{(1)}$. Because the momenta of the particles in the loop is not fixed through the momenta of the external particles, we have to integrate over them. Unfortunately, these *loop integrals* can be divergent for large momenta (ultraviolet, UV) or soft or collinear momenta (infrared, IR). Hence, the first thing we need to do is to *regularise* these divergences. This is usually done by shifting the dimension of space-time away from 4 to $d = 4 - 2\epsilon$ (dimensional regularisation, DREG). Both IR and UV singularities now appear as poles in $1/\epsilon$. We will explain how to do this formally and mathematically consistent in Chapter 3.

The loop integrals required to solve practical processes tend to be rather complicated. This complexity obviously increases the more loops are included. Further, the problem is also made more complicated through the inclusion of more external particles (with potentially different masses) as this increases the number of relevant or *active scales* μ_i that enter in the actual loop integrals. This is in contrast to other scales (inactive scales) that do not enter loop integrals like the mass of spectator particles.

Further background information on these topics can be found in various textbooks such as [51–53].

2.1 Renormalisation

When computing scattering amplitudes with the Lagrangian (2.1) beyond leading order, we encounter UV singularities that are indicative of our ignorance of the physics at very high scales. These UV singularities are dealt with through *renormalisation*. The main idea is to express scattering amplitudes in terms of renormalised fields and renormalised parameters, rather than their bare counterparts, s.t. no UV singularities are present. If to all orders in perturbation theory all UV singularities can systematically be absorbed by a finite number of *renormalisation constants*

Z_i , we call the theory *renormalisable*. It can be shown that QED as well as the full SM are renormalisable.

At this stage we will start using $\psi_{0,i}$, A_0^μ and $m_{0,i}$ for the bare quantities of (2.1). The variables ψ_i etc. shall henceforth be reserved for the renormalised quantities. In Section 2.1.1 we will be more specific what is meant by that.

Relating the bare quantities $\psi_{0,i}$, A_0^μ and $m_{0,i}$ of the Lagrangian (2.1) to the renormalised ones²

$$\psi_{0,i} = Z_{2,i}^{1/2} \psi_i, \quad m_{0,i} = Z_{m,i} m_i \quad \text{and} \quad A_0^\mu = Z_3^{1/2} A^\mu, \quad (2.4a)$$

we obtain

$$\mathcal{L} = \sum_i Z_{2,i} \bar{\psi}_i (i\not{\partial} - Z_{m,i} m_i) \psi_i - \frac{1}{4} Z_3 (F^{\mu\nu})^2 - \sum_i Z_2 Z_3^{1/2} e_0 \bar{\psi}_i A \psi. \quad (2.4b)$$

Z_2 and Z_3 are called the wave-function renormalisation factors, whereas Z_m is the mass renormalisation. We also need to renormalise the coupling e_0 . This is usually expressed in terms of the vertex-renormalisation factor Z_1 as

$$e_0 = e \frac{Z_1}{Z_2 Z_3^{1/2}} = Z_3^{-1/2} e. \quad (2.4c)$$

In the last step we have used that to all orders in QED $Z_1 = Z_2$, due to the *Ward identity*.

In (2.1) we have omitted the gauge-fixing terms, containing the gauge parameter, usually called ξ . We will always set this term to $\xi = 1$, i.e. perform all calculations in Feynman gauge. In general, ξ has to be renormalised as well. However, it can be shown that, as long as one only considers on-shell scattering amplitudes or renormalisation constants, this does not matter at any order in QED [54–56] (also cf. [57] showing that this ceases to be true in QCD at the three-loop level).

2.1.1 Renormalisation schemes

In DREG, the UV poles are manifest as poles $1/\epsilon_{UV}$, where we temporarily use the UV label to distinguish UV from IR poles. At n loops, the highest UV pole is of order $1/\epsilon_{UV}^n$. The UV part of the $Z_i = 1 + \delta Z_i$ is uniquely fixed by the requirement that all UV singularities are absorbed. At one-loop accuracy they are

$$\begin{aligned} Z_1 = Z_2 &= 1 + \frac{\alpha}{4\pi} \frac{-1}{2\epsilon_{UV}} + \mathcal{O}(\epsilon_{UV}^0, \alpha^2), \\ Z_m &= 1 + \frac{\alpha}{4\pi} \frac{-3}{2\epsilon_{UV}} + \mathcal{O}(\epsilon_{UV}^0, \alpha^2), \\ Z_3 &= 1 + \frac{\alpha}{4\pi} \frac{\beta_0}{\epsilon_{UV}} + \mathcal{O}(\epsilon_{UV}^0, \alpha^2), \end{aligned} \quad (2.5)$$

where $\beta_0 = -4/3N_F$ in a theory with N_F flavours. However, there is quite some freedom in choosing a *renormalisation scheme*, i.e. prescription how to fix the terms of the renormalisation

²In the notation of [53] $Z_2 = Z_\psi$ and $Z_3 = Z_A = Z_\alpha^{-1}$.

factors that are UV finite. Note that, to the loop order given in (2.5), it does not matter whether α has been renormalised or not, as the difference would be $\mathcal{O}(\alpha^2)$.

For most choices of the renormalisation scheme, the renormalised parameters α and m start to exhibit a behaviour known as *running*. These parameters become dependent on the *renormalisation scale* μ , the scale at which the UV subtraction is made. In particular, this is encountered for the coupling whose scale dependence is governed by the β function as

$$\frac{\partial\alpha(\mu)}{\partial\log\mu} = 2\beta(\alpha(\mu)) \quad \text{with} \quad \beta(\alpha) = -\alpha\left(\frac{\alpha}{4\pi}\beta_0 + \mathcal{O}(\alpha^2)\right). \quad (2.6)$$

This is a first example of what is called a *renormalisation group equation* (RGE). By choosing the renormalisation scale at the appropriate scale of the experiment, Q^2 , one avoids large logarithms $\log Q^2/\mu^2$ that arise when integrating (2.6).

The most common renormalisation schemes are the \overline{MS} *scheme*, where the finite terms vanish up to some common factors, and the *on-shell scheme* (OS). The latter will be the default in this project, s.t. for example m and α refer to the OS mass and coupling. Hence, the OS scheme deserves some further elaboration.

The OS scheme is constructed to most faithfully reproduce the classical limit for the input parameters at $Q^2 = 0$ without the parameters ever experiencing running. For example, this means that the electron mass really is $m_e \simeq 0.511 \text{ MeV}$. To achieve this, let us consider the one-loop corrections to the fermion propagator as (following [53])

$$\Sigma(p) = m_0 \Sigma_1(p^2) + (\not{p} - m_0) \Sigma_2(p^2). \quad (2.7)$$

To get the physical propagator S from the bare propagator $S_0 = 1/(\not{p} - m_0)$ we have to sum an infinite number of Σ

$$\begin{aligned} S(p) &= S_0(p) + S_0 \Sigma(p) S_0 + S_0 \Sigma(p) S_0 \Sigma(p) S_0 + \dots \\ &= \frac{1}{S_0^{-1} - \Sigma} = \frac{1}{\not{p} - m_0 - \Sigma}. \end{aligned} \quad (2.8)$$

We now want to describe this in the renormalised quantities, i.e.

$$S(p) \frac{1}{\not{p} - m_0 - \Sigma} \stackrel{!}{=} \frac{Z_2}{\not{p} - m} + \text{regular}, \quad (2.9)$$

where regular refers to terms that do not contribute to the pole as $\not{p} \rightarrow m$. The OS mass of the electron is now just defined as the pole of the propagator. In principle we could just plug (2.7) into (2.9) and obtain

$$Z_m = 1 - \Sigma(m) \quad \text{and} \quad Z_2 = 1 + \left. \frac{d\Sigma}{d\not{p}} \right|_{p^2=m^2}. \quad (2.10)$$

However, calculating $\Sigma'(m)$ can be cumbersome, especially beyond the one-loop level. Hence, we follow the method set out by [58]: we begin by writing down the perturbative expansion of Σ ,

Z_m , and Z_2 with the most general dependence of p^2 and m_0 allowed by the loop integration

$$\begin{aligned} Z_2 &= 1 + \sum_{n=1}^{\infty} \left(\frac{\alpha_0}{m^{2\epsilon}} \right)^n F(n), \\ Z_m &= 1 + \sum_{n=1}^{\infty} \left(\frac{\alpha_0}{m^{2\epsilon}} \right)^n M(n), \\ \Sigma &= \sum_{n=1}^{\infty} \left(\frac{\alpha_0}{(p^2)^\epsilon} \right)^n \left(m_0 \Sigma_1^{(n)} \left(\frac{m_0^2}{p^2} \right) + (\not{p} - m_0) \Sigma_2^{(n)} \left(\frac{m_0^2}{p^2} \right) \right), \end{aligned} \quad (2.11)$$

where everything is expressed in the bare coupling α_0 . This is now what we plug into (2.9) with $m = Z_m^{-1} m_0$, expanding to the desired order in α . At one-loop accuracy

$$M(1) = -\Sigma_1^{(1)}(1) \quad \text{and} \quad F(1) = \Sigma_2^{(1)}(1) - 2\Sigma_1^{\prime(1)}(1) - 2\epsilon \Sigma_1^{(1)}(1). \quad (2.12)$$

It turns out that this way we still need to calculate $\Sigma_i(1)$ and $\Sigma_i'(1)$ but we are allowed to set $p^2 = m_0^2$ before the loop integration.

For the photon field – and by extension the coupling – we proceed similarly, finding

$$Z_3 = \frac{1}{1 - \Pi(0)}, \quad (2.13)$$

where Π is the usual photon self energy, defined through

$$\Pi^{\mu\nu}(p) = (p^2 g^{\mu\nu} - p^\mu p^\nu) \Pi(p^2). \quad (2.14)$$

For a theory with only one massive fermion $\Pi(0)$ depends only on the mass of this flavour. One can easily calculate that [53]

$$\Pi^{(1)}(0) = -\frac{4}{3} \frac{e_0^2}{(4\pi)^{d/2}} m^{-2\epsilon} \Gamma(\epsilon). \quad (2.15)$$

This way, we have a relation between the $\overline{\text{MS}}$ coupling $\bar{\alpha}$ and the OS coupling α at one-loop accuracy

$$\bar{\alpha}(\mu) = \alpha \left(1 + \frac{4}{3} \frac{\alpha}{4\pi} \log \frac{\mu^2}{m^2} \right). \quad (2.16)$$

In principle we are free to renormalise the masses and coupling in any scheme we wish. For the fermion masses, we will always choose the on-shell scheme. This mass is scale independent and corresponds directly to the measured value of the lepton masses. Our standard choice for the coupling is also the on-shell scheme. In this scheme the coupling is scale independent and corresponds to the measured value $\alpha \sim 1/137$ in the Thomson limit. However, we occasionally work with $\bar{\alpha}$, the coupling in the $\overline{\text{MS}}$ -scheme. As mentioned above, this coupling depends on the renormalisation scale μ . If we consider processes at high energies Q (compared to the fermion masses) this scheme can be useful, as setting $\mu \sim Q$ allows to resum large logarithms.

All renormalisation constants required up to two-loop accuracy can be found, expressed in the bare coupling, in Appendix B.

2.1.2 Practical renormalisation

In order to obtain scattering matrix elements at a particular order in perturbation theory, we start by computing all connected and amputated Feynman diagrams to the required order. Amputated means we do not include diagrams with self-energy insertions on external lines. According to the LSZ reduction formula, such contributions are properly included by multiplying the unrenormalised amplitude by $\sqrt{Z_i}$ for each external line, where Z_i is the wave-function renormalisation factor in the on-shell scheme. This results in the renormalised scattering amplitude, but still expressed in terms of the bare coupling, masses, and gauge parameter. To absorb all UV singularities the bare parameters have to be expressed in terms of the corresponding renormalised parameters.

Renormalisation beyond one-loop has certain subtleties, most of which can be explained by pure counting of powers of the coupling α . At the one-loop level, the renormalisation constants $\delta Z_i^{(1)}$ always just multiply a tree-level amplitude $\mathcal{A}^{(0)}$. This ceases to be sufficient at the two-loop level. Now, additionally to the product of two-loop renormalisation constants $\delta Z_i^{(2)}$ with the tree-level amplitude $\mathcal{A}^{(0)}$, we need to include one-loop renormalisation of the one-loop amplitude $\mathcal{A}^{(1)} \times \delta Z_i^{(1)}$. Further, the two-loop renormalisation constants $\delta Z_i^{(2)}$ themselves need to be renormalised using constants $\delta Z_i^{(1)}$. This is called *sub-renormalisation*.

Particular attention has to be given to the fermion-mass renormalisation. Replacing $m_{0,i} = Z_{m,i} m_i = m_i + \delta m_i^{(1)} + \dots$ in the lower-order amplitudes and expanding in α produces all mass counterterms, also those on external lines. However, the latter have already been taken into account by the LSZ reduction. Hence, in practical calculations it is advantageous to perform mass renormalisation by explicitly computing Feynman diagrams with mass counterterms $\delta m_i^{(l)}$ on internal lines only.

Hence, we arrive at the following practical procedure for two-loop renormalisation:

1. For every massive external particle, add the wave function renormalisation for heavy fermions Z_h

$$\left(\frac{1}{2} \delta Z_h^{(2)} - \frac{1}{8} (\delta Z_h^{(1)})^2 \right) \times \mathcal{A}^{(0)} \quad \text{and} \quad \frac{1}{2} \delta Z_h^{(1)} \times \mathcal{A}^{(1)}. \quad (2.17)$$

2. For every massless external fermion, add $\frac{1}{2} \delta Z_l^{(2)} \times \mathcal{A}^{(0)}$, keeping in mind that these contributions are induced through terms proportional to the number of heavy flavours. This means that $Z_l = 1$ to all orders in theories without at least one massive flavour.
3. For every external photon, we have to add the corresponding $\frac{1}{2} \delta Z_3^{(1)} + \dots$ as above.
4. Perform the mass renormalisation of the fermions, i.e. add counterterm diagrams obtained through the substitution

$$\frac{i}{\not{p} + m} \rightarrow \frac{i}{\not{p} + m} \delta m^{(l)} \frac{i}{\not{p} + m} \quad (2.18)$$

for internal fermion lines at the amplitude level. We need $l = 2$ for tree-level diagrams and $l = 1$ for one-loop diagrams, as well as double insertions with $l = 1$ for tree-level diagrams. Note that this does not correspond to replacing $m_0 = Z_m m$ and expanding again in α at the matrix element level, as this would lead to the double counting of the mass renormalisation of external lines as discussed above.

5. Perform the coupling renormalisation by shifting $\alpha_0 \rightarrow (1 + \delta Z_\alpha^{(1)} + \delta Z_\alpha^{(2)}) \times \alpha$ and sorting terms according to the now renormalised coupling, dropping every term with too high a power in α .

If we have no internal photons at LO, i.e. the number of external photons coincides with the number of QED vertices, this step and Step 2 above cancel exactly thanks to the Ward identity, meaning neither is necessary (cf. (2.4c)).

2.2 Effective theories and the muon decay

A recurring theme of this project is the muon decay as an example process of high phenomenological relevance. However, the muon does not decay in pure QED as the only *weak-isospin* changing particle in the SM is the W -boson. The amplitude for $\mu(p) \rightarrow e(q)\nu_\mu(q_3)\bar{\nu}_e(q_4)$ in the SM can be written as

$$\mathcal{A} = \frac{ig}{\sqrt{2}} \left[\bar{u}_{\nu_\mu}(q_3)\gamma^\alpha P_L u_\mu(p) \right] \frac{-i}{q_W^2 - m_W^2} \left(g^{\alpha\beta} - \frac{q_W^\alpha q_W^\beta}{m_W^2} \right) \frac{ig}{\sqrt{2}} \left[\bar{u}_e(q)\gamma^\beta P_L u_{\nu_e}(q_4) \right], \quad (2.19)$$

with the W coupling g and the usual left-handed projector $P_L = \frac{1}{2}(1 - \gamma_5)$. While it is of course possible to perform all calculations, including radiative corrections, in the full SM, that is often unnecessary. Because the W momentum $q_W = p - q_3 \sim m_\mu$ is much smaller than its mass m_W , the W propagator simplifies to

$$\frac{-i}{q_W^2 - m_W^2} \left(g^{\alpha\beta} - \frac{q_W^\alpha q_W^\beta}{m_W^2} \right) = \frac{i}{m_W^2} g^{\alpha\beta} + \mathcal{O}\left(\frac{q_W^2}{m_W^2}\right), \quad (2.20)$$

resulting in

$$\mathcal{A} = -i \frac{g^2}{2m_W^2} \left[\bar{u}_{\nu_\mu}(q_3)\gamma^\alpha P_L u_\mu(p) \right] \left[\bar{u}_e(q)\gamma^\alpha P_L u_{\nu_e}(q_4) \right] + \mathcal{O}\left(\frac{q_W^2}{m_W^2}\right). \quad (2.21)$$

Further, because of the large W mass, radiative corrections due to the W are also suppressed by $\mathcal{O}(m_\mu^2/m_W^2)$. Hence, instead of introducing a propagating W boson, we augment (2.1) by

$$\mathcal{L} = \mathcal{L}_{\text{QED}} - \frac{4G_F}{\sqrt{2}} (\bar{\psi}_{\nu_\mu}\gamma^\mu P_L \psi_\mu) (\bar{\psi}_e\gamma^\mu P_L \psi_{\nu_e}). \quad (2.22)$$

Here, we have introduced a *dimension-six operator* with a dimensionful coupling G_F . At energies far below m_W , the exchange of a W boson is described well by (2.22). This is a first example of an *effective field theory* (EFT). We have encoded the high-energy dynamics of the W into a so-called *Wilson coefficient* G_F . The relation of G_F with parameters of the full SM is found through a *matching calculation* by calculating a process both in the full SM and in the EFT and then fixing G_F s.t. in the expansion of the EFT, i.e. $m_W \rightarrow \infty$, both agree. In our case we find at LO

$$\frac{G_F}{\sqrt{2}} = \frac{g^2}{8m_W^2} = \frac{1}{2v^2}, \quad (2.23)$$

where v is the vacuum expectation value of the Higgs field in the Standard Model.

There is one more simplification to be done in (2.22). Since we cannot measure the neutrinos it is unfortunate that they take such a prominent role in the calculation. Instead, we would prefer

everything related to neutrinos to factorise. Fortunately, there exist so-called *Fierz identities* to re-arrange spinor bilinears such as the ones in (2.22). In our case we find

$$\mathcal{L} = \mathcal{L}_{\text{QED}} - \frac{4G_F}{\sqrt{2}} (\bar{\psi}_e \gamma^\mu P_L \psi_\mu) (\bar{\psi}_{\nu_\mu} \gamma^\mu P_L \psi_{\nu_e}) . \quad (2.24)$$

Because (2.24) is the theory we will be using to calculate radiative corrections to the muon decay, we have to face the issue that in the strict meaning of the word, (2.24) is not renormalisable, requiring in general an infinite number of Z_i . However, as long as we do not consider a perturbative expansion in G_F , we can maintain predictability by renormalising G_F as just another coupling through a new Z_{G_F} which would usually be assumed in the $\overline{\text{MS}}$ scheme. However, it turns out that we do not even have to do that as $Z_{G_F} = 1$ to all orders in QED.

To see this, we first note that \mathcal{L} is invariant under the exchange $\psi_e \rightarrow \gamma^5 \psi_e$ and $m_e \rightarrow -m_e$ [59]. However, because this exchanges the vector and axial-vector current, we only really need to consider a vectorial coupling. Further, because the neutrinos are uncharged, there is no difference between G_F and the normal QED coupling from a renormalisation aspect. Hence, the QED Ward identity $Z_1 = Z_2$ still holds. The only contribution left to influence Z_{G_F} is the equivalent of Z_3 . The QED contribution to this quantity can be fixed by considering QED corrections to $\nu\nu \rightarrow \nu\nu$. Because the neutrinos are uncharged under QED, these vanish exactly. Of course, terms that are higher order in G_F exist in principle.

To summarise, we will be using (2.24) for all calculations involving the muon decay. As long as we only consider LO in G_F , the results will be UV finite after QED renormalisation. Higher-order corrections in G_F have been considered in [60].

2.3 Infrared safety

After the UV renormalisation, our *virtual* matrix element is unfortunately still IR divergent. This is in so-far physical that IR singularities cannot just be absorbed through redefinition of quantities. Instead, such fully *exclusive* quantities are just not physical until they are combined with *real* matrix elements involving extra radiation. While it is of course possible to distinguish events with extra hard radiation in an appropriate detector, there always exist a physical cut-off Δ below which radiation cannot be detected any more. As cross sections usually scale like $\log \Delta$, the cross section would diverge when integrating over the entire phase space including $\Delta \rightarrow 0$. This *soft* divergence is exactly cancelled by the IR divergence of the virtual matrix element. Observables for which this is true are called *IR safe*. Totally inclusive cross sections like

$$\sigma(a + b \rightarrow c + d + \text{any number of } \gamma) \quad \text{where } c, d \neq \gamma \quad (2.25)$$

are examples for IR safe observables. The existence of these observables is guaranteed by the Kinoshita-Lee-Nauenberg theorem (KLN) that states that any sufficiently inclusive observable (such as the total cross section) will always be finite. The condition imposed by the KLN theorem can be translated into a condition on the measurement function as we will see later [50].

As mentioned above, we would very much like to integrate over the phase space numerically. However, we cannot do that in d dimensions. Instead, we need special methods to treat these divergences in d dimensions without spoiling our ability to integrate numerically. We will discuss one such method in detail in Chapter 4.

In a theory with massless fermions there is an additional source of singularities due to (hard) radiation becoming *collinear* with a massless fermion. This is not an immediate problem as we will mostly be dealing with massive particles where the mass m serves as a regulator, giving rise to $\log m$. However, these *pseudo-collinear singularities* (PCS) cause a lot of numerical instabilities making them difficult to integrate over as we will discuss in Section 4.4.3 and again in Section 6.4.1.

An unfortunate aspect of perturbative calculations is that, for processes with very different scales μ_i , logarithms of the form $L \sim \log \mu_1^2/\mu_2^2$ become very large. Hence, each new loop order not just brings a new power of α but also often two powers of L – one due to soft and one due to collinear emission. At least in QCD, this can easily become large enough s.t. $\alpha_s L^2 \sim 1$, spoiling the expansion completely. But even in QED this is troublesome as it would require computations to an infeasibly high order.

This means that we have to revise our counting (2.3), assuming that we get two powers of L per loop order

$$\begin{aligned} \sigma = & \sigma_0^{(0)} + \left(\frac{\alpha}{\pi}\right)^1 L^2 \sigma_2^{(1)} + \left(\frac{\alpha}{\pi}\right)^1 L^1 \sigma_1^{(1)} + \left(\frac{\alpha}{\pi}\right)^1 L^0 \sigma_0^{(1)} \\ & + \left(\frac{\alpha}{\pi}\right)^2 L^4 \sigma_4^{(2)} + \left(\frac{\alpha}{\pi}\right)^2 L^3 \sigma_3^{(2)} + \left(\frac{\alpha}{\pi}\right)^2 L^2 \sigma_2^{(2)} + \left(\frac{\alpha}{\pi}\right)^2 L^1 \sigma_1^{(2)} + \left(\frac{\alpha}{\pi}\right)^1 L^0 \sigma_0^{(1)} \\ & + \left(\frac{\alpha}{\pi}\right)^3 L^6 \sigma_6^{(3)} + \left(\frac{\alpha}{\pi}\right)^3 L^5 \sigma_5^{(3)} + \left(\frac{\alpha}{\pi}\right)^3 L^4 \sigma_4^{(3)} + \dots \end{aligned} \quad (2.26)$$

The rows of this equation correspond to the *fixed-order* results obtained above. However, we can use the fact that the terms $\sigma_{2i}^{(i)}$ usually follow a predictable pattern. Hence, if we use $\alpha L^2/\pi$ as the expansion parameter instead of α/π we can get control over these logarithms. This process is known as *resummation*. The first column is known as *leading-logarithm* (LL), the second as *next-to-leading logarithm* (NLL) and so on.

A particularly efficient way to calculate the LL contribution is a *parton shower* (PS). This involves including a cascade of soft and collinear radiation to all involved particles. This is particularly interesting because PS can be constructed independent of the measurement function. Unfortunately, at the time of this writing, no NLL PS has been presented though work is ongoing towards a construction of such a method. Until then, NLL resummation must be done anew for each observable. However, much work has been dedicated to obtaining results that are almost NLL accurate.

2.4 Infrared prediction

When performing multi-loop calculations, an important cross-check is the cancellation of IR singularities. However, to use this as a practical tool, it is necessary to predict the IR poles without having to calculate the (potentially very difficult) real corrections.

For this discussion we assume that we work in QCD with (some) massless flavours instead as the IR structure will be much richer. We will come back to massive QED later.

Infrared predictions have been worked out for massless QCD in dimensional regularisation [61–64]. This was extended to gauge theories with massive fermions [65].

To predict the IR structure of QCD we remember that in an EFT, the Wilson coefficients need to be renormalised. However, the UV singularities removed this way were not present in the full theory. This implies that the part of the calculation entering the Wilson coefficient is IR divergent. We now need to construct a low-energy theory s.t. its UV divergences match the IR poles of QCD because we can predict UV singularities using renormalisation theory. The EFT in question is *soft-collinear effective theory* (SCET) [66–68] (for a pedagogical introduction, for example cf. [69]) that splits soft and collinear modes off from the full underlying theory, be it QED or QCD.

While a full derivation of the IR prediction is well beyond the scope of this work, we can sketch the necessary concepts, especially because we will encounter some of them later.

Let us define the, in principle, all-order renormalised³ matrix element \mathcal{M} for an arbitrary process as the sum of ℓ -loop contributions $\mathcal{M}^{(\ell)}$

$$\mathcal{M} = \sum_{\ell=0}^{\infty} \mathcal{M}^{(\ell)} = \mathcal{M}^{(0)} + \mathcal{M}^{(1)} + \mathcal{M}^{(2)} + \dots, \quad (2.27)$$

where each $\mathcal{M}^{(\ell)}$ contains one power more of $\bar{\alpha}$. We now define the corresponding \mathbf{Z} s.t.

$$\mathcal{M}_{\text{sub}} = (\mathbf{Z})^{-1} \mathcal{M} \quad \text{with} \quad \mathbf{Z} = 1 + \delta\mathbf{Z}^{(1)} + \delta\mathbf{Z}^{(2)} + \dots \quad (2.28)$$

is finite in the limits $\epsilon \rightarrow 0$. We call \mathcal{M}_{sub} *$\overline{\text{MS}}$ -like subtracted*, because \mathbf{Z} is constructed to contain no finite parts, up to trivial terms induced by the loop measure. However, just like $\overline{\text{MS}}$ renormalisation introduces a renormalisation scale, the factorisation into IR finite and IR divergent quantities of (2.28) introduces a new *factorisation scale*.

It is important to note, that, while important for what follows, there is nothing wrong with defining a different \mathbf{Z}' that contains finite parts but no factorisation scale (cf. Chapter 4). For now, however, we will stick to $\overline{\text{MS}}$ -like subtraction and re-write (2.28) to account for the new scale μ

$$\mathcal{M}_{\text{sub}}(\mu) = (\mathbf{Z}(\mu))^{-1} \mathcal{M}. \quad (2.29)$$

Next, we note that, even though \mathcal{M}_{sub} and \mathbf{Z} depend on the factorisation scale, the original matrix element \mathcal{M} does not. Hence, we can obtain a RGE for $\mathcal{M}_{\text{sub}}(\mu)$ by differentiating (2.29) w.r.t. μ , resulting in

$$\frac{d}{d \log \mu} \mathcal{M}_{\text{sub}}(\mu) = \mathbf{\Gamma}(\mu) \mathcal{M}_{\text{sub}}(\mu). \quad (2.30a)$$

with

$$\mathbf{\Gamma}(\mu) = -\frac{d \log \mathbf{Z}}{d \log \mu}. \quad (2.30b)$$

Here, $\mathbf{\Gamma}(\mu)$ is the *anomalous dimension* of the process. This is very similar to how the anomalous dimension of, for example, the fermion that is obtained by

$$\gamma_f = \frac{d \log \bar{Z}_2}{d \log \mu_F}, \quad (2.31)$$

³We will assume that the coupling is renormalised in the $\overline{\text{MS}}$ scheme to be consistent with the literature

with the $\overline{\text{MS}}$ fermion wave function renormalisation \bar{Z}_2 .

The formal solution of (2.30b) is [64]

$$\log \mathbf{Z}(\mu) = \int_{\mu}^{\infty} \frac{d\mu'}{\mu'} \mathbf{\Gamma}(\mu') = \int_{\log \mu}^{\infty} d(\log \mu') \mathbf{\Gamma}(\mu'). \quad (2.32)$$

Unfortunately, integrating (2.30b) is complicated by the fact that $\mathbf{\Gamma}$ is not just a function of μ but also of the $\overline{\text{MS}}$ coupling $\bar{\alpha}(\mu)$ that has its own RGE (2.6)⁴

$$\frac{\partial \alpha(\mu)}{\partial \log \mu} = 2\beta(\alpha(\mu)). \quad (2.33)$$

Hence, we need to distinguish the explicit scale dependence from the one induced by the running of $\bar{\alpha}$. We substitute $\mu' \rightarrow \alpha'(\mu')$ and write schematically

$$\log \mathbf{Z}(\mu) = \int_0^{\bar{\alpha}} \frac{d\alpha'}{-2\beta(\alpha')} \left(\mathbf{\Gamma}(\alpha') + \int_0^{\alpha} \frac{d\alpha''}{-2\beta(\alpha'')} \frac{\partial \mathbf{\Gamma}(\alpha'')}{\partial (\log \mu)} \right), \quad (2.34)$$

where we have used that the only explicit dependency of $\log \mu$ in $\mathbf{\Gamma}$ is linear as we will see below. By identifying $\mathbf{\Gamma}'$ as

$$\mathbf{\Gamma}' = \frac{\partial \mathbf{\Gamma}}{\partial \log \mu}, \quad (2.35)$$

we can solve this order-by-order [63, 64]

$$\log \mathbf{Z} = \left(\frac{\bar{\alpha}}{4\pi} \right) \left(\frac{\mathbf{\Gamma}'_1}{4\epsilon^2} + \frac{\mathbf{\Gamma}_1}{2\epsilon} \right) + \left(\frac{\bar{\alpha}}{4\pi} \right)^2 \left(-\frac{3\beta \cdot \mathbf{\Gamma}'_1}{16\epsilon^3} - \frac{\beta \cdot \mathbf{\Gamma}_1}{4\epsilon^2} + \frac{\mathbf{\Gamma}'_2}{16\epsilon^2} + \frac{\mathbf{\Gamma}_2}{4\epsilon} \right) + \mathcal{O}(\alpha^3), \quad (2.36)$$

where $\mathbf{\Gamma}_i$ ($\mathbf{\Gamma}'_i$) is the $\mathcal{O}(\alpha^i)$ coefficient of $\mathbf{\Gamma}$ ($\mathbf{\Gamma}'$) and $\beta \cdot \mathbf{\Gamma}_1 = \beta_0 \cdot \mathbf{\Gamma}_1$ in the notation of [70] and Appendix B.

It has been conjectured by [63] that, assuming a theory without massive flavours, the anomalous dimension $\mathbf{\Gamma}$ can be constructed to all orders by just considering two-particle correlations. This ceases to be true in a theory with massive particles [71], requiring a more complicated structure [65] that we will not reproduce here.

For the two-parton case $\mathbf{\Gamma}$ is constructed from a *cusplike anomalous dimension* γ_{cusp} relating two partons and quark anomalous dimensions γ_i (or γ_I for massive quarks) that has to do with just one parton. Assuming trivial colour-flow (as in $t \rightarrow Wb$ or of course any QED calculation)

$$\begin{aligned} \mathbf{\Gamma}(\mu) &= \sum_{i,j} \gamma_{\text{cusp}} \log \frac{\mu^2}{-\text{sign}_{ij} 2p_i \cdot p_j} + \sum_i \gamma_i \\ &\quad - \sum_{I,J} \gamma_{\text{cusp}} (\chi_{IJ}) + \sum_I \gamma_I \\ &\quad + \sum_{I,j} \gamma_{\text{cusp}} \log \frac{m_I \mu}{-\text{sign}_{Ij} 2p_I \cdot p_j}. \end{aligned} \quad (2.37)$$

We use capital letters I to indicate massive particles and lower-case letters for massless particles. The signs in front of the scalar product depend on the types of spinors involved [63]. To be precise,

⁴In [64], β is defined as $\beta_{[64]} = 2\beta$.

$\text{sign}_{ij} = (-1)^{n_{ij}+1}$, where n_{ij} is the number of incoming particles or outgoing antiparticles among the particles i and j .

In a theory without massive particles, the first line of (2.37) describes the anomalous dimension of any number of particles with the sum going over all possible unordered pairs as conjectured by [63].

The angle χ_{IJ} of the fully massive case is sometimes called *cusp angle*

$$\chi_{IJ} = \text{arcosh} \frac{-\text{sign}_{IJ} p_I \cdot p_J}{m_I m_J}. \quad (2.38)$$

A comprehensive list of the anomalous dimensions required at the two-loop level can be found in Appendix B.2.

The procedure to cross-check IR poles is now:

1. Calculate the $\overline{\text{MS}}$ -renormalised matrix element.
2. In a theory with massive flavours, perform a *decoupling transformation* relating SCET parameters, in which heavy fermions have been integrated out, and fields such as α_{SCET} to those of the full theory [72]

$$\alpha_{\text{full}} = \zeta_\alpha \times \alpha_{\text{SCET}}, \quad (2.39)$$

where ζ_α is given in Appendix B.2. In a theory without massive flavours there is no need for decoupling.

3. Calculate the anomalous dimension $\mathbf{\Gamma}$ for the process under consideration.
4. Use (2.36) to calculate \mathbf{Z} and use (2.29) to check whether \mathcal{M}_{sub} is finite.

We will see an example of this in Chapter 3.

Even though the above discussion holds in QED, there is a much simpler way to predict IR singularities in massive QED. This is done by noting that soft singularities exponentiate. This means that $\log \mathbf{Z}$ vanishes at all orders, except the first.

This can be re-formulated to all orders as

$$\sum_{\ell=0}^{\infty} \mathcal{M}^{(\ell)} = e^{-\alpha S} \times \text{finite}. \quad (2.40)$$

This was shown by Yennie, Frautschi, and Suura (YFS) [73]. Only the pole of S is fixed by this equation; its finite and $\mathcal{O}(\epsilon)$ contribution can be chosen at will. In Section 4.1 we will find a particularly helpful choice of S .

Chapter 3

Regularisation schemes

As mentioned before, loop integrals are usually divergent and require regularisation. The most common way to achieve this is to formally shift the space-time dimension [74–78] (dimensional regularisation, DREG) to

$$d = 4 - 2\epsilon. \quad (3.1)$$

Correspondingly, we change the loop integration to⁵

$$\int \frac{d^4 k}{(2\pi)^4} \rightarrow \mu^{4-d} \int \frac{d^d k_{[d]}}{(2\pi)^d} \equiv \int [dk], \quad (3.2)$$

where we have defined a convenient integral measure $[dk]$ (cf. (A.1)). We use $k_{[\text{dim}]}$ to indicate a vector of (quasi-)dimension dim . We will specify what precisely is meant by this in Section 3.1.

UV and IR singularities now manifest as poles of the form $1/\epsilon^n$. DREG is indeed a consistent prescription and the resulting integrals still fulfil properties like linearity and invariance under shifts [79, 80].

Note that (3.2) only specifies the dimensionality of the integration momentum k . The dimensionality of other objects such as γ matrices are not yet constrained. In order to systematically classify different approaches, one has to consider two questions

- are all parts of a diagram regularised or only those leading to divergences?
- are algebraic objects like metric tensors or γ matrices regularised in d dimensions or in a different dimensionality?

In Section 3.1 we will introduce a unified framework for the discussion of (dimensional) *regularisation schemes* (RS). Using this, we will briefly discuss γ_5 in DREG in Section 3.2. In Section 3.3 we will use our unified framework to discuss the muon decay in the common schemes HV [75], CDR [80], and FDH [81, 82]. In particular, in Section 3.3.5 we will provide a practitioner’s guide to a particularly simple formulation of FDH, the FDF scheme [83] by once again calculating the muon decay. Finally, we will discuss how we can use IR prediction (cf. Section 2.4) to predict the regularisation scheme dependence, both generally and on the example of the muon decay.

⁵In many of the original references, \hat{k} , \tilde{k} , \bar{k} etc. were used with different meanings depending on paper, scheme, and context. We avoid that by instead using the notation developed in [2].

3.1 Formal aspects

To study the questions asked above and to elegantly unify all common variations of DREG, we need to introduce a series of vector spaces [79, 80, 84]: the strictly four-dimensional Minkowski space $S_{[4]}$ as well as the infinite-dimensional spaces $QS_{[d_s]}$, $QS_{[d]}$, and $QS_{[n_\epsilon]}$. The infinite-dimensional spaces are equipped with the correct quasi-dimensionality, s.t. the metric tensor for each space fulfils

$$(g_{[\text{dim}]}^{\mu\nu})^2 = \text{dim}. \quad (3.3)$$

Most aspects of DREG can be understood from the hierarchy between these spaces

$$S_{[4]} \subset QS_{[d]} \quad \text{and} \quad QS_{[d_s]} = QS_{[d]} \oplus QS_{[n_\epsilon]}. \quad (3.4)$$

The space $QS_{[d]}$ is the space in which $k_{[d]}$ exist. It is *enlarged* to the bigger space $QS_{[d_s]}$ by the orthogonal sum with $QS_{[n_\epsilon]}$. The dimensionality d_s is

$$d_s = d + n_\epsilon = 4 - 2\epsilon + n_\epsilon. \quad (3.5)$$

Note that for many actual calculations we will be setting $d_s = 4$ and $n_\epsilon = 2\epsilon$. For now, however, we will keep all values independent.

Using (3.4) we can now construct all necessary d_s -dimensional objects

$$g_{[d_s]}^{\mu\nu} = g_{[d]}^{\mu\nu} + g_{[n_\epsilon]}^{\mu\nu} \quad \text{and} \quad \gamma_{[d_s]}^\mu = \gamma_{[d]}^\mu + \gamma_{[n_\epsilon]}^\mu. \quad (3.6)$$

Of course these objects have no finite-dimensional representation. To practically work with them, we rely on their algebraic properties

$$(g_{[d]}g_{[n_\epsilon]})^{\mu\nu} = 0, \quad \{\gamma_{[\text{dim}]}^\mu, \gamma_{[\text{dim}]}^\nu\} = 2g_{[\text{dim}]}^{\mu\nu}, \quad \{\gamma_{[d]}^\mu, \gamma_{[n_\epsilon]}^\nu\} = 0. \quad (3.7)$$

Finally, we need to distinguish between two types of vector fields⁶:

- Fields associated with particles in one-particle irreducible (1PI) diagrams or with soft and collinear radiation are called *singular*,
- all other fields are *regular*.

In general, there is no need to regularise regular fields so that there is some freedom regarding their treatment. We can now identify the four flavours of DREG through their answers to the questions considered above, i.e. what particles are treated in which of the three spaces.

	CDR	HV	FDH	DRED
Singular fields	$QS_{[d]}$	$QS_{[d]}$	$QS_{[d_s]}$	$QS_{[d_s]}$
Regular fields	$QS_{[d]}$	$S_{[4]}$	$S_{[4]}$	$QS_{[d_s]}$
	‘dim. reg.’		‘dim. red.’	

⁶Again, we refer to the notation of [2] instead of using the old names internal and external, respectively.

CDR and HV belong to a class of schemes that used to be referred to as ‘dimensional regularisation’ while FDH and DRED belong to what was called ‘dimensional reduction’. We will not be using these terms further to avoid confusion and refer to all four schemes as DREG.

This seems to suggest that FDH is ideal for the calculation of multi-loop contributions because all quantities are either strictly or quasi four-dimensional, keeping the algebra simple without introducing too many new problems (cf. Section 3.3.4). Similarly, DRED is ideal for any type of real corrections because it does not distinguish between singular and regular fields while still minimising the nightmare that are the ϵ/ϵ contributions [85].

3.2 γ_5 in dimensional schemes

In $S_{[4]}$, γ_5 is defined through two equivalent relations

$$\{\gamma_{[4]}^\mu, \gamma_5\} = 0 \quad \text{or} \quad \text{tr}\left(\underbrace{\gamma_{[4]}^\mu \gamma_{[4]}^\nu \gamma_{[4]}^\rho \gamma_{[4]}^\sigma}_{\Gamma_{[4]}} \gamma_5\right) = 4i\epsilon_{[4]}^{\mu\nu\rho\sigma} \equiv 4i\epsilon^{\mu\nu\rho\sigma}, \quad (3.8)$$

where we have defined

$$\Gamma_{[\text{dim}]} = \gamma_{[\text{dim}]}^\mu \gamma_{[\text{dim}]}^\nu \gamma_{[\text{dim}]}^\rho \gamma_{[\text{dim}]}^\sigma \quad (3.9)$$

in an arbitrary dimension dim . However, these definitions are equivalent only on $S_{[4]}$. In any of the other spaces, they are mutually exclusive if we want to keep the cyclicity of traces. The proof of this is simple but lengthy [86] but results in

$$2\left((g_{[d]}^{\alpha\beta})^2 - 4\right) \text{tr}(\Gamma_{[d]} \gamma_5) + \text{tr}(\Gamma_{[d]} \gamma_{[d]}^\alpha \{\gamma_5, \gamma_{[d]}^\alpha\}) = 0, \quad (3.10)$$

which is only valid if $d = (g_{[d]}^{\alpha\beta})^2 = 4$. A similar proof can be found in [87], resulting in

$$0 = (d-4)(d-3)^2(d-2)^2(d-1)^2d. \quad (3.11)$$

This suggests that the two definitions are only equivalent in for integer d .

There are two commonly used solutions to this problem that change the definition of γ_5 that maintain cyclic traces

- γ_5 is constructed to fulfil the trace relation as done in the original HV scheme [75] and later picked up by Breitenlohner and Maison (BM) [88]

$$\gamma_5^{\text{BM}} = \frac{i}{4!} \left(\epsilon^{\mu\nu\rho\sigma} \Gamma \right)_{[4]} = \frac{i}{4!} \epsilon_{[4]}^{\mu\nu\rho\sigma} \Gamma_{[d]}. \quad (3.12)$$

This way, we still have the γ -algebra in $QS_{[d]}$ but also generate many more γ -matrices, complicating traces.

In this scheme, we find for FDH and DRED

$$\{\gamma_5^{\text{BM}}, \gamma_{[4]}^\mu\} = 0 \quad \text{and} \quad [\gamma_5^{\text{BM}}, \gamma_{[n\epsilon]}^\mu] = [\gamma_5^{\text{BM}}, \gamma_{[-2\epsilon]}^\mu] = 0. \quad (3.13)$$

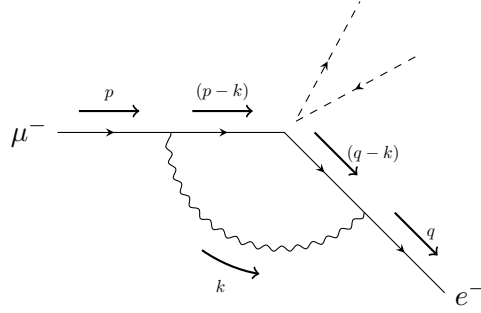


Figure 3.1: The Feynman diagram contributing to the muon decay at the one-loop level with momentum routing. The dimensionality of the momenta will depend on the scheme used.

This also implies that [88]

$$\{\gamma_5^{\text{BM}}, \gamma_{[d]}^\mu\} = 2\gamma_{[-2\epsilon]}^\mu \gamma_5^{\text{BM}} \quad (3.14)$$

and similarly for $\{\gamma_5^{\text{BM}}, \gamma_{[d_s]}^\mu\}$.

Unfortunately, in combination with DREG BM breaks the chiral symmetry because for $P_{L,R} = \frac{1}{2}(1 \pm \gamma_5)$ to be a chiral projectors for both ψ and $\bar{\psi}$, $\{\gamma^0, \gamma^5\} = 0$ is required. This no longer naively works meaning that chiral symmetry is broken. Hence, we require another finite renormalisation [89, 90]

$$\gamma_5^{\text{BM}} \rightarrow Z_5 \gamma_5^{\text{BM}} \quad \text{with} \quad Z_5 = 1 + \frac{\alpha}{4\pi} \left(\frac{n_\epsilon}{\epsilon} - 4 \right). \quad (3.15)$$

We will later see an explicit example of this.

- Alternatively we can define γ_5 algebraically s.t. the anti-commutator vanishes [90–92]

$$\{\gamma_5^{\text{AC}}, \gamma_{[d]}^\mu\} = \{\gamma_5^{\text{AC}}, \gamma_{[n_\epsilon]}^\mu\} = \{\gamma_5^{\text{AC}}, \gamma_{[d_s]}^\mu\} = 0. \quad (3.16)$$

This scheme is workable but not in the strict sense consistent as it fails to reproduce the Adler-Bell-Jackiw or triangle anomaly [93–95]. Despite this, it was proposed by [86] that we can use AC if we restore the anomaly by hand afterwards wherever necessary (though it often is not). One way to make AC consistent is by giving up the cyclicity of the trace [91, 92].

Both methods, if used properly, lead to consistent results. A more complete review of γ_5 in FDH and DRED can be found in [90].

3.3 The muon decay in all schemes

As an illustration of the various aspects of the different schemes, we will calculate the muon decay

$$\mu(p) \rightarrow \nu(q_3) \bar{\nu}(q_4) e(q), \quad (3.17)$$

with $p^2 = M^2 \equiv m_\mu^2$ and $q^2 = 0$ in the three schemes CDR, HV, and FDH. In particular, we will set the electron mass to zero in this section because it will result in a more interesting

singularity structure – helping us to understand the different schemes better. Note that we keep all mass-effects in the phenomenological discussion later.

To simplify this discussion, we will perform the computation in the Fierz rearranged effective theory of the muon decay (2.24). As we have already discussed in Section 2.2, \mathcal{L} is invariant under the exchange $\psi_e \rightarrow \gamma^5 \psi_e$ (and $m_e \rightarrow -m_e$ had we not assumed $m_e = 0$) [59], allowing us to relate the axial-vector current to the vector current. Hence, we can calculate the matrix elements without needing to worry about γ_5 .

When considering this process, we need to compute one diagram at tree level and one diagram at one-loop, the latter is shown in Figure 3.1. As aids, we will be using the Mathematica programs TRACER [96] for the Dirac algebra and Package-X [97] for the one-loop calculus.

All renormalisation constants necessary for this calculation can be found in Appendix B.1.

3.3.1 Neutrino average

As a first step that is universal to all schemes, we will deal with the neutrinos, realising that we cannot actually measure them. Hence, we would like to remove them as much from the calculation as possible. To do this we note that when we calculate any observable using (2.24), a term corresponding to the neutrino current

$$\mathcal{N}^\mu = \bar{u}(q_3)\gamma^\mu u(q_4) \quad (3.18)$$

will be present in the amplitudes. We can factor out the neutrino tensor $\mathcal{N}^\mu \mathcal{N}^{*\nu}$ that appears in the squared amplitude by averaging over all possible neutrino momenta. To do this, we note that

$$\mathcal{N}^\mu \mathcal{N}^{*\nu} = 4q_3^\mu q_4^\nu + 4q_3^\nu q_4^\mu + 4q_3 \cdot q_4 g^{\mu\nu}, \quad (3.19)$$

where q_3 and q_4 are the momenta of the neutrinos. Here and henceforth, the sum over spin states is implicit. Had we not removed the γ_5 earlier, there would also be anti-symmetric terms that would not change the discussion below. We now define the average of an arbitrary function $f(q_3, q_4)$ as the normalised $1 \rightarrow 2$ phase space integration

$$\langle f(q_3, q_4) \rangle = \frac{\int d\Phi f(q_3, q_4)}{\int d\Phi 1} = 8\pi \int d\Phi f(q_3, q_4). \quad (3.20)$$

However, it turns out that, as long as $\langle 1 \rangle = 1$, it does not matter how the phase space is defined as long as it is Lorentz invariant and integrates over the neutrinos.

When we average over q_3 and q_4 , the result can only depend on $Q = q_3 + q_4$. Hence, the most general ansatz for $\langle q_3^\mu q_4^\nu \rangle$ is

$$\langle q_3^\mu q_4^\nu \rangle = A \frac{Q^\mu Q^\nu}{Q^2} + B g^{\mu\nu}. \quad (3.21)$$

By applying the projectors $g^{\mu\nu}$ and $Q^\mu Q^\nu$ we find

$$\begin{aligned} g^{\mu\nu} \langle q_3^\mu q_4^\nu \rangle &= \langle q_3 \cdot q_4 \rangle = A + B d \\ Q^\mu Q^\nu \langle q_3^\mu q_4^\nu \rangle &= \langle Q \cdot q_3 Q \cdot q_4 \rangle = Q^2(A + B). \end{aligned} \quad (3.22)$$

Using that $q_3^2 = q_4^2 = 0$, i.e. $Q^2 = 2q_3 \cdot q_4$, we can re-write these equations

$$\frac{1}{2}Q^2\langle 1 \rangle = A + B d \quad \text{and} \quad \frac{1}{4}(Q^2)^2\langle 1 \rangle = Q^2(A + B), \quad (3.23)$$

allowing us to determine A and B

$$A = \frac{d-2}{d-1} \frac{Q^2}{4} \langle 1 \rangle \quad \text{and} \quad B = \frac{1}{d-1} \frac{Q^2}{4} \langle 1 \rangle. \quad (3.24)$$

And hence with $\langle 1 \rangle = 1$

$$\mathcal{N}^{\mu\nu} = \langle \mathcal{N}^\mu \mathcal{N}^{*\nu} \rangle = 2 \frac{d-2}{d-1} Q^2 \left(\frac{Q^\mu Q^\nu}{Q^2} - g^{\mu\nu} \right). \quad (3.25)$$

Note that the neutrino tensor $\mathcal{N}^{\mu\nu}$ will be the same in all parts of the calculation (both real and virtual) as a global pre-factor. While the dimensionality of \mathcal{N} certainly influences intermediary results, any physical quantity must be independent of its dimensionality as it will only influence terms $\mathcal{O}(\epsilon)$ that vanish in the limit $\epsilon \rightarrow 0$. This means that we could choose its dimensionality independently of the scheme under consideration.

3.3.2 Conventional dimensional regularisation (CDR)

In CDR all quantities are considered d -dimensional, even the external momenta. However, because $S_{[4]} \subset \text{QS}_{[d]}$ the dimension of the external fermion momenta does not matter and they could in principle be chosen from either space. Nevertheless, for consistency we will still keep them in the space they would be in if they were internal momenta.

The tree-level amplitude is

$$\mathcal{A}_{\text{CDR}}^{(0)} = \frac{1}{2} \times \frac{4G_F}{\sqrt{2}} \left(-\bar{u}(q_{[d]}) \gamma_{[d]}^\mu u(p_{[d]}) \mathcal{N}_{[d]}^\mu \right). \quad (3.26)$$

Here, the factor $1/2$ arises from the projector $P_L = (1 - \gamma^5)/2$. The matrix element⁷ is

$$\begin{aligned} \mathcal{M}_{\text{CDR}}^{(0)} &= \frac{1}{2} \left| \mathcal{A}_{\text{CDR}}^{(0)} \right|^2 = \frac{1}{2} \times \frac{4G_F^2}{2} \text{tr} \left[\not{q}_{[d]} \gamma_{[d]}^\mu (\not{p}_{[d]} + M) \gamma_{[d]}^\nu \right] \times \mathcal{N}_{[d]}^{\mu\nu} \\ &= \frac{8}{3} G_F^2 M^4 x (3 + 2x(\epsilon - 1) - 2\epsilon), \end{aligned} \quad (3.27)$$

with $x = 2p \cdot q/M^2$ the dimensionless quantity describing the process. To obtain this result we have used standard d -dimensional trace techniques as implemented in **TRACER**.

At the one-loop level, we have to calculate

$$\begin{aligned} \mathcal{M}_{\text{CDR}}^{(1)} \Big|_{\text{bare}} &= \frac{1}{2} \times 2\Re(\mathcal{A}_{\text{CDR}}^{(1)} \times \mathcal{A}_{\text{CDR}}^{(0)}) \\ &= \frac{\alpha_0 G_F^2}{\pi} \int [dk] \frac{\text{tr} \left[\not{q}_{[d]} \gamma_{[d]}^\sigma (\not{k}_{[d]} - \not{q}_{[d]}) \gamma_{[d]}^\mu (\not{k}_{[d]} - \not{p}_{[d]} - M) \gamma_{[d]}^\sigma (\not{p}_{[d]} + M) \gamma_{[d]}^\nu \right]}{\mathcal{D}_1 \mathcal{D}_2 \mathcal{D}_3} \mathcal{N}_{[d]}^{\mu\nu}, \end{aligned} \quad (3.28)$$

⁷By 'matrix element' we denote the result of squaring the amplitude. In particular, we refrain from calling it the matrix element squared

with

$$\mathcal{D}_1 = k_{[d]}^2, \quad \mathcal{D}_2 = (k_{[d]} + p_{[d]})^2 - M^2, \quad \mathcal{D}_3 = (k_{[d]} - q_{[d]})^2. \quad (3.29)$$

(3.28) can be evaluated using standard techniques, obtaining the unrenormalised CDR result

$$\begin{aligned} \mathcal{M}_{\text{CDR}}^{(1)} \Big|_{\text{bare}} = \frac{\alpha_0}{\pi} \left(\frac{\mu^2}{M^2 x^2} \right)^\epsilon \mathcal{M}_{\text{CDR}}^{(0)} \left(-\frac{1}{2\epsilon^2} - \frac{1}{2\epsilon} - 2 - \frac{3}{2}\zeta_2 + \frac{x}{2x-3} \log(x) \right. \\ \left. + \log(1-x) \log(x) + \text{Li}_2(x) \right), \end{aligned} \quad (3.30)$$

with the dilogarithm $\text{Li}_2(x)$, the first polylogarithm with order $o = 2$, and $\zeta(2) = \pi^2/6$ the Riemann ζ -function. This and many more expressions we will encounter can be compactly written by using so-called *harmonic polylogarithms* (HPL), introduced in [98] and implemented for Mathematica in [99]. These functions extend the notion of polylogarithms by generalising the order o to a weight vector \vec{w} . In particular, introducing $\vec{w} = \{0\}$ and $\vec{w} = \{1, 0\}$

$$H_0(x) = \log(x) \quad \text{and} \quad H_{1,0}(x) = -\log(1-x) \log(x) - \text{Li}_2(x), \quad (3.31)$$

we find

$$\mathcal{M}_{\text{CDR}}^{(1)} \Big|_{\text{bare}} = \frac{\alpha_0}{\pi} \left(\frac{\mu^2}{M^2 x^2} \right)^\epsilon \mathcal{M}_{\text{CDR}}^{(0)} \left(-\frac{1}{2\epsilon^2} - \frac{1}{2\epsilon} - 2 - \frac{3}{2}\zeta_2 + \frac{x}{2x-3} H_0(x) - H_{1,0}(x) \right), \quad (3.32)$$

We now need to renormalise this quantity. No mass renormalisation is necessary because $\mathcal{A}^{(0)}$ does not contain M . Masses from the spin-sum are taken care through the renormalisation of the wave function in the OS scheme as mandated by the LSZ formula. For the muon, this means we have to multiply with (in Feynman gauge)

$$\sqrt{Z_{2,\text{CDR}}^\mu} = 1 + \frac{\alpha_0}{2\pi} \left(-\frac{3}{2\epsilon} + \frac{3}{2} \log \frac{M^2}{\mu^2} - \frac{4}{2} \right). \quad (3.33)$$

Technically, the α_0 here is unrenormalised. However, at the current loop order there is no difference because $\alpha = \alpha_0 + \mathcal{O}(\alpha^2)$. The corresponding factor $Z_2^\epsilon = 1 + \mathcal{O}(\alpha^2)$ because we treat the electron massless. Hence, we have

$$\mathcal{M}_{\text{CDR}}^{(1)} = \frac{\alpha}{\pi} \left(\frac{\mu^2}{M^2 x^2} \right)^\epsilon \mathcal{M}_{\text{CDR}}^{(0)} \left(-\frac{1}{2\epsilon^2} - \frac{5}{4\epsilon} - 3 - \frac{3}{2}\zeta_2 - \frac{9-4x}{6-4x} H_0(x) - H_{1,0}(x) \right). \quad (3.34)$$

In particular we do not renormalise the electromagnetic coupling α because no QED vertex is present at LO (cf. Section 2.1.2).

3.3.3 The original scheme (HV)

In HV, we treat the regular fields four dimensionally. This means that at tree level we do a strictly four-dimensional calculation

$$\begin{aligned} \mathcal{M}_{\text{HV}}^{(0)} &= \frac{1}{2} \times \frac{4G_F^2}{2} \text{tr} \left[\not{q}_{[4]} \gamma_{[4]}^\mu (\not{p}_{[4]} + M) \gamma_{[4]}^\nu \right] \times \mathcal{N}_{[4]}^{\mu\nu} = \frac{8G_F^2}{3} M^4 x (3-2x) \\ &= \mathcal{M}_{\text{CDR}}^{(0)} \Big|_{d=4}. \end{aligned} \quad (3.35)$$

At one-loop we have to be more careful as we have objects of different dimensions in one trace

$$\mathcal{M}_{\text{HV}}^{(1)}\Big|_{\text{bare}} = \frac{\alpha_0 G_F^2}{\pi} \int [dk] \frac{\text{tr} \left[\not{q}_{[4]} \gamma_{[d]}^\sigma (\not{k}_{[d]} - \not{q}_{[d]}) \gamma_{[4]}^\mu (\not{k}_{[d]} - \not{p}_{[d]} - M) \gamma_{[d]}^\sigma (\not{p}_{[4]} + M) \gamma_{[4]}^\nu \right]}{\mathcal{D}_1 \mathcal{D}_2 \mathcal{D}_3} \mathcal{N}_{[4]}^{\mu\nu}. \quad (3.36)$$

Note that the only meaningful difference to the CDR discussion is the dimensionality of the γ^μ and γ^σ . When calculating in HV, we need to utilise that $S_{[4]} \subset \text{QS}_{[d]}$. This is a rather powerful statement because it allows us to calculate the product of two vectors in different spaces as

$$a_{[d]} \cdot b_{[4]} = a_{[4]} \cdot b_{[4]}. \quad (3.37)$$

This relation goes both ways. After using standard trace techniques (taking care of the dimensionality of each γ matrix) we can use it the other way around to write the numerator again in terms of the familiar $k_{[d]} \cdot p_{[d]}$, $k_{[d]} \cdot q_{[d]}$, and $k_{[d]} \cdot k_{[d]}$. However, we also have a new type numerator with $k_{[4]} \cdot k_{[4]}$ from

$$\text{tr} \left[k_{[d]} \gamma_{[4]}^\mu k_{[d]} \gamma_{[4]}^\mu \right] = 8k_{[4]} \cdot k_{[4]} - 16k_{[d]} \cdot k_{[d]}. \quad (3.38)$$

Using these relations, we find

$$\begin{aligned} \mathcal{M}_{\text{HV}}^{(1)}\Big|_{\text{bare}} = \frac{\alpha_0}{\pi} \frac{8G_F^2}{3} \int [dk] & \frac{1}{\mathcal{D}_1 \mathcal{D}_2 \mathcal{D}_3} \left(2(3M^2 - 2s)s^2 \right. \\ & + 4(3M^4 - 4M^2s + 2s^2)(k_{[d]} \cdot q_{[d]}) - 4(3M^2 - 2s)s(k_{[d]} \cdot p_{[d]}) \\ & + 4(d-2)M^2(k_{[d]} \cdot q_{[d]})^2 + 4(d-2)(M^2 - 2s)(k_{[d]} \cdot p_{[d]})(k_{[d]} \cdot q_{[d]}) \\ & \left. - (d-2)(2s - 3M^2)s(k_{[d]} \cdot k_{[d]}) - 2(M^2 - s)s(d-2)(k_{[4]} \cdot k_{[4]}) \right). \end{aligned} \quad (3.39)$$

With the $(k_{[4]} \cdot k_{[4]})$ in the numerator, we have in principle a new class of integrals to discuss. These will be related to the μ -integrals of Section 3.3.5. However, for now we can just solve these integrals using Passarino-Veltman decomposition [100] (for a didactic introduction cf. [101])

$$\int [dk] \frac{k_{[4]} \cdot k_{[4]}}{\mathcal{D}_1 \mathcal{D}_2 \mathcal{D}_3} = g_{[4]}^{\mu\nu} \int [dk] \frac{k_{[d]}^\mu k_{[d]}^\nu}{\mathcal{D}_1 \mathcal{D}_2 \mathcal{D}_3}, \quad (3.40)$$

because $S_{[4]} \subset \text{QS}_{[d]}$.

Solving the loop integral and renormalising with $Z_{2,\text{HV}}^\mu = Z_{2,\text{CDR}}^\mu$ we find a familiar result

$$\mathcal{M}_{\text{HV}}^{(1)} = \frac{\alpha}{\pi} \left(\frac{\mu^2}{M^2 x^2} \right)^\epsilon \mathcal{M}_{\text{HV}}^{(0)} \left(-\frac{1}{2\epsilon^2} - \frac{5}{4\epsilon} - 3 - \frac{3}{2}\zeta_2 - \frac{9-4x}{6-4x} H_0(x) - H_{1,0}(x) \right). \quad (3.41)$$

Note that here we pulled out a factor $\mathcal{M}_{\text{HV}}^{(0)}$ instead of $\mathcal{M}_{\text{CDR}}^{(0)}$. This makes the fully expanded result simpler in comparison with the fully expanded result of $\mathcal{M}_{\text{CDR}}^{(1)}$ as there are no terms ϵ/ϵ from the poles with the linear parts of the tree level result. We refer to this as *trivial scheme dependence* because nothing relevant has changed. This is similar to the scheme dependence due to the neutrino tensor. The $\mathcal{M}_{\text{RS}}^{(0)}$ term will appear in all parts of the calculations, i.e. both real and virtual. Intermediary results will have to be different due to the trivial scheme dependence but any physical, i.e. finite, result will be independent because $\mathcal{M}_{\text{RS}}^{(0)}$ acts as a pre-factor.

3.3.4 The four-dimensional helicity scheme (FDH)

The goal of FDH is to treat as many objects in $d_s \equiv 4$ dimensions as possible. While this simplifies things a lot, ‘there ain’t no such thing as a free lunch’. This popular saying manifests itself in the existence of so-called ϵ -scalars.

We treat singular vector fields in $\text{QS}_{[d_s]} = \text{QS}_{[d]} \oplus \text{QS}_{[n_\epsilon]}$ which means that we have to write the covariant derivative as

$$D_{[d_s]}^\mu \psi_0 = \partial_{[d]}^\mu \psi_0 + i(e_0(A_0)_{[d]}^\mu + e_{e,0}(A_0)_{[n_\epsilon]}^\mu) \psi_0, \quad (3.42)$$

with a bare ϵ -scalar $(A_0)_{[n_\epsilon]}^\mu$ with an evanescent coupling $e_{e,0}$ to fermions. This split, that spoils FDH’s simplicity, is necessary as $e_{e,0}$ is not protected by the d -dimensional gauge symmetry and is renormalised differently. In QED, the corresponding β -functions are [102] (cf. Appendix B.1)

$$\begin{aligned} \beta &= -\alpha \left(\left(\frac{\alpha}{4\pi} \right) \underbrace{\left[-\frac{4}{3} N_F \right]}_{\beta_0 \equiv \beta_{20}} + \mathcal{O}(\alpha^2) \right), \\ \beta_e &= -\alpha_e \left(\left(\frac{\alpha_e}{4\pi} \right) \underbrace{\left[-4 - 2N_F \right]}_{\beta_{02}} + \left(\frac{\alpha}{4\pi} \right) \underbrace{\left[+6 \right]}_{\beta_{11}} + \mathcal{O}(\alpha_i^2) \right). \end{aligned} \quad (3.43)$$

Therefore, one would have to perform any ℓ -loop calculation with both ϵ -scalars and normal gauge bosons, keeping the couplings e and e_e different. After renormalisation one can safely set $e_e \rightarrow e$. This increases the number of diagrams by $\mathcal{O}(2^\ell)$.

Fortunately, there is a silver lining: because the effect of ϵ -scalars is limited the their coupling’s renormalisation, there is actually no need to use (3.42) at the ℓ -loop level. This gives us the following prescription for an ℓ -loop calculation

- Use (3.42) for anything up to the $(\ell - 1)$ -level and renormalise correctly.
- At the ℓ -loop level, perform the calculation using only quasi-four-dimensional objects.
- Add everything up and set $e_e \rightarrow e$ and $n_\epsilon \rightarrow 2\epsilon$. If necessary, convert to a different renormalisation scheme for the coupling now.

Especially for one-loop ϵ -scalars are not needed at all because the renormalisation could only influence tree level ϵ -scalars that do not exist because there are no singular fields at leading order. Hence, one-loop calculations can be performed without worrying about ϵ -scalars (for a particular efficient way to exploit this, cf. Section 3.3.5). This would still work in QCD when including PDFs [82].

At tree level in FDH, we obtain the same result as in HV because both schemes treat regular fields in $S_{[4]}$. For illustration, we will calculate the one-loop FDH result twice: once carefully differentiating ϵ -scalar contributions with ϵ -scalars and once ignoring ϵ -scalars at one-loop, while instead working in $d_s \equiv 4$ dimensions.

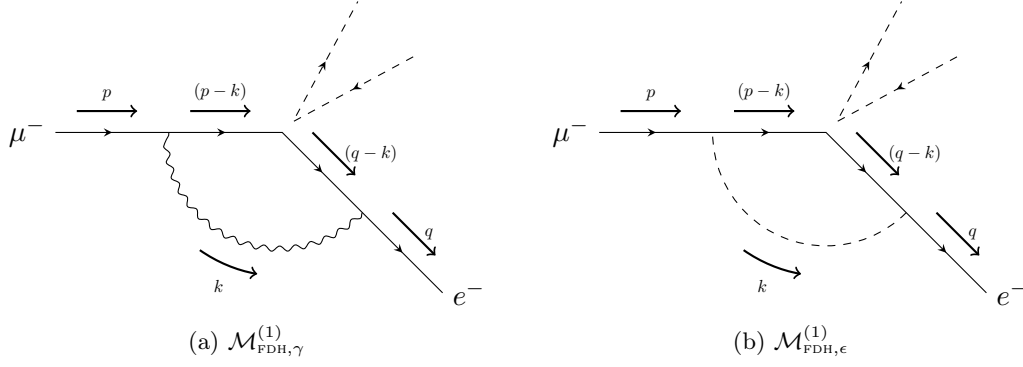


Figure 3.2: The two diagrams in full FDH. The first diagram is identical to Figure 3.1.

Calculation with ϵ -scalars

We have to calculate the two diagrams of Figure 3.2: one diagram with a virtual photon, Figure 3.2a,

$$\mathcal{M}_{\text{FDH},\gamma}^{(1)} = \frac{\alpha_0 G_F^2}{\pi} \int [dk] \frac{\text{tr} \left[\not{q}_{[4]} \gamma_{[d_s]}^\sigma (\not{k}_{[d]} - \not{q}_{[d]}) \gamma_{[4]}^\mu (\not{k}_{[d]} - \not{p}_{[d]} - M) \gamma_{[d_s]}^\sigma (\not{p}_{[4]} + M) \gamma_{[4]}^\nu \right]}{\mathcal{D}_1 \mathcal{D}_2 \mathcal{D}_3} \mathcal{N}_{[4]}^{\mu\nu}, \quad (3.44a)$$

and one with a virtual ϵ -scalar, Figure 3.2b,

$$\mathcal{M}_{\text{FDH},\epsilon}^{(1)} = \frac{\alpha_{e,0} G_F^2}{\pi} \int [dk] \frac{\text{tr} \left[\not{q}_{[4]} \gamma_{[n_\epsilon]}^\sigma (\not{k}_{[d]} - \not{q}_{[d]}) \gamma_{[4]}^\mu (\not{k}_{[d]} - \not{p}_{[d]} - M) \gamma_{[n_\epsilon]}^\sigma (\not{p}_{[4]} + M) \gamma_{[4]}^\nu \right]}{\mathcal{D}_1 \mathcal{D}_2 \mathcal{D}_3} \mathcal{N}_{[4]}^{\mu\nu}, \quad (3.44b)$$

where $\alpha_{e,0} = e_{e,0}^2/(4\pi)$ in accordance with the definition of α_0 . Because $\not{k}_{[d]} = \gamma_{[d]}^\mu k_{[d]}^\mu = \gamma_{[d_s]}^\mu k_{[d]}^\mu$, we can do most of the algebra of $\mathcal{M}_{\text{FDH},\gamma}^{(1)}$ in d_s dimensions as long as we keep track of the dimensionality of the k .

By employing the same tricks as above for the Dirac algebra, we find without specifying d_s for the bare matrix element

$$\mathcal{M}_{\text{FDH},\gamma}^{(1)} \Big|_{\text{bare}} = \frac{\alpha_0}{\pi} \left(\frac{\mu^2}{M^2 x^2} \right)^\epsilon \mathcal{M}_{\text{FDH}}^{(0)} \left(-\frac{1}{2\epsilon^2} - \frac{6-d_s}{4\epsilon} - \frac{10-d_s}{4} - \frac{3}{2} \zeta_2 \right. \\ \left. + \frac{(d_s-4)(3-x) - 2x}{6-4x} H_0(x) - H_{1,0}(x) \right), \quad (3.45a)$$

$$\mathcal{M}_{\text{FDH},\epsilon}^{(1)} \Big|_{\text{bare}} = \frac{\alpha_{e,0}}{\pi} n_\epsilon \left(\frac{\mu^2}{M^2 x^2} \right)^\epsilon \mathcal{M}_{\text{FDH}}^{(0)} \left(\frac{1}{4\epsilon} + \frac{1}{4} + \frac{3-x}{6-4x} H_0(x) \right). \quad (3.45b)$$

For the renormalisation we need to consider the effect of ϵ -scalars to Z_2^μ

$$\sqrt{Z_{2,\text{FDH}}^\mu} = 1 + \frac{\alpha_0}{2\pi} \left(-\frac{3}{2\epsilon} + \frac{3}{2} \log \frac{M^2}{\mu^2} - \frac{4}{2} \right) + \frac{\alpha_{e,0}}{2\pi} n_\epsilon \left(-\frac{1}{4\epsilon} + \frac{1}{4} \log \frac{M^2}{\mu^2} - \frac{1}{4} \right). \quad (3.46)$$

Our renormalised FDH result is therefore

$$\begin{aligned}
\mathcal{M}_{\text{FDH}}^{(1)} &= \mathcal{M}_{\text{FDH},\gamma}^{(1)} + \mathcal{M}_{\text{FDH},\epsilon}^{(1)} \\
&= \left(\frac{\mu^2}{M^2 x^2} \right)^\epsilon \mathcal{M}_{\text{FDH}}^{(0)} \left[\frac{\alpha}{\pi} \left(-\frac{1}{2\epsilon^2} + \frac{d_s - 9}{4\epsilon} - \frac{10 + (4 - d_s)}{4} - \frac{3}{2}\zeta_2 \right. \right. \\
&\quad \left. \left. + \frac{(d_s - 4)(3 - x) - 9 + 4x}{6 - 4x} H_0(x) - H_{1,0}(x) \right) \right. \\
&\quad \left. + \frac{\alpha_e n_\epsilon}{\pi} \frac{1}{4} \left(\frac{1}{2\epsilon} + \frac{1}{2} - \frac{3}{2x - 3} H_0(x) \right) \right]. \tag{3.47}
\end{aligned}$$

This result is what we refer to as *two-loop ready*. It has the explicit dependence on the ϵ -scalars so that we could – and in Chapter 5 will – perform the two-loop calculation in FDH with the correct renormalisation of α_e .

Calculation without ϵ -scalars

Assuming we do not actually want to perform a two-loop calculation, we can simplify the calculation by just setting $d_s \equiv 4$ and $n_\epsilon = 0$ in the one-loop calculation from the get-go with $\alpha_e = \alpha$. However, we still need to keep in mind that $S_{[4]} \subset \text{QS}_{[d_s]} \equiv \text{QS}_{[4]}$, i.e. that $a_{[d]} \cdot b_{[d_s]} = a_{[d]} \cdot b_{[d]}$, allowing us to perform the algebra $d_s \equiv 4$ dimensionally. For complicate processes this can simplify the algebra massively as there is no need to keep track of ϵ -terms induced by the algebra. We of course lose the generality of two-loop readiness.

Our one-loop bare result is just (3.45a) with $d_s = 4$. However, we need to keep the n_ϵ in Z_2^μ resulting in

$$\mathcal{M}_{\text{FDH}}^{(1)} \Big|_{\text{bare}} = \frac{\alpha}{\pi} \left(\frac{\mu^2}{M^2 x^2} \right)^\epsilon \mathcal{M}_{\text{FDH}}^{(0)} \left(-\frac{1}{2\epsilon^2} - \frac{1}{2\epsilon} - \frac{3}{2} - \frac{3}{2}\zeta_2 - \frac{2x}{6 - 4x} H_0(x) - H_{1,0}(x) \right), \tag{3.48a}$$

$$Z_{2,\text{FDH}}^\mu = 1 + \frac{\alpha}{2\pi} \left(-\frac{3}{2\epsilon} + \frac{3}{2} \log \frac{M^2}{\mu^2} - \frac{5}{2} \right). \tag{3.48b}$$

This directly results in what we find if we set $d_s = 4 - 2\epsilon$ and $n_\epsilon = 2\epsilon$ in (3.47)

$$\mathcal{M}_{\text{FDH}}^{(1)} = \frac{\alpha}{\pi} \left(\frac{\mu^2}{M^2 x^2} \right)^\epsilon \mathcal{M}_{\text{FDH}}^{(0)} \left(-\frac{1}{2\epsilon^2} - \frac{5}{4\epsilon} - \frac{11}{4} - \frac{3}{2}\zeta_2 - \frac{9 - 4x}{6 - 4x} H_0(x) - H_{1,0}(x) \right). \tag{3.49}$$

Compare this result to the HV result from (3.41). The only difference is the rational number in the finite part that changes from $-3 \rightarrow -11/4$. This the first time we have encountered *non-trivial scheme dependence* (this is in contrast to the trivial scheme dependence between CDR and HV). As we will see in Section 3.4, we can predict the scheme dependence without having to calculate the different contributions.

It is important that all non-trivial scheme dependence will cancel as soon as $\mathcal{M}_{\text{RS}}^{(1)}$ is combined with the real correction in the same scheme RS. This is crucial as otherwise the different schemes would not be consistent.

Renormalisation of FDH beyond leading order

Beyond what we have discussed in Section 2.1, the renormalisation in FDH is complicated by the presence of ϵ -scalars at the one-loop level. Additionally to the issue of the different coupling we have already discussed, there is one more subtlety in a theory with massive flavours. In contrast to the vector boson propagator, there is no symmetry that protects the propagator of the ϵ -scalar from acquiring a mass term $\propto m^2 g_{[n_\epsilon]}^{\mu\nu}$ [103, 104]. This effectively shifts the scalar's mass from zero, requiring an appropriate counter term to restore a vanishing ϵ -scalar mass. Hence, we add the following steps in the discussion of Section 2.1.2

5. Maintain the masslessness of the ϵ -scalars by substituting

$$\frac{-ig_{[n_\epsilon]}^{\mu\nu}}{p^2} \rightarrow \delta m_\epsilon^{(l)} \frac{-ig_{[n_\epsilon]}^{\mu\nu}}{p^2} \quad (3.50)$$

at tree level and one-loop.

6. Perform the coupling renormalisation by shifting $\alpha_{0,i} \rightarrow (1 + \delta Z_{\alpha_i}^{(1)} + \delta Z_{\alpha_i}^{(2)}) \times \alpha_i$ and sorting terms according to the now renormalised coupling, dropping every term with too high a power in α_i .
7. Identify $\alpha_\epsilon \equiv \alpha$ and set $n_\epsilon = 2\epsilon$.

3.3.5 Four-dimensional formulation of FDH (FDF)

At the one-loop level, FDH is seemingly complicated by the presence of objects with different dimensions in the traces and the need to include ϵ -scalars at tree level. There is also still the problem of γ^5 which we have ignored so-far. The four-dimensional formulation of FDH (FDF) solves both problems at one-loop [83].

Originally, the FDF scheme was constructed to best use unitarity methods for one-loop calculation. This is done by essentially constructing one-loop amplitudes by sewing together tree-level amplitudes, allowing for extremely efficient numerical evaluation of one-loop amplitudes as done by e.g. GoSam [105]. However, for this to work all momenta including the loop momentum must be in $S_{[4]}$. We will not be discussing these methods further as FDF is for us just a particularly efficient way to calculate complicated one-loop amplitudes.

We can simplify FDH by realising that all our problems arise because of the $k_{[4]}^2$ -terms in numerators of integrals that we have postponed in our discussion of HV. To understand these terms better, we will introduce another space $QS_{[-2\epsilon]}$

$$QS_{[d]} = S_{[4]} \oplus QS_{[-2\epsilon]}. \quad (3.51a)$$

We can now write $k_{[4]}^2$ as

$$k_{[d]}^2 = k_{[4]}^2 - \mu^2, \quad (3.51b)$$

where μ^2 is the remnant of the part of the loop momentum from $QS_{[-2\epsilon]}$. However, we can realise this already at the level of γ matrices by setting

$$\not{k}_{[d]} = \not{k}_{[4]} + i\gamma^5 \mu. \quad (\text{Rule I})$$

One can easily verify that this definition satisfies (3.51b). We can now perform the entire calculation in $S_{[4]}$, up to terms $\mu \in \text{QS}_{[-2\epsilon]}$ for which we use

$$\text{Odd powers of } \mu \text{ are set to zero.} \quad (\text{Rule II})$$

In our case, we write (cf. (3.36))

$$\begin{aligned} \mathcal{M}_{\text{FDF}}^{(1)} \Big|_{\text{bare}} = \frac{\alpha}{\pi} \frac{8G_F^2}{3} \left[\int [dk] \frac{1}{k_{[d]}^2 \mathcal{D}_2 \mathcal{D}_3} \left(2(3M^2 - 2s)s^2 \right. \right. \\ \left. \left. + 4(3M^4 - 4M^2s + 2s^2)(k_{[4]} \cdot q_{[4]}) - 4(3M^2 - 2s)s(k_{[4]} \cdot p_{[4]}) \right. \right. \\ \left. \left. + 8M^2(k_{[4]} \cdot q_{[4]})^2 + 8(M^2 - 2s)(k_{[4]} \cdot p_{[4]})(k_{[4]} \cdot q_{[4]}) \right. \right. \\ \left. \left. + 2M^2s k_{[4]}^2 \right) - 2 \int [dk] \frac{\mu^2}{k_{[d]}^2 \mathcal{D}_2 \mathcal{D}_3} s(3M^2 - 2s) \right]. \end{aligned} \quad (3.52)$$

Obtaining a result such as this was the original goal of FDF. All momenta are strictly four-dimensional, allowing to use (numerical) unitarity. We, however, are not interested in unitarity, instead wanting to use standard tools to calculate these integrals. For this we need to be able to cancel the $k_{[4]}^2$ -terms against denominators containing $k_{[d]}^2$. Hence, we reverse (3.51b), properly implementing (3.40)

After completing the algebra, use

$$\int [dk] \frac{k_{[4]}^2}{k_{[d]}^2 \mathcal{D}_2 \cdots \mathcal{D}_n} = \int [dk] \frac{1}{\mathcal{D}_2 \cdots \mathcal{D}_n} + \int [dk] \frac{\mu^2}{k_{[d]}^2 \mathcal{D}_2 \cdots \mathcal{D}_n}. \quad (\text{Rule III})$$

Now only terms of the form $k_{[4]} \cdot p_{[4]}$ remain in the numerators. These terms map directly to $k_{[d]} \cdot p_{[4]}$ because external momenta have no contribution in $\text{QS}_{[-2\epsilon]}$. Hence, we can now safely set $k_{[4]} \rightarrow k_{[d]}$ and solve the μ^2 -independent integrals using standard one-loop calculus as implemented in Package-X. For the μ -integrals, one can show that [106]

$$\int [d^d k] \frac{(\mu^2)^r}{\mathcal{D}_1 \cdots \mathcal{D}_n} = -\epsilon(4\pi)^r \frac{\Gamma(r - \epsilon)}{\Gamma(1 - \epsilon)} \int [d^{d+2r}] \frac{1}{\mathcal{D}_1 \cdots \mathcal{D}_n}. \quad (\text{Rule IV})$$

As these dimensionally shifted integrals are at most UV-divergent, we only ever need their UV pole which is generally very simple to obtain. In our case,

$$\mathcal{M}_{\text{FDF}}^{(1)} \Big|_{\mu\text{-integral}} = -\frac{16G_F^2}{3} M^4 (x - 1) x \epsilon \times \left(-\frac{1}{2\epsilon} + \mathcal{O}(\epsilon^0) \right). \quad (3.53)$$

Thus, we have reproduced the bare FDH result (3.45a) with techniques more amenable for automated calculations without introducing unnecessary terms such as in CDR. Unfortunately, the FDF scheme has only been shown to work at one-loop. Worse yet, the simplest extension to the two-loop level is known to be incorrect.

γ^5 in FDF

We have avoided the γ^5 problem by using the $\psi_e \rightarrow \gamma^5 \psi_e$ symmetry. However, a side effect of Rule I is that FDF comes with a hard-coded γ^5 scheme [90]. Because all objects except μ are in $S_{[4]}$, our γ^5 is anti-commuting in practice. However, due to the implementation of the $\text{QS}_{[-2\epsilon]}$

terms as $\sim \gamma^5 \mu$, these terms effectively commute with γ^5 . This means that we have implemented the BM scheme. Hence, FDF requires the additional Z_5 renormalisation.

In practice the Born matrix element is

$$\mathcal{M}_{\text{FDF}}^{(0)} = \frac{4G_F^2}{2} \text{tr} \left[(\not{p}_{[4]} + M) P_L \gamma_{[4]}^\mu \not{q}_{[4]} P_L \gamma_{[4]}^\nu \right] \times \mathcal{N}_{[4]}^{\mu\nu}, \quad (3.54)$$

where we set

$$P_L = \frac{1}{2}(1 - Z_5 \gamma^5), \quad (3.55)$$

with Z_5 as in (3.15).

3.4 Regularisation-scheme dependence and IR prediction

As mentioned in the prologue to this chapter, we ideally want to compute every part of the calculation in the best suited scheme. For this it is important to understand how to convert from one scheme to another.

For this we distinguish two different types of scheme dependence: a trivial scheme dependence that is due to the dimensionality of the Born matrix element and non-trivial scheme dependence. The trivial scheme dependence is best described between CDR and HV. As suggested in (3.41) this is just

$$\mathcal{M}_{\text{CDR}}^{(\ell)} = \frac{\mathcal{M}_{\text{CDR}}^{(0)}}{\mathcal{M}_{\text{HV}}^{(0)}} \mathcal{M}_{\text{HV}}^{(\ell)}. \quad (3.56)$$

The scheme dependence between HV and FDH is more interesting. It is encapsulated by divergent diagrams involving ϵ -scalars. At one-loop we have

$$\mathcal{M}_{\text{FDH}}^{(1)} - \mathcal{M}_{\text{HV}}^{(1)} = 2\epsilon \times \mathcal{M}_{\text{FDH}}^{(1)} \Big|_{n_\epsilon \text{ coefficient}} = \Delta_{\text{RS}}. \quad (3.57)$$

In our case, $\Delta_{\text{RS}} = M^4 x(3 - 2x)/6 + \mathcal{O}(\epsilon)$. Had we assumed a finite electron mass instead, we would have found $\Delta_{\text{RS}}^{m_e > 0} \propto \epsilon$ and hence no non-trivial scheme dependence. At NLO, scheme dependence is induced by collinear singularities [107] of which there are none for finite electron masses. Beyond NLO, also soft singularities contribute to the scheme dependence, i.e. even in the case of non-vanishing electron mass there is a non-trivial scheme dependence.

To formalise the scheme dependence, we need to extend our discussion of IR predictions from Section 2.4 to FDH in QCD. The relevant results are given in Appendix B. We begin by noting that the *light-quark*⁸ anomalous dimension γ_i has terms proportional to n_ϵ

$$\gamma_i = \left(\frac{\alpha}{4\pi} \right) (-3C_F) + \left(\frac{\alpha_\epsilon}{4\pi} \right) n_\epsilon \frac{C_F}{2} + \mathcal{O}(\alpha_i^2). \quad (3.58)$$

The *heavy-quark* anomalous dimension γ_I on the other hand has no scheme dependence

$$\gamma_I = \left(\frac{\alpha}{4\pi} \right) (-2C_F), \quad (3.59)$$

⁸The terms light and heavy quark are universally used to describe massless and massive quark, respectively.

meaning that non-trivial scheme dependence is due collinear singularities at one-loop. The cusp-anomalous dimension

$$\gamma_{\text{cusp}} = \left(\frac{\alpha}{4\pi}\right)(4) \quad (3.60)$$

also has no scheme dependence at one-loop but develops a term $\propto \alpha^2 C_A n_\epsilon$ at two-loop. Up to at least two-loop, γ_{cusp} has *Casimir scaling*, i.e. $\gamma_{\text{cusp}}^g/C_F = \gamma_{\text{cusp}}^g/C_A = \gamma_{\text{cusp}}$.

A further source of scheme dependence in \mathbf{Z} is that we now have to include terms induced by the ϵ -scalar coupling (cf. Appendix B.2). This makes $\log \mathbf{Z}_{\text{RS}}$ regularisation scheme dependent as indicated by the subscript RS. Note that, because \mathbf{Z}_{RS} matches the IR poles exactly, the $\overline{\text{MS}}$ -like subtracted matrix element $\mathcal{M}_{\text{sub}}(\mu)$ is regularisation scheme independent in the limit $n_\epsilon \rightarrow 2\epsilon$ and $\epsilon \rightarrow 0$. This allows us to predict the regularisation scheme dependence of any matrix element by predicting the scheme dependence $\log \mathbf{Z}_{\text{RS}}$ using the IR prediction discussed in Section 2.4.

To illustrate this method, let us predict the IR pole of $\mathcal{M}_{\text{RS}}^{(0)}$. For this, we first need to write down $\mathbf{\Gamma}$ as

$$\begin{aligned} \mathbf{\Gamma}_1(\mu) &= \gamma_i + \gamma_I - \gamma_{\text{cusp}} \log \frac{M\mu}{2p \cdot q} \\ &= -\frac{5\alpha}{4\pi} + \frac{\alpha_e}{8\pi} n_\epsilon - \frac{\alpha}{\pi} \log \frac{\mu}{Mx}. \end{aligned} \quad (3.61)$$

We now can construct $\log \mathbf{Z}_{\text{RS}}$ as in (B.10)

$$\begin{aligned} \log \mathbf{Z}_{\text{RS}} &= \frac{\mathbf{\Gamma}'_1}{2\epsilon^2} + \frac{\mathbf{\Gamma}_1}{\epsilon} + \mathcal{O}(\alpha_i^2) \\ &= \frac{\alpha}{\pi} \left(-\frac{1}{2\epsilon^2} - \frac{1}{\epsilon} \left[\frac{5}{4} + 2 \log \frac{\mu^2}{M^2} - \log x \right] \right) + \frac{\alpha_e}{\pi} n_\epsilon \left(\frac{1}{8\epsilon} \right) + \mathcal{O}(\alpha_i^2), \end{aligned} \quad (3.62)$$

where we have used that $\mathbf{\Gamma}'_1 = \partial_{\log \mu} \mathbf{\Gamma} = \gamma_{\text{cusp}}$. By exponentiating $\log \mathbf{Z}_{\text{RS}}$ we can obtain $\mathbf{Z}_{\text{RS}}^{-1}$ as required by (2.29)

$$\mathbf{Z}_{\text{RS}}^{-1} = 1 + \frac{\alpha}{\pi} \left(-\frac{1}{2\epsilon^2} - \frac{1}{\epsilon} \left[\frac{5}{4} + 2 \log \frac{\mu^2}{M^2} - \log x \right] \right) + \frac{\alpha_e}{\pi} n_\epsilon \left(\frac{1}{8\epsilon} \right) + \mathcal{O}(\alpha_i^2). \quad (3.63)$$

This, once multiplied with $\mathcal{M}_{\text{RS}}^{(0)} + \mathcal{M}_{\text{RS}}^{(1)}$, produces a finite, scheme independent result in the limit $d_s \rightarrow 4 - 2\epsilon$, $n_\epsilon \rightarrow 2\epsilon$, $\alpha_e \rightarrow \alpha$, and finally $\epsilon \rightarrow 0$

$$\begin{aligned} \mathbf{Z}_{\text{RS}}^{-1} \left(\mathcal{M}_{\text{RS}}^{(0)} + \mathcal{M}_{\text{RS}}^{(1)} \right) &= \mathcal{M}_{\text{RS}}^{(0)} \left(1 + \frac{\alpha}{\pi} \left[\left\{ 3 \frac{x-1}{2x-3} + L \right\} - \frac{5}{4}L - \frac{1}{4}L^2 - 3 \right. \right. \\ &\quad \left. \left. - \frac{3}{2}\zeta_2 - 2H_{0,0}(x) - H_{1,0}(x) \right] + \mathcal{O}(\alpha^2) \right), \end{aligned} \quad (3.64)$$

with $L = \log(\mu^2/M^2)$ for all schemes $\text{RS} \in \{\text{CDR}, \text{HV}, \text{FDH}\}$.

After calculating $\mathbf{Z}_{\text{RS}}^{-1} \left(\mathcal{M}_{\text{RS}}^{(0)} + \mathcal{M}_{\text{RS}}^{(1)} \right)$ in any scheme RS we can obtain $\mathcal{M}_{\text{RS}'}^{(1)}$ in any other scheme RS' by multiplying with the corresponding $\mathbf{Z}_{\text{RS}'}$. This is a very powerful statement, allowing us to perform any part of any one- and two-loop calculation in any scheme we wish and convert to any other scheme. In calculations for the LHC this is particularly important because the parton distribution functions (PDFs) are usually only available in CDR.

Chapter 4

The FKS² scheme

As already discussed in Section 2.3, cross sections beyond LO are constructed of several IR divergent parts. In this chapter, we will focus on the IR divergences arising during the phase-space integration of real corrections. As already mentioned, we would like to do this integration numerically. However, we cannot do this in d dimensions. A common way to circumvent this problem is called a *subtraction scheme*. The basic idea is to write the divergent integrand over the extra emission as

$$\int_{n+1} d\sigma_{n+1} = \int_{n+1} (d\sigma_{n+1} - d\text{CT}) + \int_n \int_1 d\text{CT}, \quad (4.1)$$

where the subscript refers to the number of particles integrated over. $d\text{CT}$ is constructed to ensure that the first integral is finite while being easy enough so that the integral over the one-particle phase space can be done analytically in d dimensions.

In the case of massive QED the only IR singularity is due to soft photon emission; collinear divergences are regulated by the presence of fermion masses. Hence, $d\text{CT}$ can be quite simple as we will see below.

In this chapter we will review one of the central pieces of this project, the FKS² subtraction scheme (Section 4.2), as well as its predecessor, the FKS scheme (Section 4.1). Next, we will comment on the possibility of extending the scheme beyond NNLO in Section 4.3. Finally, we will comment on properties of FKS² in Section 4.4.

4.1 FKS for soft singularities at NLO

In this section we will briefly summarise the necessary aspects of the FKS scheme at NLO. Because we only treat soft singularities, FKS is dramatically simplified. The NLO correction to a cross section is split into virtual and real parts

$$\sigma^{(1)} = \int (d\sigma_v^{(1)} + d\sigma_r^{(1)}) = \int d\Phi_n \mathcal{M}_n^{(1)} + \int d\Phi_{n+1} \mathcal{M}_{n+1}^{(0)}. \quad (4.2)$$

In (4.2) we implicitly assume the presence of the flux factor (or the analogous factor for a decay rate) as well as a measurement function that defines the observable in terms of the particle

momenta. The measurement function has to respect infrared safety, i.e. the observable it defines must not depend on whether or not one or more additional soft photons are present as arguments of this function.

The real corrections

$$d\sigma_r^{(1)} = d\Phi_{n+1} \mathcal{M}_{n+1}^{(0)} \quad (4.3)$$

are obtained by integrating the tree-level matrix element $\mathcal{M}_{n+1}^{(0)}$ over the phase space $d\Phi_{n+1}$. To simplify the discussion we assume that in the tree-level process described by $\mathcal{M}_n^{(0)}$ no final-state photons are present. Hence, in $\mathcal{M}_{n+1}^{(0)}$ only the particle (photon) with label $n+1$ can potentially become soft. If there are additional photons (i.e. photons in the LO process) the measurement function and combinatorics become slightly more involved, but the essential part of the discussion is not affected.

When computing a cross section in the centre-of-mass frame, we choose coordinates where the beam axis is in z direction. Further, we denote the (partonic) centre-of-mass energy by \sqrt{s} . When computing a decay width we instead parametrise one of the outgoing particles in z direction and, if necessary, rotate the coordinate system afterwards.

Following [108] we parametrise the momentum of the additionally radiated particle $n+1$ as⁹

$$k_1 = p_{n+1} = \frac{\sqrt{s}}{2} \xi_1 (1, \sqrt{1-y_1^2} \vec{e}_\perp, y_1), \quad (4.4)$$

where \vec{e}_\perp is a $(d-2)$ dimensional unit vector and the ranges of y_1 (the cosine of the angle) and ξ_1 (the scaled energy) are $-1 \leq y_1 \leq 1$ and $0 \leq \xi_1 \leq \xi_{\max}$, respectively. The upper bound ξ_{\max} depends on the masses of the outgoing particles. Following [109] we find

$$\xi_{\max} = 1 - \frac{(\sum_i m_i)^2}{s}. \quad (4.5)$$

Further kinematic constraints are assumed to be implemented through the measurement function. We write the single-particle phase-space measure for particle $n+1$ as

$$d\phi_1 \equiv \mu^{4-d} \frac{d^{d-1} k_1}{(2\pi)^{d-1} 2k_1^0} = \frac{\mu^{2\epsilon}}{2(2\pi)^{d-1}} \left(\frac{\sqrt{s}}{2} \right)^{d-2} \xi_1^{1-2\epsilon} (1-y_1^2)^{-\epsilon} d\xi_1 dy_1 d\Omega_1^{(d-2)} = d\Upsilon_1 d\xi_1 \xi_1^{1-2\epsilon}, \quad (4.6)$$

where the angular integrations and other trivial factors are collected in $d\Upsilon_1$. Denoting by $d\Phi_{n,1}$ the remainder of the $(n+1)$ -parton phase space, i.e. $d\Phi_{n+1} = d\Phi_{n,1} d\phi_1$, we write the real part of the NLO differential cross section as

$$d\sigma_r^{(1)} = d\Phi_{n,1} d\phi_1 \mathcal{M}_{n+1}^{(0)} = d\Upsilon_1 d\Phi_{n,1} d\xi_1 \xi_1^2 \mathcal{M}_{n+1}^{(0)} \xi_1^{-1-2\epsilon}. \quad (4.7)$$

To isolate the soft singularities in the phase-space integration we use the identity

$$\xi^{-1-2\epsilon} = -\frac{\xi_c^{-2\epsilon}}{2\epsilon} \delta(\xi) + \left(\frac{1}{\xi^{1+2\epsilon}} \right)_c, \quad (4.8)$$

$$\left\langle \left(\frac{1}{\xi^n} \right)_c, f \right\rangle = \int_0^1 d\xi \frac{f(\xi) - f(0)\theta(\xi_c - \xi)}{\xi^n},$$

⁹Note that this parametrisation could also tackle initial-state collinear singularities because y_1 corresponds to the angle between the photon and the incoming particles. However, a different parametrisation may be sensible (and is allowed here) to better account for PCS from light particles (cf. Section 4.4.3 and Section 6.4.1). What is important in the following is that the scaled energy ξ_1 is chosen as a variable in the parametrisation to ensure a consistent implementation of the distributions defined in (4.8).

to expand $\xi_1^{-1-2\epsilon}$ in terms of a *c-distribution*. Here we have introduced an unphysical free parameter ξ_c that can be chosen arbitrarily [108, 109] as long as

$$0 < \xi_c \leq \xi_{\max}. \quad (4.9)$$

The dependence of ξ_c has to drop out exactly since no approximation was made. Therefore, any fixed value could be chosen. However, keeping it variable is useful to test the implementation of the scheme.

Using (4.8) we split the real cross section into a hard and a soft part¹⁰

$$d\sigma_r^{(1)} = d\sigma_s^{(1)}(\xi_c) + d\sigma_h^{(1)}(\xi_c), \quad (4.10a)$$

$$d\sigma_s^{(1)}(\xi_c) = -d\Upsilon_1 d\Phi_{n,1} \frac{\xi_c^{-2\epsilon}}{2\epsilon} \delta(\xi_1) d\xi_1 \left(\xi_1^2 \mathcal{M}_{n+1}^{(0)} \right), \quad (4.10b)$$

$$d\sigma_h^{(1)}(\xi_c) = +d\Upsilon_1 d\Phi_{n,1} \left(\frac{1}{\xi_1^{1+2\epsilon}} \right)_c d\xi_1 \left(\xi_1^2 \mathcal{M}_{n+1}^{(0)} \right). \quad (4.10c)$$

In $d\sigma_s^{(1)}$ we can now (trivially) perform the ξ_1 integration. To do this systematically, we define for photons the general soft limit \mathcal{S}_i of the i -th particle

$$\mathcal{S}_i \mathcal{M}_m^{(0)} \equiv \lim_{\xi_i \rightarrow 0} \xi_i^2 \mathcal{M}_m^{(0)} = \mathcal{E}_i \mathcal{M}_{m-1}^{(0)} \quad \text{with} \quad \xi_i = \frac{2E_i}{\sqrt{s}}, \quad (4.11)$$

where $\mathcal{M}_{m-1}^{(0)}$ is the matrix element for the process without particle i . The *eikonal factor*

$$\mathcal{E}_i \equiv 4\pi\alpha \sum_{j,k} \frac{p_j \cdot p_k}{p_j \cdot n_i p_k \cdot n_i} \text{sign}_{jk} \quad \text{with} \quad p_i = \xi_i n_i, \quad (4.12)$$

is assembled from self- and mixed-eikonals. $\text{sign}_{jk} = (-1)^{n_{jk}+1}$ as in Section 2.4, where n_{jk} is the number of incoming particles or outgoing antiparticles among the particles j and l . Further, we define the *integrated eikonal*

$$\hat{\mathcal{E}}(\xi_c) \equiv -\frac{\xi_c^{-2\epsilon}}{2\epsilon} \int d\Upsilon_i \mathcal{E}_i = \xi_c^{-2\epsilon} \hat{\mathcal{E}}(1) = \sum_{j,k} \hat{\mathcal{E}}_{jk}(\xi_c). \quad (4.13)$$

$\hat{\mathcal{E}}$ has been computed for example in [108, 109] and can be found in Appendix C. This definition of $\hat{\mathcal{E}}$ completes the definition of the YFS split (2.40) with $\alpha S = \hat{\mathcal{E}}$. After $d\Upsilon_1$ and $d\xi_1$ integration (under which $d\Phi_{n,1} \rightarrow d\Phi_n$) we obtain

$$d\sigma_s^{(1)}(\xi_c) \xrightarrow{\int d\Upsilon_1 d\xi_1} d\Phi_n \hat{\mathcal{E}}(\xi_c) \mathcal{M}_n^{(0)}. \quad (4.14)$$

This part now contains explicit $1/\epsilon$ poles that cancel against poles in the virtual cross section. The second term of the real corrections, $d\sigma_h^{(1)}$ given in (4.10c), is finite and can be integrated numerically after setting $d=4$. Combining the real and virtual corrections, the NLO correction is given by

$$\sigma^{(1)} = \sigma_n^{(1)}(\xi_c) + \sigma_{n+1}^{(1)}(\xi_c), \quad (4.15a)$$

$$\sigma_n^{(1)}(\xi_c) = \int d\Phi_n^{d=4} \left(\mathcal{M}_n^{(1)} + \hat{\mathcal{E}}(\xi_c) \mathcal{M}_n^{(0)} \right) = \int d\Phi_n^{d=4} \mathcal{M}_n^{(1)f}, \quad (4.15b)$$

$$\sigma_{n+1}^{(1)}(\xi_c) = \int d\Phi_{n+1}^{d=4} \left(\frac{1}{\xi_1} \right)_c (\xi_1 \mathcal{M}_{n+1}^{(0)f}). \quad (4.15c)$$

¹⁰In [108] the second term is called $d\sigma^{(ns)}$ for ‘non-soft’. We will label it h (for ‘hard’) instead to avoid confusion when we need more than one such label later.

We have defined $\mathcal{M}_{n+1}^{(0)f} = \mathcal{M}_{n+1}^{(0)}$ and absorbed one of the ξ_1 factors multiplying $\mathcal{M}_{n+1}^{(0)}$ in (4.10c) in the phase space $d\Phi_{n+1}^{d=4}$. Contrary to (4.2), there are no soft singularities present in (4.15). According to (2.40) the explicit $1/\epsilon$ poles cancel between the two terms in the integrand of (4.15b) and the phase-space integration in (4.15c) is also manifestly finite.

In (4.15) we see first terms of the build-up of the YFS split (2.40)

$$e^{\alpha\hat{\mathcal{E}}} \sum_{\ell=0}^{\infty} \mathcal{M}_n^{(\ell)} = \sum_{\ell=0}^{\infty} \mathcal{M}_n^{(\ell)f} = \mathcal{M}_n^{(1)} + \hat{\mathcal{E}}(\xi_c) \mathcal{M}_n^{(0)} + \mathcal{O}(\alpha^2). \quad (4.16)$$

Finally, we note that \mathcal{S}_i is invariant under rotations, but not Lorentz invariant, because it contains the explicit energy E_i . Hence, also \mathcal{E}_i and $\hat{\mathcal{E}}$ are only invariant under rotations but not under general Lorentz transformations. The integrated eikonal $\hat{\mathcal{E}}_{jk}$ has been computed in [109], dropping terms of $\mathcal{O}(\epsilon)$. As we will see this is sufficient even beyond NLO. The expression is given in Appendix C, using our conventions.

4.2 FKS²: NNLO extension

In the following, we discuss the extension of FKS to NNLO, while still limiting ourselves to massive QED. To simplify the discussion in this section, we assume that all (suitably renormalised) matrix elements are known to sufficient order in the coupling and expansion in ϵ . In Section 4.4.1 we will state what precisely is needed for a NNLO computation.

We write the NNLO cross section $\sigma^{(2)}$ as

$$\sigma^{(2)} = \int \left(d\sigma_{vv}^{(2)} + d\sigma_{rv}^{(2)} + d\sigma_{rr}^{(2)} \right) = \int d\Phi_n \mathcal{M}_n^{(2)} + \int d\Phi_{n+1} \mathcal{M}_{n+1}^{(1)} + \int d\Phi_{n+2} \mathcal{M}_{n+2}^{(0)}. \quad (4.17)$$

The double-virtual corrections are obtained by integrating $\mathcal{M}_n^{(2)}$ over the Born phase space $d\Phi_n$. Here $\mathcal{M}_n^{(2)}$ contains all terms of the n -particle (renormalised) matrix element with two additional powers of the coupling α . This includes the interference term of the two-loop amplitude with the tree-level amplitude as well as the one-loop amplitude squared. Similarly, the real-virtual contribution is obtained by integration of $\mathcal{M}_{n+1}^{(1)}$, the interference of the (renormalised) $(n+1)$ -particle one-loop amplitude with the corresponding tree-level amplitude, over the $(n+1)$ -particle phase space $d\Phi_{n+1}$. Finally, for the double-real contribution the tree-level matrix element with two additional particles, $\mathcal{M}_{n+2}^{(0)}$, is integrated over the corresponding phase space.

4.2.1 Real-virtual correction

The treatment of the real-virtual contribution

$$d\sigma_{rv}^{(2)} = d\Phi_{n+1} \mathcal{M}_{n+1}^{(1)} \quad (4.18)$$

proceeds along the lines of normal FKS because it is a $(n+1)$ -particle contribution. Again we assume that there is only one external particle, with label $n+1$, that can potentially become soft. We use (4.8) with another unphysical cut-parameter ξ_{c_A} to split the real-virtual cross section into a soft and a hard part

$$d\sigma_{rv}^{(2)} = d\sigma_s^{(2)}(\xi_{c_A}) + d\sigma_h^{(2)}(\xi_{c_A}). \quad (4.19)$$

For $d\sigma_s^{(2)}$ the analogy to the NLO case is particularly strong because there is no genuine one-loop eikonal contribution [110, 111], i.e. the soft limit of the real-virtual matrix element is

$$\mathcal{S}_{n+1}\mathcal{M}_{n+1}^{(1)} = \mathcal{E}_{n+1}\mathcal{M}_n^{(1)}, \quad (4.20)$$

with the same \mathcal{E}_{n+1} as in (4.12). Therefore, compared to (4.14) the definition of the soft part remains essentially unchanged

$$d\sigma_s^{(2)}(\xi_{c_A}) \xrightarrow{\int d\Upsilon_1 d\xi_1} d\Phi_n \hat{\mathcal{E}}(\xi_{c_A}) \mathcal{M}_n^{(1)}. \quad (4.21)$$

However, $d\sigma_s^{(2)}$ has a double-soft $1/\epsilon^2$ pole from the overlap of the soft $1/\epsilon$ poles of $\hat{\mathcal{E}}$ and $\mathcal{M}_n^{(1)}$.

Unfortunately, $d\sigma_h^{(2)}$ is not yet finite as it contains an explicit $1/\epsilon$ pole from the loop integration. With the $\overline{\text{MS}}$ -like IR subtraction of Section 2.4, we already found one way to remove this pole by defining $\mathbf{Z} = 1 + \alpha\delta\mathbf{Z}$ s.t.

$$\mathcal{M}_{\text{sub}}(\mu) = \mathcal{M}_{n+1}^{(1)} - \delta\mathbf{Z}(\mu)\mathcal{M}_{n+1}^{(0)} \quad (4.22)$$

is finite. This is (2.29) expanded in α and applied to our discussion. However, it turns out that a different subtraction, called *eikonal subtraction*, is more advantageous. We split the real-virtual matrix element according to

$$\mathcal{M}_{n+1}^{(1)f} = \mathcal{M}_{n+1}^{(1)}(\xi_{c_B}) + \hat{\mathcal{E}}(\xi_{c_B})\mathcal{M}_{n+1}^{(0)} \quad (4.23)$$

into a finite and a divergent piece. The pole of $\mathcal{M}_{n+1}^{(1)}$ is now contained in the integrated eikonal of $\hat{\mathcal{E}}(\xi_{c_B})\mathcal{M}_{n+1}^{(0)}$, whereas the eikonal-subtracted matrix element $\mathcal{M}_{n+1}^{(1)f}$ is free from poles. This is again the YFS split, mentioned in (2.40) and (4.16). In (4.23) we have introduced yet another initially independent cut-parameter ξ_{c_B} .

With the help of (4.23) we can now write

$$\begin{aligned} d\sigma_h^{(2)}(\xi_{c_A}) &= d\Upsilon_1 d\Phi_{n,1} d\xi_1 \left(\frac{1}{\xi_1^{1+2\epsilon}} \right)_{c_A} (\xi_1^2 \mathcal{M}_{n+1}^{(1)}) \\ &= d\sigma_f^{(2)}(\xi_{c_A}, \xi_{c_B}) + d\sigma_d^{(2)}(\xi_{c_A}, \xi_{c_B}), \end{aligned} \quad (4.24a)$$

where c_A indicates that the subtraction should be performed with the cut parameter ξ_{c_A} . The finite piece

$$d\sigma_f^{(2)}(\xi_{c_A}, \xi_{c_B}) = d\Upsilon_1 d\Phi_{n,1} d\xi_1 \left(\frac{1}{\xi_1^{1+2\epsilon}} \right)_{c_A} (\xi_1^2 \mathcal{M}_{n+1}^{(1)f}(\xi_{c_B})) \quad (4.24b)$$

can be integrated numerically with $\epsilon = 0$. Integrating the divergent piece, $d\sigma_d^{(2)}$, over the complete phase space we obtain

$$\int d\sigma_d^{(2)}(\xi_{c_A}, \xi_{c_B}) = - \int d\Upsilon_1 d\Phi_{n,1} d\xi_1 \left(\frac{1}{\xi_1^{1+2\epsilon}} \right)_{c_A} (\hat{\mathcal{E}}(\xi_{c_B}) \xi_1^2 \mathcal{M}_{n+1}^{(0)}) \equiv -\mathcal{I}(\xi_{c_A}, \xi_{c_B}), \quad (4.24c)$$

where in \mathcal{I} the first argument refers to the cut-parameter of the ξ integration and the second to the argument of $\hat{\mathcal{E}}$. This process- and observable-dependent function is not finite and generally very tedious to compute. Even for the simplest cases such as the muon decay it gives rise to

complicated analytic expressions including for example Appell's F_i functions. However, as we will see it is possible to cancel its contribution exactly with the double-real emission.

To summarise, the real-virtual corrections are given by

$$d\sigma_{rv}^{(2)} = d\sigma_s^{(2)}(\xi_{c_A}) + d\sigma_f^{(2)}(\xi_{c_A}, \xi_{c_B}) + d\sigma_d^{(2)}(\xi_{c_A}, \xi_{c_B}), \quad (4.25)$$

where the expressions for $d\sigma_s^{(2)}$, $d\sigma_f^{(2)}$, and $d\sigma_d^{(2)}$ can be read off from (4.21), (4.24b), and (4.24c), respectively. We point out that $d\sigma_{rv}^{(2)}$ is independent of both ξ_{c_A} and ξ_{c_B} .

4.2.2 Double-real correction

For the double-real contribution

$$d\sigma_{rr}^{(2)} = d\Phi_{n+2} \mathcal{M}_{n+2}^{(0)} \quad (4.26)$$

we have to consider $\mathcal{M}_{n+2}^{(0)}$, the matrix element for the process with two additional photons (with labels $n+1$ and $n+2$) w.r.t. the tree-level process. We extend the parametrisation (4.4) accordingly to

$$k_1 = p_{n+1} = \frac{\sqrt{s}}{2} \xi_1 (1, \sqrt{1-y_1^2} \vec{e}_\perp, y_1), \quad k_2 = p_{n+2} = \frac{\sqrt{s}}{2} \xi_2 R_\phi (1, \sqrt{1-y_2^2} \vec{e}_\perp, y_2), \quad (4.27)$$

with $-1 \leq y_i \leq 1$, $0 \leq \xi_i \leq \xi_{\max}$ and a $(d-2)$ -dimensional rotation matrix R_ϕ . Writing the phase space as $d\Phi_{n+2} = d\Phi_{n,2} d\phi_1 d\phi_2$, the double-real contribution becomes

$$\begin{aligned} d\sigma_{rr}^{(2)} &= d\Phi_{n,2} d\phi_1 d\phi_2 \frac{1}{2!} \mathcal{M}_{n+2}^{(0)} \\ &= d\Upsilon_1 d\Upsilon_2 d\Phi_{n,2} d\xi_1 d\xi_2 \frac{1}{2!} (\xi_1^2 \xi_2^2 \mathcal{M}_{n+2}^{(0)}) \xi_1^{-1-2\epsilon} \xi_2^{-1-2\epsilon}, \end{aligned} \quad (4.28)$$

where we have used analogous definitions as in (4.6) and (4.7). The only difference between $d\Phi_{n,1}$ and $d\Phi_{n,2}$ is in the argument of the δ function that ensures momentum conservation. Note that the factor $1/2!$ is the symmetry factor due to two identical particles.

Again, we use (4.8) with two new cut parameters ξ_{c_1} and ξ_{c_2} to expand $d\sigma_{rr}^{(2)}$ in terms of distributions as

$$d\sigma_{rr}^{(2)} = d\sigma_{ss}^{(2)}(\xi_{c_1}, \xi_{c_2}) + d\sigma_{sh}^{(2)}(\xi_{c_1}, \xi_{c_2}) + d\sigma_{hs}^{(2)}(\xi_{c_1}, \xi_{c_2}) + d\sigma_{hh}^{(2)}(\xi_{c_1}, \xi_{c_2}), \quad (4.29)$$

$$\left\{ \begin{array}{l} d\sigma_{ss}^{(2)}(\xi_{c_1}, \xi_{c_2}) \\ d\sigma_{hs}^{(2)}(\xi_{c_1}, \xi_{c_2}) \\ d\sigma_{sh}^{(2)}(\xi_{c_1}, \xi_{c_2}) \\ d\sigma_{hh}^{(2)}(\xi_{c_1}, \xi_{c_2}) \end{array} \right\} = d\Upsilon_1 d\Upsilon_2 d\Phi_{n,2} \frac{1}{2!} \left\{ \begin{array}{l} \frac{\xi_{c_1}^{-2\epsilon}}{2\epsilon} \delta(\xi_1) \frac{\xi_{c_2}^{-2\epsilon}}{2\epsilon} \delta(\xi_2) \\ -\frac{\xi_{c_2}^{-2\epsilon}}{2\epsilon} \delta(\xi_2) \left(\frac{1}{\xi_1^{1+2\epsilon}} \right)_{c_1} \\ -\frac{\xi_{c_1}^{-2\epsilon}}{2\epsilon} \delta(\xi_1) \left(\frac{1}{\xi_2^{1+2\epsilon}} \right)_{c_2} \\ \left(\frac{1}{\xi_1^{1+2\epsilon}} \right)_{c_1} \left(\frac{1}{\xi_2^{1+2\epsilon}} \right)_{c_2} \end{array} \right\} d\xi_1 d\xi_2 \xi_1^2 \xi_2^2 \mathcal{M}_{n+2}^{(0)}.$$

We note that for $\xi_{c_1} = \xi_{c_2} \equiv \xi_c$ we have $\int d\sigma_{sh}^{(2)}(\xi_c, \xi_c) = \int d\sigma_{hs}^{(2)}(\xi_c, \xi_c)$.

The contribution from $d\sigma_{hh}^{(2)}$ can be integrated numerically with $\epsilon = 0$ because it is finite everywhere.

For the mixed contributions $d\sigma_{hs}^{(2)}$ and $d\sigma_{sh}^{(2)}$ we use

$$\mathcal{S}_i \mathcal{M}_{n+2}^{(0)} = \mathcal{E}_i \mathcal{M}_{n+1}^{(0)} \quad \text{with} \quad i \in \{n+1, n+2\}. \quad (4.30)$$

Considering first $d\sigma_{hs}^{(2)}$, we perform the ξ_2 integration (under which $d\Phi_{n,2} \rightarrow d\Phi_{n,1}$) and use (4.13) to do the $d\Upsilon_2$ integration to obtain

$$\int d\sigma_{hs}^{(2)}(\xi_{c_1}, \xi_{c_2}) = \int d\Upsilon_1 d\Phi_{n,1} \frac{1}{2!} \int d\xi_1 \left(\frac{1}{\xi_1^{1+2\epsilon}} \right)_{c_1} (\xi_1^2 \mathcal{M}_{n+1}^{(0)}) \hat{\mathcal{E}}(\xi_{c_2}) = \frac{1}{2!} \mathcal{I}(\xi_{c_1}, \xi_{c_2}). \quad (4.31a)$$

Similarly, we get

$$\int d\sigma_{sh}^{(2)}(\xi_{c_1}, \xi_{c_2}) = \frac{1}{2!} \mathcal{I}(\xi_{c_2}, \xi_{c_1}). \quad (4.31b)$$

Thus, we find again the integral \mathcal{I} of (4.24c).

Finally, we turn to the double-soft contribution $d\sigma_{ss}^{(2)}$. Since

$$(\mathcal{S}_i \circ \mathcal{S}_j) \mathcal{M}_{n+2}^{(0)} = (\mathcal{S}_j \circ \mathcal{S}_i) \mathcal{M}_{n+2}^{(0)} = \mathcal{E}_i \mathcal{E}_j \mathcal{M}_n^{(0)} \quad \text{with} \quad i \neq j \in \{n+1, n+2\}, \quad (4.32)$$

the ξ integrals in $d\sigma_{ss}^{(2)}$ factorise. Therefore, we can do the $d\xi_1 d\Upsilon_1$ integrations independently from the $d\xi_2 d\Upsilon_2$ integrations and obtain

$$d\sigma_{ss}^{(2)}(\xi_{c_1}, \xi_{c_2}) \xrightarrow{\int d\Upsilon_{1,2} d\xi_{1,2}} d\Phi_n \frac{1}{2!} \hat{\mathcal{E}}(\xi_{c_1}) \hat{\mathcal{E}}(\xi_{c_2}) \mathcal{M}_n^{(0)}. \quad (4.33)$$

It is clear that the simplicity of the infrared structure of QED with massive fermions is crucial for reducing the complexity of the procedure described in the steps above.

4.2.3 Combination

At this stage we have introduced four different cutting parameters ξ_{c_A} and ξ_{c_B} as well as ξ_{c_1} and ξ_{c_2} . All of these are unphysical, arbitrary parameters that can take any value $0 < \xi_{c_i} \leq \xi_{\max}$. In total we have to deal with seven different contributions. Two of them, $d\sigma_s^{(2)}$ and $d\sigma_{ss}^{(2)}$, are very simple as they just depend on the eikonal. Another two contributions $d\sigma_f^{(2)}$ and $d\sigma_{hh}^{(2)}$ can be calculated numerically with $\epsilon = 0$.

The sum of the three remaining *auxiliary contributions* $d\sigma_d^{(2)}$, $d\sigma_{sh}^{(2)}$, and $d\sigma_{hs}^{(2)}$, only depend on the function \mathcal{I} defined above

$$\begin{aligned} \int d\sigma_{aux}^{(2)}(\{\xi_{c_i}\}) &\equiv \int \left(d\sigma_d^{(2)}(\xi_{c_A}, \xi_{c_B}) + d\sigma_{hs}^{(2)}(\xi_{c_1}, \xi_{c_2}) + d\sigma_{sh}^{(2)}(\xi_{c_1}, \xi_{c_2}) \right) \\ &= -\mathcal{I}(\xi_{c_A}, \xi_{c_B}) + \frac{1}{2!} \mathcal{I}(\xi_{c_1}, \xi_{c_2}) + \frac{1}{2!} \mathcal{I}(\xi_{c_2}, \xi_{c_1}). \end{aligned} \quad (4.34)$$

Note that, due to the sign difference and the symmetry factor, $d\sigma_{aux}^{(2)}$ vanishes if we choose

$$\xi_c \equiv \xi_{c_A} = \xi_{c_B} = \xi_{c_1} = \xi_{c_2}. \quad (4.35)$$

This cancellation will not be affected by the measurement function. Thus, in what follows we will make the choice (4.35), avoiding the computation of the potentially difficult \mathcal{I} function.

It is possible to compute the auxiliary contribution $d\sigma_{aux}^{(2)}$ numerically keeping all ξ_{c_i} different by implementing the d -dimensional phase space mapping explicitly. While this complicates the implementation of the scheme it can be helpful to validate the code by confirming that physical quantities are in fact ξ_c independent. We have indeed done that by calculating $\mathcal{I}(\xi_{c_1}, \xi_{c_2})$ for the muon decay.

We can now collect the non-vanishing contributions, sorted by remaining integrations

$$\sigma^{(2)} = \sigma_n^{(2)}(\xi_c) + \sigma_{n+1}^{(2)}(\xi_c) + \sigma_{n+2}^{(2)}(\xi_c), \quad (4.36a)$$

$$\sigma_n^{(2)}(\xi_c) = \int \left(d\Phi_n \mathcal{M}_n^{(2)} + d\sigma_s^{(2)} + d\sigma_{ss}^{(2)} \right), \quad (4.36b)$$

$$\sigma_{n+1}^{(2)}(\xi_c) = \int d\sigma_f^{(2)} = \int d\Upsilon_1 d\Phi_{n,1} d\xi \left(\frac{1}{\xi^{1+2\epsilon}} \right)_c \xi^2 \mathcal{M}_{n+1}^{(1)f}(\xi_c), \quad (4.36c)$$

$$\sigma_{n+2}^{(2)}(\xi_c) = \int d\sigma_{hh}^{(2)} = \int d\Upsilon_1 d\Upsilon_2 d\Phi_{n,2} d\xi_1 d\xi_2 \frac{1}{2!} \left(\frac{1}{\xi_1^{1+2\epsilon}} \right)_c \left(\frac{1}{\xi_2^{1+2\epsilon}} \right)_c \left(\xi_1^2 \xi_2^2 \mathcal{M}_{n+2}^{(0)} \right). \quad (4.36d)$$

The three terms of the integrand of $\sigma_n^{(2)}$ are separately divergent. However, in the sum the $1/\epsilon$ poles cancel. The other parts, $\sigma_{n+1}^{(2)}$ and $\sigma_{n+2}^{(2)}$, are finite by construction. Hence, we can set $d = 4$ everywhere (except in the individual pieces of the integrand of $\sigma_n^{(2)}$) and obtain

$$\sigma_n^{(2)}(\xi_c) = \int d\Phi_n^{d=4} \left(\mathcal{M}_n^{(2)} + \hat{\mathcal{E}}(\xi_c) \mathcal{M}_n^{(1)} + \frac{1}{2!} \mathcal{M}_n^{(0)} \hat{\mathcal{E}}(\xi_c)^2 \right) = \int d\Phi_n^{d=4} \mathcal{M}_n^{(2)f}, \quad (4.37a)$$

$$\sigma_{n+1}^{(2)}(\xi_c) = \int d\Phi_{n+1}^{d=4} \left(\frac{1}{\xi} \right)_c \left(\xi \mathcal{M}_{n+1}^{(1)f}(\xi_c) \right), \quad (4.37b)$$

$$\sigma_{n+2}^{(2)}(\xi_c) = \int d\Phi_{n+2}^{d=4} \left(\frac{1}{\xi_1} \right)_c \left(\frac{1}{\xi_2} \right)_c \left(\xi_1 \xi_2 \mathcal{M}_{n+2}^{(0)f} \right). \quad (4.37c)$$

This is the generalisation of (4.15) to NNLO. In the integrand of (4.37a) the build-up of the exponentiated singular part $e^{\hat{\mathcal{E}}}$ is recognisable (cf. (2.40) and (4.16)). For $\mathcal{M}_n^{(\ell)f}$ to be finite, $\hat{\mathcal{E}}$ has to contain the soft $1/\epsilon$ pole. However, any choice of the finite part is possible in principle. We have chosen to define the finite matrix elements through eikonal subtraction, (4.23). This ensures that the auxiliary contributions cancel and the remaining parts $\sigma_{n+1}^{(2)}$ and $\sigma_{n+2}^{(2)}$ have a very simple form. Terms of $\mathcal{O}(\epsilon)$ in $\hat{\mathcal{E}}$ have no effect since they do not modify $\mathcal{M}_n^{(\ell)f}$ after setting $d = 4$. This means we can set them to zero and there is no need to compute the integral (4.13) beyond finite terms.

4.3 Beyond NNLO

4.3.1 FKS³: extension to N³LO

First steps towards extending universal schemes beyond NNLO have been made in QCD [49]. The simplicity of FKS² suggests that this paradigm is a promising starting point for further extension to N³LO in massive QED, provided that all matrix elements are known.

At N³LO, we have four terms

$$\sigma^{(3)} = \int d\Phi_n \mathcal{M}_n^{(3)} + \int d\Phi_{n+1} \mathcal{M}_{n+1}^{(2)} + \int d\Phi_{n+2} \mathcal{M}_{n+2}^{(1)} + \int d\Phi_{n+3} \mathcal{M}_{n+3}^{(0)}, \quad (4.38)$$

which are separately divergent. In order to reorganise these four terms into individually finite terms, we repeatedly use (4.8) to split the phase-space integrations into hard and soft and (4.23) to split the matrix element into finite and divergent parts. In principle we could choose many different ξ_c parameters. However, from the experience of FKS² we expect decisive simplifications if we choose them all to be the same. Indeed, as is detailed in Appendix D, there are now at least three different auxiliary integrals that enter in intermediate steps. However, if all ξ_c parameters are chosen to be equal, their contributions cancel for any cross section, similar to (4.34). Hence, writing

$$d\sigma^{(3)} = d\sigma_n^{(3)}(\xi_c) + d\sigma_{n+1}^{(3)}(\xi_c) + d\sigma_{n+2}^{(3)}(\xi_c) + d\sigma_{n+3}^{(3)}(\xi_c), \quad (4.39)$$

all terms are separately finite and, as discussed in detail in Appendix D, given by

$$d\sigma_n^{(3)}(\xi_c) = d\Phi_n^{d=4} \mathcal{M}_n^{(3)f}, \quad (4.40a)$$

$$d\sigma_{n+1}^{(3)}(\xi_c) = d\Phi_{n+1} \left(\frac{1}{\xi_1} \right)_c \left(\xi_1 \mathcal{M}_{n+1}^{(2)f}(\xi_c) \right), \quad (4.40b)$$

$$d\sigma_{n+2}^{(3)}(\xi_c) = \frac{1}{2!} d\Phi_{n+2} \left(\frac{1}{\xi_1} \right)_c \left(\frac{1}{\xi_2} \right)_c \left(\xi_1 \xi_2 \mathcal{M}_{n+2}^{(1)f}(\xi_c) \right), \quad (4.40c)$$

$$d\sigma_{n+3}^{(3)}(\xi_c) = \frac{1}{3!} d\Phi_{n+3} \left(\frac{1}{\xi_1} \right)_c \left(\frac{1}{\xi_2} \right)_c \left(\frac{1}{\xi_3} \right)_c \left(\xi_1 \xi_2 \xi_3 \mathcal{M}_{n+3}^{(0)f}(\xi_c) \right). \quad (4.40d)$$

Once more we have used the fact that for tree-level amplitudes $\mathcal{M}_{n+3}^{(0)} = \mathcal{M}_{n+3}^{(0)f}$. As always, the ξ_c dependence cancels between the various parts s.t. $d\sigma^{(3)}$ is independent of this unphysical parameter.

4.3.2 FKS^ℓ: extension to N^ℓLO

The pattern that has emerged in the previous cases leads to the following extension to an arbitrary order ℓ in perturbation theory:

$$d\sigma^{(\ell)} = \sum_{j=0}^{\ell} d\sigma_{n+j}^{(\ell)}(\xi_c), \quad (4.41a)$$

$$d\sigma_{n+j}^{(\ell)}(\xi_c) = d\Phi_{n+j}^{d=4} \frac{1}{j!} \left(\prod_{i=1}^j \left(\frac{1}{\xi_i} \right)_c \xi_i \right) \mathcal{M}_{n+j}^{(\ell-j)f}(\xi_c). \quad (4.41b)$$

The eikonal subtracted matrix elements

$$\mathcal{M}_m^{(\ell)f} = \sum_{j=0}^{\ell} \frac{\hat{\xi}^j}{j!} \mathcal{M}_m^{(\ell-j)}, \quad (4.42)$$

(with the special case $\mathcal{M}_m^{(0)f} = \mathcal{M}_m^{(0)}$ included) are free from $1/\epsilon$ poles, as indicated in (2.40). Furthermore, the phase-space integrations are manifestly finite.

4.4 Comments on and properties of FKS^ℓ

With the scheme now established, let us discuss a few non-trivial properties that are helpful during implementation and testing.

4.4.1 Regularisation-scheme and scale dependence

As we have explained in Section 2.1, it is advantageous to calculate the matrix elements $\mathcal{M}_n^{(\ell)}$ in the on-shell scheme for α (and the masses) because it best exploits the Ward identity. This way the only μ dependence is in a global prefactor $\mu^{2\epsilon}$ induced through the integral measure. The same holds for the integrated eikonal. Hence, for the finite matrix elements $\mathcal{M}_n^{(\ell)f}$ there is no μ dependence after setting $d = 4$.

A similar argument can be made for the regularisation-scheme dependence. As discussed in Section 3.4, the renormalised and $\overline{\text{MS}}$ -like IR subtracted \mathcal{M}_{sub} is scheme independent for $\epsilon \rightarrow 0$ because it is free of terms $\propto n_\epsilon/\epsilon$. The same argument can also be made for the eikonal subtracted matrix element $\mathcal{M}_n^{(\ell)f}$ because the integrated eikonal $\hat{\mathcal{E}}$ is scheme independent, dealing only with singular vector fields. Of course, this hinges on there being no collinear singularities.

4.4.2 Ingredients required at NNLO

To be concrete, we list the input that is required for a computation of a physical cross section at NNLO in QED. The important point is that once the final expressions for a NNLO cross section, (4.37), or beyond, (4.41), are obtained, we can set $d = 4$ everywhere.

- The two-loop matrix element $\mathcal{M}_n^{(2)}$ is known with non-vanishing masses up to $\mathcal{O}(\epsilon^0)$. In general this is a bottleneck because the necessary master integrals are only known for a very select class of processes, not to mention the algebraic complexity. However, it is possible to approximate $d\sigma^{(2)}$ using ‘massification’ of $\mathcal{M}_n^{(2)}$ [5, 112, 113] (see Section 5.5).
- The renormalised one-loop matrix element $\mathcal{M}_n^{(1)}$ of the n -particle process is known including $\mathcal{O}(\epsilon^1)$ terms. This is usually the case for NNLO calculation as it is needed for the sub-renormalisation $\mathcal{M}_n^{(2)} \supset \delta Z \times \mathcal{M}_n^{(1)}$ as well as the one-loop amplitude squared, which is part of $\mathcal{M}_n^{(2)}$. Once these pieces are assembled to $\mathcal{M}_n^{(2)f}$, the $\mathcal{O}(\epsilon)$ terms can be dropped.
- The renormalised real-virtual matrix element $\mathcal{M}_{n+1}^{(1)}$ is known with non-vanishing masses. Terms $\mathcal{O}(\epsilon)$ are not required.
- $\mathcal{M}_{n+2}^{(0)}$ is known in four dimensions. In intermediate steps, the matrix elements $\mathcal{M}_n^{(0)}$ and $\mathcal{M}_{n+1}^{(0)}$ are required to $\mathcal{O}(\epsilon^2)$ and $\mathcal{O}(\epsilon)$, respectively. However, depending on the regularisation scheme, such terms might actually be absent. In any scheme, once $\mathcal{M}_n^{(2)f}$ and $\mathcal{M}_{n+1}^{(1)f}$ is assembled, the $\mathcal{O}(\epsilon)$ terms can be dropped.

4.4.3 Phase-space parametrisation

A further issue in connection with small lepton masses is related to the phase-space parametrisation. The phase space has to be constructed in any way that allows the distributions to be implemented. The easiest way to do this is to ensure that ξ_i is as an integration variable of the numerical integrator. In addition, for small m there are potentially numerical problems due to PCS. In fact, these regions produce precisely the $\log(m)$ terms that correspond to the collinear ‘singularities’ of the real part. These $\log(m)$ terms will cancel the virtual collinear ‘singularities’ of similar origin. Hence, for small m there is a numerically delicate cancellation. This requires a dedicated tuning of the phase-space parametrisation. We will discuss this in detail in [Section 6.4.1](#).

Chapter 5

Two-loop calculation

The major bottleneck in most higher-order calculations is the evaluation of the n -particle amplitude to the required number of loops. In our case of NNLO calculations these are two-loop diagrams. The difficulty originates in part from the algebraic complexity, though this can sometimes be reduced by the choice of the regularisation scheme. The biggest problem is in any case the lack of analytic results for the so-called master integrals. This is because – especially in massive QED – we have often a lot of active scales some of which are internal and external masses.

There is a traditional procedure for multi-loop calculations that was developed over the last decade for the analytic QCD calculations for the LHC which we have adopted for massive QED:

1. Generate all Feynman diagrams contributing to the process. While this is straightforward to do by hand for amplitudes with few external particles and few loops, it quickly becomes a daunting task as the number of diagrams grows factorially at higher loops or multiplicities. Hence, this step is usually performed with a dedicated computer program such as QGRAF [114].
2. Apply the Feynman rules and perform algebraic simplification. This also includes simplifying the Dirac and Lorentz structure of the expression to obtain scalar quantities that can be treated later. Common ways to do this include

- The reduction to helicity amplitudes, i.e. fixing the helicity and polarisation of every external particle and then employ completeness relations and Fierz identities to simplify the result. This works very well for tree and one-loop diagrams involving few massless particles as the number of helicity combinations is small. For massive particles, this is still possible but in practice a lot more involved.

We will not be using helicity amplitudes in this project.

- The standard approach of squaring the amplitude \mathcal{A} to obtain the matrix element $\mathcal{M} = |\mathcal{A}|^2$ and using the completeness relation of spinors to convert the expression of \mathcal{M} to traces.
- The projection onto form factors. This is done by writing the most general expression that satisfies all symmetries of the theory with arbitrary coefficients and fixing those by applying projectors onto the amplitude. This procedure has the advantage of being completely general and independent of the observable to be calculated. However, this mechanism also falls short when too many particles are involved because too many form factors need to be defined.

3. Take stock of all integrals appearing and try to find relations between them.
4. Calculate all remaining master integrals using various methods.

In this chapter, we will briefly discuss all these steps as a short tutorial on two-loop calculations. As an example we will be using the calculations in MCMULE but the discussion is far more general. In fact, the relevant calculations were performed in QCD first and only later was the abelian limit taken. We begin by discussing ways of organising a calculation in a gauge-invariant fashion in Section 5.1. Next, we will discuss various aspects of the actual loop integration, focussing on reductions to scalar (Section 5.2) and master integrals (Section 5.3) as well as the eventual calculation of these integrals in Section 5.4. Finally, we will discuss a method of coping with massive fermions in Section 5.5.

5.1 Gauge-invariant splitting of amplitudes

Often we would like to be able to decompose our expressions into simpler contributions. If we do not want to break gauge invariance, we cannot use Feynman diagrams for this. Instead, we are forced to find a different strategy to classify the contributions.

A natural strategy in QCD is to sort the expression by *colour factors*, the result of solving the colour algebra. While public codes are available for this (for example [115]), it is often easier to just implement the colour algebra directly. After solving the traces in colour space, one is left with combinations of the different colour factors of Table 5.1.

When adapting results from QCD for QED, the limit of the Casimir operators $C_F \rightarrow 1$ and $C_A \rightarrow 0$ is trivial. However, the factor associated to closed fermion loops $T_R n_i$ is often written assuming $T_R = 1/2$ s.t. adapting amplitudes may require $n_i \rightarrow 2n_i$ before use.

Note that even for QED without colour structure it may make sense to separate purely photonic contributions ($\propto C_F^\ell$) from fermionic contributions with their n_i .

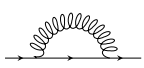
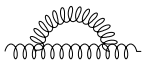
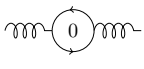
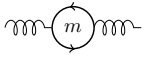
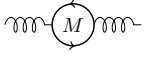
	example diagram	QCD value	QED value	
C_F		$(N^2 - 1)/(2N)$ $= 4/3$	1	Casimir operator of the fundamental repr.
C_A		$N = 3$	0	Casimir operator of the adjoint repr.
$T_R n_f$		$\frac{1}{2} \times 4$	1×0	no. of massless fermions
$T_R n_m$		$\frac{1}{2} \times 1$	1×1	no. of light fermions
$T_R n_h$		$\frac{1}{2} \times 1$	1×1	no. of heavy fermions

Table 5.1: Colour factors in QCD and QED. The values for the n_i refer to calculation of $t \rightarrow W^\pm b$ and $\mu \rightarrow \nu \bar{\nu} e$, respectively.

Unfortunately, sorting the contributions by colour factor is often not sufficient in QED as there are just not enough different colour factors. Assuming we have multiple flavours of leptons, as is the case in most MCMULE processes, we can exploit this as a new strategy [45, 116] by assigning (formally) different charges to each flavour. For example, the amplitude for μ - e scattering at LO can be written as

$$\mathcal{A}^{(0)}(\mu e \rightarrow \mu e) = qQ \left(\begin{array}{c} \rightarrow \rightarrow \rightarrow \\ | \\ \leftarrow \leftarrow \leftarrow \end{array} \right), \quad (5.1a)$$

where q (Q) is the charge of electron (muon). The one-loop amplitude can now be split as

$$\mathcal{A}^{(1)} = q^3 Q \left(\begin{array}{c} \rightarrow \rightarrow \rightarrow \\ | \\ \leftarrow \leftarrow \leftarrow \end{array} \right) + qQ^3 \left(\begin{array}{c} \rightarrow \rightarrow \rightarrow \\ | \\ \leftarrow \leftarrow \leftarrow \end{array} \right) + q^2 Q^2 \left(\begin{array}{c} \rightarrow \rightarrow \rightarrow \\ | \\ \leftarrow \leftarrow \leftarrow \end{array} \right). \quad (5.1b)$$

Hence, we now can consider the terms separately without breaking gauge invariance.

A counting that include logarithms as well as powers of α suggests that the $q^3 Q$ (qQ^3) term would be $\alpha^3 \log \frac{m_s^2}{s}$ ($\alpha^3 \log \frac{M_s^2}{s}$). Hence, the splitting (5.1b) allows us to use the large hierarchy between the lepton masses to prioritise the $q^3 Q$ term over the much more complicated $q^2 Q^2$ term because we expect the former to be much larger than the latter. This was indeed found at NLO [45].

This decomposition is very similar to the colour decomposition used in connection with helicity amplitudes (for a review, cf. [117]). When using this method to calculate \mathcal{A} directly, one collects the different colour structures at the amplitude level to split that into different gauge-invariant subparts.

5.2 Scalar integrals

Beyond the one-loop level, it is generally advisable to work with scalar objects. Unfortunately, calculations involving fermions will eventually require the manipulation of Dirac matrices. While computer algebra programs can certainly handle this, it is generally a good idea to reduce the expression to only contain scalar quantities as soon as possible. As discussed above, this could be achieved by interfering the amplitude with the corresponding Born amplitude. However, one stays more flexible in the calculation when instead decomposing the amplitude into form factors using appropriate projectors. This has the added advantage of reducing the amount of algebra necessary if the number of form factors is not unreasonably large. This is due to the simple fact that projectors can often be written with less objects than the physical Born amplitude.

The next step is the removal of scalar products involving one (or more) loop momenta from the numerator. For this, we need to identify one of the propagators of the diagram and use it to cancel the scalar product. If no propagator of the diagram contains this scalar product, we need to add a fictitious propagator that does. We call a set of propagators that is guaranteed to achieve this for any scalar product a *family*. For a process with ρ external momenta (after applying momentum conservation) and ℓ loop momenta there are

$$p = \binom{\rho + \ell}{2} - \binom{\rho}{2} = \ell \frac{1 + \ell + 2\rho}{2} \quad (5.2)$$

possible scalar products, requiring a family of that size. Here, we have defined the multichoose function

$$\binom{n}{k} = \binom{n+k-1}{k} = \frac{(n+k-1)!}{k!(n-1)!}, \quad (5.3)$$

that counts the number of ways one can pick k unordered elements from a set of n elements, allowing for repetition.

Once the families are fixed, the next step is to bring the expression into the following form

$$\sum_n C_n \times \int \prod_{j=1}^{\ell} [dk_j] \frac{1}{\mathcal{P}_{1,n}^{\alpha_{1,n}} \dots \mathcal{P}_{p,n}^{\alpha_{p,n}}}. \quad (5.4)$$

The powers α_i of the propagators \mathcal{P}_i may be negative or zero and the C_n are functions of the external kinematics and the dimension d . These integrals are referred to as *reducible scalar integrals*.

In virtually no case are all $\alpha_i > 0$. Hence, it makes sense to group integrals into so-called *sectors* by looking at the propagators \mathcal{P} that are present as denominators (with whatever power). As this is a boolean decision for every i , each group can be represented as a binary number. An integral that has t propagators with $\alpha_i > 0$ shall have sector ID [118]

$$\text{ID} = \sum_{k=1}^t 2^{i_k-1} \quad \text{with} \quad \alpha_{i_1}, \dots, \alpha_{i_t} > 0. \quad (5.5)$$

This serves to organise integrals because as soon as one integral in a sector can be calculated all integrals of the sector can be calculated, at least in principle. We call the easiest integral of each sector, i.e. the one with $\alpha_{i_1} = \dots = \alpha_{i_t} = 1$, the *corner integral* of this sector. To further categorise integrals, we also define

$$r = \alpha_{i_1} + \dots + \alpha_{i_t} \quad \text{and} \quad s = - \sum_{\alpha_i < 0} \alpha_i, \quad (5.6)$$

as the sum of positive and negative propagator indices, respectively. Obviously $s \geq 0$ and $r \geq t$ with $r = t$ for the corner integral.

5.3 Integration-by-parts reduction

At this stage, one has a large number of scalar loop integrals. As the calculation of any one of them can be incredibly difficult, one would like to reduce them to a minimal set of so-called *master integral*. We will mostly follow [119] in the discussion below.

It turns out that such a reduction to master integrals can indeed be achieved with the use of *integration-by-parts* (IBP) identities [120]. In contrast to the standard integration-by-parts theorem

$$\int dx u v' = uv - \int dx u' v,$$

where one chooses u and v s.t. $u'v$ is simpler, we now use that the surface term uv vanishes in dimensional regularisation. In particular, we have

$$\int \prod_{j=1}^{\ell} [dk_j] \frac{\partial}{\partial k_i} \cdot \left(q \frac{1}{\mathcal{P}_1^{\alpha_1} \dots \mathcal{P}_t^{\alpha_t}} \right) = 0, \quad i = 1, \dots, \ell, \quad (5.7)$$

where q represents either a loop or an external momentum. Note that q is inside the derivative s.t. if $q = k_i$ the product rule has to be used on the integrand with

$$\frac{\partial}{\partial k} \cdot k \equiv \frac{\partial}{\partial k_\mu} k^\mu = d. \quad (5.8)$$

IBP relations now allow us to get identities between different integrals.

To illustrate the usefulness of these IBP identities in the calculation of a large number of loop integrals, we consider as a toy example a simple class of one-loop integrals

$$I(a, b) = \int [dk] \frac{1}{[k^2 - m^2]^a [(k-p)^2 - M^2]^b} \quad \text{with } p^2 = M^2. \quad (5.9)$$

For now we will only consider the case where $m = 0$. Of course, this integral could be trivially calculated for arbitrary powers of a and b . However, even if this is possible in practice, it is often not very helpful because the resulting functions of a and b might be very complicated.

Setting $q = k$, we apply (5.7)

$$\begin{aligned} i(a, b) &= \frac{\partial}{\partial k_\mu} \left(k^\mu \frac{1}{[k^2]^a [(k-p)^2 - M^2]^b} \right) \\ &= k^\mu \frac{\partial}{\partial k_\mu} \left(\frac{1}{[k^2]^a [(k-p)^2 - M^2]^b} \right) + \left(\frac{\partial}{\partial k_\mu} k^\mu \right) \frac{1}{[k^2]^a [(k-p)^2 - M^2]^b} \\ &= -2k^\mu \left(\frac{a k^\mu}{[k^2]^{1+a} [(k-p)^2 - M^2]^b} + \frac{b (k^\mu - p^\mu)}{[k^2]^a [(k-p)^2 - M^2]^{1+b}} \right) \\ &\quad + \frac{d}{[k^2]^a [(k-p)^2 - M^2]^b} \\ &= \frac{(d - 2a - 2b)k^2 + 2(2a + b - d)k \cdot p}{[k^2]^a [(k-p)^2 - M^2]^{b+1}}. \end{aligned} \quad (5.10)$$

We now again use the algorithm described in Section 5.2 to turn this expression back into scalar integrals of the form $I(a', b')$. After loop integration and setting $\int [dk] i(a, b) = 0$ we finally have our first *seed identity*

$$0 = -bI(a-1, b+1) + (d-2a-b)I(a, b). \quad (5.11)$$

We can write this and the seed identity from $q = p$ using the short-hand notation of [119]. \mathbf{n}^\pm indicates that the power of the n -th propagator is raised (lowered) by one.

$$\begin{aligned} 0 &= d - 2a - b - b \mathbf{1}^- \mathbf{2}^+, \\ 0 &= -a + b - b \mathbf{1}^- \mathbf{2}^+ + a \mathbf{2}^- \mathbf{1}^+ + 2bM^2 \mathbf{2}^+. \end{aligned} \quad (5.12)$$

It is a good idea to consider an integral family with p propagators as an element of a p -dimensional vector space of the $\{\alpha_i\}$. The IBP relations then provide linear dependences between vectors of this space.

Let us now choose $b = 1$ and use the fact that

$$\mathbf{2}^- I(a, 1) = I(a, 0) = 0 \quad (5.13)$$

is scaleless. We now have

$$\begin{aligned} 0 &= (d-1-2a) I(a, 1) - I(a-1, 2) \\ 0 &= (+1-a) I(a, 1) - I(a-1, 2) + 2M^2 I(a, 2), \end{aligned} \quad (5.14a)$$

which is usually expressed as a matrix equation

$$\begin{pmatrix} d-1-2a & 0 & -1 \\ 1-a & 2M^2 & -1 \end{pmatrix} \cdot \begin{pmatrix} I(a, 1) \\ I(a, 2) \\ I(a-1, 2) \end{pmatrix} = 0. \quad (5.14b)$$

This system of equations is under-determined, but we could make it over-determined by varying a , a common feature of IBP relations.

For now, we will eliminate $I(a, 1)$ and obtain a recursion relation (shifting $a \rightarrow a + 1$)

$$I(a + 1, 2) = \frac{1}{2M^2} \frac{3 + a - d}{3 + 2a - d} I(a, 2). \quad (5.15a)$$

Alternatively, we eliminate $I(a - 1, 2)$ and obtain

$$I(a, 2) = -\frac{2 + a - d}{2M^2} I(a, 1). \quad (5.15b)$$

This is again classic behaviour for IBP reduction. We have multiple ways of solving the system and have to make decisions on what integrals are more complicated. In our case we arrive at

$$I(a + 1, 2) = -\frac{2 + a - d}{4M^4} \frac{3 + a - d}{3 + 2a - d} I(a, 1), \quad (5.15c)$$

where $I(1, 1)$ is a *master integral* that has to be computed.

In real-world calculations it is often not possible to write down a simple recursion relation as (5.15). Instead, one writes down the linear system (5.14) for $b = 1, \dots, b_{\max}$ for whatever b_{\max} the problem under consideration mandates. One would naively assume that this system grows out of control rapidly as more and more integrals are added. However, assuming a cut-off point such as b_{\max} , the system is naturally over-determined because the number of new integrals grows slower than the number of equations. We now define what is called a *lexicographic ordering* that, given two integrals, determines which is more complicated. The exact specification of this ordering does not matter as long as it is consistent. We can keep generating seed identities and solve the resulting matrix through Gaussian elimination, favouring integrals that were deemed simpler by the lexicographic ordering. This is called Laporta's algorithm [121, 122].

There are many public codes that implement Laporta's algorithm or other, similar algorithms such as LiteRed [123], AIR [124], FIRE [125], Kira [126], and `reduze` [118]. We will be focusing on the latter two. Additionally to the IBP reduction, `reduze` and `Kira` are also capable of exploiting shift symmetries, i.e. shifting the loop momenta $k_i \rightarrow k_i + p$. This means that it can find relations between sectors of different families which reduces the number of integrals that need to be manually considered. More importantly yet, this feature can also be used to find shift relations between diagrams, reducing the number of families that need to be considered.

Note that there are other relations that can be used to generate seed identities that use other properties of loop integrals such as Lorentz invariance.

5.4 Calculation of master integrals

We now turn to the calculation of master integrals, beginning with some general comments on Feynman parametrisation in Section 5.4.1, followed by a discussion of how mass hierarchies can be best exploited in Section 5.4.2 (for heavy scales) and Section 5.4.3 (for light scales). A more detailed discussion can be found in [8].

5.4.1 Feynman parametrisation

If we want to calculate loop integrals in whatever form, we often employ *Feynman parametrisation* as some stage. For an ℓ -loop integral¹¹

$$I = \int \prod_{j=1}^{\ell} [dk_j] \frac{1}{\mathcal{P}_1^{\alpha_1} \dots \mathcal{P}_t^{\alpha_t}} \quad \text{with } \alpha_1, \dots, \alpha_t > 0 \quad (5.16)$$

we could either solve the loops one by one or all in one go. Both methods are equivalent though difficult to relate in practical examples. We will be focusing on the latter case as the former can be viewed as a sub-class. Following [127], we write

$$\frac{1}{\mathcal{P}_1^{\alpha_1} \dots \mathcal{P}_t^{\alpha_t}} = \frac{\Gamma(r)}{\prod_j \Gamma(\alpha_j)} \int_0^\infty \prod_{j=1}^t dx_j x_j^{\alpha_j-1} \delta\left(\sum_{i \in \nu} x_i - 1\right) \frac{1}{(\mathcal{P}_1 x_1 + \dots + \mathcal{P}_t x_t)^r}. \quad (5.17)$$

where $r = \sum_j \alpha_j$ and ν a non-empty subset of $\{1, \dots, t\}$ (Cheng-Wu theorem, [128]). The x_i are called *Feynman parameters*. Note that most books on QFT will assume $\nu = \{1, \dots, t\}$, reducing the integration region to $[0, 1] \times [1, 1 - x_1] \times \dots$. However, for analytic calculations we have found that having just one element, say $i = 1$, in $\nu = \{1\}$ is a better choice, setting one $x_1 = 1$ and keeping the integration bounds at $[0, \infty]^{t-1}$.

The denominator can be written as

$$D = \mathcal{P}_1 x_1 + \dots + \mathcal{P}_t x_t = k^T \cdot M(x_i) \cdot k - 2Q(x_i, q_j)^T k + J(x_i, s_{jk}), \quad (5.18)$$

with a $\ell \times \ell$ matrix M , ℓ -vectors $k = (k_1, \dots, k_\ell)$ and Q , depending on the Feynman parameters x_i , external momenta q_j and invariants $s_{jk} = 2q_j \cdot q_k$. By shifting $k \rightarrow k + M^{-1}Q$ we cancel the linear term so that after diagonalising M (with eigenvalues λ_i) we have

$$D = k^T \cdot \text{diag}(\lambda_i) \cdot k - \Delta \quad \text{with } \Delta = Q^T M^{-1} Q - J. \quad (5.19)$$

After rescaling $k_i \rightarrow \lambda_i^{-1/2} k_i$ we have factorised the loop integrations and can use that

$$\int [dk] \frac{1}{(k^2 - \Delta)^r} = (-1)^r \Gamma(1 - \epsilon) \frac{\Gamma(r - d/2)}{\Gamma(r)} \left(\frac{1}{\Delta}\right)^{r-d/2} \quad (5.20)$$

to find the general Feynman-parametrised form of the ℓ -loop integral I , keeping in mind that we chose to have only x_i in the δ function

$$I = (-1)^r \Gamma(1 - \epsilon) \frac{\Gamma(r - \ell d/2)}{\prod_j \Gamma(\alpha_j)} \int_0^\infty \prod_{j=1}^t dx_j x_j^{\alpha_j-1} \delta(x_i - 1) \underbrace{\frac{\mathcal{U}^{r-(\ell+1)d/2}}{\mathcal{F}^{r-\ell d/2}}}_{\mathcal{G}}, \quad (5.21a)$$

$$\mathcal{U} = \det M = \prod_j \lambda_j, \quad \mathcal{F} = \det M \times \Delta. \quad (5.21b)$$

We dub the polynomials \mathcal{U} and \mathcal{F} *graph polynomials* or Symanzik polynomials because they can be computed without having to go through the motions of finding and diagonalising M by instead studying graph theoretical aspects of the Feynman diagram corresponding to I as implemented in UF [127].

¹¹The propagators can be either physical propagators of the form $(k_j + p)^2 - m^2$ or linear propagators $k_j \cdot p$ that appear in Section 5.4.2

Note that I can now be viewed (up to a pre-factor) as the $(p-1)$ -dimensional *Mellin transform* of \mathcal{G} evaluated at the indices $\vec{\alpha} = (\alpha_2, \dots, \alpha_p)$

$$\{\mathcal{M}\mathcal{G}\}(\vec{\alpha}) = \int_0^\infty d\vec{x} \vec{x}^{\vec{\alpha}-1} \mathcal{G}(\vec{x}) = \int_0^\infty \left(\prod_{j=1}^p dx_j x_j^{\alpha_j-1} \right) \mathcal{G}(\vec{x}) \propto I, \quad (5.22)$$

where we have assumed that $\nu = \{1\}$ for simplicity.

The actual calculation of the Feynman integral (5.21a) is naturally quite involved. However, in most cases, once a solution has been found for the corner integral, other integrals with the same structure can be found relatively easily. For methods to compute I , see for example [8, 119].

There is one last subtlety related to numerators. As discussed in Section 5.2, we implement numerators in integrals by setting some $\alpha_i < 0$. However, that would make the Feynman parametrisation ill-defined because the Γ function diverges for negative integers. To solve this problem [127], we note an identity for Mellin transforms called *Ramanujan's master theorem*. In our language it states that the Mellin transform of a function $f(x)$ evaluated at negative integers $-n$ can be written as the n -th derivative of f

$$\{\mathcal{M}f\}(-n) = \int dx x^{-n-1} f(x) = \Gamma(-n) f^{(n)}(0). \quad (5.23)$$

Now the $\Gamma(-n)$ cancels, finally leading to our master formula [129]

$$I = (-1)^r \Gamma(1-\epsilon)^\ell \Gamma(r-s-\ell d/2) \int_0^\infty \delta(x_i-1) \left(\prod_{j=1}^t dx_j \frac{x_j^{\alpha_j-1}}{\Gamma(\alpha_j)} \right) \left(\prod_{j=t+1}^p \frac{\partial^{-\alpha_j}}{\partial x_j^{-\alpha_j}} \right) \frac{\mathcal{U}^{r-s-(\ell+1)d/2}}{\mathcal{F}^{r-s-\ell d/2}} \Big|_{x_{t+1}=\dots=x_p=0}, \quad (5.24)$$

with r (s) the sum of positive (negative) indices, t the number of positive indices and p the length of the family as defined above and in [118]. This implies that

$$\alpha_1, \dots, \alpha_t > 0 \quad \text{and} \quad \alpha_{t+1}, \dots, \alpha_p \leq 0. \quad (5.25)$$

Let us now use Feynman parametrisation to calculate the integral $I(a, b)$ we have introduced above. The polynomials \mathcal{U} and \mathcal{F} can be easily calculated using [127]

$$\mathcal{U} = x_1 + x_2, \quad \text{and} \quad \mathcal{F} = M^2 x_2^2 + m^2 x_1(x_1 + x_2). \quad (5.26)$$

With our master formula $l = 1$, $\alpha_1 = a$, $\alpha_2 = b$, and $r = a + b$

$$I(a, b) = (-1)^{a+b} \frac{\Gamma(a+b-\frac{d}{2})\Gamma(1-\epsilon)}{\Gamma(a)\Gamma(b)} \int_0^\infty dx_1 dx_2 \delta(1-x_2) x_1^{a-1} x_2^{b-1} \frac{(x_1+x_2)^{a+b-d}}{(M^2 x_2^2 + m^2 x_1(x_1+x_2))^{a+b-d/2}}. \quad (5.27)$$

We can see that if we can solve this integral for $a = b = 1$, we will most likely be able to solve it for any value of a and b .

For now we will again set $m = 0$ to simplify this integral. Calculating the full integral either requires more complicated integration techniques (for example cf. [8]) or a clever substitution¹²,

¹²The substitution in question is $m \rightarrow M\sqrt{-(\chi-1)^2/\chi^2}$ with $\chi \in \mathbb{C}$

resulting in complicated hypergeometric functions that could be expanded in ϵ with `HypExp` [130]. Needless to say, this goes beyond the scope of this simple example.

The δ -function makes the x_2 -integral trivial. The x_1 -integral we are left with is

$$\begin{aligned} I(a, b) &= (-1)^{a+b} [M^2]^{d/2-a-b} \frac{\Gamma(a+b-d/2)\Gamma(1-\epsilon)}{\Gamma(a)\Gamma(b)} \int_0^\infty dx_1 x_1^{a-1} (1+x_1)^{a+b-d} \\ &= (-1)^{a+b} [M^2]^{d/2-a-b} \frac{\Gamma(a+b-d/2)\Gamma(d-2a-b)\Gamma(1-\epsilon)}{\Gamma(b)\Gamma(d-a-b)}. \end{aligned} \quad (5.28)$$

5.4.2 Method of regions

In general, the calculation of master integrals with full dependence of any parameter is very difficult and time consuming. However, in many cases this is not needed, often because the parameters have a strong hierarchy such as the electron mass m being much smaller than the muon mass M or typical momentum transfers \sqrt{s} . In this case, we instead calculate the integrals expanded in m . The technique used to achieve this is the *method of regions* [131].

We consider a loop integral that contains two or more disparate scales, as in the case of the muon decay where $m^2 \ll M^2 \sim p \cdot q$. If the integral under consideration is hard to calculate, the obvious idea is to expand the integrand in the small parameter with the hope of achieving a simplification. The method that allows to consistently perform such an expansion is the method of regions.

To motivate this method, we again consider the toy example from above

$$I \equiv I(1, 1) = \int [dk] \frac{1}{[k^2 - m^2 + i0^+]^a [k^2 - 2k \cdot p + i0^+]^b} \quad \text{with } m^2 \ll p^2 = M^2. \quad (5.29)$$

It is useful to keep track of the $i0^+$ prescription in this discussion. We once again ignore that this integral can be calculated with the full m dependence and instead try to expand it at the level of the integrand. Note that the naive expansion

$$\frac{1}{k^2 - m^2} = \frac{1}{k^2} \left(1 + \frac{m^2}{k^2} + \dots \right) \quad (5.30)$$

is not allowed due to the region of the integration domain where $k \sim m \ll M$. The key idea of the method of regions is therefore to split the domain into regions of constant order of magnitude. In the case of our toy example, we introduce as an intermediary step an additional scale Λ with $m \ll \Lambda \ll M$ and write¹³

$$I = \underbrace{\int_0^\Lambda [dk] \frac{1}{[k^2 - m^2 + i0^+] [k^2 - 2k \cdot p + i0^+]}}_{=I_s^\Lambda} + \underbrace{\int_\Lambda^\infty [dk] \frac{1}{[k^2 - m^2 + i0^+] [k^2 - 2k \cdot p + i0^+]}}_{=I_h^\Lambda}, \quad (5.31)$$

where I_s^Λ corresponds to the region where the loop momentum is *soft* and I_h^Λ to the one where it is *hard*.

¹³Note that we have not actually defined what is meant by these integration boundaries w.r.t. the Minkowski metric. Thus, the arguments are somewhat heuristic but could be formalised.

We are now able to expand the integrand in each region according to the respective scaling regime, namely¹⁴

$$\begin{aligned} I_s^\Lambda \stackrel{k \sim m \ll p}{=} \sum_{n=0}^{\infty} \int_0^\Lambda [dk] \frac{(-k^2)^n}{[k^2 - m^2 + i0^+][-2k \cdot p + i0^+]^{n+1}}, \\ I_h^\Lambda \stackrel{m \ll p \sim k}{=} \sum_{n=0}^{\infty} \int_\Lambda^\infty [dk] \frac{(m^2)^n}{[k^2 + i0^+]^{n+1}[k^2 - 2k \cdot p + i0^+]}. \end{aligned} \quad (5.32)$$

The I_s^Λ become more and more UV divergent as n grows while the I_h^Λ becomes UV finite as soon as $n > 0$ but more IR divergent. The sum, however, always keeps the same degrees of divergence.

Before actually calculating I_s^Λ and I_h^Λ , let us see what we can deduce directly. Clearly, the new integrals are much simpler as they both only have one scale (m and p^2 , respectively). Further, the integrand of I_s^Λ is proportional to p^{-n-1} while $I_h^\Lambda \propto m^{2n}$. Because both integrals have mass dimension zero, we can now write

$$I_s^\Lambda \propto \left(\frac{m^2}{M^2}\right)^{(n+1)/2} \quad \text{and} \quad I_h^\Lambda \propto \left(\frac{m^2}{M^2}\right)^n. \quad (5.33)$$

Note that the symmetry $p \rightarrow -p$ is broken by the presence of the $i0^+$ term. Naively, this would suggest that $I_s^\Lambda = 0$ for n even. This, however, is not the case. Assuming we want to calculate I to some order in m/M , we already now know how far in n to expand from these simple considerations without ever calculating I_s^Λ or I_h^Λ .

Once we actually do calculate the leading term, i.e. $n = 0$, we see that the newly introduced cut-off scale Λ drops out in the sum $I_s^\Lambda + I_h^\Lambda$. This, of course, is to be expected since there is no Λ present in the original integral, defined in (5.29).

Ideally, we like for the integration to cover the full domain to avoid introducing the superfluous scale Λ , i.e. $\Lambda \rightarrow \infty$ for I_s^Λ and $\Lambda \rightarrow 0$ for I_h^Λ . However, this potentially introduces additional contributions that need to be calculated. For example in the first case of I_s^Λ , the added term is

$$\int_\Lambda^\infty [dk] \frac{(k^2)^n}{[k^2 - m^2][-2k \cdot p + i0^+]^{n+1}} \stackrel{m \ll \Lambda}{=} \sum_{i=0}^{\infty} [m^2]^i \int_0^\infty [dk] \frac{(k^2)^n}{[k^2]^{1+i}[-2k \cdot p + i0^+]^{n+1}}, \quad (5.34)$$

which is scaleless and therefore vanishes in DREG. A similar argument can also be made for I_h^Λ . Hence, we are allowed to remove Λ and find

$$I_s = \lim_{\Lambda \rightarrow \infty} I_s^\Lambda = \left(\frac{m^2}{M^2}\right)^{\frac{n+1}{2}} \left(\frac{\mu^2}{m^2}\right)^\epsilon \Gamma(1 - \epsilon) \frac{\Gamma(\frac{n+1}{2})\Gamma(\frac{n-1}{2} + \epsilon)}{2\Gamma(1 + n)} \quad (5.35a)$$

$$I_h = \lim_{\Lambda \rightarrow 0} I_h^\Lambda = (-1)^n \left(\frac{m^2}{M^2}\right)^n \left(\frac{\mu^2}{M^2}\right)^\epsilon \Gamma(1 - \epsilon) \frac{\Gamma(1 - 2n - 2\epsilon)\Gamma(n + \epsilon)}{\Gamma(2 - n - 2\epsilon)}. \quad (5.35b)$$

Had we calculated I with full mass dependence using appropriate tricks or referred to a one-loop library such as Package-X [97], we would have found

$$I = \frac{1}{\epsilon} + 2 + 2\beta\sqrt{\beta^2 - 1} \left[i\pi + 2 \log(\beta + \sqrt{\beta^2 - 1}) \right] + 2(\beta^2 - 1) \log \frac{M^2}{m^2} + \log \frac{\mu^2}{M^2}, \quad (5.36)$$

with $\beta = \sqrt{1 - m^2/(4M^2)}$. We can expand this in m/M , obtaining

$$I = \frac{1}{\epsilon} + 2 - \pi \frac{m}{M} + \mathcal{O}(m^2), \quad (5.37)$$

¹⁴We assume as usual that infinite summation and integration commutes.

which is in agreement with (5.35) for $n = 0$.

We are now ready to formulate the method of regions in general:

1. Identify all momentum regions that yield non-zero contributions. Note that in real-life applications more regions than just hard ($k \sim M$) and soft ($k \sim m$) may contribute.
2. Expand the integrand in each region and integrate the result over the full domain.
3. Sum up the contributions from all regions.

When following these steps, one ends up with the expanded solution of the integral. The method of region is intimately linked with the concept of EFTs as both exploit hierarchies of scales. In fact, the EFT framework can be viewed as a field-theoretical formulation of the method of region. Assuming only soft and hard contribution exists, the soft contribution can be viewed as a calculation in an EFT and the hard contribution as a matching calculation to determine the Wilson coefficients of the EFT. Indeed, the UV poles of the soft contributions (EFT calculation) match the IR poles of the hard contribution (Wilson coefficients).

5.4.3 Light-cone coordinates and momentum regions

The discussion of the method of regions above deals mostly with heavy degrees of freedom that we remove. However, as we have seen in Section 2.4 it is also possible to remove light degrees of freedom. This is particularly interesting if we want to study (small) mass effects in a hard scattering process using SCET, an EFT that splits soft and collinear modes off from the full underlying theory, be it QED or QCD. A full review of SCET is well beyond the scope of this review, hence we refer to [69]. Instead, we will just discuss those points we need in order to extend our previous discussion to also cover (anti-)collinear and ultrasoft regions. Both of these are relevant for the muon decay which we will calculate in a SCET-inspired way.

Coordinates suitable for the description of the relevant regions (i.e. hard, soft, collinear) are the light-cone coordinates, which are based on the light-like momenta $e = (1, \vec{0}, 1)/\sqrt{2}$ and $\bar{e} = (1, \vec{0}, -1)/\sqrt{2}$.¹⁵ These allow to decompose any momentum l into its light-cone components as

$$l^\mu = l_+^\mu + l_-^\mu + l_\perp^\mu = (l_+, l_-, l_\perp) = (e \cdot l, \bar{e} \cdot l, l_\perp). \quad (5.38)$$

Let r be another arbitrary momentum, then these components satisfy the properties

$$l_\pm^2 = l_\pm \cdot l_\perp = 0, \quad l \cdot r = l_+ \cdot r_- + l_- \cdot r_+ + l_\perp \cdot r_\perp, \quad l^2 = 2l_+ \cdot l_- + l_\perp^2. \quad (5.39)$$

As an example, let us now write the kinematics of the muon decay in terms of these coordinates. If the muon is considered at rest, we find $p = (M, M, 0)/\sqrt{2}$ in light-cone coordinates. Furthermore, we choose the electron momentum as $q = (0, q_-, q_\perp) = (0, \sqrt{2}E, q_\perp)$. This yields for the kinematic invariants

$$p^2 = 2p_+ \cdot p_- = M^2 \sim \lambda^0, \quad q^2 = q_\perp^2 = m^2 \sim \lambda^2, \quad s = 2p \cdot q = 2p_+ \cdot q_- = 2ME \sim \lambda^0. \quad (5.40)$$

We use λ to indicate the relative size of the parameters and as a book keeping tool that was not strictly necessary in the discussion above. Next, we need a componentwise scaling of the momenta p and q that reproduces these scalings

$$p \sim (M, M, 0) \sim (1, 1, 0), \quad q \sim (0, E, q_\perp) \sim (0, 1, \lambda). \quad (5.41)$$

¹⁵Our definition of e and \bar{e} differs from the standard convention by the normalisation factor $1/\sqrt{2}$.

A region of the loop momentum k is then defined as a specific choice of parameters a , b , and c where $k \sim (\lambda^a, \lambda^b, \lambda^c)$. At this point we expect an infinite number of regions corresponding to the infinite possible choices of a , b , and c . Fortunately, almost all of the infinite number of regions turn out to be zero.

From the SCET point of view, we expect the following contributing regions:

$$\text{hard: } k \sim (1, 1, 1) \quad (5.42a)$$

$$\text{soft: } k \sim (\lambda, \lambda, \lambda) \quad (5.42b)$$

$$\text{anti-collinear: } k \sim (1, \lambda^2, \lambda) \quad (5.42c)$$

$$\text{collinear: } k \sim (\lambda^2, 1, \lambda) \quad (5.42d)$$

$$\text{ultrasoft: } k \sim (\lambda^2, \lambda^2, \lambda^2), \quad (5.42e)$$

We have included the anti-collinear region for completeness even though it does not enter in the muon decay. All regions can appear on the level of individual integrals and even diagrams. However, once all diagrams are summed, we expect all regions except hard, soft, and collinear to drop out.

Let us discuss a simple one-loop example to illustrate how loop integrations are performed in light-cone coordinates. The integral

$$I = \int [dk] \frac{1}{[-2k_- \cdot p_+][(k - q)^2 - m^2]} \quad (5.43)$$

occurs in the method of regions calculation of the one-loop bubble master integral. In order to perform this integration in the standard way, we need to write the integrand as a function of k instead of its light-cone components. This can be achieved with the identity $k_- \cdot p_+ = k \cdot p_+$. Now we can proceed as usual: Feynman parametrisation, shift to remove all terms linear in k and integration over loop momentum. Using (5.39) and (5.40) as well as our master formula for the Feynman parametrisation (5.24), we find

$$\begin{aligned} I &= M^{2\epsilon} \Gamma(1 - \epsilon) \Gamma(\epsilon) \int_0^1 dx x^{-2+\epsilon} (s + m^2 x)^{-\epsilon} \\ &= -\frac{m^2}{s\epsilon} + \frac{m^2[-1 + 2\log(m/M)]}{s} + \mathcal{O}(\epsilon). \end{aligned} \quad (5.44)$$

5.5 Massification

The procedure set out above allows, at least in principle, to expand any amplitude to whatever power in m/M necessary. And while it is certainly much simpler than the full computation of the amplitude with massive electron, it would still be a lot of effort to repeat it anew for each process. However, if we are only interested in the leading term $(m/M)^0$, we do not have to because we can view the light mass as an IR regulator of collinear singularities. This way the terms $\log m$ we are after can be obtained by considering a regularisation scheme dependence. This formalises the discussion of Section 5.4.3 above in the SCET framework. We call the resulting procedure *massification*.

Massification has been worked out at NNLO. Initially this was done for QED in the context of Bhabha scattering [132]. Later, a more general approach has been presented [112, 113] that relies on factorisation and is also valid in QCD. [5] has extended this to include also heavy flavours. Very recently, these considerations have been extended beyond NNLO, in particular for the heavy-quark form factor [133–135].

To be concrete, massification allows us to write for example

$$\mathcal{A}_{t \rightarrow W^\pm b}(m) = \sqrt{Z_q} \times \mathcal{S} \times \mathcal{A}_{t \rightarrow W^\pm b}(0) + \mathcal{O}(m/M), \quad (5.45a)$$

$$\mathcal{A}_{\gamma^* \rightarrow ee} = \sqrt{Z_q \times \bar{Z}_q} \times \mathcal{S}' \times \mathcal{A}_{\gamma^* \rightarrow ee}(0) + \mathcal{O}(m^2/s), \quad (5.45b)$$

allowing us to relate the massive amplitude $\mathcal{A}(m)$ to the (partially) massless amplitude $\mathcal{A}(0)$. For this we need a process-dependent soft contribution $\mathcal{S}^{(\prime)}$ as well as a process-independent collinear contribution Z_q and an anti-collinear contribution \bar{Z}_q . The latter two are universal and can be obtained by solving (5.45b) (cf. Appendix B.3). For this, we have to calculate the amplitude expanded in m . For the case of the heavy-quark form factor that only contains HPLs, we can just take the full result [136] and expand using the Mathematica package HPL [99]. However, obtaining \mathcal{A} is more involved for the heavy-to-light form factor which contains *generalised polylogarithms* (GPL). Hence, we have to resort to the method of regions discussed in Section 5.4.2.

With the expressions for Z_q and \bar{Z}_q , we have now the following recipe to massify any amplitude. The hard part corresponds to the corresponding amplitude with $m = 0$. For each external collinear (anti-collinear) fermion of mass m , we multiply by the corresponding $Z_q^{1/2}$ ($\bar{Z}_q^{1/2}$). Finally, we add a process dependent soft function.

In the following we will discuss the soft contributions for both processes (Section 5.5.1 and Section 5.5.3), commenting on subtleties that, in this context, were first discussed in [5]. Next in Section 5.5.4, we will compare Z_q and \bar{Z}_q , the explicit expressions of which can be found in Appendix B.3, with the literature, especially [113].

5.5.1 The soft function for $t \rightarrow W^\pm b$

For the soft part \mathcal{S} , we only need to consider diagrams with internal fermion loops. Indeed, by performing the formal decoupling of gluon and fermion fields in the SCET framework, one can show that purely gluonic contributions to the soft part vanish to all orders [67, 113]. A simple counting argument implies that only the fermion bubble with mass m contributes (cf. Figure 5.2). Therefore, the unrenormalised soft part \mathcal{S}_0 can easily be calculated from first principle in the SCET framework using (5.42b), i.e.

$$\mathcal{S}_0 = 1 + \left(\frac{\alpha_0^2}{4\pi}\right) C_F \int [dk] \frac{(-2p^\mu)(-2q^\nu)}{(k^2)^2(2p \cdot k)(2q_- \cdot k)} \Pi_{(n_m)}^{\mu\nu}(k). \quad (5.46)$$

In accordance with (5.42b), we only use the large component of the collinear momentum q . Even though the calculation is performed in FDH, there is no contributions $\propto n_\epsilon$, because ϵ -scalars do not couple to fermions in the eikonal approximation [103]. The function $\Pi_{(n_m)}^{\mu\nu}$ is the contribution of n_m fermions with mass m to the usual tensorial vacuum polarisation (2.14). When calculating \mathcal{S}_0 , one encounters an anomaly, i.e. the breaking of naive factorisation [137, 138]. Following [139], we call this *factorisation anomaly*¹⁶. This is a new feature that is only present due to the large mass $p^2 = M^2$.

The factorisation anomaly first appears because the integral (5.46) is not fully regularised in DREG and hence requires further *analytic regularisation*. We shift the power of the propagator $p \cdot k$ at the diagrammatic level according to [69, 141]

$$\frac{1}{(k-p)^2 - M^2 + i0^+} \rightarrow \frac{1}{-2p \cdot k + i0^+} \rightarrow (-\nu^2)^\eta \frac{1}{(-2p \cdot k + i0^+)^{1+\eta}}, \quad (5.47)$$

where the regulator η has to be expanded before the dimensional regulator ϵ . This regularisation also introduces an associated scale ν that drops out in the final result. The only further

¹⁶This is also referred to as collinear anomaly or rapidity divergence [140].

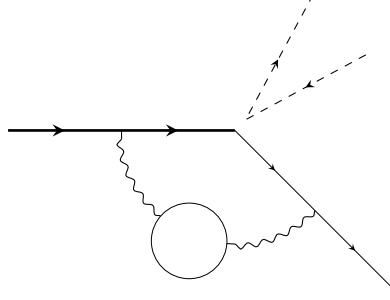


Figure 5.2: The n_m -bubble giving rise to the soft contribution of $t \rightarrow W^\pm b$.

soft contribution is from n_m terms in the wave-function renormalisation of the heavy fermion. Including this contribution, Z_2^S , we obtain

$$\begin{aligned} \mathcal{S} = \sqrt{Z_2^S} \times \mathcal{S}_0 = 1 + (a_0(Mm))^2 C_F n_m & \left[\frac{2}{3} \frac{1}{\eta} \left(-\frac{1}{\epsilon^2} + \frac{5}{3\epsilon} - \frac{28}{9} - 2\zeta_2 \right) \right. \\ & + \frac{1}{2\epsilon^3} - \frac{1}{9\epsilon^2} + \frac{1}{\epsilon} \left(-\frac{26}{27} + \zeta_2 \right) \\ & \left. + \frac{11}{3} - \frac{2}{3}\zeta_3 - \frac{2}{9}\zeta_2 \right] + \mathcal{O}(a^3, \epsilon, \eta), \end{aligned} \quad (5.48)$$

where we define $a_0(x)$ through the bare coupling as

$$a_{0,i}(x) = \left(\frac{\alpha_{i,0}}{4\pi} \right) \left(\frac{\mu^2}{m^2} \right)^\epsilon (-2 + i0^+)^{\eta/2} \left(\frac{-\nu^2}{x} \right)^{\eta/2}, \quad i \in \{s, e\}, \quad (5.49)$$

with an analogous expression for the renormalised couplings.

5.5.2 Collinear contribution for $t \rightarrow W^\pm b$

Looking at (5.48), the pole in $1/\eta$ seems like a catastrophe as we are required to set $\eta \rightarrow 0$ in the end. Luckily, there is still the contribution from collinear region to consider. Z_q is much more complicated than \mathcal{S} with the full result given in (B.17). The relevant n_m bit however is simple enough

$$\begin{aligned} \sqrt{Z_q}|_{n_m} = (a_0(s))^2 C_F n_m \frac{2}{3} & \left[\frac{1}{\eta} \left(\frac{1}{\epsilon^2} - \frac{5}{3\epsilon} + \frac{28}{9} + 2\zeta_2 \right) - \frac{1}{\epsilon^3} + \frac{1}{2\epsilon^2} + \frac{1}{\epsilon} \left(-\frac{55}{24} - 3\zeta_2 \right) \right. \\ & \left. + \frac{1675}{432} - 2\zeta_2 + \zeta_3 \right] + \mathcal{O}(a_s^3, \epsilon, \eta). \end{aligned} \quad (5.50)$$

Because Z_q also has a pole in η , their sum, as mandated by (5.45a) is finite in the analytic regulator η . In other words, after finishing the massification, the result is again free of extra divergences and reproduces the result obtained by calculating the amplitude directly.

However, in doing so a new anomalous logarithm is created because the arguments of a_0 in Z_q and \mathcal{S} differ. Schematically,

$$\sqrt{Z_q} + \mathcal{S} \sim \left(\frac{-\nu^2}{s} \right)^{\eta/2} \frac{1}{\eta} - \left(\frac{-\nu^2}{mM} \right)^{\eta/2} \frac{1}{\eta} = \frac{1}{2} \log \frac{mM}{s} + \mathcal{O}(\eta). \quad (5.51)$$

Combined with the terms $\log(\mu^2/m^2)$ from expanding a_0 in ϵ , this means that the two-loop form factors contain terms $(\log m)^3$ instead of just $(\log m)^2$ suggested by naive counting. This extraneous logarithm is cancelled when the process is combined with the pair-production process $t \rightarrow W^\pm b + bb$.

5.5.3 The soft function for $\gamma^* \rightarrow qq$

For this process, the soft function was first calculated in [113] as

$$\mathcal{S}'_{[113]} = 1 + \left(\frac{\alpha}{4\pi}\right)^2 C_F \int [dk] \frac{(-2p^\mu)(-2q^\nu)}{(k^2)^2(2p \cdot k)(2q \cdot k)} \Pi_{(n_m)}^{\mu\nu}(k). \quad (5.52)$$

This definition is motivated by the eikonal approximation and does not lead to a factorisation anomaly. Our definition of the soft contribution to the heavy-quark form factor is motivated by SCET. For consistency with the collinear contribution, one also has to introduce the same regulator here. Our definition therefore reads

$$\mathcal{S}' = 1 + \left(\frac{\alpha}{4\pi}\right)^2 C_F \int [dk] \frac{(-2p_+^\mu)(-2q_-^\nu)}{(k^2)^2(2p_+ \cdot k)^{1+\eta}(2q_- \cdot k)} \Pi_{(n_m)}^{\mu\nu}(k), \quad (5.53)$$

where p is assumed to scale anti-collinear and q collinear. Because any integral of the form

$$I(n_1, n_2, n_3) \equiv \int [dk] \frac{1}{(k^2)^{n_1}(2p_+ \cdot k)^{n_2}(2q_- \cdot k)^{n_3}} \Pi_{(n_m)}^{\mu\nu}(k) \quad (5.54)$$

depends on p_+ and q_- only through $s = 2p_+ \cdot q_-$, it is invariant under simultaneous rescaling $p_+ \rightarrow \lambda p_+$, $q_- \rightarrow q_-/\lambda$. This implies $I(n_1, n_2, n_3) = \lambda^{-n_2} \lambda^{n_3} I(n_1, n_2, n_3)$ and, hence, $I = 0$ unless $n_2 = n_3$. However, due to the regulator (5.47), n_2 can never be equal to n_3 . Hence, all occurring integrals vanish and $\mathcal{S}' = 1$ at two loops. For the heavy-quark form factor, the factorisation anomaly in Z_q is therefore not cancelled by an anomaly in the soft contribution. In the following we show that, instead, it is cancelled by an anomaly in \bar{Z}_q . This is a contribution analogous to Z_q , but due to the anti-collinear fermion.

5.5.4 Comparison with the heavy-quark form factor

The collinear contribution, Z_q , agrees with a corresponding expression obtained in [112] apart from the n_m terms that were not considered there. However, the different treatment of the soft function makes a direct comparison with [113] difficult. Instead, we have to include the anti-collinear contribution \bar{Z}_q whose n_m term (cf. (B.19))

$$\begin{aligned} \sqrt{\bar{Z}_q} \Big|_{n_m} &= \left(a_s^0(m^2)\right)^2 C_F n_m \frac{2}{3} \left[-\frac{1}{\eta} \left(\frac{1}{\epsilon^2} - \frac{5}{3\epsilon} + \frac{28}{9} + 2\zeta_2 \right) + \frac{1}{2\epsilon^3} - \frac{5}{6\epsilon^2} - \frac{253}{72\epsilon} \right. \\ &\quad \left. + \frac{5083}{432} - \frac{14}{3}\zeta_2 - \zeta_3 \right] + \mathcal{O}(a_s^3, \epsilon, \eta) \end{aligned} \quad (5.55)$$

is different from the one of Z_q , again cancelling the pole in η . We find agreement for

$$Z_{[112]} = \sqrt{Z_q \times \bar{Z}_q} \Big|_{n_m \rightarrow 0} \quad \text{and} \quad Z_{[113]} \times \mathcal{S}'_{[113]} = \sqrt{Z_q \times \bar{Z}_q} \times \mathcal{S}'. \quad (5.56)$$

Hence, our results agree with previous ones but extend them to processes where additional fermions with a large mass are present. This agreement as well as the fact that Z_q is the same for the heavy-to-light and heavy-quark form factors is a strong indication that the factorisation presented here is general.

5.5.5 Summary

With massification we have an extremely powerful tool at hand to calculate the leading mass effects, i.e. the logarithms $\log m$, of any one- or two-loop matrix element where m is the smallest scale involved. Unfortunately, this means that massification cannot yet be used to calculate real-virtual or real-virtual-virtual matrix elements because those will contain a scale associated to the energy of the real photon. When integrating over phase space with FKS², this energy can become arbitrarily small s.t. the assumption that the mass m is the smallest scale is no longer justified.

For any valid process, we need to write

$$\mathcal{A}(m) = \prod_{\text{inc}} \sqrt{\bar{Z}_q} \times \prod_{\text{out}} \sqrt{Z_q} \times \mathcal{S} \times \mathcal{A}(0) + \mathcal{O}\left(\frac{m^2}{\{s, t, M^2, \dots\}}\right). \quad (5.57)$$

This is very similar to the LSZ formula except that the products only run over incoming and outgoing light but non massless flavours (n_m). The function $\mathcal{S} = 1 + \delta\mathcal{S}$ is process dependent but $\delta\mathcal{S} \propto n_m$ and hence is relatively simple to calculate.

There is one remaining problem related to the factorisation anomaly. In (5.49), we are forced to choose a scale of the anomaly that is different in Z_q , \bar{Z}_q , and \mathcal{S} . Presently it is unclear how this scale must be chosen.

The anomaly also has the unfortunate side effect of giving rise to logarithms with higher power than suggested by naive counting. For example at two-loop, the higher power one would naively expect is $\log^2 m$. This is raised to $\log^3 m$ due to the anomaly. Hence, power-suppressed terms $m^i \log^j m$ too might be larger than expected. Luckily all of this happens only in the n_m part of the amplitude that is generally easier to obtain with full m dependence than the remaining amplitude.

This is especially true considering that one might also need to include contributions from the HVP that in any case need to be done numerically. Some progress has been made to efficiently include HVP effects also in complicated loop diagrams [142, 143]. As a side effect, this also allows the exact numerical calculation of the n_m terms with just one finite numerical integration.

Chapter 6

The Monte Carlo code MCMULE

MCMULE (Monte carlo for Muons and other leptons) is a generic framework for higher-order QED calculations of scattering and decay processes involving leptons. It is written in Fortran 95 with two types of users in mind. First, several processes are implemented, some at NLO, some at NNLO. For these processes, the user can define an arbitrary (infrared safe), fully differential observable and compute cross sections and distributions. MCMULE's processes, present and future, are listed in Table 6.1 together with the relevant experiments for which the cuts are implemented. Second, the program is set up s.t. additional processes can be implemented by supplying the relevant matrix elements.

The code can be found at

<https://gitlab.psi.ch/mcmule/mcmule>

The internal version of the code can be found at

<https://gitlab.psi.ch/mcmule/monte-carlo>

Access will be granted by the MCMULE core team (MMCT), usually for new collaborators who wish to extend MCMULE in meaningful ways.

This chapter will often refer to MCMULE's online manual [144] for specific details. This is to avoid deprecating this document as new processes are added and technical details may change. In any case, the online manual will be authoritative.

MCMULE consists of several modules with a simple, mostly hierarchic structure. In this chapter we will describe this structure as follows: First, we give an overview with a brief description of all modules and how they are connected in Section 6.1. Next, we discuss in Section 6.2 how the code works and how to run it on the basis of a simple process, the radiative tau decay $\tau \rightarrow \nu\bar{\nu}e\gamma$. We also discuss tools to analyse the output of MCMULE. Technical aspects of MCMULE are discussed in Section 6.4. Finally, we describe in Section 6.5 on how to implement additional processes in MCMULE.

6.1 Structure of MCMULE

MCMULE is written in Fortran 95 with helper and analysis tools written in python. To obtain a copy of MCMULE we recommend the following approach

```
$ git clone --recursive https://gitlab.psi.ch/mcmule/mcmule
```

To build MCMULE, a Fortran compiler such as gfortran and a python installation is needed. The main executable can be compiled by running

```
$ ./configure
$ make mcmule
```

process	order	experiments	comments	status
$\mu \rightarrow \nu \bar{\nu} e$	NNLO	MEG I&II	polarised, massified & exact	[6]
$\mu \rightarrow \nu \bar{\nu} e \gamma$	NLO	MEG I	polarised	[3]
$\mu \rightarrow \nu \bar{\nu} e e e$	NLO	Mu3e	polarised	[1]
$\mu \rightarrow \nu \bar{\nu} e \gamma \gamma$	LO	MEG	polarised	priv. comm.
$\tau \rightarrow \nu \bar{\nu} e \gamma$	NLO	BaBar	cuts in lab frame	[3]
$\tau \rightarrow \nu \bar{\nu} l l l$	NLO	Belle II		*
$e \mu \rightarrow e \mu$	NLO	MUonE		complete
	NNLO		purely electronic corrections	[7]
			mixed (massified)	†
$\ell p \rightarrow \ell p$	NNLO	P2, MUSE, Prad	only leptonic corrections	complete
$e^- e^- \rightarrow e^- e^-$	NNLO	Prad		*
$e^+ e^- \rightarrow e^+ e^-$	NNLO			†
$e^+ e^- \rightarrow \gamma \gamma$	NNLO	PADME		†
$e^+ e^- \rightarrow \mu^+ \mu^-$	NNLO	Belle	massified	†

Table 6.1: A list of processes that are either already included in MCMULE, almost implemented (*), or planned to be implemented (†).

Alternatively, we provide a Docker container [145] for easy deployment and legacy results. In multi-user environments, *udocker* [146] can be used instead. In either case, a pre-compiled copy of the code can be obtained by calling

```
$ docker pull yulrich/mcmule # requires Docker to be installed
$ udocker pull yulrich/mcmule # requires uDocker to be installed
```

When started, *mcmule* reads options from *stdin* as specified in Table 6.5 (cf. Section 6.2). The value and error estimate of the integration is printed to *stdout* and the full status of the integration is written in a machine-readable format into a folder called *out/* (see below).

The structure of the code and the relation between the most important Fortran modules is depicted in Figure 6.2. A solid arrow indicates “using” the full module, whereas a dashed arrow is indicative of partial use. In what follows we give a brief description of the various modules and mention some variables that play a prominent role in the interplay between the modules.

global_def: This module simply provides some parameters such as fermion masses that are needed throughout the code. It also defines *prec* as a generic type for the precision used.¹⁷ Currently, this simply corresponds to double precision.

functions: This module is a library of basic functions that are needed at various points in the code. This includes dot products, eikonal factors, the integrated eikonal, and an interface for scalar integral functions among others.

collier: This is an external module [147–150]. It will be linked to MCMULE during compilation and provides the numerical evaluations of the scalar, and in some cases tensor, integral functions in *functions*.

phase_space: The routines for generating phase-space points and their weights are collected in this module. Phase-space routines ending with FKS are prepared for the FKS subtraction procedure with a single unresolved photon. In the weight of such routines a factor ξ_1 is omitted to allow the implementation of the distributions in the FKS method. This

¹⁷For quad precision *prec=16* and the compiler flag *-fdefault-real-16* is required.

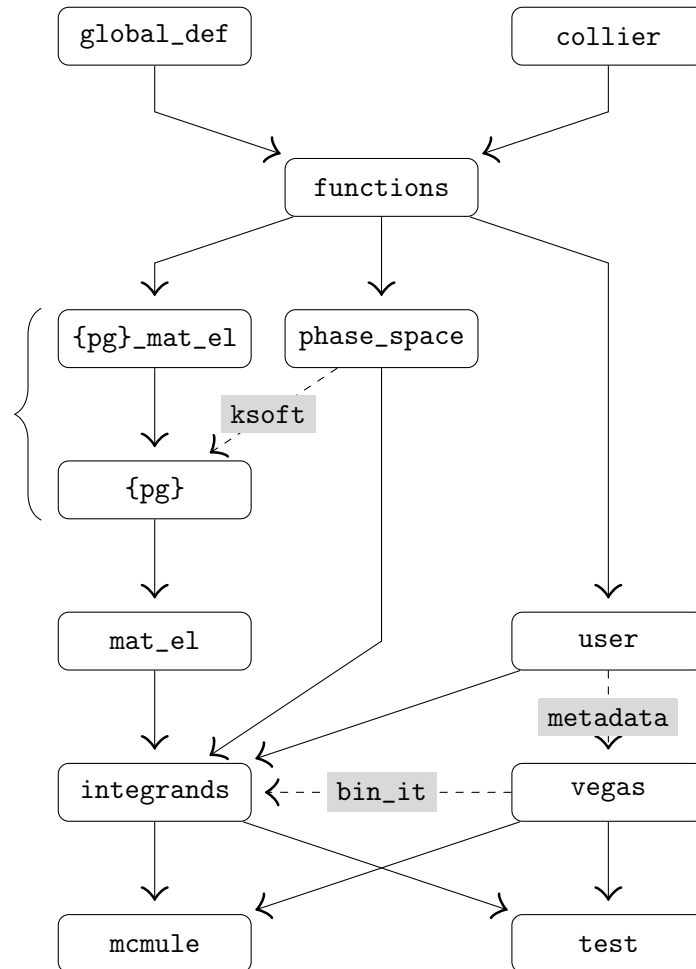


Figure 6.2: The structure of MCMULE.

corresponds to a global variable `xiout1`. This factor has to be included in the integrand of the module `integrands`. Also the variable `ksoft1` is provided that corresponds to the photon momentum without the (vanishing) energy factor ξ_1 . Routines ending with `FKSS` are routines with two unresolved photons. Correspondingly, a factor $\xi_1 \xi_2$ is missing in the weight and `xiout1` and `xiout2`, as well as `ksoft1` and `ksoft2` are provided. To ensure numerical stability it is often required to tune the phase-space routine to a particular kinematic situation.

`{pg}_mat_el` : Matrix elements are grouped into *process groups* such as muon decay (`mudec`) or μ - e and μ - p scattering (`mue`). Each process group contains a `mat_el` module that provides all matrix elements for its group. Simple matrix elements are coded directly in this module. More complicated results are imported from sub-modules not shown in Figure 6.2. A matrix element starting with `P` contains a polarised initial state. A matrix element ending in `av` is averaged over a neutrino pair in the final state (cf. Section 3.3.1).

`{pg}`: In this module the soft limits of all applicable matrix elements of a process group are provided to allow for the soft subtractions required in the FKS scheme. These limits are simply the eikonal factor evaluated with `ksoft` from `phase_space` times the reduced matrix element, provided through `mat_el`.

This module also functions as the interface of the process group, exposing all necessary functions that are imported by

`mat_el`, which collects all matrix elements as well as their particle labelling or *particle identification* (PID).

`user`: For a user of the code who wants to run for an already implemented process, this is the only relevant module. At the beginning of the module, the user has to specify the number of quantities to be computed, `nr_q`, the number of bins in the histogram, `nr_bins`, as well as their lower and upper boundaries, `min_val` and `max_val`. The last three quantities are arrays of length `nr_q`. The quantities themselves, i.e. the measurement function, is to be defined by the user in terms of the momenta of the particles in `quant`. Cuts can be applied by setting the logical variable `pass_cut` to false¹⁸. Some auxiliary functions like (pseudo)rapidity, transverse momentum etc. are predefined in `functions`. Each quantity has to be given a name through the array `names`.

Further, `user` contains a subroutine called `inituser`. This allows the user to read additional input at runtime, for example which of multiple cuts should be calculated. It also allows the user to print some information on the configuration implemented. Needless to say that it is good idea to do this for documentation purposes.

`vegas`: As the name suggests this module contains the adaptive Monte Carlo routine `vegas` [151]. The binning routine `bin_it` is also in this module, hence the need for the binning metadata, i.e. the number of bins and histograms (`nr_bins` and `nr_q`, respectively) as well as their bounds (`min_val` and `max_val`) and names, from `user`.

`integrands`: In this module the functions that are to be integrated by `vegas` are coded. There are three types of integrands: non-subtracted, single-subtracted, and double-subtracted integrands, corresponding to, for example, the three parts of (4.36). The matrix elements to be evaluated and the phase-space routines used are set using function pointers through a subroutine `initpiece`. The factors ξ_i that were omitted in the phase-space weight have to be included here for the single- and double-subtracted integrands.

¹⁸Technically, `pass_cut` is a list of length `nr_q`, allowing to decide whether to cut for each histogram separately.

mcmule: This is the main program, but actually does little else than read the inputs and call `vegas` with a function provided by `integrands`.

test: For developing purposes, a separate main program exists that is used to validate the code after each change. Reference values for matrix elements and results of short integrations are stored here and compared against.

The library of matrix elements deserves a few comments. As matrix elements quickly become very large, we store them separately from the main code. This makes it also easy to extend the program by minimising the code that needs to be changed. We group matrix elements into process groups, *generic processes*, and *generic pieces* as shown in Figure 6.3. The generic process is a prototype for the physical process such as $\ell \rightarrow \nu \bar{\nu} l \gamma$ where the flavour of the leptons ℓ and l is left open. The generic piece describes a part of the calculation such as the real or virtual corrections, i.e. the different pieces of (4.15) (or correspondingly (4.37) at NNLO), that themselves may be further subdivided as is convenient. In particular, in some cases a generic piece is split into various partitions (cf. Section 6.4.1 for details on why that is important). The example shown concerns the real part of NLO contributions to the electronic corrections to μ - e scattering.

When running `mcmule`, the code generates a statefile from which the full state of the integrator can be reconstructed should the integration be interrupted (cf. Section 6.4.4 for details). This makes the statefile ideal to also store results in a compact format. To analyse these results, we provide a python tool `pymule`, additionally to the main code for MCMULE. `pymule` uses `numpy` [152] for data storage and `matplotlib` for plotting [153]. While `pymule` works with any python interpreter, IPython [154] is recommended. We will encounter `pymule` in Section 6.2.2 when we discuss how to use it to analyse results. A full list of functions provided can be found in the online manual of `pymule` [144].

6.2 Running MCMULE: an example

In order to provide a simple example with concrete instructions on how to run the code and to illustrate how it works, we consider the radiative decay of the tau $\tau \rightarrow e[\nu\bar{\nu}]\gamma$. Since the neutrinos are not detected, we average over them, indicated by the brackets (cf. Section 3.3.1). Hence, we have to be fully inclusive w.r.t. the neutrinos. Still, the code allows to make any cut on the other final-state particles. As we will see, the BR for this process, as measured by BABAR [39, 40] has a discrepancy of more than 3σ from the SM value. This will illustrate the importance of fully differential NLO corrections in QED.

6.2.1 Preparations

To be concrete let us assume that we want to compute two distributions, the invariant mass of the $e\gamma$ pair, $m_{\gamma e} \equiv \sqrt{(p_e + p_\gamma)^2}$, and the energy of the electron, E_e , in the rest frame of the tau. To avoid an IR singularity in the BR, we have to require a minimum energy of the photon. We choose this to be $E_\gamma \geq 10$ MeV as used in [39, 40].

As mentioned in Section 6.1 the quantities are defined in the module `user` (`src/user.f95`). At the beginning of the module we set

```
nr_q = 2
nr_bins = 90
min_val = (/ 0._prec, 0._prec /)
max_val = (/ 1800._prec, 900._prec /)
```



Figure 6.3: The structure of process group, generic process, and generic piece as used by MCMULE.

where we have decided to have 90 bins for both distributions and `nr_q` determines the number of distributions. The boundaries for the distributions are set as $0 < m_{\gamma e} < 1800 \text{ MeV}$ and $0 \leq E_e \leq 900 \text{ MeV}$.

The quantities themselves are defined in the function `quant` of the module `user`. This function takes arguments, `q1` to `q7`. These are the momenta of the particles, arrays of length 4 with the fourth entry the energy. Depending on the process though not all momenta are needed and may be zero.

The PID, i.e. which momentum corresponds to which particle, can be looked up in the online documentation of MCMULE as well as the file `mat_e1.f95`, as it may change as new processes are added or modified. In our case we have `q1` for the incoming τ , `q2` for the outgoing e , and `q5` for the outgoing γ . At NLO, we will also need `q6` for the second γ . The momenta of the neutrinos do not enter, as we average over them.

Schematically, the function `quant` is shown in Listing 6.4. Here we have used `sq` provided by `functions` to compute the square of a four-vector. We have also specified the polarisation vector `pol1` s.t. the initial tau is considered unpolarised. The variable `pass_cut` controls the cuts. Initially it is set to true, to indicate that the event is kept. Applying a cut amounts to setting `pass_cut` to false. The version of `quant` in Listing 6.4 will work for a LO calculation, but will need to be adapted for the presence of a second photon in an NLO computation. Being content with LO for the moment, all that remains to be done is prepare the input read by `mcmule` from `stdin`, as specified in Table 6.5.

To be concrete let us assume we want to use 10 iterations with 1000×10^3 points each for pre-conditioning and 50 iterations with 1000×10^3 points each for the actual numerical evaluation (cf. Section 6.3.1 for some heuristics to determine the statistics needed). We pick a *random seed* between 0 and $2^{31} - 1$ (cf. Section 6.4.3), say 70998, and for the input variable `which_piece` we enter `m2enng0`. This stands for the generic process $\mu \rightarrow \nu \bar{\nu} e \gamma$ and 0 for tree level. The `flavour` variable is now set to `tau-e` to change from the generic process $\mu \rightarrow \nu \bar{\nu} e \gamma$ to the process we are actually interested in, $\tau \rightarrow \nu \bar{\nu} e \gamma$. This system is used for other processes as well. The input variable `which_piece` determines the generic process and the part of it that is to be computed (i.e. tree level, real, double virtual etc.). In a second step, the input `flavour` associates actual numbers to the parameters entering the matrix elements and phase-space generation.

Obviously, in practice the input will typically not be given by typing in by hand. In Listing 6.6, we have listed four equivalent ways to input this data into `mcmule`. The two variables `xinormcut1` and `xinormcut2` have no effect at all for a tree-level calculation and will be discussed below in the context of the NLO run. We also ignore the optional input for the moment.

Now the mule is ready to trot. The first step it does in `mcmule` is to associate the numerical values of the masses, as specified through `flavour`. In particular, we set the generic masses `Mm` and `Me` to `Mtau` and `Me1`. This is done in `initflavour`, defined in `global_def`. For other processes this might also involve setting e.g. centre-of-mass energies `scms` to default values.

Next, the function to be integrated by `vegas` is determined. This is a function stored in `integrand`s. There are basically three types of integrands: a standard, non-subtracted integrand `sigma_0`, a single-subtracted integrand needed beyond LO `sigma_1`, and a double-subtracted integrand needed beyond NLO `sigma_2`. Which integrand is needed and what matrix elements and phase-space it depends on is determined by calling the function `initpiece` which uses the variable `which_piece` to point function pointers at the necessary procedures. For our LO case, `initpiece` sets the integrand to `sigma_0` and fixes the dimension of the integration to `ndim = 8`. The matrix element pointer is assigned to the matrix element that needs to be called, `Pm2enngAV(q1,n1,q2,q3,q4,q5)`. The name of the function suggests we compute $\mu(q_1, n_1) \rightarrow [\nu(q_3)\bar{\nu}(q_4)]e(q_2)\gamma(q_5)$ with the polarisation vector `n1` of the initial lepton, and the neutrinos are averaged over. Note that the momenta of the neutrinos are given as arguments, even if they are

```

FUNCTION QUANT(Q1,Q2,Q3,Q4,Q5,Q6,Q7)
...
pass_cut = .true.

if(q5(4) < 10._prec) pass_cut = .false.
pol1 = (/ 0._prec, 0._prec, 0._prec, 0._prec /)

names(1) = 'minv'
quant(1) = sqrt(sq(q2+q5))

names(2) = 'Ee'
quant(2) = q2(4)

END FUNCTION QUANT

```

Listing 6.4: An example for the function `quant` to calculate the radiative τ decay. Note that this is only valid at LO and should not be used in any actual calculation.

Variable name	Data type	Comment
nenter_ad	integer	calls / iteration during pre-conditioning
itmx_ad	integer	iterations during pre-conditioning
nenter	integer	calls / iteration during main run
itmx	integer	iterations during main run
ran_seed	integer	random seed z_1
xinormcut	real(prec)	the $0 < \xi_c \leq 1$ parameter
delcut	real(prec)	the δ_{cut} parameter (or at NNLO the second ξ_c)
which_piece	char(10)	the part of the calculation to perform
flavour	char(8)	the particles involved
(opt)	unknown	the user can request further input during <code>userinit</code>

Table 6.5: The options read from `stdin` by MCMULE. The calls are multiplied by 1000.

```

$ ./mcmule
1000
10
10000
50
70998
1.0
1.0
m2enng0
tau-e
$ ./mcmule < b1.in
$ echo "1000\n10\n10000\n50\n70998\n1.0\n1.0\nm2enng0\ntau-e" \
| ./mcmule

```

Listing 6.6: Methods to enter configuration into MCMULE. All four invocations will result in the same run assuming the text file `r1.in` contains the correct data.

redundant. This simplifies the code a lot because it means that all matrix elements have the same calling convention.

The interplay between the function `sigma_0(x,wgt,ndim)` and `vegas` is as usual, through an array of random numbers `x` of length `ndim`. In addition there is the `vegas` weight of the event, `wgt` due to the Jacobian introduced by the importance sampling. The function `sigma_0` simply evaluates the complete weight `wg` of a particular event by combining `wgt` with the matrix element supplemented by symmetry, flux, and phase-space factors. In a first step a phase-space routine of `phase_space` is called. For our LO calculation, `initpiece` pointed a pointer to the phase-space routine `psd5_25(x, p1,Mm, p2,Me, p3,0., p4,0., p5,0., weight)`. The `d` in the name of the phase-space routine indicates that we are considering a decay process (one initial state particle), the `5` indicates the total number of momenta generated and the meaning of `fks` will be explained below. The other labels indicate the particular tuning and partition which are irrelevant in this case (cf. Section 6.4.1). With these momenta the observables to be computed are evaluated with a call to `quant`. If one of them passes the cuts, the variable `cuts` is set to true. This triggers the computation of the matrix element and the assembly of the full weight. In a last step, the routine `bin_it`, stored in `vegas`, is called to put the weight into the correct bins of the various distributions. If the variable under- or overshoots the bounds specified by `min_val` and `max_val`, the event is placed into dedicated, infinitely big under- and overflow bins. These steps are done for all events and those after pre-conditioning are used to obtain the final distributions.

For a corresponding computation at NLO, a few things need to be modified. First, the observables have to be specified more carefully. In particular, we need to decide how we treat the additional photon due to real radiation. In our example we will consider the exclusive radiative decay, i.e. we request precisely one photon with energy $E_\gamma > 10$ MeV. The function `quant` will have to take this into account with the additional argument `q6`, the momentum of the second photon.

An example of how this could be done is shown in Listing 6.7. Here we have just defined the harder and softer photon `gah` and `gas`, respectively, and require that the former (latter) has energy larger (smaller) than 10 MeV. This version of `quant` is also suitable for the LO calculation, and to ensure infrared-safety, it is generally advisable to use a single `quant` function for all parts of a computation. This is also mandatory if LO and NLO runs are done in one go, as discussed below.

With this version of `quant` we evaluate the virtual and real corrections, as well as the infrared counterterm (i.e. the integrated eikonal times the tree-level matrix element.) The latter is often combined with the virtual corrections. The corresponding `which_piece` are `m2enngV`, `m2enngR`, and `m2enngC`, respectively. If the counterterm is combined with the virtual part, we would use `m2enngF` which is not implemented.

6.2.2 Running and analysing

When we run MCMULE, we will want to choose various random seeds and different values for the unphysical parameter ξ_c . Checking the independence of physical results on the latter serves as a consistency check. To do this, it helps to disentangle `m2enngF` into `m2enngV` and `m2enngC`. Only the latter depends on ξ_c and this part is typically much faster in the numerical evaluation. However, this can quickly lead to a rather large number of runs that need to be taken care of. We often also disentangle the *vacuum polarisation* (VP) contributions. In this case they would be called `m2enngA` though this particular piece does not exist.

```

FUNCTION QUANT(Q1,Q2,Q3,Q4,Q5,Q6,Q7)
...
  pass_cut = .true.

  qq5 = 0._prec
  qq6 = 0._prec
  if(present(q5)) qq5=q5
  if(present(q6)) qq6=q6

  if (qq5(4) > qq6(4)) then
    gah = qq5 ; gas = qq6
  else
    gah = qq6 ; gas = qq5
  endif

  if (gah(4) < 10.) pass_cut = .false.
  if (gas(4) > 10.) pass_cut = .false.

names(1) = 'minv'
quant(1) = sqrt(sq(q2+gah))

names(2) = 'Ee'
quant(2) = q2(4)

END FUNCTION QUANT

```

Listing 6.7: An example for the function `quant` to calculate the radiative τ decay at NLO. This implementation is IR safe and exclusive w.r.t. extra photons.

```

$ python pymule create -i
What generic process? [m2enn] m2enng
Which flavour combination? [mu-e] tau-e
How many / which seeds? [5]
Which xi cuts? [[0.5, 0.25, 0.125]]
Where to store data? [m2enngtau-e] babar-tau-e
Which pieces? [['0', 'V', 'R']] 0, V, C, R
How much statistics for 0 (pc, pi, c, i)? [(10000, 20, 100000, 100)]
    ↪ 1000,10,1000,50
How much statistics for V (pc, pi, c, i)? [(10000, 20, 100000, 100)]
    ↪ 1000,10,1000,50
How much statistics for C (pc, pi, c, i)? [(10000, 20, 100000, 100)]
    ↪ 1000,10,1000,50
How much statistics for R (pc, pi, c, i)? [(10000, 20, 100000, 100)]
    ↪ 5000,50,10000,100
Building files. To rerun this, execute
python pymule create\
    --seeds 70998 66707 69184 75845 63937 \
    -xi 0.5 0.25 0.125 \
    --flavour tau-e \
    --genprocess m2enng \
    --output-dir babar-tau-e \
    --prog mcmule \
    --stat R,5000,50,10000,100 \
    --stat 0,1000,10,1000,50 \
    --stat V,1000,10,1000,50 \
    --stat C,1000,10,1000,50
Expect 3750 iterations, 20.250000G calls
Created menu, config and submit script in babar-tau-e
Please change the ntasks and time options accordingly

```

Listing 6.8: The steps necessary to use `pymule` to prepare running MCMULE. Input by the user is shown in bold. A red arrow indicates a graphical line wrap. Note that numbers listed as seeds are random and hence not reproducible.

A particularly convenient way to run MCMULE is using *menu files*¹⁹. A menu file contains a list of jobs to be computed s.t. the user will only have to vary the random seed and ξ_c by hand as the statistical requirements are defined globally in a *config file*. This is completed by a *submission script*, usually called `submit.sh`. The submit script is what will need to be launched. It will take care of the starting of different jobs. It can be run on a normal computer or on a Slurm cluster [155].

To prepare the run in this way we can use `pymule` as shown in Listing 6.8. When using the tool, we are asked various questions, most of which have a default answer in square brackets. In the end `pymule` will create a directory that the user decided to call `babar-tau-e`, where all results will be stored. The menu and config files generated by `pymule` are shown in Figure 6.9

To start `mcmule`, we now just need to execute the created `babar-tau-e/submit.sh`. Note

¹⁹The name menu was originally used by the cryptanalysts at Bletchley Park to describe a particular set of configurations for the ‘computer’ to try

```

## Generated at 16:00 on February 28 2020 by yannickulrich
# git version: redesign (b558978)

conf babar-tau-e/m2enng-tau-e.conf

run 70998 0.500000 m2enng R tau-e 0
run 66707 0.500000 m2enng R tau-e 0
...

run 70998 0.250000 m2enng R tau-e 0
...

run 70998 1.000000 m2enng0 tau-e 0
...

run 70998 1.000000 m2enng V tau-e 0
...

run 70998 0.500000 m2enng C tau-e 0
...
run 70998 0.250000 m2enng C tau-e 0
...

```

(a) Menu file menu-m2enn-tau-e.menu

```

## Generated at 16:00 on February 28 2020 by yannickulrich
# git version: redesign (b558978)

# specify the program to run relative to 'pwd'
binary=mcmule

# specify the output folder
folder=babar-tau-e/

# Specify the variables nenter_ad, itmx_ad, nenter and itmx
# for each piece you want to run.
declare -A STAT=(
  ["m2enngR"]="5000\n50\n10000\n100"
  ["m2enng0"]="1000\n10\n1000\n50"
  ["m2enngV"]="1000\n10\n1000\n50"
  ["m2enngC"]="1000\n10\n1000\n50"
)

```

(b) Configuration file m2enng-tau-e.conf

Listing 6.9: The files required for the present calculations as generated in Listing 6.8. The file has been massively shortened for presentation. The online manual of MCMULE has the full file.

that per default this will spawn at most as many jobs as the computer `pymule` ran on had CPU cores. If the user wishes a different number of parallel jobs, change the fifth line of `babar-tau-e/submit.sh` to

```
#SBATCH --ntasks=<number of cores>
```

After running the code, we need to combine the various `which_pieces` into physical results that we will want to use to create plots. For this purpose, we provide the python tool `pymule`, though of course other tools can be used as well. Here, we will only cover the aspects of `pymule` required for the present analysis as shown in Listing 6.10; a full documentation can be found in the `docstrings` used in `pymule` as well as the online manual [144]. First, we import `pymule`. Next, we need to point `pymule` to the output directory of `mcmule` with the `setup` command. In our example this is `babar-tau-e/out`.

As a next step, we import the LO and NLO `which_pieces` and combine them using two central `pymule` commands: `sigma` and `mergefks`. `sigma` takes the `which_piece` as an argument and imports matching results, already merging different random seeds. `mergefks` takes the results of (multiple) `sigma` invocations, adds results with matching ξ_c values and combines the result. In the present case, $\sigma_n^{(1)}$ is split into multiple contributions, namely `m2enngV` and `m2enngC`. This is indicated by the `anyxi` argument.

Users should keep in mind that MCMULE ships with a version of `global_def` where the couplings $G_F = \mathbf{GF}$ and $\alpha = \mathbf{alpha}$ are set to $G_F = \alpha = 1$. Hence, we use `pymule`'s function `scaleset` to multiply the result with the correct values of G_F (in MeV^{-1}) and α (in the OS scheme).

Next, we can use some of `pymule`'s tools (cf. Listing 6.10) to calculate the full NLO BRs from the corrections and the LO results

$$\mathcal{B}|_{\text{LO}} = 1.8339(1) \times 10^{-2}, \quad \mathcal{B}|_{\text{NLO}} = 1.6451(1) \times 10^{-2}, \quad (6.1)$$

which agree with [3, 38], but $\mathcal{B}|_{\text{NLO}}$ is in tension with the value $\mathcal{B}|_{\text{exp}} = 1.847(54) \times 10^{-2}$ reported by BABAR [39, 40]. As discussed in [3, 4] it is very likely that this tension would be removed if a full NLO result was used to take into account the effects of the stringent experimental cuts to extract the signal. We will come back to this issue in Section 7.4.

As a last step, we can use the `matplotlib`-backed `kplot` command to present the results for the distributions (logarithmic for $m_{e\gamma}$ and linear for E_e). The results are shown in Figure 6.11. The upper panel of Figure 6.11a shows the results for the invariant mass $m_{e\gamma}$ at LO (green) and NLO (blue) in the range $0 \leq m_{e\gamma} \leq 1 \text{ GeV}$. Note that this, for the purposes of the demonstration, does not correspond to the boundaries given in the run.

The distribution falls sharply for large $m_{e\gamma}$. Consequently, there are only few events generated in the tail and the statistical error becomes large. This can be seen clearly in the lower panel, where the NLO K factor is shown. It is defined as

$$K^{(1)} = 1 + \delta K^{(1)} = 1 + \frac{d\sigma^{(1)}/dx}{d\sigma^{(0)}/dx}, \quad (6.2)$$

and the band represents the statistical error of the Monte Carlo integration. To obtain a reliable prediction for larger values of $m_{e\gamma}$, i.e. the tail of the distribution, we would have to perform tailored runs. To this end, we should introduce a cut $m_{\text{cut}} \ll m_\tau$ on $m_{e\gamma}$ to eliminate events with larger invariant mass. Due to the adaption in the numerical integration, we then obtain reliable and precise results for values of $m_{e\gamma} \lesssim m_{\text{cut}}$.

Figure 6.11b shows the electron energy distribution, again at LO (green) and NLO (blue). As for $m_{e\gamma}$ the corrections are negative and amount to roughly 10%. Since this plot is linear, they can be clearly seen by comparing LO and NLO. In the lower panel once more the K factor

```

from pymule import *

# To normalise branching ratios, we need the tau lifetime
lifetime = 1/(1000*(6.582119e-25)/(2.903e-13))

# The folder where McMule has stored the statefiles
setup(folder='babar-tau-e/out/')

# Import LO data and re-scale to branching ratio
LO = scaleset(mergefks(sigma('m2enng0')), GF**2*lifetime*alpha)

# Import NLO corrections from the three pieces
NLO = scaleset(mergefks(
    sigma('m2enngR'),      # real corrections
    sigma('m2enngCT'),    # counter term
    anyxi=sigma('m2enngV') # virtual corrections
), GF**2*lifetime*alpha**2)

# The branching ratio at NLO = LO + correction
fullNLO = plusnumbers(LO['value'], NLO['value'])

# Print results
print "BR_0□=□", printnumber(LO['value'])
print "dBR_□□=□", printnumber(NLO['value'])
print "BR_1□=□", printnumber(fullNLO)

# Produce energy plot
fig1, (ax1, ax2) = kplot(
    {'lo': LO['Ee'], 'nlo': NLO['Ee']},
    labelx=r"$E_e\,/\/\,{\rm□MeV}$",
    labelsigma=r"$\D\mathcal{B}/\D□E_e$"
)
ax2.set_ylim(-0.2,0.01)

# Produce visible mass plot
fig2, (ax1, ax2) = kplot(
    {'lo': LO['minv'], 'nlo': NLO['minv']},
    labelx=r"$m_{e\gamma}\,/\/\,{\rm□MeV}$",
    labelsigma=r"$\D\mathcal{B}/\D□m_{e\gamma}$"
)

ax1.set_yscale('log')
ax1.set_xlim(1000,0)
ax1.set_ylim(5e-9,1e-3)
ax2.set_ylim(-0.2,0.)

```

Listing 6.10: An example code to analyse the results for $\tau \rightarrow \nu\bar{\nu}e\gamma$ in pymule. Note that, in the Fortran code $G_F = \alpha = 1$. In pymule they are at their physical values [156].

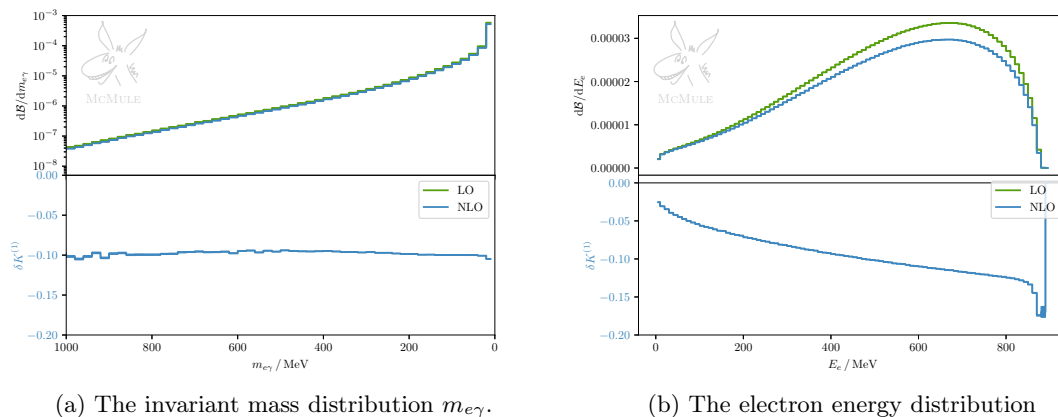


Figure 6.11: Results of the toy run to compute $m_{e\gamma}$ (left) and E_e (right) for $\tau \rightarrow \nu\bar{\nu}e\gamma$. Upper panels show the LO (green) and NLO (blue) results, the lower panels show the NLO K factor.

is depicted. Unsurprisingly, at the very end of the distribution, $E_e \sim 900$ MeV, the statistics is out of control.

6.3 General aspects of using MCMULE

In this section, we will collect a few general points of interest regarding MCMULE. In particular, we will discuss heuristics on how much statistics is necessary for different contributions in Section 6.3.1. This is followed by a more in-depth discussion of the analysis strategy in Section 6.3.2.

6.3.1 Statistics

MCMULE is a Monte Carlo program. This means it samples the integrand at N (pseudo-)random points to get an estimate for the integral. However, because it uses the adaptive Monte Carlo integration routine `vegas` [151], we split $N = i \times n$ into i iterations (`itmx`), each with n points (`nenter`). After each iteration, `vegas` changes the way it will sample the next iteration based on the results of the previous one. Hence, the performance of the integration is a subtle interplay between i and n – it is not sufficient any more to consider their product N .

Further, we always perform the integration in two steps: a pre-conditioning with $i_{\text{ad}} \times n_{\text{ad}}$ (`nenter_ad` and `itmx_ad`, respectively), that is used to optimise the integration strategy and after which the result is discarded, and a main integration that benefits from the integrator’s understanding of the integrand.

Of course there are no one-size-fits-all rules of how to choose the i and n for pre-conditioning and main run. However, the following heuristics have proven helpful:

- n is always much larger than i . For very simple integrands, $n = \mathcal{O}(10 \cdot 10^3)$ and $i = \mathcal{O}(10)$.
- Increasing n reduces errors that can be thought of as systematic because it allows the integrator to ‘discover’ new features of the integrand. Increasing i on the other hand will rarely have that effect and only improves the statistical error. This is especially true for distributions.
- There is no real limit on n , except that it has to fit into the datatype used – integrations with $n = \mathcal{O}(2^{31} - 1)$ are not too uncommon – while i is rarely (much) larger than 100.

- For very stringent cuts it can happen that that typical values of n_{ad} are too small for any point to pass the cuts. In this case `vegas` will return `NaN`, indicating that no events were found. Barring mistakes in the definition of the cuts, a pre-pre-conditioning with extremely large n but $i = 1-2$ can be helpful.
- n also needs to be large enough for `vegas` to reliably find all features of the integrand. It is rarely obvious that it did, though sometimes it becomes clear when increasing n or looking at intermediary results as a function of the already-completed iterations.
- The main run should always have larger i and n than the pre-conditioning. Judging how much more is a delicate game though $i/i_{\text{ad}} = \mathcal{O}(5)$ and $n/n_{\text{ad}} = \mathcal{O}(10-50)$ have been proven helpful.
- If, once the integration is completed, the result is unsatisfactory, take into account the following strategies
 - A large $\chi^2/\text{d.o.f.}$ indicates a too small n . Try to increase n_{ad} and, to a perhaps lesser extent, n .
 - Increase i . Often it is a good idea to consciously set i to a value so large that the integrator will never reach it and to keep looking at ‘intermediary’ results.
 - If the error is small enough for the application but the result seems incorrect (for example because the ξ_c dependence does not vanish), massively increase n .
- Real corrections need much more statistics in both i and n ($\mathcal{O}(10)$ times more for n , $\mathcal{O}(2)$ for i) than the corresponding LO calculations because of the higher-dimensional phase-space.
- Virtual corrections have the same number of dimensions as the LO calculation and can go by with only a modest increase to account for the added functional complexity.
- `vegas` tends to underestimate the numerical error.

These guidelines are often helpful but should not be considered infallible as they are just that – guidelines.

MCMULE is not parallelised; however, because Monte Carlo integrations require a random seed anyway, it is possible to calculate multiple estimates of the same integral using different random seeds z_1 and combining the results obtained this way. This also allows to for a better, more reliable understanding of the error estimate.

6.3.2 Analysis

Once the Monte Carlo has run, an offline analysis of the results is required. This entails loading, averaging, and combining the data. This is automatised in `pymule` but the basic steps are

0. Load the data into a suitable analysis framework such as `python`.
1. Combine the different random seeds into one result per contribution and ξ_c . The $\chi^2/\text{d.o.f.}$ of this merging must be small. Otherwise, try to increase the statistics or choose of different phase-space parametrisation.
2. Add all contributions that combine into one of the physical contributions (4.41b). This includes any partitioning done in Section 6.4.1.

3. (optional) At N^ℓLO, perform a fit²⁰

$$\sigma_{n+j}^{(\ell)} = c_0^{(j)} + c_1^{(j)} \log \xi_c + c_2^{(j)} \log^2 \xi_c + \cdots + c_\ell^{(j)} \log^\ell = \sum_{i=0}^{\ell} c_i^{(j)} \log^i \xi_c. \quad (6.3)$$

This has the advantage that it very clearly quantifies any residual ξ_c dependence. We will come back to this issue in Section 6.5.1.

4. Combine all physical contributions of (4.41a) into $\sigma^{(\ell)}(\xi_c)$ which has to be ξ_c independent.
5. Perform detailed checks on ξ_c independence. This is especially important on the first time a particular configuration is run. Beyond NLO, it is also extremely helpful to check whether the sum of the fits (6.3) is compatible with a constant. In case it is not, try to run the Monte Carlo again with an increased n . `pymule`'s `mergefkswithplot` can be helpful here.
6. Merge the different estimates of (4.41a) from the different ξ_c into one final number $\sigma^{(\ell)}$. The $\chi^2/\text{d.o.f.}$ of this merging must be small.
7. Repeat the above for any distributions produced, though often bin-wise fitting as in Point 3 is rarely necessary or helpful.

If a total cross section is ξ_c independent but the distributions (or a cross section obtained after applying cuts) are not, this is a hint that the distribution (or the applied cuts) is not IR safe.

These steps have been almost completely automatised in `pymule` and Mathematica. Though all steps of this pipeline could be easily implemented in any other language by following the specification of the file format below (Section 6.4.4).

6.4 Technical aspects of MCMULE

In this section, we will review the very technical details of the implementation. This is meant for those readers, who wish to truly understand the nuts and bolts holding the code together. We begin by discussing the phase-space generation and potential pitfalls in Section 6.4.1. Next, in Section 6.4.2, we discuss how the FKS scheme of Chapter 4 is implemented in Fortran code. This is followed by a brief review of the random number generator used in MCMULE in Section 6.4.3. Finally, we give an account of how the statefiles work and how they are used to store distributions in Section 6.4.4.

6.4.1 Phase-space generation

We use the `vegas` algorithm for numerical integration [151]. As `vegas` only works on the hypercube, we need a routine that maps $[0, 1]^{3n-4}$ to the momenta of an n -particle final state, including the corresponding Jacobian. The simplest way to do this uses iterative two-particle phase-spaces and boosting the generated momenta all back into the frame under consideration. An example of how this is done is shown in Listing 6.12.

As soon as we start using FKS, we cannot use this simplistic approach any longer. The c -distributions of FKS require the photon energies ξ_i to be variables of the integration. We can fix this by first generating the photon explicitly as (4.4) and (4.6) and then generate the remaining particles iteratively again. This can always be done and is guaranteed to work.

²⁰Note that it is important to perform the fit after combining the phase-space partitionings (cf. Section 6.4.1) but before adding (4.41a) as this model is only valid for the terms of (4.41b)

For processes with one or more PCS this approach is suboptimal. The numerical integration can be improved by orders of magnitude by aligning the pseudo-singular contribution to one of the variables of the integration, as this allows `vegas` to optimise the integration procedure accordingly. As an example, consider once again $\mu \rightarrow \nu \bar{\nu} e \gamma$. The PCS comes from

$$\mathcal{M}_{n+1}^{(\ell)} \propto \frac{1}{(q \cdot k)^2} = \frac{1}{\xi^2} \frac{1}{(1 - y\beta)^2}, \quad (6.4)$$

where y is the angle between photon (k) and electron (q). For large velocities β (or equivalently small masses), this becomes almost singular as $y \rightarrow 1$. If now y is a variable of the integration this can be mediated. An example implementation is shown in Listing 6.13.

The approach outlined above is very easy to do in the case of the muon decay as the neutrinos can absorb any timelike four-momentum. This is because the δ function of the phase-space was solved through the neutrino's `pair_dec`. However, for scattering processes where all final state leptons could be measured, this fails. Writing a routine for μ - e -scattering

$$e(p_1) + \mu(p_2) \rightarrow e(p_3) + \mu(p_4) + \gamma(p_5), \quad (6.5)$$

that optimises on the incoming electron is rather trivial because its direction stays fixed s.t. the photon just needs to be generated according to (4.4). The outgoing electron p_3 is more complicated. Writing the p_4 -phase-space four- instead of three-dimensional

$$d\Phi_5 = \delta^{(4)}(p_1 + p_2 - p_3 - p_4 - p_5) \delta(p_4^2 - M^2) \Theta(E_4) \frac{d^4 \vec{p}_4}{(2\pi)^4} \frac{d^3 \vec{p}_3}{(2\pi)^3 2E_3} \frac{d^3 \vec{p}_5}{(2\pi)^3 2E_5}, \quad (6.6)$$

we can solve the four-dimensional δ function for p_4 and proceed for the generation p_3 and p_5 almost as for the muon decay above. Doing this we obtain for the final δ function

$$\delta(p_4^2 - M^2) = \delta\left(m^2 - M^2 + s(1 - \xi) + E_3 \sqrt{s} \left[\xi - 2 - y\xi\beta_3(E_3)\right]\right). \quad (6.7)$$

When solving this for E_3 , we need to take care to avoid extraneous solutions of this radical equation [157]. We have now obtained our phase-space parametrisation, albeit with one caveat: for anti-collinear photons, i.e. $-1 < y < 0$ with energies

$$\xi_1 = 1 - \frac{m}{\sqrt{s}} + \frac{M^2}{\sqrt{s}(m - \sqrt{s})} < \xi < \xi_{\max} = 1 - \frac{(m + M)^2}{s} \quad (6.8)$$

there are still two solutions. One of these corresponds to very low-energy electron that are almost produced at rest. This is rather fortunate as most experiments will have an electron detection threshold higher than this. Otherwise, phase-spaces optimised this way also define a `which_piece` for this *corner region*.

There is one last subtlety when it comes to these type of phase-space optimisations. Optimising the phase-space for emission from one leg often has adverse effects on terms with dominant emission from another leg. In other words, the numerical integration works best if there is only one PCS on which the phase-space is tuned. As most processes have more than one PCS we need to resort to something that was already discussed in the original FKS paper [108]. Scattering processes that involve multiple massless particles have overlapping singular regions. The FKS scheme now mandates that the phase-space is partitioned in such a way as to isolate at most one singularity per region with each region having its own phase-space parametrisation. Similarly we have to split the phase-space to contain at most one PCS as well as the soft singularity. In MCMULE μ - e scattering for instance is split as follows²¹

$$1 = \theta(s_{15} > s_{35}) + \theta(s_{15} < s_{35}), \quad (6.9)$$

²¹When implementing this, care must be taken to ensure that the split is also well defined if the photon is soft, i.e. if $\xi = 0$.

with $s_{ij} = 2p_i \cdot p_j$ as usual. The integrand of the first θ function has a final-state PCS and hence we use the parametrisation obtained by solving (6.7). The second θ function, on the other hand, has an initial-state PCS which can be treated by just directly parametrisating the photon in the centre-of-mass frame as per (4.4). This automatically makes $s_{15} \propto (1 - \beta_{\text{in}} y_1)$ a variable of the integration.

For the double-real corrections of μ - e scattering, we proceed along the same lines except now the argument of the δ function is more complicated.

6.4.2 Implementation of FKS schemes

Now that we have a phase-space routine that has ξ_i as variables of the integration, we can start implementing the relevant c -distributions (4.8)

$$\begin{aligned} d\sigma_h^{(1)}(\xi_c) &= d\Upsilon_1 d\Phi_{n,1} \left(\frac{1}{\xi_1} \right)_c d\xi_1 \left(\xi_1^2 \mathcal{M}_{n+1}^{(0)} \right) \\ &= d\xi_1 \frac{1}{\xi_1} \left(d\Upsilon_1 d\Phi_{n,1} \left(\xi_1^2 \mathcal{M}_{n+1}^{(0)} \right) - d\Upsilon_1 d\Phi_{n,1} \left(\mathcal{E} \mathcal{M}_n^{(0)} \right) \theta(\xi_c - \xi_1) \right). \end{aligned} \quad (6.10)$$

We refer to the first term as the *event* and the second as the *counter-event*.

Note that, due to the presence of $\delta(\xi_1)$ in the counter-event (that is implemented through the eikonal factor \mathcal{E} , cf. (4.12)) the momenta generated by the phase-space $d\Upsilon_1 d\Phi_{n,1}$ are different. Thus, it is possible that the momenta of the event pass the cuts or on-shell conditions, while those of the counter event fail, or vice versa. This subtlety is extremely important to properly implement the FKS scheme and many problems fundamentally trace back to this.

Finally, we should note that, in order to increase numerical stability, we introduce cuts on ξ and sometimes also on a parameter that encodes the PCS such as $y = y_2$ in (4.4) and Listing 6.13. Events that have values of ξ smaller than this *soft cut* are discarded immediately and no subtraction is considered. The dependence on this slicing parameter is not expected to drop out completely and hence, the soft cut has to be chosen small enough to not influence the result.

An example implementation can be found in Listing 6.14.

6.4.3 Random number generation

A Monte Carlo integrator relies on a (pseudo) *random number generator* (RNG or PRNG) to work. The pseudo-random numbers need to be of high enough quality, i.e. have no discernible pattern and a long period, to consider each point of the integration independent but the RNG needs to be simple enough to be called many billion times without being a significant source of runtime. RNGs used in Monte Carlo applications are generally poor in quality and often predictable s.t. they could not be used for cryptographic applications.

A commonly used trade-off between unpredictability and simplicity, both in speed and implementation, is the Park-Miller RNG, also known as `minstd` [158]. As a linear congruential generator, its $(k+1)$ th output x_{k+1} can be found as

$$z_{k+1} = a \cdot z_k \bmod m = a^{k+1} z_1 \bmod m \quad \text{and} \quad x_k = z_k / m \in (0, 1), \quad (6.11)$$

where m is a large, preferably prime, number and $2 < a < m - 1$ an integer. The initial value z_1 is called the random seed and is chosen integer between 1 and $m - 1$. It can easily be seen that any such RNG has a fixed period²² $p < m$ s.t. $z_{k+p} = z_k$ because any z_{k+1} only depends on z_k

²²Note that, because of the simple recursion the RNG will not repeat any number until the full period is complete

```

! use a random number to decide how much energy should
! go into the first particle
minv3 = ra(1)*energy

! use two random numbers to generate the momenta of
! particles 1 and the remainder in the CMS frame
call pair_dec(ra(2:3),energy,q2,m2,qq3,minv3)

! adjust the Jacobian
weight = minv3*energy/pi
weight = weight*0.125*sq_lambda(energy**2,m2,minv3)/energy**2/pi

! use a random number to decide how much energy should
! go into the second particle
minv4 = ra(4)*energy
! use two random numbers to generate the momenta of
! particles 2 and the remainder in their rest frame
call pair_dec(ra(5:6),minv3,q3,m3,qq4,minv4)

! adjust the Jacobian
weight = weight*minv4*energy/pi
weight = weight*0.125*sq_lambda(minv3**2,m3,minv4)/minv3**2/pi

! repeat this process until all particles are generated

! boost all generated particles back into the CMS frame

q4 = boost_back(qq4, q4)
q5 = boost_back(qq4, q5)

q3 = boost_back(qq3, q3)
q4 = boost_back(qq3, q4)
q5 = boost_back(qq3, q5)

```

Listing 6.12: Example implementation of iterative phase-space. Not shown are the checks to make sure that all particles have at least enough energy for their mass, i.e. that $E_i \geq m_i$.

```

xi5 = ra(1)
y2 = 2*ra(2) - 1.

! generate electron q2 and photon q5 s.t. that the
! photon goes into z diractions

eme = energy*ra(3)
pme = sqrt(eme**2-m2**2)
q2 = (/ 0., pme*sqrt(1. - y2**2), pme*y2, eme /)
q5 = (/ 0., 0., 1., 1. /)
q5 = 0.5*energy*xi5*q5

! generate euler angles and rotate all momenta

euler_mat = get_euler_mat(ra(4:6))

q2 = matmul(euler_mat,q2)
q5 = matmul(euler_mat,q5)

qq34 = q1-q2-q5
minv34 = sqrt(sq(qq34))

! The event weight, note that a factor xi5**2 has been ommited
weight = energy**3*pme/(4.*(2.*pi)**4)

! generate remaining neutrino momenta

call pair_dec(ra(7:8),minv34,q3,m3,q4,m4,enough_energy)
weight = weight*0.125*sq_lambda(minv34**2,m3,m4)/minv34**2/pi

q3 = boost_back(qq34, q3)
q4 = boost_back(qq34, q4)

```

Listing 6.13: Example implementation of a so-called FKS phase-space where the fifth particle is an FKS photon that may becomes soft. Not shown are checks whether $E_i \geq m_i$.

```

FUNCTION SIGMA_1(x, wgt, ndim)

! The first random number x(1) is xi.
arr = x

! Generate momenta for the event using the function pointer ps
call gen_mom_fks(ps, x, masses(1:nparticle), vecs, weight)

! Whether unphysical or not, take the value of xi
xifix = xiout

! Check if the event is physical ...
if(weight > zero ) then
! and whether it passes the cuts
var = quant(vecs(:,1), vecs(:,2), vecs(:,3), vecs(:,4), ...)
cuts = any(pass_cut)
if(cuts) then
! Calculate the  $\xi^2 * M_{n+1}^0$  using the pointer matel
mat = matel(vecs(:,1), vecs(:,2), vecs(:,3), vecs(:,4), ...)
mat = xifix*weight*mat
sigma_1 = mat
end if
end if

! Check whether soft subtraction is required
if(xifix < xicut1) then
! Implement the delta function and regenerate events
arr(1) = 0._prec
call gen_mom_fks(ps, arr, masses(1:nparticle), vecs, weight)
! Check whether to include the counter event
if(weight > zero) then
var = quant(vecs(:,1), vecs(:,2), vecs(:,3), vecs(:,4), ...)
cuts = any(pass_cut)
if(cuts) then
mat = matel_s(vecs(:,1), vecs(:,2), vecs(:,3), vecs(:,4),
↪ ...)
mat = weight*mat/xifix
sigma_1 = sigma_1 - mat
endif
endif
endif
END FUNCTION SIGMA_1

```

Listing 6.14: An example implementation of the FKS scheme in Fortran. Not shown are various checks performed, the binning as well as initialisation blocks.

and there are finitely many possible z_k . We call the RNG attached to (m, a) to be of *full period* if $p = m - 1$, i.e. all integers between 1 and $m - 1$ appear in the sequence z_k .

Assuming $z_1 = 1$ then the existence of p s.t. $z_{p+1} = 1$ is guaranteed by Fermat's Theorem²³. This means that the RNG is of full period iff a is a primitive root modulo m , i.e.

$$\forall g \text{ co-prime to } m \quad \exists k \in \mathbb{Z} \quad \text{s.t.} \quad a^k \equiv g \pmod{m}. \quad (6.12)$$

Park and Miller suggest to use the Mersenne prime $m = 2^{31} - 1$, noting that there are 534,600,000 primitive roots of which 7 is the smallest. Because $7^b \pmod{m}$ is also a primitive root as long as b is co-prime to $(m-1)$, [158] settled on $b = 5$, i.e. $a = 16807$ as a good choice for the multiplier that, per construction, has full period and passes certain tests of randomness.

The points generated by any such RNG will fall into $\sqrt[n]{n! \cdot m}$ hyperplanes if scattered in an n dimensional space [159]. However, for bad choices of the multiplier a the number of planes can be a lot smaller²⁴.

Presently, the period length of $p = m - 1 = 2^{31} - 2$ is believed to be sufficient though detailed studies quantifying this would be welcome.

6.4.4 Differential distributions and intermediary state files

Distributions are always calculated as histograms by binning each event according to its value for the observable S . This is done by having an $(n_b \times n_q)$ -dimensional array²⁵ `quant` where n_q is the number of histograms to be calculated (`nr_q`) and n_b is the number of bins used (`nr_bins`). The weight of each event $d\Phi \times \mathcal{M} \times w$ is added to the correct entry in `bit_it` where $w = \text{wgt}$ is the event weight assigned by `vegas`.

After each iteration of `vegas` we add `quant` (`quant2`) to an accumulator of the same dimensions called `quantsum` (`quantsumsq`). After i iterations, we can calculate the value and error as

$$\frac{d\sigma}{dS} \approx \frac{\text{quantsum}}{\Delta \times i} \quad \text{and} \quad \delta\left(\frac{d\sigma}{dS}\right) \approx \frac{1}{\Delta} \sqrt{\frac{\text{quantsumsq} - \text{quantsum}^2/i}{i(i-1)}}, \quad (6.13)$$

where Δ is the bin-size.

Related to this discussion is the concept of intermediary state files. Their purpose is to record the complete state of the integrator after every iteration in order to recover should the program crash – or more likely be interrupted by a batch system. MCMULE uses a custom file format `.vegas` for this purpose which uses Fortran's record-based (instead of stream- or byte-based) format. This means that each entry starts with 32bit unsigned integer, i.e. 4 byte, indicating the record's size and ends with the same 32bit integer. As this is automatically done for each record, it minimises the amount of metadata that have to be written.

The current version (`v3`) must begin with the magic header and version self-identification shown in Figure 6.15. The latter includes file version information and the first five characters the source tree's SHA1 hash, obtained using `make hash`.

The header is followed by records describing the state of the integrator as shown in Figure 6.16. Additionally to information required to continue integration such as the current value and grid information, this file also has 300 bytes for a message. This is usually set by the routine to store information on the fate of the integration such as whether it was so-far uninterrupted or whether there is reason to believe it to be inconsistent.

²³If p is prime, for any integer a , $a^p - a$ is a multiple of p .

²⁴An infamous example is `randu` that used $a = 2^{16} + 3$ and $m = 2^{31}$ that in three dimension produces only 15 planes instead of the maximum 2344.

²⁵To be precise, the actual dimensions are $(n_b + 2) \times n_q$ to accommodate under- and overflow bins

The latter point is particularly important. While MCMULE cannot read intermediary files from a different version of the file format, it will continue any integration for which it can read the state file. This also includes cases where the source tree has been changed. In this case MCMULE prints a warning but continues the integration deriving potentially inconsistent results.

6.5 Implementing new processes in MCMULE

In this section we will discuss how new processes can be added to MCMULE. Not all of the points below might be applicable to any particular process. Further, all points are merely guidelines that could be deviated from if necessary as long as proper precautions are taken.

As an example, we will discuss how Møller scattering $e^-e^- \rightarrow e^-e^-$ could be implemented.

1. A new process group may need to be created if the process does not fit any of the presently implemented groups. This requires a new folder with a makefile as well as modifications to the main makefile as discussed in the online manual.

In our case, $ee \rightarrow ee$ does not fit any of the groups, so we create a new group that we shall call `ee`.

2. Calculate the tree-level matrix elements needed at LO and NLO: $\mathcal{M}_n^{(0)}$ and $\mathcal{M}_{n+1}^{(0)}$. This is relatively straightforward and – crucially – unambiguous as both are finite in $d = 4$. We will come back to an example calculation in Section 6.5.2.

3. A generic matrix element file is needed to store ‘simple’ matrix elements as well as importing more complicated matrix elements. Usually, this file should not contain matrix elements that are longer than a few dozen or so lines. In most cases, this applies to $\mathcal{M}_n^{(0)}$.

After each matrix element, the PID needs to be denoted in a comment. Further, all required masses as well as the centre-of-mass energy, called `scms` to avoid collisions with the function $\mathbf{s}(\mathbf{p}_i, \mathbf{p}_j) = 2\mathbf{p}_i \cdot \mathbf{p}_j$, need to be calculated in the matrix element to be as localised as possible.

In the case of Møller scattering, a file `ee/ee_mat_e1.f95` will contain $\mathcal{M}_n^{(0)}$. For example, $\mathcal{M}_n^{(0)}$ is implemented there as shown in Listing 6.17.

4. Further, we need an interface file that also contains the soft limits. In our case this is called `ee/ee.f95`.
5. Because $\mathcal{M}_{n+1}^{(0)}$ is border-line large, we will assume that it will be stored in an extra file, `ee/ee2eeg.f95`. The required functions are to be imported in `ee/ee_mat_e1.f95`.
6. Calculate the one-loop virtual matrix element $\mathcal{M}_n^{(1)}$, renormalised in the OS scheme. In particular VP contributions should not be included but implemented in a separate function. Of course, this could be done in any regularisation scheme. However, results in MCMULE shall be in the FDH (or equivalently the FDF) scheme. Divergent matrix elements in MCMULE are implemented as c_{-1} , c_0 , and c_1

$$\mathcal{M}_n^{(1)} = \frac{(4\pi)^\epsilon}{\Gamma(1-\epsilon)} \left(\frac{c_{-1}}{\epsilon} + c_0 + c_1\epsilon + \mathcal{O}(\epsilon^2) \right). \quad (6.14)$$

For c_{-1} and c_0 this is equivalent to the conventions employed by Package-X [97] up to a factor $1/16\pi^2$. While not strictly necessary, it is generally advisable to also include c_{-1} in the Fortran code.

offset	00	01	02	03	04	05	06	07	08	09	0A	0B	0C	0D	0E	0F
hex	09	00	00	00	20	4D	63	4D	75	6C	65	20	20	09	00	00
ASCII	\t				' '	M	c	M	u	l	e	' '	' '	\t		
offset	10	11	12	13	14	15	16	17	18	19	1A	1B	1C	1D	1E	1F
hex	00	0A	00	00	00	76	xx	xx	20	20	20	20	20	20	20	0A
ASCII		\n				v	v_1	v_2	' '	' '	' '	' '	' '	' '	' '	\n
offset	20	21	22	23	24	25	26	27	28	29	2A	2B	2C	2D	2E	2F
hex	00	00	00	05	00	00	00	xx	xx	xx	xx	xx	05	00	00	00
ASCII								s_1	s_2	s_3	s_4	s_5				

Figure 6.15: The magic header and version information used by v3. v_1 indicates the current version number and v_2 whether long integers are used (L) or not (N). s_1 - s_5 indicate the first five characters of the SHA1 hash produced by the source code at compile time (`make hash`).

Off	Len	Type	Var.	Comment
0030	000C	integer	it	the current iteration
003C	000C	integer	ndo	subdiv. on an axis
0048	0010	real	si	$\sigma/(\delta\sigma)^2$
0058	0010	real	swgt	$1/(\delta\sigma)^2$
0068	0010	real	schi	$(1 - \text{it})\chi + \sigma^2/(\delta\sigma)^2$
0078	1A98	real(50,17)	xi	the integration grid
1B10	000C	integer	randy	the current random number seed
1B1C	0014	integer	n_q	number of histograms
		integer	n_b	number of bins
		integer	n_s	len. histogram name
1B30	$10n_q + 8$	real(n_q)	minv	lower bounds
		real(n_q)	maxv	upper bounds
	$n_s n_q + 8$	character(n_s, n_q)	names	names of S
	$10n_q(n_b + 2) + 8$	real(n_q, n_b+2)	quantsum	accu. histograms
		real(n_q, n_b+2)	quantsumsq	accu. histograms squared
-0144	0010	real	time	current runtime in seconds
-0134	0134	character(300)	msg	any message
-0000			EOF	

Figure 6.16: The body of a .vegas file storing all important information. Each horizontal line indicates as dressed record. In the offset and length columns, all integers are in hexadecimal notation. Negative numbers count from the end of file (EOF).

```

FUNCTION EE2EE(p1, p2, p3, p4)
  !! e-(p1) e-(p2) -> e-(p3) e-(p4)
  !! for massive (and massless) electrons
  implicit none
  real(kind=prec), intent(in) :: p1(4), p2(4), p3(4), p4(4), ee2ee
  real(kind=prec) :: den1, den2, t, scms, m2
  t = sq(p1-p3) ; scms = sq(p1+p2) ; m2 = sq(p1)
  den1 = sq(p1-p3) ; den2 = sq(p1-p4)

  ee2ee=(8*m2**2 - 8*m2*scms + 2*s**2 + 2*scms*t + t**2)/den1**2
  ee2ee=ee2ee+2*(12*m2**2 - 8*m2*scms + scms**2) / den1 / den2
  ee2ee=ee2ee+(24*m2**2 + scms**2 + t**2 - 8*m2*(s + t))/den2**2

  ee2ee = ee2ee * 128*pi**2*alpha**2
END FUNCTION

```

Listing 6.17: An example implementation of $\mathcal{M}_n^{(0)}$ for Møller scattering. Note that the electron mass and the centre-of-mass energy are calculated locally. A global factor of $8e^4 = 128\pi^2\alpha^2$ is included at the end.

For NLO calculations, c_1 does not enter. However, we wish to include Møller scattering up to NNLO and hence will need it sooner rather than later anyway.

In our case, we will create a file `ee/ee_ee2eel.f95`, which defines a function

```

FUNCTION EE2EE1(p1, p2, p3, p4, sing, lin)
  !! e-(p1) e-(p2) -> e-(p3) e-(p4)
  !! for massive electrons
  implicit none
  real(kind=prec), intent(in) :: p1(4), p2(4), p3(4), p4(4)
  real(kind=prec) :: ee2eel
  real(kind=prec), intent(out), optional :: sing, lin
  ...
END FUNCTION

```

The function shall return c_0 in `ee2eel` and, if present c_{-1} and c_1 in `sing` and `lin`.

7. At this stage, a new subroutine in the program `test` with reference values for all three matrix elements should be written to test the Fortran implementation. This is done by generating a few points using an appropriate phase-space routine and comparing to as many digits as possible using the routine `check`.

In our case, we would construct a subroutine `TESTEEMATEL` as shown in Listing 6.18

8. Define a default observable in `user` for this process. This observable must be defined for any `which_piece` that might have been defined and test all relevant features of the implementation such as polarisation if applicable.
9. Add the matrix elements to the integrands defined in `integrands.f95` as discussed above. A second test routine should be written that runs short integrations against a reference value. Because `test_INT` uses a fixed random seed, this is expected to be possible very

precisely. To guarantee reproducibility, the reference values for these tests need to be obtained by running MCMULE in a Docker container.

10. After some short test runs, it should be clear whether new phase-space routines are required. Add those, if need be, to `phase_space` as described in Section 6.4.1.
11. Per default the stringent soft cut, that may be required to stabilise the numerical integration (cf. Section 6.4.2), is set to zero. Study what the smallest value is that still permits integration.
12. Perform very precise ξ_c independence studies. Tips on how to do this can be found in Section 6.5.1.

At this stage, the NLO calculation is complete and may, after proper integration into MCMULE and adherence to coding style has been confirmed, be added to the list of MCMULE processes in a new release. Should NNLO precision be required, the following steps should be taken

13. Calculate the real-virtual and double-real matrix elements $\mathcal{M}_{n+1}^{(1)}$ and $\mathcal{M}_{n+2}^{(0)}$ and add them to the test routines as well as integrands.
14. Prepare the n -particle contribution $\sigma_n^{(2)}$. In a pinch, massified results can be used also for $\hat{\mathcal{E}}(\xi_c)\mathcal{M}_n^{(1)}$ though of course one should default to the fully massive results.
15. Study whether the pre-defined phase-space routines are sufficient. Even if it was possible to use an old phase-space at NLO, this might no longer work at NNLO due to the added complexity. Adapt and partition further if necessary, adding more test integrations in the process.
16. Perform yet more detailed ξ_c and soft cut analyses.

In the following we comment on a few aspects of this procedure such as the ξ_c study (Section 6.5.1), the calculation of matrix elements (Section 6.5.2), and a brief style guide for MCMULE code (Section 6.5.3).

6.5.1 Study of ξ_c dependence

When performing calculations with MCMULE, we need to check that the dependence of the unphysical ξ_c parameter introduced in Chapter 4 actually drops out at NLO and NNLO. In principle it is sufficient to do this once during the development phase. However, we consider it good practice to also do this (albeit with a reduced range of ξ_c) for production runs.

Because the ξ_c dependence is induced through terms as $\xi_c^{-2\epsilon}/\epsilon$, we know the functional dependence of $\sigma_{n+j}^{(\ell)}$. For example, at NLO we have

$$\begin{aligned}\sigma_n^{(1)}(\xi_c) &= a_{0,0} + a_{0,1} \log(\xi_c), \\ \sigma_{n+1}^{(1)}(\xi_c) &= a_{1,0} + a_{1,1} \log(\xi_c),\end{aligned}\tag{6.15a}$$

where ξ_c independence of $\sigma^{(1)}$ of course requires

$$a_{0,1} + a_{1,1} = 0.\tag{6.15b}$$

```

SUBROUTINE TESTEEMATEL
implicit none
real (kind=prec) :: x(2),y(5)
real (kind=prec) :: single, finite, lin
real (kind=prec) :: weight
integer ido

call blockstart("ee_matrix_elements")
scms = 40000.
musq = me
x = (/0.75,0.5/)
call ps_x2(x,scms,p1,me,p2,me,p3,me,p4,me,weight)
call check("ee2ee",ee2ee(p1,p2,p3,p4), 2.273983244890001e4,
  ↪ threshold=2e-8)
call check("ee2eel",ee2eel(p1,p2,p3,p4), 6.964297070440638e7,
  ↪ threshold=2e-8)

scms = 40000.
y = (/0.3,0.6,0.8,0.4,0.9/)
call ps_x3_fks(y,scms,p1,me,p2,me,p3,me,p4,me,p5,weight)
call check("ee2eeg",ee2eeg(p1,p2,p3,p4,p5),7.864297444955537e2,
  ↪ threshold=2e-8)

call blockend(3)
END SUBROUTINE

SUBROUTINE TESTMEEVEGAS
xinormcut1 = 0.2
xinormcut2 = 0.3

call blockstart("Moller_VEGAS_test")

call test_INT('ee2ee0', sigma_0, 2,10,10, ??)
call test_INT('ee2eeF', sigma_0, 2,10,10, ??)
call test_INT('ee2eeR', sigma_1, 5,10,10, ??)
call blockend(3)
END SUBROUTINE

```

Listing 6.18: Test routine for $ee \rightarrow ee$ matrix elements and integrands. The reference values for the integration are yet to be determined.

At NNLO we have

$$\begin{aligned}\sigma_n^{(2)}(\xi_c) &= a_{0,0} + a_{0,1} \log(\xi_c) + a_{0,2} \log(\xi_c)^2, \\ \sigma_{n+1}^{(2)}(\xi_c) &= a_{1,0} + a_{1,1} \log(\xi_c) + a_{1,2} \log(\xi_c)^2, \\ \sigma_{n+2}^{(2)}(\xi_c) &= a_{2,0} + a_{2,1} \log(\xi_c) + a_{2,2} \log(\xi_c)^2.\end{aligned}\tag{6.16a}$$

We require

$$a_{0,i} + a_{1,i} + a_{2,i} = 0\tag{6.16b}$$

for $i = 1, 2$. However, the IR structure allows for an even stronger statement for the $a_{j,2}$ terms

$$a_{0,2} = a_{2,2} = -\frac{a_{1,2}}{2}.\tag{6.16c}$$

Of course we cannot directly calculate any of the $a_{1,i}$ or $a_{2,i}$ because we use numerical integration to obtain the $\sigma_{n+j}^{(\ell)}$. Still, knowing the coefficients can be extremely helpful when debugging the code or to just quantify how well the ξ_c dependence vanishes. Hence, we use a fitting routine to fit the Monte Carlo results *after* any phase-space partitioning has been undone. Sometimes non of this is sufficient to pin-point the source of a problem to any one integrand. However, if the goodness of, for example, $\sigma_{n+2}^{(2)}(\xi_c)$ is much worse than the one for $\sigma_{n+1}^{(2)}(\xi_c)$, a problem in the double-real corrections can be expected.

A worked example can be found in the next chapter in Section 7.1.

6.5.2 Example calculations in Mathematica

A thorough understanding of one-loop matrix elements is crucial for any higher-order calculation. In MCMULE, one-loop matrix elements either enter as the virtual contribution to NLO corrections or the real-virtual contribution in NNLO calculations. In any case, a fast numerical routine is required that computes the matrix element.

We perform all one-loop calculations in FDF as this is arguably the simplest scheme available. For theoretical background, we refer to Section 3.3.5 and references therein.

As already discussed in Section 5, we use QGRAF for the diagram generation. Using the in-house Mathematica package `qgraf.wl` we convert QGRAF's output for manipulation with Package-X [97]. This package is available on request through the MMCT

<https://gitlab.psi.ch/mcmule/qgraf>

An example calculation for the one-loop calculation of $\mu \rightarrow \nu \bar{\nu} e \gamma$ can be found in Listing 6.19. Of course this example can be made more efficient by, for example, feeding the minimal amount of algebra to the loop integration routine.

When using `qgraf.wl` for FDF some attention needs to be paid when considering diagrams with closed fermion loops. By default, `qgraf.wl` evaluates these traces in d dimensions. `RunQGraf` has an option to keep this from happening.

There is a subtlety here that only arise for complicated matrix elements. Because the function Package-X uses for box integrals, `ScalarD0IR6`, is so complicated, no native Fortran implementation exists in MCMULE. Instead, we are defaulting to COLLIER [147] and should directly evaluate the finite part of the PVD function above. The same holds true for the more complicated triangle functions. In fact, only the simple `DiscB` and `ScalarC0IR6` are natively implemented without need for external libraries. For any other functions, a judgement call is necessary of whether one should `LoopRefine` the finite part in the first place. In general, if an integral can be written through logarithms and dilogs of simple arguments (resulting in real answers) or `DiscB` and `ScalarC0IR6`, it makes sense to do so. Otherwise, it is often easier to directly link to COLLIER.

```

<<qgraf.wl
onshell = {
  p.p -> M^2, q.q -> m^2, p.q -> s/2
};

A0 = (4GF/Sqrt[2]) "diag1"/.RunQGraf[{"mum"},{"nu","elm"},0] //. {
  line[_ , x_] -> x, p1->p, q1->p-q, q2->q,
  _δZ | δm -> 0
};

A1 = pref /. RunQGraf[{"mum"},{"nu","elm"},1] //. {
  line[_ , x_] -> x, p1->p, q1->p-q, q2->q,
  _δZ | δm -> 0
};

M0=Block[{Dim=4},Simplify[Contract[
  1/2 Z2[m] Z2[M] FermionSpinSum[
    A0 /. PL -> (1 - Z5 γ5)/2,
    A0 /. PL -> (1 + Z5 γ5)/2
  ]
]] /. onshell]/.{
  Z2[M_] -> 1 + (α/(4π)) (-3/(2ε)-5/2 + 3/2 Log[M^2/Mu^2]),
  Z5      -> 1 - (α/(4π))
};

M1=Block[{Dim=4},Simplify[Contract[
  1/2 FermionSpinSum[
    A1/.γ.k1 -> γ. 4[k1]+I γ5 μ,
    A0
  ]
] /. onshell /. {
  μ^n_ /; EvenQ[n] -> μ2^(n/2), μ -> 0
}]/. {
  4[k1]. 4[k1] -> k1.k1 + μ2, 4[k1] -> k1
}]]];

M1bare = Simplify[KallenExpand[LoopRefine[LoopRelease[
  Pro2LoopIntegrate[
    Coefficient[M1, μ2, 0]/(16 π^2)
  ]
  + μIntegrate[
    Coefficient[M1, μ2, 1]/(64 π^3),
    1
  ],
  ],
  onshell
]]] /. e -> Sqrt[4 πα]];

```

Listing 6.19: An example on how to calculate the renormalised one-loop matrix element for $\mu \rightarrow \nu \bar{\nu} e$ in FDF.

6.5.3 Coding style and best practice

A large-scale code base like MCMULE cannot live without some basic agreements regarding coding style and operational best practice. These range from a (recommended but not enforced) style guide over the management of the git repository to how to best run MCMULE in development scenarios. All aspects have been discussed within the MMCT.

Fortran code in MCMULE is (mostly) written in accordance with the following style guide. If new code is added, compliance would be appreciated but deviation is allowed if necessary. If in doubt, contact any member of the MMCT.

- Indentation width is two spaces. In Vim this could be implemented by adding the following to `.vimrc`

```
autocmd FileType fortran set tabstop=8 softtabstop=0 expandtab
↔ shiftwidth=2 smarttab
```
- Function and subroutine names are in all-upper case.
- A function body is not indented beyond its definition.
- When specifying floating point literals specify the precision when possible, i.e. `1._prec`.
- Integrands should have `ndim` specified.
- Internal functions should be used where available.
- Masses and other kinematic parameters must be calculated in the matrix elements as local variables; using the global parameters `Mm` and `Me` is strictly forbidden.
- These rules also hold for matrix elements.

For python code, i.e. `pymule` as well as the analysis code, PEP8 compliance is strongly encouraged with the exception of E231 (Missing whitespace after `,`, `;`, and `:`), E731 (Do not assign a lambda expression, use a `def`) as well, in justified cases, i.e. if required by the visual layout, E272 (Multiple spaces before keyword), and E131 (Continuation line unaligned for hanging indent).

MCMULE uses two git repositories for version management. One internal repository and one public-facing one. Releasing to the latter is the responsibility of the MMCT after sufficient vetting was performed by squashing commits to avoid the accidental release of embarrassing or wrong code to the public. However, even the internal repository has certain rules attached. In general, developers are encouraged to not commit wrong or unvetted code though this can obviously not be completely avoided in practice. To avoid uncontrollable growth of the git repository, large files movements are strongly discouraged. This also means that matrix elements should not be completely overhauled barring unanimous agreement. Instead, developers are encouraged to add a new matrix element file and link to that instead.

Even when running MCMULE for development purposes the usage of menu files is strongly encouraged because the code will do its utmost to automatically document the run by storing the git version as well as any modification thereof. This allows for easy and unique reconstruction of what was running. For production runs this is not optional; these must be conducted with menu files after which the run folder must be stored with an analysis script and all data on the AFS as well as the user file library to ensure data retention.

Chapter 7

Phenomenology

In this chapter we will demonstrate example calculations with MCMULE. We will come back to the list of processes presented in Chapter 1, reviewing various scattering processes and muon decay modes sorted by experimental situation. We will begin by discussing the scattering experiments MUonE (Section 7.1) and Muse (Section 7.2). Next, we will review MEG in Section 7.3. Afterwards in Section 7.4, we review the 3σ discrepancy in the radiative τ decays we observed earlier. This is followed by a discussion of the Michel decay $\mu \rightarrow \nu\bar{\nu}e$ that is independent of any particular experiment in Section 7.5. Finally, we briefly present results for the Mu3e experiment in Section 7.6.

For the present discussion we will only provide examples that show MCMULE's capabilities. This list is not meant to be exhaustive of all results that have ever been produced. Such a list is in preparation [160].

All results presented here use the following input parameters

$$\begin{aligned} m_\mu &= 105.6583715 \text{ MeV} , & m_e &= 0.510998928 \text{ MeV} , \\ m_\tau &= 1776.82 \text{ MeV} , & m_p &= 938.2720813 \text{ MeV} , \\ \alpha &= \frac{1}{137.03599907} , & G_F &= 1.16637 \cdot 10^{-11} \text{ MeV}^{-2} \\ \text{conv} &= (c\hbar)^2 = 3.8937936 \cdot 10^8 \text{ MeV}^2\mu\text{b} , \end{aligned}$$

where the masses and the coupling is understood to be in the on-shell scheme. Here, `conv` is the factor used to convert cross sections from MeV^{-2} to μb .

7.1 MUonE ($\mu^-e^- \rightarrow \mu^-e^-$)

Following the renewed interest into μ - e scattering, previous NLO calculations [43, 44] have been redone in a fully differential Monte Carlo [45, 47] as well as MCMULE [7]. However, to match the required experimental accuracy a NNLO calculation is required (for a review cf. [116]).

The full NNLO is currently under investigation though impressive progress has been made. The required master integrals are known for vanishing electron masses [161–164]. Similarly, the real-virtual diagrams have been calculated both for $m = 0$ and $m > 0$ [116]. The signal, i.e. the HVP contribution, has been studied at NNLO [142, 143] and an integration of these results into MCMULE is being validated. Finally, the impact of BSM physics has been found to be negligible [165, 166].

For all calculations we will assume a muon beam with a fixed energy $E_{\text{beam}} = 150 \text{ GeV}$, consistent with the M2 beam line at CERN North Area [17]. Let us further remark that the total cross section is ill-defined due to the behaviour $d\sigma/dt \sim t^{-2}$ with $t_{\text{min}} \leq t \leq 0$. We

therefore have to apply a cut on the maximal value of t or equivalently on the minimal energy of the outgoing electron. In the results below we have chosen $E_{\min} = 1$ GeV (‘Setup 2’ of [45]). Further, to demonstrate the versatility of MCMULE, we apply a cut restricting photon emission in a way that could be measured by MUonE. To be precise, we require that the acoplanarity is

$$|\pi - |\phi_e - \phi_\mu|| < 3.5 \text{ mrad}, \quad (7.1)$$

in correspondence with ‘Setup 4’ of [45].

We will be more verbose in the discussion of μ - e scattering than in the other calculations presented in this chapter, as these results have not been presented elsewhere yet. However, all of them follow the same procedure.

In the following, we will present selected results for μ - e scattering in the context of MUonE. In particular, we will compare MCMULE’s NLO calculation [7] with [45] putting special emphasis on the gauge invariant split into *electronic corrections* (emission only from the electron line), *muonic corrections* (emission from the muon line), and *mixed corrections* (cf. Section 5.1). With the splitting properly motivated, we present the electronic corrections without any VP contribution at NNLO and compare with [167]. This is of course much simpler because the muon becomes a spectator, reducing the number of scales.

As discussed many times before, detailed ξ_c studies are crucial. In Section 6.5.1, we have outlined a procedure on how to best do this by fitting the MCMULE data. In Figure 7.1, the result of the fitting procedure as well as the final combination can be seen for the full NLO corrections as well as the electronic NNLO corrections. Note that while it is of course possible to use small ξ_c values such as 10^{-3} for production runs, this rarely is a good idea due to the large cancellation between the different contributions. At NLO, the ideal spot for running is the intersection between $\sigma_n^{(1)}(\xi_c)$ and $\sigma_{n+1}^{(1)}(\xi_c)$. In this case this is $\xi_c \approx 0.15$. At NNLO this is less clear cut because the three parabolas might not conveniently intersect. Here, $\xi_c \approx 0.1$ might be a good idea.

We split the total cross section σ into different contributions by order in perturbation theory and origin (either e for electronic, μ for muonic, or m for mixed)

$$\sigma = \sigma^{(0)} + \left(\sigma_e^{(1)} + \sigma_\mu^{(1)} + \sigma_m^{(1)} \right) + \left(\sigma_e^{(2)} + \dots \right) + \mathcal{O}(\alpha^5). \quad (7.2)$$

The different contributions are shown in Table 7.2 for μ^-e^- scattering. To obtain results for μ^+e^- scattering, the sign of $\sigma_m^{(1)} \propto (q^2Q^2)Q$ needs to be flipped (cf. Section 5.1). Results are compared with the results from [45, 167], finding excellent agreement. All errors given are purely statistical. Especially, parametric uncertainties and those arising from the uncomputed N³LO are not considered. It is clearly visible that the electronic corrections at NLO are by far the largest contributor to the full NLO. The high precision to which the cross sections were calculated is a side effect of wanting to obtain precise histograms. The present dataset corresponds to roughly 1.4×10^8 CPU s ≈ 4.6 CPU years on PSI’s Slurm system.

After we have justified the split into contributions for the cross section, let us now look at a differential distribution such as $d\sigma/d\theta_e$. In Figure 7.3, this distribution is shown, once without the acoplanarity cut (7.1) and with it. The K -factor is shown split into the different classes (7.2)

$$K_j^{(i)} = \frac{d\sigma_{j,i}/d\theta_e}{d\sigma_{j,i-1}/d\theta_e} = 1 + \delta K_j^{(i)} \quad \text{with } j \in \{e, \mu, m\}. \quad (7.3)$$

For now, we only do this at NLO, i.e. $i = 1$, because the mixed contributions at NNLO are not yet available. It is clearly visible that even for differential spectra, the electronic corrections are by far the largest. Indeed, considering e.g. $\theta_e = 5$ mrad, the fixed-order NLO electronic correction

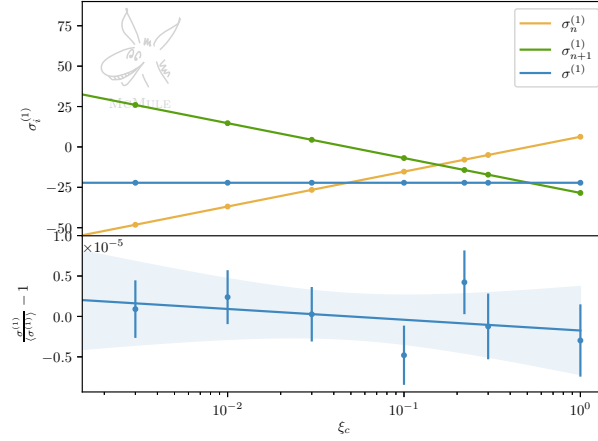
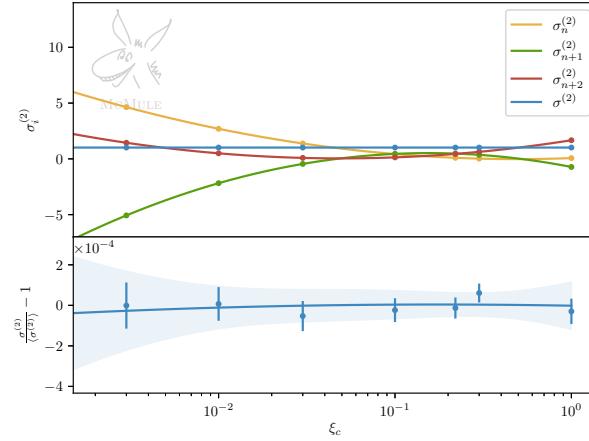
(a) The ξ_c dependence at NLO(b) The ξ_c dependence at NNLO

Figure 7.1: The ξ_c dependence at NLO and NNLO, split into different contributions and fitted to (6.15) and (6.16), respectively. The upper panels show all different contributions in μb . The lower panels show the sum normalised to the averaged value. The fit shows a 1σ band.

	[45]		MCMULE		K	
	Setup 2	Setup 4	Setup 2	Setup 4	Setup 2	Setup 4
$\sigma^{(0)}$	245.038906(3)		245.038910(1)			
$\sigma_e^{(1)}$	10.510(2)	-21.605(2)	10.51037(5)	-21.60054(3)	0.0429	-0.0882
$\sigma_\mu^{(1)}$	-0.069(2)	-0.627(2)	-0.06824902(5)	-0.62546(4)	-0.0003	-0.0026
$\sigma_m^{(1)}$	-0.360(5)	0.042(5)	-0.3599420(3)	0.04113(1)	-0.0015	0.0002
$\sigma^{(1)}$	10.081(2)	-22.188(2)	10.08218(5)	-22.18488(3)	0.0411	-0.0905
$\sigma_e^{(2)}$	10.5793(7)	1.0409(7)	0.02277(2)	1.04118(2)	0.0023	-0.0469
σ			255.14385(5)	223.89521(4)		

Table 7.2: The cross section for μ - e scattering at MUonE in Setup 2 ($E_e > 1$ GeV) and Setup 4 (also including (7.1)). The results are split into the gauge invariant subsets introduced in Section 5.1 and again in (7.2). It is apparent that at NLO, the electronic contributions are by far the largest as discussed before. To compare with [167] no VP contributions were included.

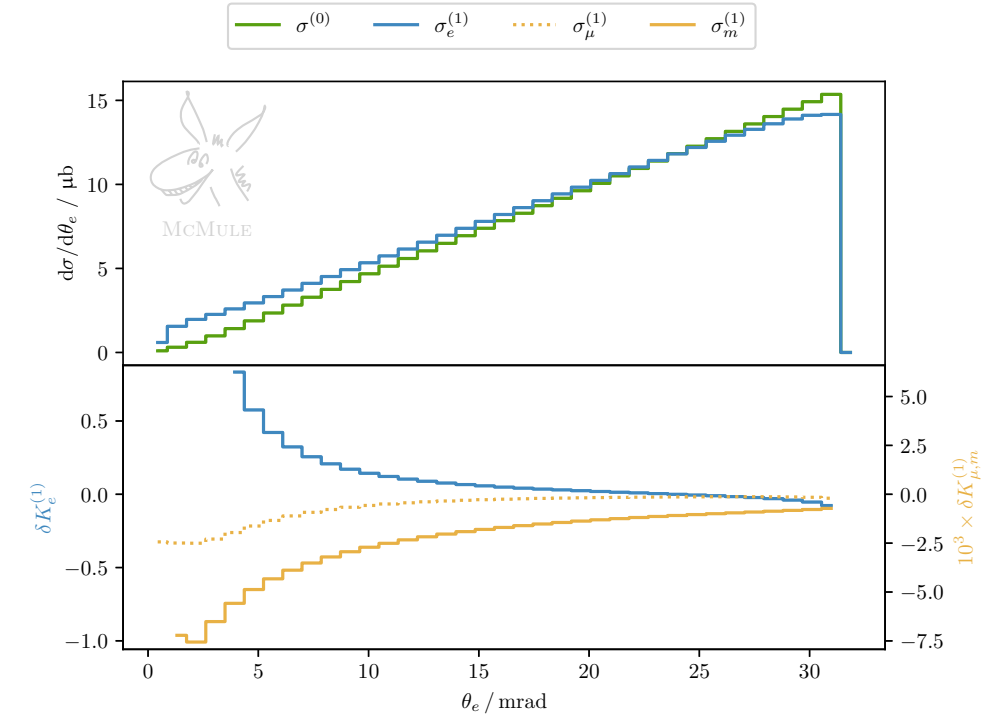
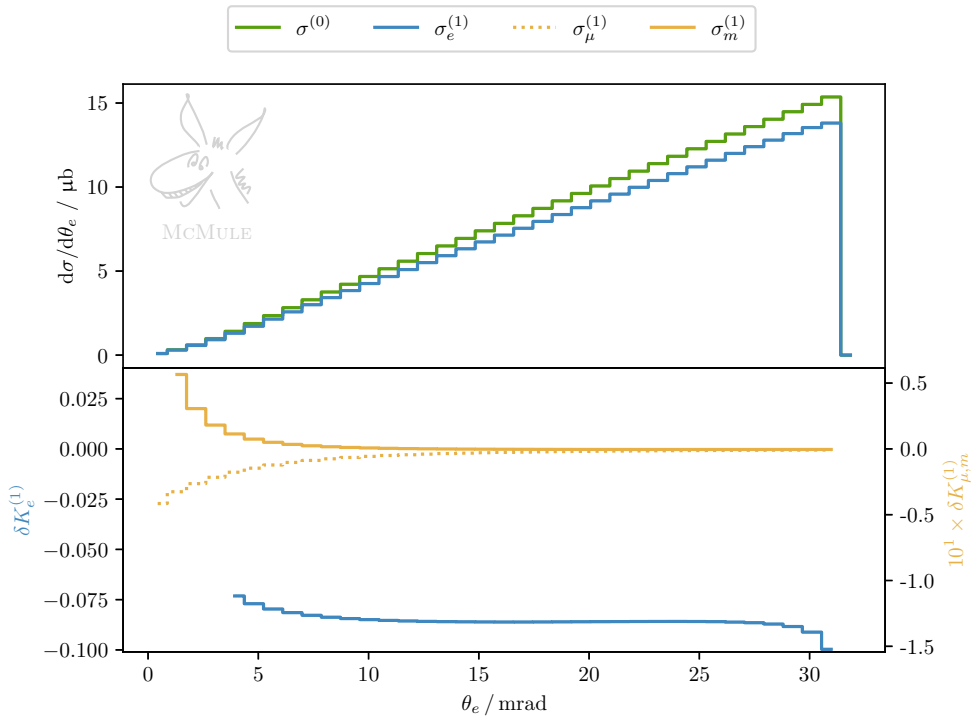
(a) $d\sigma/d\theta_e$ without the acoplanarity cut (7.1) (Setup 2)(b) $d\sigma/d\theta_e$ with the acoplanarity cut (7.1) (Setup 4)

Figure 7.3: The angular distribution $d\sigma/d\theta_e$ at NLO. The K -factors are presented split into different contributions (7.2). The electronic corrections (blue, left axis) are a lot larger than the muonic (orange, dashed, right axis) or mixed contributions (orange, right axis).

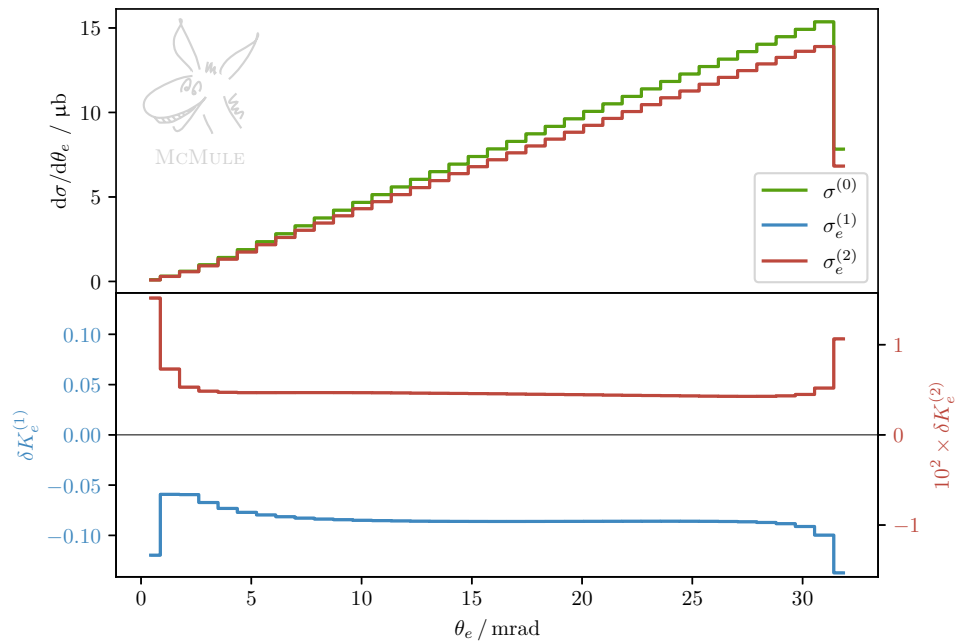
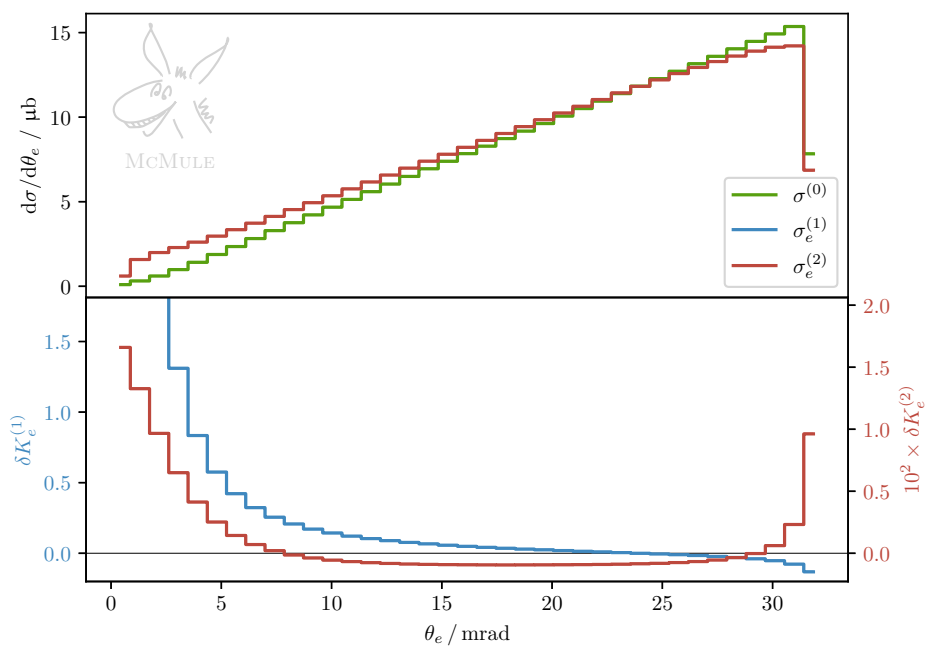
(a) $d\sigma/d\theta_e$ with the acoplanarity cut (7.1)(b) $d\sigma/d\theta_e$ without the acoplanarity cut (7.1)

Figure 7.4: The distribution of the outgoing electron's angle relative to the beam axis at LO, NLO, and NNLO. The upper panels only show the LO and NNLO curves.

K_e amount to nearly 50% (see scale on the left) whereas the muonic and mixed corrections (K_μ and K_m , respectively) are less than half a percent (see scale on the right).

Before we discuss Figure 7.3 in detail, let us add the electronic corrections at NNLO ignoring contributions due to the VP in Figure 7.4. It is clearly visible that for small scattering angles $\theta_e \rightarrow 0$ the NLO corrections become extremely large ($K > 2$ for $\theta_e < 5$ mrad). As this is the region of interest for MUonE, these corrections are especially troubling. However, they can be almost entirely accounted to the new process $\mu e \rightarrow \mu e \gamma$. Hard photon radiation can knock the electron back towards the beam axis resulting in more small-angle electrons, i.e. positive corrections. At NNLO, the radiative process $\mu e \rightarrow \mu e \gamma$ has now essentially been included at NLO. This results in reduced, but still large ($\mathcal{O}(10\%)$), corrections for small-angle electrons. As soon as the acoplanarity cut (7.1) is applied, the corrections dramatically decrease in size because the cut restricts hard photon emission.

Still, the NNLO corrections are very large in the relevant regions ($\mathcal{O}(0.5\%)$). A naive extrapolation to N³LO would suggest $\mathcal{O}(5 \times 10^{-4})$ corrections. This is a long way from the requirement that all systematic uncertainties need to be below 10^{-5} . Fortunately, the corrections are almost exclusively driven by large logarithms for $\theta_e \rightarrow 0$ that can be resummed. However, only LL resummation is feasible due to the complexity of the cuts because those can be obtained using a PS. It is unlikely that for example a cross section with the acoplanarity cut (7.1) could ever be resummed analytically to NLL. While it is of course possible to construct other observables that could be resummed to NLL or even beyond, most of those could not be measured at MUonE due to the lack of precise energy measurements of the outgoing particle.

7.2 MUSE ($ep \rightarrow ep$)

Lepton proton scattering has an extremely long history in particle physics that we will not recount in full here. On the theoretical side, higher-order corrections have been calculated long ago [168, 169] and later revisited [170–179]. Unfortunately, these calculations can often not be directly reused as they typically rely on assumptions on the energy scales involved or what particles are and are not measured. While this helps to arrive at concise formulas, these assumptions are not universally valid. Hence, we need a fully-differential NNLO calculation to best exploit past, present and future data.

Results similar to those shown here and [7] have been presented in [180], not including VP contributions. Our NLO results (without VP) agree with these results. However, we disagree substantially with the NNLO corrections of [180], even if we adapt to their calculation and include the electron loop in the two-loop vertex diagram. With respect to the results presented in Section 7.1 that have been verified independently by [167], the only new ingredients are the matrix elements. They have been compared pointwise with [180] and agree.

We can use MCMULE to calculate e - p scattering by repurposing the electronic corrections to μ - e scattering. However, unlike the muon, the proton is not point-like. For small virtualities Q^2 of the t -channel photon, we change the proton's interaction with the photon to

$$\bar{u}(m_\mu)\gamma_\mu u(m_\mu) \rightarrow \bar{u}(m_p)\left(F_1(Q^2)\gamma^\mu + F_2(Q^2)\frac{i\sigma^{\mu\nu}Q_\nu}{2m_p}\right)u(m_p), \quad (7.4)$$

where F_1 and F_2 are determined through measurements. For simplicity, we assume a dipole parametrisation of a proton with charge radius R_p

$$F_1(Q^2) = \frac{1 + \kappa\tau}{1 + \tau} \left(1 + \frac{Q^2}{\Lambda^2}\right)^{-2} \quad \text{and} \quad F_2(Q^2) = \frac{-1 + \kappa}{1 + \tau} \left(1 + \frac{Q^2}{\Lambda^2}\right)^{-2}, \quad (7.5)$$

with $\tau = Q^2/(4m_p^2)$, $\Lambda^2 = 12/R_p^2 = 0.71 \text{ GeV}^2$ and $\kappa = 2.7928$ the proton's magnetic moment. However, the specific values and parametrisation used have no large influence [180].

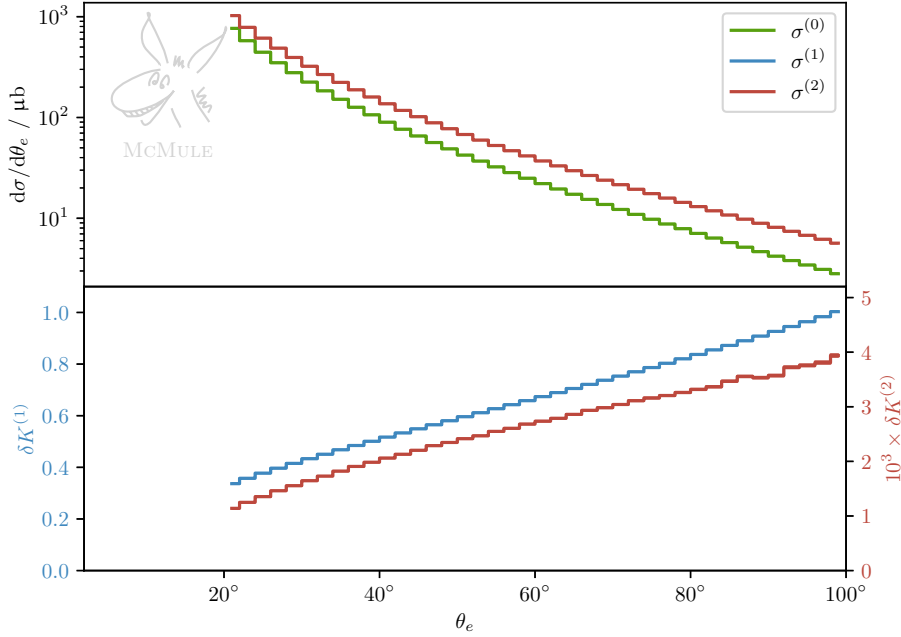


Figure 7.5: The angular distribution of the outgoing electron for a $p_{\text{in}} = 115 \text{ MeV}$ electron beam in Muse.

As an example of e - p scattering we will calculate the process for the Muse experiment [20]. It is situated on the π M1 beam line at PSI, measuring both e - p and μ - p scattering with different momenta. The geometric acceptance of the detector for outgoing electrons is

$$20^\circ < \theta_e < 100^\circ. \quad (7.6)$$

For now, we will only consider one value of the beam momentum $p_{\text{in}} = 115 \text{ MeV}$.

For this calculation, we have included only electronic effects. Just as for the discussion of μ - e scattering, we have not included HVP or leptonic vacuum polarisation effects as they are being still vetted. Hence, these results should not be considered definite.

The resulting distribution $d\sigma/d\theta_e$ is shown in Figure 7.5. Just as for MUonE, the large corrections are due to unrestricted photon emission in $ep \rightarrow ep\gamma$ that shifts the entire spectrum towards larger angles such that eventually more electrons hit the detector. This view is reaffirmed by the fact that the NNLO corrections are very small, especially compared to the NLO corrections.

7.3 MEG and MEG II

The MEG experiment and its successor MEG II are designed to search for the LFV process $\mu \rightarrow e\gamma$. However, they are also interested in the single ($\mu \rightarrow \nu\bar{\nu}e\gamma$) and double ($\mu \rightarrow \nu\bar{\nu}e\gamma\gamma$) radiative muon decays as they serve as backgrounds to searches like $\mu \rightarrow e\gamma$ and $\mu \rightarrow eJ(\rightarrow \gamma\gamma)$.

MEG and MEG II are running on the π E5 beam line that delivers (partially) polarised μ^+ that are stopped in the detector. We define the z -axis against the polarisation axis s.t. the muon polarisation $\vec{P}_\mu = -0.85 \vec{z}$ [181]. The geometric acceptance of the MEG detector is then

simulated as

$$|\cos \angle(\vec{p}_\gamma, \vec{z})| \equiv |\cos \theta_\gamma| < 0.35, \quad |\phi_\gamma| > \frac{2\pi}{3}, \quad (7.7a)$$

$$|\cos \angle(\vec{p}_e, \vec{z})| \equiv |\cos \theta_e| < 0.5, \quad |\phi_e| > \frac{\pi}{3}. \quad (7.7b)$$

Further cuts may be applied, depending on the physics search.

7.3.1 Single radiative muon decay ($\mu \rightarrow \nu \bar{\nu} e \gamma$)

The radiative muon decay $\mu \rightarrow \nu \bar{\nu} e \gamma$ is an important background to the LFV searches for $\mu \rightarrow e \gamma$ in MEG. Hence, precise understanding of this decay is crucial.

We begin by noting that the BR for this process depends on the energy cut on the photon, that is required to make the quantity well defined. For the standard choice of $E_\gamma > 10 \text{ MeV}$ the BR is roughly 1%. Given the vast number of muons that can be produced, it should be possible to study radiative muon decays with very good precision. Apart from measuring the BR and as a background to LFV searches, the SM could in principle also be tested by measuring Michel parameters of a general formula for muon decays [182–184]. Unfortunately, the cuts employed by MEG are far too restrictive to do this. Hence, we have to rely on other experiments for these measurements.

Corrections beyond the Fermi theory due to the W -boson propagator [60, 185] turn out to be much smaller than the NLO corrections. The tree-level calculation within the Fermi theory has been considered by several authors a long time ago [186–189]. Due to the photon bremsstrahlung the helicity of the final-state lepton does not have to be left-handed [190–193]. After some partial results [194, 195] a full NLO calculation for the BR was presented in [38, 196]. As for a related calculation of the rare decays of leptons [32], the results presented in [38, 196] allow to obtain the differential decay width at NLO with cuts on the photon and electron energy and angles between them. With MCMULE, we generalise these results because it allows us to implement arbitrary cuts, allowing to mirror the experimental situation more closely.

When searching for $\mu \rightarrow e \gamma$, MEG applies, in addition to (7.7), energy cuts requiring

$$E_\gamma > 40 \text{ MeV} \quad \text{and} \quad E_e > 45 \text{ MeV}, \quad (7.8a)$$

This reduces the amount of data taken without infringing on the signal which is at $E_e \approx E_\gamma = M/2$. Also, MEG will veto any event with multiple visible photons. We simulate this by requiring for the second photon (if present)

$$E_{\gamma_2} < \begin{cases} 2 \text{ MeV} & \text{if (7.7a) is satisfied} \\ \infty & \text{otherwise} \end{cases}. \quad (7.8b)$$

Of course this is rather simplistic because it assumes that the detector could tell two photons apart regardless of how closely clustered they are. In contrast to QCD, there is fortunately no mechanism driving the two photons collinear. Hence, this model is sufficient for current purposes. In Section 7.3.2, we will discuss a more detailed model that does require spatial separation in the detector.

We now can use the cuts (7.7) and (7.8) to calculate the missing energy spectrum $d\mathcal{B}/d\cancel{E}$ in Figure 7.6 where the missing energy is *defined* as

$$\cancel{E} = M - E_e - E_\gamma, \quad (7.9)$$

which includes both the neutrinos as well as a potential second photon. To obtain precise results in the region of small \cancel{E} , we perform two runs, one with the full range of \cancel{E} allowed by (7.8) (roughly $0 < \cancel{E} \lesssim 20 \text{ MeV}$) and a tailored run where $\cancel{E} < 6 \text{ MeV}$ is enforced (cf. Section 6.2.2).

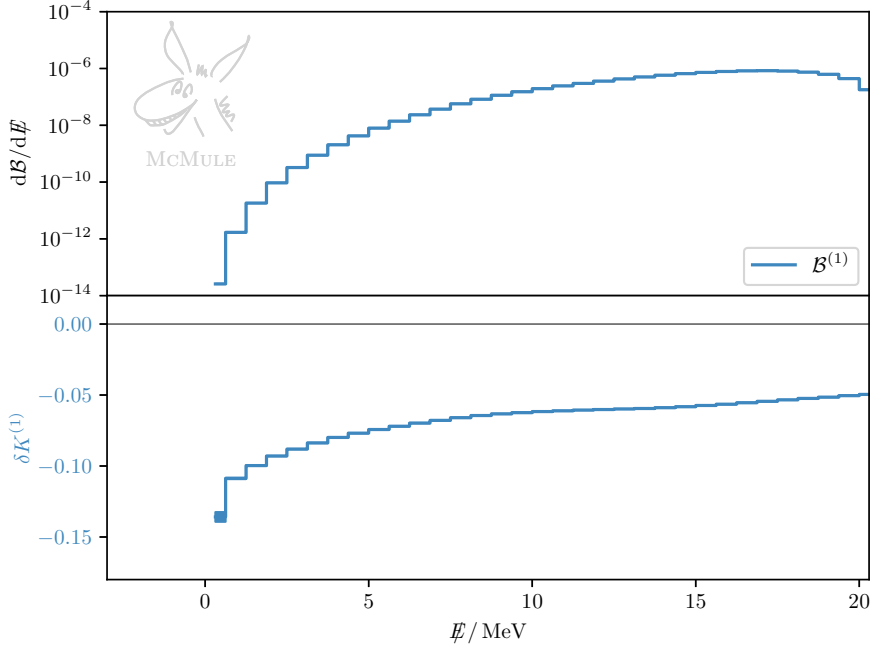


Figure 7.6: The missing energy spectrum with full MEG cuts (7.7) and (7.8) at NLO.

For the bulk of the distribution, the corrections are of the order of -5% , but in the tail they increase substantially. We also note that the distribution itself falls rapidly towards zero for $E \rightarrow 20$ MeV, due to the kinematic constraints.

7.3.2 Double radiative muon decay ($\mu \rightarrow \nu\bar{\nu}e\gamma\gamma$)

The double radiative muon decay is a background for searches of light New Physics that induces the LFV muon decay $\mu \rightarrow eJ$ where the J is a Majoron, a light but not massless new particle, that could promptly decays into $J \rightarrow \gamma\gamma$.

For this study we only apply the cuts on photon geometry (7.7a) as well as

$$E_{\gamma_i} \geq 10 \text{ MeV}, \quad (7.10a)$$

which is necessary for IR safety. Further, we require that the two photons can be separated in the calorimeter. This is implemented by specifying them to be $\delta x = 20$ cm apart on the detector surface which is at a radius of $R = 67.85$ cm resulting in

$$\langle (\vec{p}_{\gamma_1}, \vec{p}_{\gamma_2}) = \theta_{\gamma\gamma} \rangle \tan^{-1} \left(\frac{\delta x}{R} \right) \approx 16.4^\circ. \quad (7.10b)$$

With these cuts, we can now again calculate the missing energy spectrum at LO, depicted in Figure 7.7.

7.4 BABAR ($\tau \rightarrow \nu\bar{\nu}e\gamma$)

The example calculation in Section 6.2 already indicated a discrepancy between the NLO results and the experimental measurement [40, 197] for the radiative τ decay. As argued in [38] these

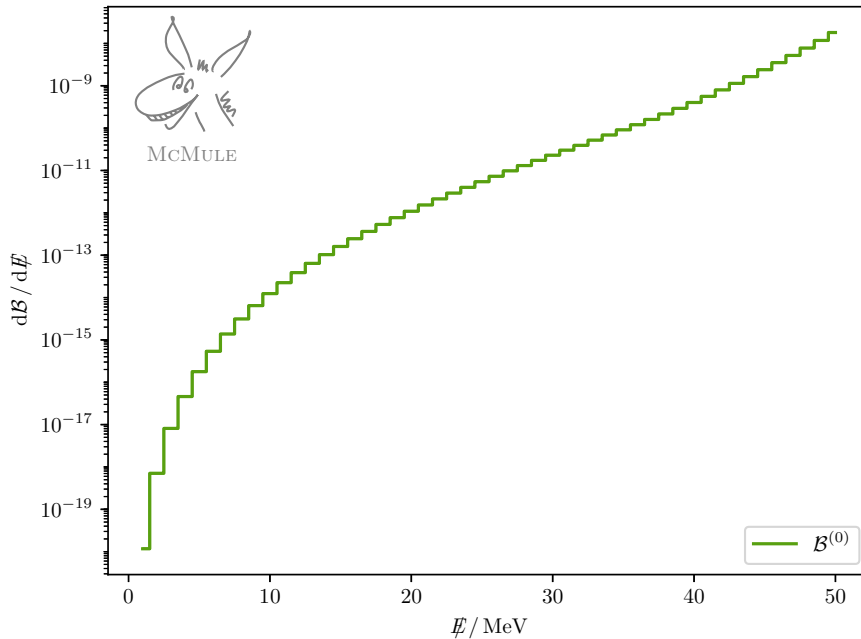


Figure 7.7: The missing energy spectrum for the double-radiative muon decay at LO.

measurements are to be compared with the exclusive BR we have calculated before

$$\begin{aligned}\mathcal{B}|_{\text{NLO}} &= 1.6451(1) \times 10^{-2} \\ \mathcal{B}|_{\text{exp}} &= 1.847(54) \times 10^{-2}.\end{aligned}\tag{7.11}$$

We will now use MCMULE to revisit this 3.5σ discrepancy, making use of our fully differential NLO computation to match the actual measurement as closely as possible.

For the BABAR measurement, tau pairs are produced through e^+e^- collisions at $\sqrt{s} = M_{\Upsilon(4S)} = 10.58 \text{ GeV}$. The event is then divided into a signal- and tag-hemisphere. In order to reduce background events, rather stringent cuts on the kinematics of the decay products e and γ in the signal hemisphere are applied. In particular, the following requirements are made:

$$\cos \theta_{e\gamma}^* \geq 0.97, \quad 0.22 \text{ GeV} \leq E_\gamma^* \leq 2.0 \text{ GeV}, \quad M_{e\gamma} \geq 0.14 \text{ GeV}.\tag{7.12}$$

All the quantities are given in the centre-of-mass frame. These cuts can be easily implemented in our code. To this end, we generate taus in their rest frame, boost them to a frame such that they have energy $\sqrt{s}/2$ and then apply the cuts (7.12) in this boosted frame. As we will see, the NLO corrections will have an important effect when ‘undoing’ the cuts, i.e. when extracting the exclusive BR (with only the cut $E_\gamma > 10 \text{ MeV}$ in the tau rest frame).

In order to illustrate this we have devised the following simplified scheme: let N_{obs} be the measured number of events including all cuts. To obtain the BR this is multiplied by a factor $\epsilon_{(\text{N})\text{LO}}^{\text{exp}}$

$$\mathcal{B}_{\text{exp}}^{(\text{N})\text{LO}} = \epsilon_{(\text{N})\text{LO}}^{\text{exp}} \cdot N_{\text{obs}} = \epsilon_{\text{det}} \cdot \epsilon_{(\text{N})\text{LO}} \cdot N_{\text{obs}}.\tag{7.13}$$

ϵ_{det} contains detector efficiencies needed to compute the fiducial BR. On the other hand, $\epsilon_{(\text{N})\text{LO}}$ is a theoretical correction factor that is needed to convert the actually measured BR with the

	$\tau \rightarrow \bar{\nu} \nu e \gamma$	$\tau \rightarrow \bar{\nu} \nu \mu \gamma$
LO	$1.834(1) \cdot 10^{-2}$	$3.662(1) \cdot 10^{-3}$
exclusive NLO	$1.645(1) \cdot 10^{-2}$	$3.571(1) \cdot 10^{-3}$
inclusive NLO	$1.727(3) \cdot 10^{-2}$	$3.604(1) \cdot 10^{-3}$
\mathcal{B}_{exp}	$1.847(54) \cdot 10^{-2}$	$3.69(10) \cdot 10^{-3}$
ϵ_{LO}	48.55(1)	4.966(1)
ϵ_{NLO}	44.80(1)	4.911(1)
$\epsilon' = \epsilon_{\text{NLO}}/\epsilon_{\text{LO}}$	0.923(1)	0.989(1)
$\epsilon' \cdot \mathcal{B}_{\text{exp}}$	$1.704(50) \cdot 10^{-2}$	$3.65(10) \cdot 10^{-3}$

Table 7.8: Branching ratios for the radiative decays of the τ . The minimum photon energy is 10 MeV. For the theoretical results only the numerical error due to the Monte Carlo integration is given. The errors on the experimental results are combined statistical and systematic errors, as given by [40].

cuts (7.12) to the desired BR with $E_\gamma \geq 10$ MeV. This factor can be computed easily at LO and NLO²⁶

$$\epsilon_{(\text{N})\text{LO}} = \frac{\sigma_{(\text{N})\text{LO}}^{\text{total}}}{\sigma_{(\text{N})\text{LO}}^{\text{with cuts}}} \Big|_{\text{theory}}, \quad (7.14)$$

where $\sigma_{(\text{N})\text{LO}}^{\text{total}}$ and $\sigma_{(\text{N})\text{LO}}^{\text{with cuts}}$ again refer to the cut $E_\gamma \geq 10$ MeV and the cuts (7.12), respectively. More precisely, we require that exactly one photon passes the cuts. To assess the importance of NLO corrections when extracting \mathcal{B}_{exp} we write

$$\mathcal{B}_{\text{exp}}^{\text{NLO}} = \epsilon_{\text{NLO}}^{\text{exp}} \cdot N_{\text{obs}} = \epsilon_{\text{NLO}} \cdot \epsilon_{\text{det}} \cdot N_{\text{obs}} = \frac{\epsilon_{\text{NLO}}}{\epsilon_{\text{LO}}} \cdot \mathcal{B}_{\text{exp}}^{\text{LO}} = \epsilon' \cdot \mathcal{B}_{\text{exp}}^{\text{LO}}, \quad (7.15)$$

where we assume that ϵ_{det} remains unchanged by the inclusion of radiative corrections. Thus, ϵ' is a purely theoretical factor that describes the difference of using a LO or NLO computation in the determination of \mathcal{B}_{exp} .

The results for the various factors described above are given in the first row of Table 7.8. The salient feature is that NLO effects are very important in the $\tau \rightarrow e \nu \bar{\nu} \gamma$ case and amount to a correction of 7%. Since the corresponding BABAR result was obtained using theory at LO the inclusion of the NLO corrections changes the result from $\mathcal{B}_{\text{exp}} = 1.847(54) \cdot 10^{-2}$ to $\epsilon' \cdot \mathcal{B}_{\text{exp}} = 1.704(50) \cdot 10^{-2}$, in much better agreement with the theoretical NLO result $\mathcal{B} = 1.645(1) \cdot 10^{-2}$.

Of course, the same procedure can be repeated for the $\tau \rightarrow \nu \bar{\nu} \mu \gamma$ decay. In this case, some of the cuts applied by BABAR are

$$\cos \theta_{\mu\gamma}^* \geq 0.99, \quad 0.10 \text{ GeV} \leq E_\gamma^* \leq 2.5 \text{ GeV}, \quad M_{\mu\gamma} \leq 0.25 \text{ GeV}. \quad (7.16)$$

A computation of the ϵ' factor reveals that the effects here are more modest and amount only to a correction of about 1%. The resulting value $\epsilon' \cdot \mathcal{B}_{\text{exp}} = 3.65(10) \cdot 10^{-3}$ agrees well with the NLO result $\mathcal{B} = 3.571(1) \cdot 10^{-3}$.

Obviously, this is only a simplistic and by far not complete simulation of the full analysis. While the cut on E_γ^* has the biggest impact, the results for the ϵ' factor actually depend quite significantly on all the details of the cuts. In particular, in the presence of a second photon it is important to precisely specify how the cuts are applied. This can also be seen from the rather large difference between the exclusive and inclusive results for $\tau \rightarrow \nu \bar{\nu} e \gamma$. We do not claim that this is the conclusive resolution to the apparent 3.5σ deviation for the measured branching ratio of $\tau \rightarrow \nu \bar{\nu} e \gamma$. However, we do claim that a proper inclusion of NLO effects is mandatory for such a measurement, in particular if stringent cuts on the decay products are applied.

²⁶Note that, to remain consistent with the discussion above, we will denote the decay rate by σ instead of Γ .

7.5 Michel decay ($\mu \rightarrow \nu\bar{\nu}e$)

The conventional Michel decay $\mu \rightarrow \nu\bar{\nu}e$ is used to determine the Fermi constant G_F by measuring the muon lifetime. Hence, this process is of high phenomenological relevance. However, many experiments have measured this and the present analysis is not connected to any one experiment.

NLO corrections to the Michel decay have been known for many decades [186, 198]. Using the optical theorem, the NNLO QED corrections to the decay width were calculated around the turn of the millennium, assuming vanishing electron masses [24]. Over the course of the next decade, the electron energy spectrum, which is not infrared finite in the limit $m_e \rightarrow 0$, was calculated. At first, only its logarithms were known analytically [199, 200]. A few years later, the full spectrum was calculated with a numerical loop integration [201] and the original calculation of [24] was extended to include mass effects [202]. It was only recently that the form factors necessary for a fully differential calculation were published [5, 203].

In what follows, we have included muon and electron loops but neither tau nor hadronic contributions [204, 205]. We treat the electromagnetic coupling α in the on-shell scheme, except in Table 7.9 where, in order to compare to [24], we need the $\overline{\text{MS}}$ coupling $\bar{\alpha} \equiv \bar{\alpha}(\mu = M)$.

Apart from the form factors needed for $d\sigma_n^{(2)}$, we also need matrix elements for $d\sigma_{n+1}^{(2)}$ and $d\sigma_{n+2}^{(2)}$ that were calculated using the strategies detailed in previous chapters.

7.5.1 Results for the decay rate

The first quantity we consider is the full decay width

$$\sigma = \sigma_0 + \frac{\bar{\alpha}}{\pi} \sigma^{(1)} + \left(\frac{\bar{\alpha}}{\pi}\right)^2 \sigma^{(2)} + \mathcal{O}(\bar{\alpha}^3), \quad (7.17)$$

where we have pulled out factors of the $\overline{\text{MS}}$ coupling $\bar{\alpha}/\pi$. We compute $\sigma^{(2)}$ using the massified form factors to obtain the leading terms in $z = m/M$, as well as the form factor with full m dependence [5, 203]. We will label these two results ‘massified’ and ‘massive’, respectively. In the case of the massified result, we expand all three parts of the integrand contributing to $\sigma_n^{(2)}$, see (4.36b) and (4.37a). Of course, the exact mass dependence of $d\sigma_s^{(1)}$ and $d\sigma_{ss}^{(2)}$ is usually much easier to obtain than for $\mathcal{M}_n^{(2)}$. However, the complete cancellation of singularities requires a consistent expansion in z of all contributions at the n -particle level.

Because the full decay rate does not contain terms $\log z \sim \log m$ the limit $m \rightarrow 0$ exists and we can compare our massified and massive results with the result for a massless electron [24]. We note that in this particular case (contrary to distributions, where $\log m$ terms exist), the massified result is not expected to be superior to the massless computation.

Following [24], we split the result into three parts: photonic corrections $\sigma_\gamma^{(1)}$ and $\sigma_\gamma^{(2)}$, corrections due to an electron pair (real or virtual) $\sigma_e^{(2)}$, and corrections due to a muon pair (virtual) $\sigma_\mu^{(2)}$. These parts have been defined and their analytic results in the massless case given in equations (2.11), (2.13) and (2.15) of [24]. The individual results for the NNLO corrections are shown in Table 7.9, where the Monte Carlo error is smaller than the significant digits. Note that [24] had to include the ‘open-lepton production’ $\mu \rightarrow \nu\bar{\nu}e ee$ into their calculation of $\sigma_e^{(2)}$ to guarantee finiteness. We have included this process as well [1] since it contributes to $\sigma_e^{(2)}$ (two-trace contribution) and $\sigma_\gamma^{(2)}$ (one-trace contribution).²⁷

The results of Table 7.9 merit a few comments:

²⁷The amplitude for $\mu^- \rightarrow \nu\bar{\nu}e^- e^+e^-$ has a (anti)symmetry under exchange of the two e^- . This gives rise to two types of interference terms in the matrix element: first the contribution that is also present without this symmetry (two-trace) and one where the swapped is interfered with the non-swapped contribution (one-trace).

	$\sigma_\gamma^{(2)}/\sigma_0$	$\sigma_\mu^{(2)}/\sigma_0$	$\sigma_e^{(2)}/\sigma_0$	total
massified	3.42	-0.0364	3.24	6.62
massive	3.54	-0.0364	3.16	6.66
massless [24]	3.56	-0.0364	3.22	6.74
Δ_{rel} massified	3.7×10^{-2}	0	6.1×10^{-3}	1.6×10^{-2}
Δ_{rel} massive	5.0×10^{-3}	1.9×10^{-4}	2.0×10^{-2}	1.1×10^{-2}

Table 7.9: The different contributions to $\sigma^{(2)}$. Note that $\sigma_e^{(2)}$ also includes the process $\mu \rightarrow \nu \bar{\nu} e ee$. See text for interpretation. The coupling $\bar{\alpha}(\mu = M)$ is renormalised in the $\overline{\text{MS}}$ scheme. Δ_{rel} denotes the relative difference of our results to the massless result [24].

- The good agreement for the purely photonic contributions $\sigma_\gamma^{(2)}$ between the massive and massless result is due to the absence of terms $\log m$ and $m \log m$ as discussed by [24].
- The massified results differs by about 3% from the massive (and massless) result for $\sigma_\gamma^{(2)}$. This is due to the mismatch between the real corrections, that were calculated with the full electron mass dependence, and the massified two-loop amplitude that only includes logarithmically enhanced mass effects.
- The massified results agrees perfectly with [24] for the $\sigma_\mu^{(2)}$ part because the contribution comes purely from one two-loop diagram that is free of any soft or collinear logarithms and hence effectively massless.
- The massive and massless results for $\sigma_e^{(2)}$ agree only up to two percent. This difference can be accounted for through the two-trace contribution of the open-lepton production. In the pure electron trace m must not be neglected to lead to finite expressions. However, in the other trace the electron mass can be set to zero. Our value of 3.16 was calculated with full electron mass dependence. If we were to set $m \rightarrow 0$ in the this trace, we would obtain 3.23 in much better agreement with [24].
- The $\sigma_e^{(2)}$ part contains the factorisation anomaly, already discussed in Chapter 5 and [5].

Note that in any case the ‘massive’ result should be considered the reference. Our results agree with [202]. For the pure mass effects of the photonic part, this agreement is only at the 20% level. This is due to large numerical cancellations between $\sigma_n^{(2)}$, $\sigma_{n+1}^{(2)}$ and $\sigma_{n+2}^{(2)}$ which make the extraction of a few-percent effect on the NNLO corrections numerically challenging. In fact, an efficient numerical evaluation of the integrals with full mass dependence [203] has only recently been implemented [206].

7.5.2 The electron energy spectrum

In order to validate our computation, we consider the NNLO corrections to the normalised electron energy spectrum $x_e = 2E_e/M$ and compare them to results available in the literature. If two (negatively charged) electrons are present in the final state, we include both of them in the x_e distribution. The leading and sub-leading logarithmic contributions for this observable were calculated in [199, 200]. Because this corresponds to a strict expansion in z , we expect good agreement for large x_e as noticed in [5]. In Figure 7.10 we compare the two results and see that the differences are compatible with the constant (logarithm-free) terms missing in [199, 200]. These terms were computed numerically and shown in a plot for $x_e > 0.3$ in [201]. If we include these constant terms of [201], we obtain perfect agreement with our result, using the massive

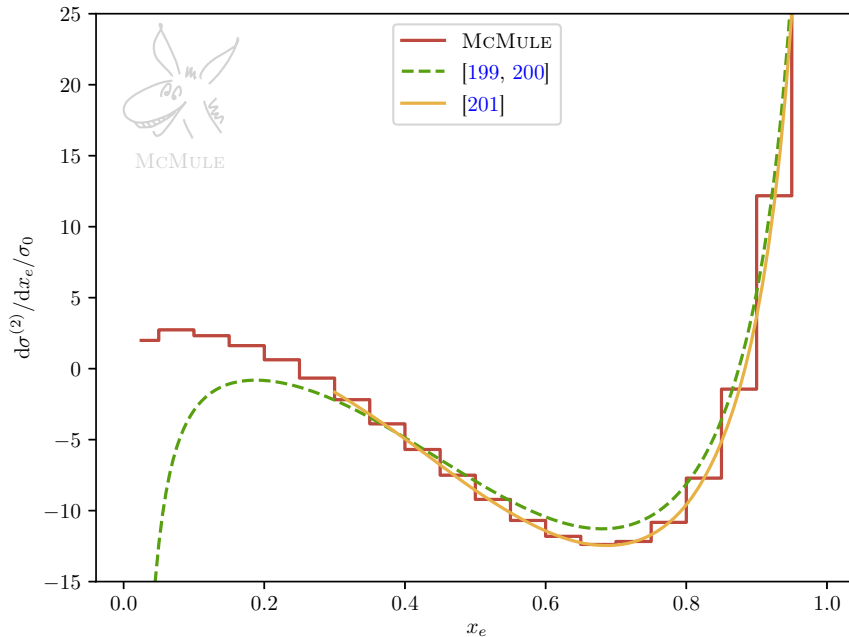


Figure 7.10: The NNLO corrections to the electron energy spectrum, omitting a factor $(\alpha/\pi)^2$. The logarithmic contributions of [199, 200] (green dashed) agree reasonably well with our massive result (red histogram) for large x_e . Adding the constant terms of [201] (orange) we obtain very good agreement.

form factors. Note that the difference between massified and massive result in Figure 7.10 is at the percent level and only becomes visible around the zero crossing at $x_e \approx 0.21$ and $x_e \approx 0.88$, never changing the overall picture. The on-shell coupling $(\alpha/\pi)^2$ is omitted in the results shown in the Figure 7.10.

With a fully differential Monte Carlo code, we can compute arbitrary distributions, including cuts. As an example, we consider again the normalised electron energy spectrum but impose a cut on photon emission through lepton isolation. Concretely, we restrict the total energy of all photons within a cone of angle $\theta \equiv \angle(\vec{p}_e, \vec{p}_\gamma) = 37^\circ$ (i.e. a cone with $|\cos \theta| > 0.8$) around the electron to be less than 10 MeV.

The results are shown in Figure 7.11. Comparing the normalised NNLO result (red histogram) to the normalised LO result (green histogram) in the top panel reveals that only for large x_e the corrections to the shape are relevant. This is driven by the NLO corrections. They are large at both ends of the x_e spectrum, as shown by the NLO $K^{(1)}$ factor

$$K^{(i)} = \frac{d\sigma_i/dx_e}{d\sigma_{i-1}/dx_e} = 1 + \delta K^{(i)}. \quad (7.18)$$

Typically, the NNLO corrections are below 0.1 % and even in the regions of huge NLO corrections they are below 0.5%.

7.5.3 Michel decay as a background in MEG

The Michel decay is not just a signal for the measurement of the muon lifetime. It also serves as a background to BSM searches. The light new LFV particle J – introduced above as the signal

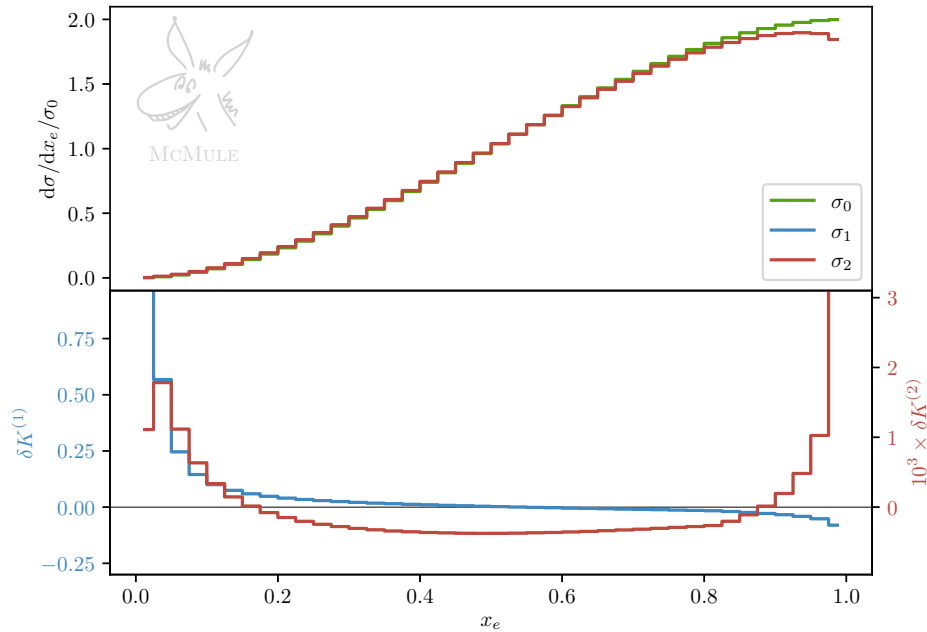


Figure 7.11: Top panel: The normalised electron energy spectrum at LO (green histogram) and NNLO (red histogram) with a cut on photon emission. The lower panel shows the NLO and NNLO K factors.

over $\mu \rightarrow \nu \bar{\nu} e \gamma \gamma$ – for example may not decay promptly but actually leave the detector as missing energy, resulting in the difficult signature $\mu \rightarrow e + \text{invisible}$. This process is indistinguishable from the Michel decay $\mu \rightarrow \nu \bar{\nu} e$. The experimental searches are now hunting for a miniscule deviation from the only spectrum available – $d\mathcal{B}/dx_e$.

Unfortunately, the delicate experimental situation requires a full detector simulation based on the best possible theory prediction. Hence, we need to generalise the discussion above. MEG will not be using the photon detector in search for $\mu \rightarrow e J$. Hence, we can be inclusive w.r.t. photon emission, simplifying our analysis. We exploit that the decay of a polarised muon is completely described to all orders by an *isotropic*, i.e. polarisation independent, and an *anisotropic*, i.e. polarisation dependent, part

$$\frac{d^2\sigma}{dx_e d(\cos\theta)} = \Gamma_0 (f(x_e) + P \cdot \cos\theta g(x_e)), \quad (7.19)$$

where x_e is the electron energy fraction and θ the angle between the polarisation axis and the outgoing electron. Neglecting mass effects, f and g can be written at LO as

$$\begin{aligned} f^{(0)}(x_e) &= x_e^2 (3 - 2x_e), \\ g^{(0)}(x_e) &= x_e^2 (1 - 2x_e). \end{aligned} \quad (7.20)$$

For the allowed energies $x_e \lesssim 1$, f is always positive. However, g crosses zero at $x_e' = 1/2$.²⁸

²⁸Taking into account mass effects, this happens at $x_e' = 1/2 + (3/2)m^2/M^2$

Beyond LO, we can calculate $f(x_e)$ and $g(x_e)$ with two runs of MCMULE²⁹ by defining

$$\frac{d\sigma_-}{dx_e} = \int_{-1}^0 d(\cos\theta) \frac{d^2\sigma}{dx_e d(\cos\theta)} \quad \text{and} \quad \frac{d\sigma_+}{dx_e} = \int_0^1 d(\cos\theta) \frac{d^2\sigma}{dx_e d(\cos\theta)}. \quad (7.21)$$

By combining σ_+ and σ_- we can obtain results for f and g allowing a full detector simulation. The numerical results for f and g are shown in Figure 7.12.

These results merit a few comments

- For small and large electron energies the NLO K factor becomes very large, both for f and g . This is a fundamental change in the kinematic situation due to extra photon emission. However, these large corrections are almost entirely LL and can be resummed easily enough. Especially for large x_e , soft photon emission gives rise to logarithms of the form $\log(1-x_e)$ that can just be exponentiated. This is currently being implemented [207].
- The corrections are still quite large at NNLO towards the endpoint though nowhere nearly as large as at NLO. The build-up of the LL tower can hence be clearly seen.
- Around $x'_e \approx 1/2$ the K factor for g diverges. This is because soft-photon emissions slightly shift the zero crossing of g away from x'_e resulting in large relative corrections.

7.6 Mu3e

The rare muon decay $\mu \rightarrow \nu\bar{\nu}eee$ is a background for Mu3e, looking for $\mu \rightarrow eee$. Mu3e – just as MEG – operates on the $\pi E5$ beam line at PSI using positive muons and hence, we again define the z axis s.t. the muon polarisation is $\vec{P}_\mu = -0.85\vec{z}$. We model the Mu3e detector with the cuts

$$|\cos\theta_i| < 0.8 \quad \text{and} \quad E_i > 10 \text{ MeV}. \quad (7.22)$$

Without special modifications, Mu3e is not sensitive to photons so that we accept any photon emission.

A simple observable is the invisible energy \cancel{E}

$$\cancel{E} = M - \sum_i E_i, \quad (7.23)$$

where the sum runs over all charged tracks, i.e. the electron and the two positrons. Note that this includes the energy of undetected photons. The resulting spectrum is shown in Figure 7.13. For this plot, too, we had to perform dedicated runs with a cut of $\cancel{E} < 20$ MeV in order to obtain a good enough precision for this region. This is the reason why the statistical error briefly goes down again for small \cancel{E} .

The NLO corrections are negative except for a small region of maximal \cancel{E} . In the low-energy tail, the corrections exceed 10%, due to the ever-present large logarithms. Hence, there are fewer background events to $\mu \rightarrow 3e$ from the rare decay than expected from tree-level simulations. The cuts on the electron and positrons (7.22) are the reason for the sharp fall of the distribution at $\cancel{E} = M - 30$ MeV.

The kink in the distribution is at about $M/2$, shifted to somewhat lower values due to the effects of the non-vanishing electron mass. In fact, due to the additional real radiation of a photon, the NLO corrections amount to shifting the distribution $d\mathcal{B}/d\cancel{E}$ to higher energies.

²⁹In reality there are more runs required to sample the x distributions precise enough

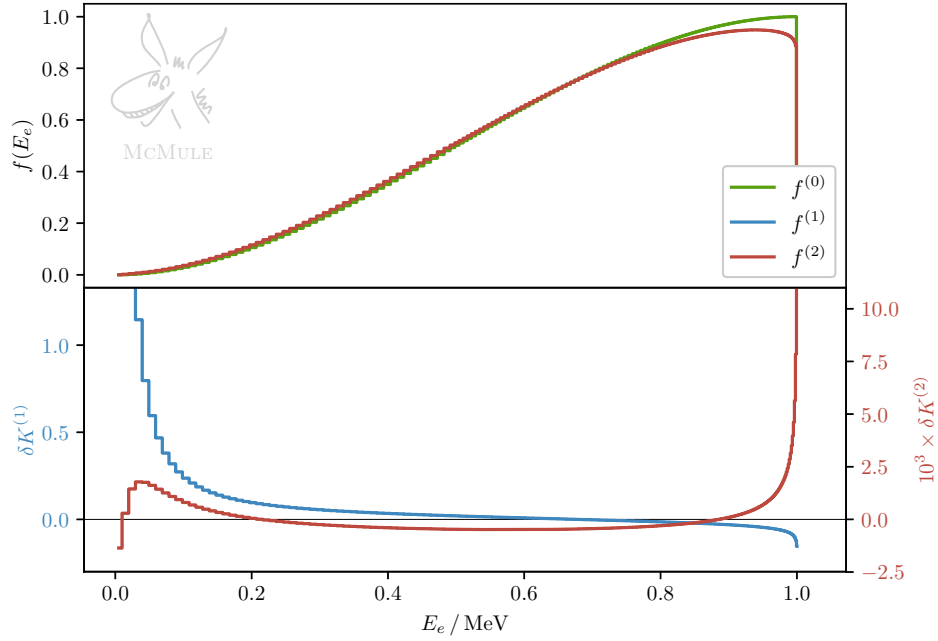
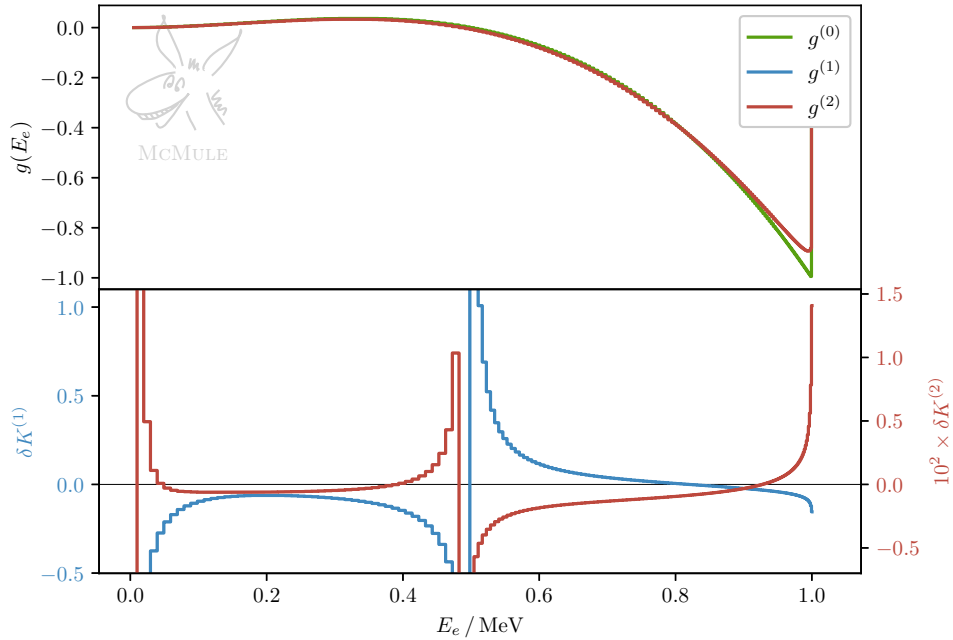
(a) The isotropic f function(b) The anisotropic g function

Figure 7.12: The isotropic and anisotropic functions $f(x_e)$ and $g(x_e)$ as defined in (7.19). The upper panel shows the functions and the lower panel the effect due to radiative corrections as $\delta K^{(i)} = f^{(i)}/f^{(i-1)}$. The left axis of the lower panel shows the NLO $\delta K^{(1)}$ and the right axis the NNLO $\delta K^{(2)}$. See text for a detailed discussion

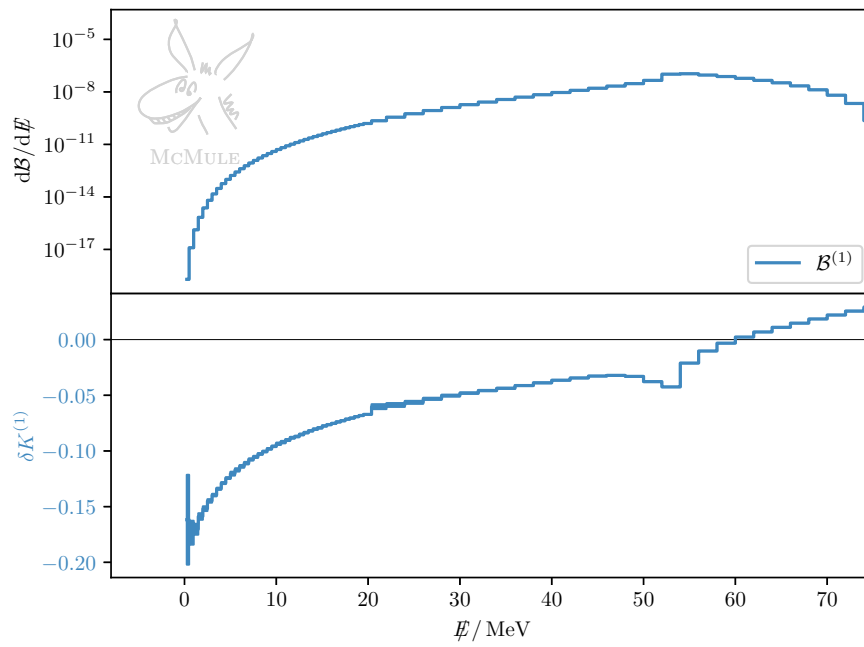


Figure 7.13: The invisible energy spectrum with the Mu3e cuts at NLO.

Chapter 8

Outlook

MCMULE supports various phenomenologically relevant processes at NLO and NNLO in QED with massive fermions. The code's development was driven by and implemented in close cooperation with the experiments that it will continue to serve.

When designing MCMULE we have two more or less distinct groups of users in mind: those who just wish to calculate tailored observables and those who wish to extend it by adding new processes. The code's structure serves both groups.

Defining new observables is as easy as changing a single file; in fact we will provide a library of legacy results [160] with the user files to reproduce all previous works by (or related to) MCMULE [1, 3, 4, 6, 7].

Thanks to the technical development of massification and FKS², adding new processes at NNLO is also relatively painless. This is good too because the demand for massive QED calculation will not abate. If anything, it will grow as more low-energy experiments push for higher and higher accuracy.

The bottleneck in the computation of cross sections for massive QED at NNLO is the availability of the matrix element $\mathcal{M}_n^{(2)}$. These computations are usually much simpler if some (or all) fermion masses m are set to zero. Unfortunately, this also spoils FKS². However, if m is small compared to the other kinematic quantities, an option is to start from the massless case and subsequently massify $\mathcal{M}_n^{(2)}$. As we have seen, this converts the collinear $1/\epsilon$ singularities of $\mathcal{M}_n^{(2)}(m=0)$ into $\log(m)$ terms that will cancel against corresponding 'singularities' of the real corrections. In addition, it retains the finite $\log(m)$ terms in $d\sigma_n^{(2)}$ that are present in differential distributions. However, terms $m \log(m)$ that vanish in the limit $m \rightarrow 0$ will be neglected. Using full m dependence in $d\sigma_{n+1}^{(2)}$, but only partial m dependence in $d\sigma_n^{(2)}$ through a massified $\mathcal{M}_n^{(2)}$ results in a mismatch in terms $m \log(m)$. Since the whole procedure of massification is anyway only correct up to such terms, the mismatch should not cause additional problems, as the terms relevant to the ξ_c independence can be included exactly.

It should be noted that a similar procedure in $d\sigma_{n+1}^{(2)}$ is less straightforward. It is not possible to naively use massification for $\mathcal{M}_{n+1}^{(1)}$. The remaining phase-space integration over the additional particle requires a non-vanishing m to avoid a collinear singularity. While this could be patched, massification relies on the fact that the small mass is the smallest scale of the process. While this is certainly often the case, it ceases to be true once we allow for soft or collinear photon emission. Hence, a crucial step will be working out the massification for real-emission matrix elements.

The extension of massification is closely connected to the problem of collinear stabilisation, i.e. finding an efficient numerical treatment of PCSs. So far we have solved this problem by dedicated tuning of the phase-space. However, this ceases to be feasible for high-multiplicity

processes. In fact, both problems – numerical stabilisation and massification of real-emissions matrix elements might be solved with the same method. The idea is to subtract pseudo-collinear regions from the integrand and add them back in integrated form [208]. However, care must be taken when integrating these terms analytically to retain a fully-differential code. This is because, in contrast to QCD where collinear emission cannot be resolved, collinear photon emission of an electron can very much be resolved experimentally.

To actually compute $\mathcal{M}_{n+1}^{(1)}$, we use FDF in conjunction with COLLIER. The usage of FDF over CDR is already a major simplification. However, maybe a much better strategy exists. Fundamentally, we are not interested in $\mathcal{M}_{n+j}^{(\ell)}$ but in the eikonal-subtracted $\mathcal{M}_{n+j}^{(\ell)f}$ that we traditionally obtain from $\mathcal{M}_{n+j}^{(\ell)}$. However, $\mathcal{M}_{n+j}^{(\ell)f}$ is *finite*. This seems to suggest that it should be possible to calculate it without ever leaving $S_{[4]}$ using numerical methods. Schematically, this is similar to the FDU scheme (four-dimensional unsubtraction) [209–212] that directly combines real and virtual corrections using only four-dimensional quantities.

Unfortunately, just adding new processes at NNLO – Møller scattering and photon pair production come to mind – is not enough. Already now, NNLO accuracy fails to be good enough for some applications. To reach the required accuracy for MUonE, it may become necessary to calculate the electronic N³LO corrections. While we do have a suitable subtraction scheme with FKS³, the relevant matrix elements are presently not known and most likely will not become known with the full mass dependence in time. Further, even if they were available, they would likely be very complicated analytic functions that are not directly suited for numerical integration. The big bottleneck here is the real-virtual-virtual contribution $\mathcal{M}_{n+1}^{(2)}$. The electronic corrections can be constructed from $\gamma^* \rightarrow q\bar{q}g$ [213, 214] that are only known for vanishing quark (or in our case, electron) masses. This makes the need for massification of real-emission matrix element even more pressing.

Whatever happens with the N³LO calculation, it presently seems exceedingly unlikely that we could go beyond even that to N⁴LO. Unfortunately, a naive extrapolation of the trend observed so-far in the radiative corrections to μ - e scattering seem to suggest that we need exactly that. Luckily, resummation provides a way out as most of the corrections come from a single source: large – and predictable – logarithms. In the framework of MCMULE, the only way to implement resummation is adding a PS that will resum the full LL tower. This way, we can capture the largest contributions of all orders without sacrificing our ability to calculate arbitrary observables.

To summarise, MCMULE has allowed for relatively easy implementation of NNLO calculations in QED with massive fermions while paving the way to N³LO calculations. In the near future, these will be matched to PS in order to resum the LL tower. Further, more exotic technical development, such as the numerical and direct evaluation $\mathcal{M}_{n+j}^{(\ell)f}$, is being proposed.

Appendix A

Conventions

When calculating loop integrals one often encounters factors of $\log(4\pi)$ and γ_E . These are artefacts of expanding the d -dimensional spherical integration in ϵ and hence not physical. Because they will drop out in any physical result, there is no need to include them to begin with. Hence, we remove the relevant factor directly by defining the loop measure as [215]

$$\mu^{2\epsilon} \frac{d^d k}{(2\pi)^d} \rightarrow [dk] = \mu^{2\epsilon} \Gamma(1 - \epsilon) \frac{d^d k}{i(4\pi)^{-d/2}} \quad (\text{A.1})$$

With this conventions, the tadpole integral reads

$$\int [dk] \frac{1}{(k^2 - \Delta)^\alpha} = (-1)^\alpha \Delta^{2-\epsilon-\alpha} \times \frac{\Gamma(1 - \epsilon) \Gamma(\alpha - 2 + \epsilon)}{\Gamma(\alpha)} \quad (\text{A.2})$$

Here we also have removed a factor $16\pi^2$ that is physical but cumbersome to write. What factors to include is somewhat arbitrary as long as this is done consistently for virtual and real correction and all factors that remain for $\epsilon \rightarrow 0$ are added back. In fact, Package-X [97] uses a different convention

$$[dk]_X = \left(\frac{ie^{-\gamma_E \epsilon}}{(4\pi)^{d/2}} \right)^{-1} d^d k. \quad (\text{A.3})$$

Both conventions have the effect of removing unwanted and distracting constants and are equally valid. However, they do differ at $\mathcal{O}(\epsilon^2)$ so attention must be paid for massless calculations where the highest pole is ϵ^{-2} or when requiring the $\mathcal{O}(\epsilon)$ terms of a massive one-loop amplitude. The relevant conversion factor is

$$\frac{[dk]}{[dk]_X} = \frac{\Gamma(1 - \epsilon)}{e^{\epsilon \gamma_E}} = 1 + \frac{\zeta_2}{2} \epsilon^2 + \frac{\zeta_3}{3} \epsilon^3 + \mathcal{O}(\epsilon^4). \quad (\text{A.4})$$

Of course other conventions exist as well.

Appendix B

Constants in FDH

For the benefit of the reader, we will collect all relevant constants for FDH calculations in this chapter. These include renormalisation constants (Section B.1), the anomalous dimensions required for the IR prediction (Section B.2) and the massification constants (Section B.3). In all cases, the CDR or HV limit can be obtained by setting $n_\epsilon \rightarrow 0$.

All results present here were previously published in [58, 102, 103] for the renormalisation constants, [102, 103] for the SCET constants and [5] for the massification constants. Some results in different schemes have obviously been published before.

All results presented use Feynman gauge.

B.1 Renormalisation constants

In this section we present the renormalisation constants Z_2 and Z_m up to $\mathcal{O}(\alpha^2)$ as well as Z_α and Z_{m_ϵ} up to $\mathcal{O}(\alpha)$. With this we can calculate processes to the muon decay as well as the electronic corrections to μ - e scattering.

All results (except Z_{α_i}) in this section are given in the *unrenormalised* coupling in accordance to the procedure set out in Section 2.1.2. Further, the scale μ of the integration is set to the muon mass $\mu = M$, assuming we are renormalising the muon field and mass. Obtaining the results for the electron is straightforward by re-introducing logarithms from $(m^2/\mu^2)^\epsilon$ per coupling.

Using the technology we set out in Chapter 3 we find for δm_ϵ

$$\begin{aligned} \delta m_\epsilon &= \left(\frac{\alpha_{0,\epsilon}}{4\pi}\right) (2M^2 n_h) \Gamma(1-\epsilon) \Gamma(\epsilon-1) + \mathcal{O}(\alpha^2) \\ &= \left(\frac{\alpha_{0,\epsilon}}{4\pi}\right) (-2M^2 n_h) \left[\frac{1}{\epsilon} + 1 + (1+\zeta_2)\epsilon + (1+\zeta_2)\epsilon^2 \right] + \mathcal{O}(\alpha^2, \epsilon^3) \end{aligned} \quad (\text{B.1})$$

A similar term is required for n_m and m^2 .

The mass renormalisation is

$$\begin{aligned} Z_m &= 1 + \left(\frac{\alpha_0}{4\pi}\right) C_F \left[-\frac{3}{\epsilon} - 4 + (-3\zeta_2 - 8)\epsilon + (-4\zeta_2 - 16)\epsilon^2 + \mathcal{O}(\epsilon^3) \right] \\ &\quad + \left(\frac{\alpha_{0,\epsilon}}{4\pi}\right) C_F n_\epsilon \left[-\frac{1}{2\epsilon} - \frac{1}{2} - \frac{1}{2}(\zeta_2 + 1)\epsilon - \frac{1}{2}(\zeta_2 - 1)\epsilon^2 + \mathcal{O}(\epsilon^3) \right] \\ &\quad + \left(\frac{\alpha_0}{4\pi}\right)^2 \left\{ C_F^2 \left[\frac{9}{2\epsilon^2} + \frac{45}{4\epsilon} - 21\zeta_2 - 12\zeta_3 + 48\zeta_2 \log 2 + \frac{199}{8} + \mathcal{O}(\epsilon) \right] \right. \\ &\quad \left. + C_A C_F \left[-\frac{11}{2\epsilon^2} - \frac{91}{4\epsilon} - 3\zeta_2 + 6\zeta_3 - 24\zeta_2 \log 2 - \frac{605}{8} + \mathcal{O}(\epsilon) \right] \right\} \end{aligned}$$

$$\begin{aligned}
& + C_A C_F n_\epsilon \left[\frac{1}{4\epsilon^2} + \frac{9}{8\epsilon} + \frac{3}{2}\zeta_2 + \frac{63}{16} + \mathcal{O}(\epsilon) \right] \\
& + n_f C_F \left[\frac{1}{\epsilon^2} + \frac{7}{2\epsilon} + 6\zeta_2 + \frac{45}{4} + \mathcal{O}(\epsilon) \right] + n_h C_F \left[\frac{1}{\epsilon^2} + \frac{7}{2\epsilon} - 6\zeta_2 + \frac{69}{4} + \mathcal{O}(\epsilon) \right] \\
& + n_m C_F \left[\frac{1}{\epsilon^2} + \frac{7}{2\epsilon} + \frac{11}{16} - \frac{1}{2}z + \left(\frac{3}{2} - 2z^2 + z^4 \right) \zeta_2 + 8z^4 H_{0,0}(z) + 4z^2 H_0(z) \right. \\
& \quad \left. + 4(z-1)^2(z^2+z+1)H_{1,0}(z) - 4(z^4+z^3+z+1)H_{-1,0}(z) + \mathcal{O}(\epsilon) \right] \Big\} \\
& + \left(\frac{\alpha_0}{4\pi} \right) \left(\frac{\alpha_{0,e}}{4\pi} \right) n_\epsilon \left\{ C_F^2 \left[-\frac{3}{2\epsilon} + 6\zeta_2 - \frac{23}{4} + \mathcal{O}(\epsilon) \right] + C_A C_F \left[-\frac{3}{4\epsilon} - 3\zeta_2 - \frac{11}{8} + \mathcal{O}(\epsilon) \right] \right\} \\
& + \left(\frac{\alpha_{0,e}}{4\pi} \right)^2 n_\epsilon \left\{ C_F^2 \left[\frac{1}{\epsilon^2} + \frac{3}{\epsilon} + 6 + \mathcal{O}(\epsilon) \right] + C_F^2 n_\epsilon \left[-\frac{1}{8\epsilon^2} - \frac{13}{16\epsilon} + \frac{5}{4}\zeta_2 - \frac{75}{32} + \mathcal{O}(\epsilon) \right] \right. \\
& \quad C_A C_F \left[-\frac{1}{2\epsilon^2} - \frac{3}{2\epsilon} - 3 + \mathcal{O}(\epsilon) \right] + C_A C_F n_\epsilon \left[\frac{1}{4\epsilon^2} + \frac{3}{4\epsilon} + \frac{3}{2} + \mathcal{O}(\epsilon) \right] \\
& \quad + C_F n_f \left[\frac{1}{4\epsilon^2} + \frac{5}{8\epsilon} + \frac{3}{2}\zeta_2 + \frac{11}{16} + \mathcal{O}(\epsilon) \right] + C_F n_h \left[\frac{1}{4\epsilon^2} + \frac{5}{8\epsilon} + \frac{1}{2}\zeta_2 + \frac{3}{16} + \mathcal{O}(\epsilon) \right] \\
& \quad + C_F n_m \left[\frac{1}{4\epsilon^2} + \frac{5}{8\epsilon} + \frac{11}{16} - \frac{1}{2}z^2 + \left(\frac{3}{2} - 2z^2 + z^4 \right) \zeta_2 + 2(z^2-2)z^2 H_{0,0}(z) - z^2 H_0(z) \right. \\
& \quad \left. - (z^2-1)^2 H_{-1,0}(z) + (z^2-1)^2 H_{1,0}(z) + \mathcal{O}(\epsilon) \right] \Big\} + \mathcal{O}(\alpha^3). \tag{B.2}
\end{aligned}$$

Similarly, the wave-function is renormalised through

$$\begin{aligned}
Z_2 = & 1 + \left(\frac{\alpha_0}{4\pi} \right) C_F \left[-\frac{3}{\epsilon} - 4 + (-3\zeta_2 - 8)\epsilon + (-4\zeta_2 - 16)\epsilon^2 + \mathcal{O}(\epsilon^3) \right] \\
& + \left(\frac{\alpha_{0,e}}{4\pi} \right) C_F n_\epsilon \left[-\frac{1}{2\epsilon} - \frac{1}{2} - \frac{1}{2}(\zeta_2 + 1)\epsilon - \frac{1}{2}(\zeta_2 - 1)\epsilon^2 + \mathcal{O}(\epsilon^3) \right] \\
& + \left(\frac{\alpha_0}{4\pi} \right)^2 \left\{ C_F^2 \left[\frac{9}{2\epsilon^2} + \frac{51}{4\epsilon} - 69\zeta_2 - 24\zeta_3 + 96\zeta_2 \log 2 + \frac{433}{8} + \mathcal{O}(\epsilon) \right] \right. \\
& \quad C_A C_F \left[-\frac{11}{2\epsilon^2} - \frac{101}{4\epsilon} + 19\zeta_2 + 12\zeta_3 - 48\zeta_2 \log 2 - \frac{803}{8} + \mathcal{O}(\epsilon) \right] \\
& \quad + C_A C_F n_\epsilon \left[\frac{1}{4\epsilon^2} + \frac{11}{8\epsilon} + \frac{3}{2}\zeta_2 + \frac{81}{16} + \mathcal{O}(\epsilon) \right] \\
& \quad + C_F n_f \left[\frac{1}{\epsilon^2} + \frac{9}{2\epsilon} + 6\zeta_2 + \frac{59}{4} + \mathcal{O}(\epsilon) \right] + C_F n_h \left[\frac{2}{\epsilon^2} + \frac{19}{6\epsilon} + \frac{1139}{36} - 12\zeta_2 + \mathcal{O}(\epsilon) \right] \\
& \quad + C_F n_m \left[\frac{2}{\epsilon^2} + \frac{1}{\epsilon} \left(\frac{19}{6} - 4H_0(z) \right) + \frac{635}{36} + 14z^2 + (8 - 18z - 30z^3 + 12z^4)\zeta_2 \right. \\
& \quad \quad - 2(6z^4 + 5z^3 + 3z + 2)H_{-1,0}(z) + 2(6z^4 - 5z^3 - 3z + 2)H_{1,0}(z) \\
& \quad \quad \left. + 8(3z^4 + 2)H_{0,0}(z) + (8z^2 + \frac{16}{3})H_0(z) + \mathcal{O}(\epsilon) \right] \Big\} \\
& + \left(\frac{\alpha_0}{4\pi} \right) \left(\frac{\alpha_{0,e}}{4\pi} \right) n_\epsilon \left\{ + C_F^2 \left[\frac{3}{2\epsilon} + \frac{47}{4} - 6\zeta_2 + \mathcal{O}(\epsilon) \right] + C_A C_F \left[-\frac{9}{4\epsilon} + \zeta_2 - \frac{77}{8} + \mathcal{O}(\epsilon) \right] \right\}
\end{aligned}$$

$$\begin{aligned}
& + \left(\frac{\alpha_{0,\epsilon}}{4\pi}\right)^2 n_\epsilon \left\{ C_F^2 \left[\frac{1}{\epsilon^2} + \frac{2}{\epsilon} + 4\zeta_2 - 3 + \mathcal{O}(\epsilon) \right] + C_F^2 n_\epsilon \left[-\frac{1}{8\epsilon^2} - \frac{3}{16\epsilon} + \frac{91}{32} - \frac{7}{4}\zeta_2 + \mathcal{O}(\epsilon) \right] \right. \\
& + C_A C_F \left[-\frac{1}{2\epsilon^2} - \frac{1}{\epsilon} + \frac{3}{2} - 2\zeta_2 + \mathcal{O}(\epsilon) \right] + C_A C_F n_\epsilon \left[\frac{1}{4\epsilon^2} + \frac{1}{2\epsilon} + \zeta_2 - \frac{3}{4} + \mathcal{O}(\epsilon) \right] \\
& + C_F n_f \left[\frac{1}{4\epsilon^2} + \frac{7}{8\epsilon} + \frac{3\zeta_2}{2} + \frac{21}{16} + \mathcal{O}(\epsilon) \right] + C_F n_h \left[\frac{1}{4\epsilon^2} + \frac{7}{8\epsilon} + \frac{\zeta_2}{2} - \frac{3}{16} + \mathcal{O}(\epsilon) \right] \\
& + C_F n_m \left[\frac{1}{4\epsilon^2} + \frac{7}{8\epsilon} + \frac{21}{16} - \frac{3}{2}z^2 + \left(\frac{3}{2} - 4z^2 + 3z^4\right)\zeta_2 + (6z^4 - 8z^2)H_{0,0}(z) - 3z^2 H_0(z) \right. \\
& \left. + (-3z^4 + 4z^2 - 1)H_{-1,0}(z) + (3z^4 - 4z^2 + 1)H_{1,0}(z) + \mathcal{O}(\epsilon) \right] \left. \right\} + \mathcal{O}(\alpha^3).
\end{aligned} \tag{B.3}$$

Note that the one-loop coefficients of Z_2 and Z_m match. However, this is clearly a coincidence as it ceases to be true at two-loop.

If we work in a theory with some massless and some massive flavours we need a further renormalisation constant that renormalises diagrams where a heavy-fermion loop is inserted in the light-fermion propagator corrections. This constant starts at the two-loop level and is

$$\begin{aligned}
Z_{2,l} &= 1 + \left(\frac{\alpha_0}{2\pi}\right)^2 C_F n_h \left[\frac{1}{2\epsilon} - \frac{5}{12} + \mathcal{O}(\epsilon) \right] + \left(\frac{\alpha_\epsilon}{4\pi}\right)^2 C_F n_h n_\epsilon \left[-\frac{1}{4\epsilon^2} + \frac{3}{8\epsilon} - \frac{\zeta_2}{2} - \frac{13}{16} + \mathcal{O}(\epsilon) \right] \\
& + \mathcal{O}(\alpha^3).
\end{aligned} \tag{B.4}$$

Next, we need the renormalisation constants for the couplings. Those will be given in the $\overline{\text{MS}}$ scheme. If other schemes, such as the OS scheme for the coupling is desired, this can be fixed *after* setting $\bar{\alpha}_e = \bar{\alpha}$ and $n_\epsilon = 2\epsilon$.

$$\begin{aligned}
Z_\alpha &= 1 + \frac{\bar{\alpha}}{4\pi} \left[\frac{\beta_{20}}{\epsilon} \right] + \mathcal{O}(\bar{\alpha}_i^2) \\
Z_{\alpha_e} &= 1 + \frac{\bar{\alpha}_e}{4\pi} \left[\frac{\beta_{02}}{\epsilon} \right] + \frac{\bar{\alpha}}{4\pi} \left[\frac{\beta_{11}}{\epsilon} \right] + \mathcal{O}(\bar{\alpha}_i^2),
\end{aligned} \tag{B.5}$$

For obvious reasons, we give Z_{α_i} in the renormalised couplings. The β coefficients are

$$\begin{aligned}
\beta_{20} &= \beta_0 + n_\epsilon \left(-\frac{C_A}{6} \right), \\
\beta_{11} &= 6C_F, \\
\beta_{02} &= -4C_F + 2C_A - 2T_R N_F + n_\epsilon (C_F - C_A),
\end{aligned} \tag{B.6}$$

where $\beta_0 = 11/3C_A - 4/3T_R N_F$ is the normal β_0 of CDR. Here we have defined the shorthand $N_F = n_h + n_m + n_f$ as the sum of all active flavours, independent of mass. To convert these results into the OS scheme, we set [53]

$$\alpha = \bar{\alpha} \frac{\bar{Z}_\alpha}{Z_\alpha} = \bar{\alpha} \left[1 - \frac{4}{3} \frac{\bar{\alpha}}{4\pi} \log \frac{\mu^2}{M^2} \right], \tag{B.7}$$

for each active fermion with mass M .

B.2 Infrared prediction in QCD

In this section we will give results for QCD with some massive and some massless flavours. The QED limit is straightforward by setting $C_F \rightarrow 1$, $C_A \rightarrow 0$, and $n_f \rightarrow 0$.

As discussed in Section 2.4, we use SCET to predict the IR structure of an amplitude. For this we need to calculate the process's anomalous dimension $\mathbf{\Gamma}$ with (2.37) and determine \mathbf{Z} by solving the RGE (2.30b). \mathbf{Z} then shares the IR structure with our amplitude after we have performed the decoupling transformation [72, 103]

$$\zeta_\alpha = 1 + \left(\frac{\alpha}{4\pi}\right) n_h \frac{4}{3} \log \frac{\mu^2}{M^2} + \mathcal{O}(\alpha^2), \quad (\text{B.8})$$

$$\zeta_{\alpha_e} = 1 + \left(\frac{\alpha_e}{4\pi}\right) n_h 2 \log \frac{\mu^2}{M^2} + \mathcal{O}(\alpha^2). \quad (\text{B.9})$$

In FDH, the presence of the evanescent coupling makes the RGE more complicated [70]. We restrict ourselves mostly to QED again because three- and four-gauge vertices become very complicated as soon as they involve ϵ -scalars. We have

$$\begin{aligned} \log \mathbf{Z} &= \left(\frac{\vec{\alpha}}{4\pi}\right) \left(\frac{\vec{\mathbf{\Gamma}}'_1}{4\epsilon^2} + \frac{\vec{\mathbf{\Gamma}}_1}{2\epsilon}\right) \\ &+ \sum_{m+n=2} \left(\frac{\alpha}{4\pi}\right)^m \left(\frac{\alpha_e}{4\pi}\right)^n \left(-\frac{3\vec{\beta}_{mn} \cdot \vec{\mathbf{\Gamma}}'_1}{16\epsilon^3} - \frac{\vec{\beta}_{mn} \cdot \vec{\mathbf{\Gamma}}_1}{4\epsilon^2} + \frac{\mathbf{\Gamma}'_{mn}}{16\epsilon^2} + \frac{\mathbf{\Gamma}_{mn}}{4\epsilon}\right) + \mathcal{O}(\alpha^3), \end{aligned} \quad (\text{B.10})$$

where we have defined the shorthand notation for terms involving only one-loop quantities

$$\begin{aligned} \vec{\alpha} \cdot \vec{\mathbf{\Gamma}}_1 &= \alpha \mathbf{\Gamma}_{10} + \alpha_e \mathbf{\Gamma}_{01}, \\ \vec{\beta} \cdot \vec{\mathbf{\Gamma}}_1 &= \beta_{10} \mathbf{\Gamma}_{10} + \beta_{01} \mathbf{\Gamma}_{01}. \end{aligned} \quad (\text{B.11})$$

Here, we have used $\mathbf{\Gamma}_{mn}$ (β_{mn}) to indicate the $\alpha^m \alpha_e^n$ coefficient of $\mathbf{\Gamma}$ (β). $\vec{\beta}$ is given in (B.6) and $\mathbf{\Gamma}$ is constructed as in (2.37)

$$\begin{aligned} \mathbf{\Gamma}(\mu) &= \sum_{i,j} \gamma_{\text{cusp}} \log \frac{\mu^2}{-\text{sign}_{ij} 2p_i \cdot p_j} + \sum_i \gamma_i \\ &- \sum_{I,J} \gamma_{\text{cusp}}(\chi_{I,J}) + \sum_I \gamma_I \\ &+ \sum_{I,j} \gamma_{\text{cusp}} \log \frac{m_I \mu}{-\text{sign}_{Ij} 2p_I \cdot p_j}. \end{aligned} \quad (\text{B.12})$$

Let us go through the four anomalous dimensions appearing here:

- The light-quark anomalous dimension γ_i [70]

$$\begin{aligned} \gamma_i &= \left(\frac{\alpha}{4\pi}\right) (-3C_F) + \left(\frac{\alpha_e}{4\pi}\right) n_\epsilon \frac{C_F}{2} \\ &+ \left(\frac{\alpha}{4\pi}\right)^2 \left[C_F^2 \left(-\frac{3}{2} + 12\zeta_2 - 24\zeta_3\right) + C_F n_f \left(\frac{130}{27} + 4\zeta_2\right) \right. \\ &\quad \left. + C_A C_F \left(-\frac{961}{54} - 11\zeta_2 + 26\zeta_3\right) \right] \\ &+ \left(\frac{\alpha}{4\pi}\right) \left(\frac{\alpha_e}{4\pi}\right) n_\epsilon \left[C_A C_F \frac{11}{2} - C_F^2 (2 + 2\zeta_2) \right] + \left(\frac{\alpha_e}{4\pi}\right)^2 n_\epsilon \left[-\frac{1}{8} n_\epsilon C_F^2 - \frac{3}{2} n_f \right] + \mathcal{O}(\alpha^3). \end{aligned} \quad (\text{B.13})$$

- The heavy-quark anomalous dimension γ_i [103]

$$\gamma_I = \left(\frac{\alpha}{4\pi}\right)(-2C_F) + \left(\frac{\alpha}{4\pi}\right)^2 \left[C_A C_F \left(-\frac{98}{9} + 4\zeta_2 - 4\zeta_3 + \frac{8}{9}n_\epsilon \right) + C_F n_f \frac{40}{9} \right] + \mathcal{O}(\alpha^3). \quad (\text{B.14})$$

- The normal cusp anomalous dimension γ_{cusp} is [70]

$$\gamma_{\text{cusp}} = \left(\frac{\alpha}{4\pi}\right)(4) + \left(\frac{\alpha}{4\pi}\right)^2 \left[C_A \left(\frac{268}{9} - 8\zeta_2 \right) - \frac{80}{9}n_f - n_\epsilon C_A \frac{16}{9} \right] + \mathcal{O}(\alpha^3). \quad (\text{B.15})$$

- Finally, we have the velocity dependent cusp anomalous dimension $\gamma_{\text{cusp}}(\chi)$ [103]

$$\begin{aligned} \gamma_{\text{cusp}}(\chi) = & \gamma_{\text{cusp}} \chi \coth \chi + \left(\frac{\alpha}{4\pi}\right)^2 8C_A \left\{ \chi^2 + \zeta_2 + \zeta_3 \right. \\ & + \coth \chi \left[\text{Li}_2(e^{-2\chi}) - 2\chi \log(1 - e^{-2\chi}) - \zeta_2(1 + \chi) - \chi^2 - \frac{\chi^3}{3} \right] \\ & \left. + \coth^2 \chi \left[\text{Li}_3(e^{-2\chi}) + \chi \text{Li}_2(e^{-2\chi}) - \zeta_3 + \zeta_2 \chi + \frac{\chi^3}{3} \right] \right\} + \mathcal{O}(\alpha^3). \end{aligned} \quad (\text{B.16})$$

Beyond the one-loop level, these anomalous dimensions do not have C_F^2 , $C_F n_m$, or $C_F n_h$ terms. This implies that soft singularities associated to these terms exponentiate – just as expected.

B.3 Massification

Our discussion of massification was still missing the explicit expression of Z_q

$$\begin{aligned} \sqrt{Z_q} = & 1 + a_0 C_F \left\{ \frac{1}{\epsilon^2} + \frac{1}{2\epsilon} + \zeta_2 + 2 + \left(4 + \frac{1}{2}\zeta_2\right)\epsilon + \left(8 + 2\zeta_2 + \frac{7}{4}\zeta_4\right)\epsilon^2 + \mathcal{O}(\epsilon^3) \right\} \\ & + a_{0,e} C_F \frac{n_\epsilon}{4} \left\{ -\frac{1}{\epsilon} - 1 - (1 + \zeta_2)\epsilon - (1 + \zeta_2)\epsilon^2 + \mathcal{O}(\epsilon^3) \right\} \\ & + \left(a_0(s)\right)^2 \left\{ C_F^2 \left[\frac{1}{2\epsilon^4} + \frac{1}{2\epsilon^3} + \frac{1}{\epsilon^2} \left(\frac{51}{24} + \zeta_2 \right) + \frac{1}{\epsilon} \left(\frac{43}{8} - 2\zeta_2 + 6\zeta_3 \right) \right. \right. \\ & \left. \left. + \frac{369}{16} + \frac{61}{4}\zeta_2 - 18\zeta_4 - 24\zeta_2 \log 2 - 3\zeta_3 \right] \right. \\ & + C_F C_A \left[\frac{11}{12\epsilon^3} + \frac{1}{\epsilon^2} \left(\frac{25}{9} - \frac{1}{2}\zeta_2 \right) + \frac{1}{\epsilon} \left(\frac{1957}{216} + \frac{13}{2}\zeta_2 - \frac{15}{2}\zeta_3 \right) \right. \\ & \left. \left. + \frac{31885}{1296} + \frac{38}{3}\zeta_2 - 13\zeta_4 + 12\zeta_2 \log 2 + \frac{13}{3}\zeta_3 \right] \right. \\ & - C_F C_A \frac{n_\epsilon}{12} \left[\frac{1}{2\epsilon^3} + \frac{11}{6\epsilon^2} + \frac{1}{\epsilon} \left(\frac{215}{36} + 3\zeta_2 \right) + \frac{4559}{216} + 11\zeta_2 + 4\zeta_3 \right] \\ & \left. + C_F n_f \frac{1}{6} \left[-\frac{1}{\epsilon^3} - \frac{8}{3\epsilon^2} - \frac{1}{\epsilon} \left(\frac{149}{18} + 6\zeta_2 \right) - \frac{3269}{108} - 16\zeta_2 - 8\zeta_3 \right] \right\} \end{aligned}$$

$$\begin{aligned}
& + C_F n_m \frac{2}{3} \left[\frac{1}{\eta} \left(\frac{1}{\epsilon^2} - \frac{5}{3\epsilon} + \frac{28}{9} + 2\zeta_2 \right) - \frac{1}{\epsilon^3} + \frac{1}{2\epsilon^2} + \frac{1}{\epsilon} \left(-\frac{55}{24} - 3\zeta_2 \right) \right. \\
& \quad \left. + \frac{1675}{432} - 2\zeta_2 + \zeta_3 \right] \\
& + a_{0,e} a_0 \left\{ C_F^2 \frac{n_\epsilon}{4} \left[-\frac{1}{\epsilon^3} - \frac{9}{2\epsilon^2} - \frac{15}{2\epsilon} - 23\zeta_2 - 2\zeta_3 + 1 \right] \right. \\
& \quad \left. + C_A C_F \frac{n_\epsilon}{8} \left[-\frac{11}{\epsilon} - \frac{105}{2} + 4\zeta_2 + 20\zeta_3 \right] \right\} \\
& + (a_{0,e})^2 \left\{ (C_F n_\epsilon)^2 \frac{1}{32} \left[-\frac{3}{\epsilon^2} - \frac{5}{\epsilon} - 30\zeta_2 + \frac{85}{2} \right] \right. \\
& \quad + C_F n_f \frac{n_\epsilon}{8} \left[\frac{1}{\epsilon^2} + \frac{7}{2\epsilon} + \frac{21}{4} + 6\zeta_2 \right] \\
& \quad + C_F n_\epsilon \left(\frac{C_F}{2} + \frac{n_\epsilon C_A}{8} - \frac{C_A}{4} \right) \left[\frac{1}{\epsilon^2} + \frac{2}{\epsilon} - 3 + 4\zeta_2 \right] \\
& \quad \left. + C_F n_\epsilon n_m \frac{1}{8} \left[\frac{1}{\epsilon^2} + \frac{7}{2\epsilon} - \frac{3}{4} + 2\zeta_2 \right] \right\} + \mathcal{O}(a_i^3, \epsilon, \eta). \tag{B.17}
\end{aligned}$$

Here, we have defined $a_i^0(x)$ as in (5.49)

$$a_i^0(x) = \left(\frac{\alpha_i^0}{4\pi} \right) \left(\frac{\mu^2}{m^2} \right)^\epsilon (-2 + i0^+)^{\eta/2} \left(\frac{-\nu^2}{x} \right)^{\eta/2}, \quad i \in \{s, e\}, \tag{B.18}$$

through the unrenormalised coupling. The factorisation anomaly, i.e. the pole in $1/\eta$, either cancels with the soft function or with a similar contribution due to the anti-collinear jet \bar{Z}_q that is identical to Z_q except for the n_m term

$$\begin{aligned}
\sqrt{\bar{Z}_q} \Big|_{n_m} & = (a_s^0(m^2))^2 C_F n_m \frac{2}{3} \left[-\frac{1}{\eta} \left(\frac{1}{\epsilon^2} - \frac{5}{3\epsilon} + \frac{28}{9} + 2\zeta_2 \right) + \frac{1}{2\epsilon^3} - \frac{5}{6\epsilon^2} - \frac{253}{72\epsilon} \right. \\
& \quad \left. + \frac{5083}{432} - \frac{14}{3}\zeta_2 - \zeta_3 \right] + \mathcal{O}(a_s^3, \epsilon, \eta). \tag{B.19}
\end{aligned}$$

B.4 Conclusion

We now have all necessary constants to perform any calculation in FDH at the two-loop level. These results are three-loop ready in that they contain n_ϵ . However, before we can use even these two-loop results in any actual three-loop calculations, we need to expand everything up to at least $\mathcal{O}(\epsilon)$ or even $\mathcal{O}(\epsilon^2)$ for Z_q . For Z_m and Z_2 , this is trivial because their exact ϵ dependence is known in terms of hypergeometric functions. This is unfortunately not true for the more complicated Z_q .

Appendix C

Eikonal integrals $\hat{\mathcal{E}}$

Here we give the explicit form of integrated eikonal required for massive QED. These expressions have been computed in [109]. As discussed in the text, we do not need terms $\mathcal{O}(\epsilon)$ or higher: terms of $\mathcal{O}(\epsilon)$ in $\hat{\mathcal{E}}$ have no effect since they do not modify $\mathcal{M}_n^{(\ell)f}$ after setting $d = 4$. This means we can set them to zero and there is no need to compute $\hat{\mathcal{E}}$ beyond finite terms.

We start with defining a few auxiliary quantities:

$$\beta_j \equiv \sqrt{1 - \frac{m_j^2}{E_j^2}}, \quad v_{kj} \equiv \sqrt{1 - \left(\frac{m_j m_k}{p_j \cdot p_k}\right)^2}, \quad a_{kj} \equiv (1 + v_{kj}) \frac{p_j \cdot p_k}{m_k^2}, \quad \nu_{kj} \equiv \frac{a_{kj}^2 m_k^2 - m_j^2}{2(a_{kj} E_k - E_j)}. \quad (\text{C.1})$$

Following [109], the integrated eikonal can then be written as

$$\hat{\mathcal{E}}_{kj} = \frac{\alpha}{2\pi} \frac{(4\pi)^\epsilon}{\Gamma(1-\epsilon)} \left(\frac{\xi_c^2 s}{\mu^2}\right)^{-\epsilon} \left(-\frac{1}{2\epsilon} \frac{1}{v_{kj}} \log \frac{1+v_{kj}}{1-v_{kj}} + \frac{a_{kj}(p_j \cdot p_k)}{2(a_{kj}^2 m_k^2 - m_j^2)} \left(J(a_{kj} E_k, \beta_k, \nu_{kj}) - J(E_j, \beta_j, \nu_{kj}) \right) \right) + \mathcal{O}(\epsilon), \quad (\text{C.2})$$

where we have used the function

$$J(x, y, z) = \left(\log^2 \frac{1-y}{1+y} + 4 \text{Li}_2 \left(1 - \frac{x(1+y)}{z} \right) + 4 \text{Li}_2 \left(1 - \frac{x(1-y)}{z} \right) \right) \quad (\text{C.3})$$

For the case $j = k$ this expression simplifies to

$$\hat{\mathcal{E}}_{jj} = \frac{\alpha}{2\pi} \frac{(4\pi)^\epsilon}{\Gamma(1-\epsilon)} \left(\frac{\xi_c^2 s}{\mu^2}\right)^{-\epsilon} \left(-\frac{1}{\epsilon} - \frac{1}{\beta_j} \log \frac{1+\beta_j}{1-\beta_j} \right) + \mathcal{O}(\epsilon) \quad (\text{C.4})$$

for the self-eikonals.

Appendix D

Explicit derivation of FKS³

In Section 4.3.1, we have skipped the detailed derivation of FKS³. While we motivated that all auxiliary integrals can be avoided by setting all ξ_c equal, we have not shown this because the iterative eikonal subtracting and expanding is rather lengthy. In the following we will go through all contributions and show that indeed all auxiliary integrals cancel. One concession we will make for simplicity is to set already those ξ_c equal that we have set equal in FKS².

At N³LO, we have four terms

$$\sigma^{(3)} = \int d\Phi_n \mathcal{M}_n^{(3)} + \int d\Phi_{n+1} \mathcal{M}_{n+1}^{(2)} + \int d\Phi_{n+2} \mathcal{M}_{n+2}^{(1)} + \int d\Phi_{n+3} \mathcal{M}_{n+3}^{(0)}, \quad (\text{D.1})$$

which are separately divergent and that we will re-organise according to the scheme's prescription.

D.1 Real-virtual-virtual contribution

Let us begin with the real-virtual-virtual part that we split again into a hard and soft contribution

$$d\sigma_{rvv}^{(3)} = d\Phi_{n+1} \mathcal{M}_{n+1}^{(2)} = d\sigma_s^{(3)}(\xi_c) + d\sigma_h^{(3)}(\xi_c) \quad (\text{D.2})$$

as in (4.19). Using that even at the two-loop level

$$\mathcal{S}_{n+1} \mathcal{M}_{n+1}^{(2)} = \mathcal{E}_{n+1} \mathcal{M}_n^{(2)}, \quad (\text{D.3})$$

the soft contribution in analogy to (4.14) and (4.21) is given by

$$d\sigma_s^{(3)}(\xi_c) \rightarrow d\Phi_n \hat{\mathcal{E}}(\xi_c) \mathcal{M}_n^{(2)}. \quad (\text{D.4})$$

The hard contribution is now

$$\begin{aligned} d\sigma_h^{(3)}(\xi_c) &= d\Upsilon_1 d\Phi_{n,1} d\xi \left(\frac{1}{\xi^{1+2\epsilon}} \right)_c (\xi^2 \mathcal{M}_{n+1}^{(2)}) \\ &= d\Upsilon_1 d\Phi_{n,1} d\xi \left(\frac{1}{\xi^{1+2\epsilon}} \right)_c \xi^2 \left(\mathcal{M}_{n+1}^{(2)f} - \hat{\mathcal{E}}(\xi_c) \mathcal{M}_{n+1}^{(1)} - \frac{1}{2!} \hat{\mathcal{E}}(\xi_c)^2 \mathcal{M}_{n+1}^{(0)} \right) \\ &= d\sigma_f^{(3)}(\xi_c) + \underbrace{d\sigma_{d1}^{(3)}(\xi_c) + d\sigma_{d0}^{(3)}(\xi_c)}_{d\sigma_d^{(3)}(\xi_c)} \end{aligned} \quad (\text{D.5})$$

where $d\sigma_f^{(3)}$ is finite and the divergent part $d\sigma_d^{(3)}$ is composed of

$$\int d\sigma_{d1}^{(3)}(\xi_c) = - \int d\Upsilon_1 d\Phi_{n,1} d\xi \left(\frac{1}{\xi^{1+2\epsilon}} \right)_c \xi^2 \left(\hat{\mathcal{E}}(\xi_c) \mathcal{M}_{n+1}^{(1)} \right) \equiv -\mathcal{I}^{(1)}(\xi_c), \quad (\text{D.6a})$$

$$\int d\sigma_{d0}^{(3)}(\xi_c) = - \int \frac{1}{2!} d\Upsilon_1 d\Phi_{n,1} d\xi \left(\frac{1}{\xi^{1+2\epsilon}} \right)_c \xi^2 \left(\hat{\mathcal{E}}(\xi_c)^2 \mathcal{M}_{n+1}^{(0)} \right) \equiv -\frac{1}{2!} \mathcal{J}(\xi_c). \quad (\text{D.6b})$$

Above we have defined two functions $\mathcal{I}^{(1)}$ and \mathcal{J} that are potentially tedious to compute. However, as we will see they cancel in the final result, similar to the function \mathcal{I} at NNLO.

D.2 Real-real-virtual contribution

The real-real-virtual contribution are similar to the double-real contribution of FKS²

$$d\sigma_{rrv}^{(3)} = d\Phi_{n+2}\mathcal{M}_{n+2}^{(1)} = d\sigma_{ss}^{(3)}(\xi_c) + d\sigma_{sh}^{(3)}(\xi_c) + d\sigma_{hs}^{(3)}(\xi_c) + d\sigma_{hh}^{(3)}(\xi_c), \quad (\text{D.7a})$$

$$\left\{ \begin{array}{l} d\sigma_{ss}^{(3)}(\xi_c) \\ d\sigma_{hs}^{(3)}(\xi_c) \\ d\sigma_{sh}^{(3)}(\xi_c) \\ d\sigma_{hh}^{(3)}(\xi_c) \end{array} \right\} = d\Upsilon_1 d\Upsilon_2 d\Phi_{n,2} \frac{1}{2!} \left\{ \begin{array}{l} \frac{\xi_c^{-2\epsilon}}{2\epsilon} \delta(\xi_1) \frac{\xi_c^{-2\epsilon}}{2\epsilon} \delta(\xi_2) \\ -\frac{\xi_c^{-2\epsilon}}{2\epsilon} \delta(\xi_2) \left(\frac{1}{\xi_1^{1+2\epsilon}} \right)_c \\ -\frac{\xi_c^{-2\epsilon}}{2\epsilon} \delta(\xi_1) \left(\frac{1}{\xi_2^{1+2\epsilon}} \right)_c \\ \left(\frac{1}{\xi_1^{1+2\epsilon}} \right)_c \left(\frac{1}{\xi_2^{1+2\epsilon}} \right)_c \end{array} \right\} d\xi_1 d\xi_2 \xi_1^2 \xi_2^2 \mathcal{M}_{n+2}^{(1)}. \quad (\text{D.7b})$$

Obviously $\int d\sigma_{hs}^{(3)} = \int d\sigma_{sh}^{(3)}$ and

$$\int d\sigma_{hs}^{(3)}(\xi_c) = d\Upsilon_1 d\Upsilon_2 d\Phi_{n,2} \frac{1}{2!} \int d\xi_1 \left(\frac{1}{\xi_1^{1+2\epsilon}} \right)_c (\xi_1^2 \mathcal{M}_{n+1}^{(1)}) \hat{\mathcal{E}}(\xi_c) = \frac{1}{2!} \mathcal{I}^{(1)}(\xi_c). \quad (\text{D.8})$$

Furthermore, as for (4.33) we find

$$d\sigma_{ss}^{(3)}(\xi_c) \rightarrow d\Phi_n \frac{1}{2!} \hat{\mathcal{E}}(\xi_c)^2 \mathcal{M}_n^{(1)}. \quad (\text{D.9})$$

The hard contribution is not yet finite due to the explicit $1/\epsilon$ pole in $\mathcal{M}_{n+2}^{(1)}$. As is customary by now we again perform an eikonal subtraction

$$\mathcal{M}_{n+2}^{(1)} \equiv \mathcal{M}_{n+2}^{(1)f}(\xi_c) - \hat{\mathcal{E}}(\xi_c) \mathcal{M}_{n+2}^{(0)}. \quad (\text{D.10})$$

and write

$$d\sigma_{hh}^{(3)}(\xi_c) = d\sigma_{hf}^{(3)}(\xi_c) + d\sigma_{hd}^{(3)}(\xi_c), \quad (\text{D.11a})$$

$$d\sigma_{hf}^{(3)}(\xi_c) = d\Upsilon_1 d\Upsilon_2 d\Phi_{n,2} \frac{1}{2!} \left(\frac{1}{\xi_1^{1+2\epsilon}} \right)_c \left(\frac{1}{\xi_2^{1+2\epsilon}} \right)_c \xi_1^2 \xi_2^2 \mathcal{M}_{n+2}^{(1)f}(\xi_c), \quad (\text{D.11b})$$

$$\int d\sigma_{hd}^{(3)}(\xi_c) = - \int d\Upsilon_1 d\Upsilon_2 d\Phi_{n,2} \frac{1}{2!} \left(\frac{1}{\xi_1^{1+2\epsilon}} \right)_c \left(\frac{1}{\xi_2^{1+2\epsilon}} \right)_c \xi_1^2 \xi_2^2 \hat{\mathcal{E}}(\xi_c) \mathcal{M}_{n+2}^{(0)} \equiv -\frac{1}{2!} \mathcal{K}(\xi_c). \quad (\text{D.11c})$$

Here we have defined a third auxiliary function \mathcal{K} that will cancel in the final result.

D.3 Triple-real contributions

The evaluation of the triple-real contributions proceeds along the lines of the FKS² double-real part, albeit with more (individually ξ_c dependent) terms

$$d\sigma_{rrr}^{(3)} = d\Phi_{n+3} \mathcal{M}_{n+3}^{(0)} = d\sigma_{hhh}^{(3)} + \underbrace{d\sigma_{hhs}^{(3)} + d\sigma_{hsh}^{(3)} + d\sigma_{shh}^{(3)}}_{3d\sigma_{hhs}^{(3)}} + \underbrace{d\sigma_{hss}^{(3)} + d\sigma_{shs}^{(3)} + d\sigma_{ssh}^{(3)}}_{3d\sigma_{hss}^{(3)}} + d\sigma_{sss}^{(3)}. \quad (\text{D.12})$$

Because we choose all ξ_c equal, it does not matter which photon is soft, just how many. Thus, we are left with four different kinds of contributions

$$\left\{ \begin{array}{l} d\sigma_{sss}^{(3)}(\xi_c) \\ d\sigma_{hss}^{(3)}(\xi_c) \\ d\sigma_{hhs}^{(3)}(\xi_c) \\ d\sigma_{hhh}^{(3)}(\xi_c) \end{array} \right\} = \prod_{i=1}^3 \left(d\Upsilon_i d\xi_i \xi_i^2 \right) d\Phi_{n,3} \frac{\mathcal{M}_{n+3}^{(0)}}{3!} \left\{ \begin{array}{l} \frac{\xi_c^{-2\epsilon}}{2\epsilon} \delta(\xi_1) \frac{\xi_c^{-2\epsilon}}{2\epsilon} \delta(\xi_2) \frac{\xi_c^{-2\epsilon}}{2\epsilon} \delta(\xi_3) \\ \frac{\xi_c^{-2\epsilon}}{2\epsilon} \delta(\xi_2) \frac{\xi_c^{-2\epsilon}}{2\epsilon} \delta(\xi_3) \left(\frac{1}{\xi_1^{1+2\epsilon}} \right)_c \\ -\frac{\xi_c^{-2\epsilon}}{2\epsilon} \delta(\xi_3) \left(\frac{1}{\xi_1^{1+2\epsilon}} \right)_c \left(\frac{1}{\xi_2^{1+2\epsilon}} \right)_c \\ \left(\frac{1}{\xi_1^{1+2\epsilon}} \right)_c \left(\frac{1}{\xi_2^{1+2\epsilon}} \right)_c \left(\frac{1}{\xi_3^{1+2\epsilon}} \right)_c \end{array} \right\}. \quad (\text{D.13})$$

The triple-hard $d\sigma_{hhh}^{(3)}$ contribution is finite and can be integrated numerically. For the triple-soft $d\sigma_{sss}^{(3)}$ we get

$$d\sigma_{sss}^{(3)}(\xi_c) = d\Phi_n \frac{1}{3!} \hat{\mathcal{E}}^3 \mathcal{M}_n^{(0)}. \quad (\text{D.14})$$

The double-soft contribution can be expressed in terms of the function $\mathcal{J}(\xi_c)$ as

$$\int d\sigma_{hss}^{(3)}(\xi_c) = \int d\Upsilon_1 d\Phi_{n,1} \frac{1}{3!} \hat{\mathcal{E}}(\xi_c)^2 \left(\frac{1}{\xi_1^{1+2\epsilon}} \right)_c d\xi_1 \xi_1^2 \mathcal{M}_{n+1}^{(0)} = \frac{1}{3!} \mathcal{J}(\xi_c). \quad (\text{D.15})$$

Similarly, the single-soft contribution

$$\int d\sigma_{hhs}^{(3)}(\xi_c) = \int d\Upsilon_1 d\Upsilon_2 d\Phi_{n,2} \frac{1}{3!} \hat{\mathcal{E}}(\xi_c) \left(\frac{1}{\xi_1^{1+2\epsilon}} \right)_c \left(\frac{1}{\xi_2^{1+2\epsilon}} \right)_c d\xi_1 d\xi_2 \xi_1^2 \xi_2^2 \mathcal{M}_{n+2}^{(0)} = \frac{1}{3!} \mathcal{K}(\xi_c) \quad (\text{D.16})$$

involves the auxiliary function \mathcal{K} .

D.4 Combination

Combining all contributions at N³LO we need to evaluate (4.39). Collecting the terms with an n -parton phase space we get

$$\begin{aligned} d\sigma_n^{(3)}(\xi_c) = & \int d\Phi_n \left(\mathcal{M}_n^{(3)} + \underbrace{\hat{\mathcal{E}}(\xi_c) \mathcal{M}_n^{(2)}}_{d\sigma_s^{(3)}} + \underbrace{\frac{1}{2!} \hat{\mathcal{E}}(\xi_c)^2 \mathcal{M}_n^{(1)}}_{d\sigma_{ss}^{(3)}} + 1 \times \underbrace{\frac{1}{3!} \hat{\mathcal{E}}(\xi_c)^3 \mathcal{M}_n^{(0)}}_{d\sigma_{sss}^{(3)}} \right) \\ & \underbrace{-\mathcal{I}(\xi_c) - \frac{1}{2!} \mathcal{J}(\xi_c)}_{d\sigma_d^{(3)}} + \underbrace{\frac{1}{2!} \mathcal{I}(\xi_c) + \frac{1}{2!} \mathcal{I}(\xi_c)}_{d\sigma_{hs}^{(3)} + d\sigma_{sh}^{(3)}} - \underbrace{\frac{1}{2!} \mathcal{K}(\xi_c)}_{d\sigma_{hd}^{(3)}} + \underbrace{3 \times \frac{1}{3!} \mathcal{J}(\xi_c)}_{d\sigma_{hss}^{(3)} + \dots} + \underbrace{3 \times \frac{1}{3!} \mathcal{K}(\xi_c)}_{d\sigma_{hhs}^{(3)} + \dots}. \end{aligned} \quad (\text{D.17})$$

The auxiliary integrals $\mathcal{I}^{(1)}$, \mathcal{J} and \mathcal{K} cancel as do the explicit $1/\epsilon$ poles in the first line. The other contributions in (4.39) are also separately finite. Thus, after setting $d = 4$ the explicit expressions of the separately finite parts of (4.39) are given by (4.40) with

$$d\sigma_{n+1}^{(3)}(\xi_c) = d\sigma_f^{(3)}; \quad d\sigma_{n+2}^{(3)}(\xi_c) = d\sigma_{hf}^{(3)}; \quad d\sigma_{n+3}^{(3)}(\xi_c) = d\sigma_{hhh}^{(3)}. \quad (\text{D.18})$$

Comparing (D.18) to (4.36c) and (4.36d) reveals the pattern of how to extend beyond N³LO as done in Section 4.3.2.

Index

We have used the following acronyms, abbreviations and terminology

1PI	one-particle irreducible	LHC	Large Hadron Collider
AC	Anti-commuting γ_5 scheme	LL	leading logarithm
BM	Breitenlohner-Maison scheme	LO	Leading order
BR	branching ratio	LSZ	Lehmann-Symanzik-Zimmermann reduction formula
BSM	Beyond the Standard Model	MMCT	MCMULE core team
CDR	Conventional dimensional regularisation	$\overline{\text{MS}}$	modified minimal subtraction
DRED	Dimensional reduction	N³LO	Next-to-next-to-next-to-leading order
DREG	Dimensional regularisation	NLL	Next-to-leading logarithm
EFT	effective field theory	NLO	Next-to-leading order
FDF	Four-dimensional formulation of FDH	NNLO	Next-to-next-to-leading order
FDH	Four-dimensional helicity scheme	OS	on-shell
FDU	Four-dimensional unsubtraction	PCS	pseudo-collinear singularity
FKS²	FKS double soft	PID	particle identification
FKS	Frixione-Kunszt-Signer subtraction scheme	PDF	parton distribution function
HPL	harmonic polylogarithm	PSI	Paul Scherrer Institut
HVP	hadronic vacuum polarisation	PS	parton shower
HV	't Hooft-Veltman scheme	QCD	Quantum chromodynamics
IBP	integration-by-parts	QED	Quantum electron dynamics
IR	infrared	QFT	Quantum field theory
KLN	Kinoshita-Lee-Nauenberg	RGE	Renormalisation-group equation
LFV	lepton-flavour violating	RNG	Random number generator
		RS	Regularisation scheme
		SCET	Soft-collinear effective theory
		SHA1	Secure Hashing Algorithm 1

SM	Standard Model	
UV	Ultraviolet	
VP	vacuum polarisation	
YFS	Yennie-Frautschi-Suura	
active scales		6
analytic regularisation		57
anisotropic		107
anomalous dimension		14
auxiliary contributions		39
c -distribution		35
Casimir scaling		31
collinear		13
colour factors		46
config file		71
corner integral		48
corner region		78
counter-event		79
cuspid angle		16
cuspid anomalous dimension		15
decoupling transformation		16
dimension-six operator		11
eikonal factor		35
eikonal subtraction		37
electronic corrections		94
exclusive		12
event		79
factorisation anomaly		57
factorisation scale		14
family		47
Feynman parameters		51
Feynman parametrisation		51
Fierz identities		12
fixed-order		13
full period		83
fully differential		6
generic pieces		65
generic processes		65
graph polynomials		51
hard		53
heavy-quark		30
integrated eikonal		35
IR safe		12
isotropic		107
lexicographic ordering		50
light-quark		30
loop diagrams		6
loop-induced		6
loop integrals		6
massification		56
master integral		48
matching calculation		11
measurement function		6
Mellin transform		52
menu files		71
method of regions		53
Michel decay		4
mixed corrections		94
$\overline{\text{MS}}$ -like subtracted		14
muonic corrections		94
non-trivial scheme dependence		27
process groups		64
radiative muon decay		2
Ramanujan's master theorem		52
random seed		67
rare muon decay		2
real		12
reducible scalar integrals		48
regular		18
regularise		6
renormalisable		7
renormalisation		6
renormalisation constants		6
renormalisation scale		8
renormalisation scheme		7
resummation		13
running		8

sectors	48	tree-level diagrams	6
seed identity	49	trivial scheme dependence	24
singular	18	two-loop ready	27
soft	12	virtual	12
soft cut	79	Ward identity	7
submission script	71	weak-isospin	11
sub-renormalisation	10	Wilson coefficient	11
subtraction scheme	33		

Bibliography

- [1] G. M. Pruna, A. Signer and Y. Ulrich, *Fully differential NLO predictions for the rare muon decay*, *Phys. Lett.* **B765** (2017) 280 [[1611.03617](#)].
- [2] C. Gnendiger et al., *To d, or not to d: recent developments and comparisons of regularization schemes*, *Eur. Phys. J.* **C77** (2017) 471 [[1705.01827](#)].
- [3] G. M. Pruna, A. Signer and Y. Ulrich, *Fully differential NLO predictions for the radiative decay of muons and taus*, *Phys. Lett.* **B772** (2017) 452 [[1705.03782](#)].
- [4] Y. Ulrich, *Fully differential NLO predictions for rare and radiative lepton decays*, *PoS NuFact2017* (2018) 124 [[1712.05633](#)].
- [5] T. Engel, C. Gnendiger, A. Signer and Y. Ulrich, *Small-mass effects in heavy-to-light form factors*, *JHEP* **02** (2018) 118 [[1811.06461](#)].
- [6] T. Engel, A. Signer and Y. Ulrich, *A subtraction scheme for massive QED*, *JHEP* **01** (2020) 085 [[1909.10244](#)].
- [7] P. Banerjee, T. Engel, A. Signer and Y. Ulrich, *QED at NNLO with McMule*, [2007.01654](#).
- [8] T. Engel, “*Two-loop corrections to the muon decay*”, Master’s thesis, Swiss Federal Institute of Technology in Zurich, 2018.
- [9] WORKING GROUP ON RADIATIVE CORRECTIONS AND MONTE CARLO GENERATORS FOR LOW ENERGIES collaboration, S. Actis et al., *Quest for precision in hadronic cross sections at low energy: Monte Carlo tools vs. experimental data*, *Eur. Phys. J.* **C66** (2010) 585 [[0912.0749](#)].
- [10] MUON G-2 collaboration, G. W. Bennett et al., *Final Report of the Muon E821 Anomalous Magnetic Moment Measurement at BNL*, *Phys. Rev.* **D73** (2006) 072003 [[hep-ex/0602035](#)].
- [11] MUON G-2 collaboration, J. Grange et al., *Muon ($g - 2$) Technical Design Report*, [1501.06858](#).
- [12] J-PARC G-2/EDM collaboration, N. Saito, *A novel precision measurement of muon $g - 2$ and EDM at J-PARC*, *AIP Conf. Proc.* **1467** (2012) 45.
- [13] A. Nyffeler, *Precision of a data-driven estimate of hadronic light-by-light scattering in the muon $g - 2$: Pseudoscalar-pole contribution*, *Phys. Rev.* **D94** (2016) 053006 [[1602.03398](#)].
- [14] T. Aoyama, T. Kinoshita and M. Nio, *Revised and Improved Value of the QED Tenth-Order Electron Anomalous Magnetic Moment*, *Phys. Rev.* **D97** (2018) 036001 [[1712.06060](#)].

- [15] C. M. Carloni Calame, M. Passera, L. Trentadue and G. Venanzoni, *A new approach to evaluate the leading hadronic corrections to the muon $g - 2$* , *Phys. Lett.* **B746** (2015) 325 [[1504.02228](#)].
- [16] G. Abbiendi and C. M. Carloni Calame and U. Marconi and C. Matteuzzi and G. Montagna and O. Nicosini and M. Passera and F. Piccinini and R. Tenchini and L. Trentadue and G. Venanzoni, *Measuring the leading hadronic contribution to the muon $g - 2$ via μe scattering*, *Eur. Phys. J.* **C77** (2017) 139 [[1609.08987](#)].
- [17] C. Matteuzzi, G. Venanzoni, D. Abbaneo, G. Abbiendi, G. Bagliesi, D. Banerjee et al., *Letter of Intent: the MUonE project*, Tech. Rep. CERN-SPSC-2019-026. SPSC-I-252, CERN, Geneva, Jun, 2019.
- [18] D. Becker et al., *The P2 experiment*, [1802.04759](#).
- [19] W. Xiong et al., *A small proton charge radius from an electron–proton scattering experiment*, *Nature* **575** (2019) 147.
- [20] MUSE collaboration, R. Gilman et al., *Studying the Proton "Radius" Puzzle with μp Elastic Scattering*, [1303.2160](#).
- [21] MOLLER collaboration, J. Benesch et al., *The MOLLER Experiment: An Ultra-Precise Measurement of the Weak Mixing Angle Using Møller Scattering*, [1411.4088](#).
- [22] QWEAK collaboration, D. Androić et al., *Precision measurement of the weak charge of the proton*, *Nature* **557** (2018) 207 [[1905.08283](#)].
- [23] MULAN collaboration, D. M. Webber et al., *Measurement of the Positive Muon Lifetime and Determination of the Fermi Constant to Part-per-Million Precision*, *Phys. Rev. Lett.* **106** (2011) 041803 [[1010.0991](#)].
- [24] T. van Ritbergen and R. G. Stuart, *On the precise determination of the Fermi coupling constant from the muon lifetime*, *Nucl. Phys.* **B564** (2000) 343 [[hep-ph/9904240](#)].
- [25] C. Anastasiou, K. Melnikov and F. Petriello, *The Electron energy spectrum in muon decay through $\mathcal{O}(\alpha^2)$* , *JHEP* **0709** (2007) 014 [[hep-ph/0505069](#)].
- [26] MEG COLLABORATION collaboration, J. Adam et al., *New constraint on the existence of the $\mu^+ \rightarrow e^+ \gamma$ decay*, *Phys.Rev.Lett.* **110** (2013) 201801 [[1303.0754](#)].
- [27] A. Baldini, F. Cei, C. Cerri, S. Dussoni, L. Galli et al., *MEG Upgrade Proposal*, [1301.7225](#).
- [28] MU3E collaboration, A.-K. Perrevoort, *Status of the Mu3e Experiment at PSI*, *EPJ Web Conf.* **118** (2016) 01028 [[1605.02906](#)].
- [29] A. Blondel, A. Bravar, M. Pohl, S. Bachmann, N. Berger et al., *Research Proposal for an Experiment to Search for the Decay $\mu \rightarrow eee$* , [1301.6113](#).
- [30] M. Raggi and V. Kozhuharov, *Proposal to Search for a Dark Photon in Positron on Target Collisions at DAΦNE Linac*, *Adv. High Energy Phys.* **2014** (2014) 959802 [[1403.3041](#)].
- [31] G. Pruna and A. Signer, *private communication*, .

- [32] M. Fael and C. Greub, *Next-to-leading order prediction for the decay $\mu \rightarrow e (e^+e^-) \nu \bar{\nu}$* , *JHEP* **01** (2017) 084 [[1611.03726](#)].
- [33] G. B. Gelmini and M. Roncadelli, *Left-Handed Neutrino Mass Scale and Spontaneously Broken Lepton Number*, *Phys. Lett.* **99B** (1981) 411.
- [34] Y. Chikashige, R. N. Mohapatra and R. D. Peccei, *Are There Real Goldstone Bosons Associated with Broken Lepton Number?*, *Phys. Lett.* **98B** (1981) 265.
- [35] A. Papa and S. Ritt, *"charged lepton flavour violation and exotic physics searches with the megii and mu3e experiments"*, .
- [36] E. Ripiccini, *Ricerca del Majorone nei decadimenti del muone con lâŽesperimento MEG*, Master's thesis, University of Rome, 2011.
- [37] N. Mitsutaka and Y. Uchiyama, *private communication*, .
- [38] M. Fael, L. Mercolli and M. Passera, *Radiative μ and τ leptonic decays at NLO*, *JHEP* **07** (2015) 153 [[1506.03416](#)].
- [39] B. Oberhof, *Measurement of $\mathcal{B}(\tau \rightarrow l\gamma\nu\bar{\nu}, l = e, \mu)$ at BaBar*, Ph.D. thesis, University of Pisa, Italy, 2015.
- [40] BABAR collaboration, J. P. Lees et al., *Measurement of the branching fractions of the radiative leptonic τ decays $\tau \rightarrow e\gamma\nu\bar{\nu}$ and $\tau \rightarrow \mu\gamma\nu\bar{\nu}$ at BABAR*, *Phys. Rev.* **D91** (2015) 051103 [[1502.01784](#)].
- [41] BELLE collaboration, J. Sasaki, *Study of five-body leptonic decays of tau at Belle experiment*, *J. Phys. Conf. Ser.* **912** (2017) 012002.
- [42] M. Fael, G. M. Pruna, A. Signer and Y. Ulrich, *In preparation*, .
- [43] D. Yu. Bardin and L. Kalinovskaya, *QED corrections for polarized elastic μe scattering*, [hep-ph/9712310](#).
- [44] N. Kaiser, *Radiative corrections to lepton-lepton scattering revisited*, *J. Phys.* **G37** (2010) 115005.
- [45] M. Alacevich, C. M. Carloni Calame, M. Chiesa, G. Montagna, O. Nicosini and F. Piccinini, *Muon-electron scattering at NLO*, *JHEP* **02** (2019) 155 [[1811.06743](#)].
- [46] T. Engel, A. Signer and Y. Ulrich, *private communication, unpublished* (2019) .
- [47] M. Fael and M. Passera, *private communication, unpublished* (2018) .
- [48] TWIST collaboration, A. Hillairet et al., *Precision muon decay measurements and improved constraints on the weak interaction*, *Phys.Rev.* **D85** (2012) 092013 [[1112.3606](#)].
- [49] J. Currie, T. Gehrmann, E. W. N. Glover, A. Huss, J. Niehues and A. Vogt, *N^3LO corrections to jet production in deep inelastic scattering using the Projection-to-Born method*, *JHEP* **05** (2018) 209 [[1803.09973](#)].
- [50] Z. Kunszt and D. E. Soper, *Calculation of jet cross-sections in hadron collisions at order α_s^3* , *Phys. Rev.* **D46** (1992) 192.
- [51] M. D. Schwartz, *Quantum Field Theory and the Standard Model*. Cambridge University Press, 2014.

- [52] M. E. Peskin and D. V. Schroeder, *An Introduction to quantum field theory*. Addison-Wesley, Reading, USA, 1995.
- [53] A. Grozin, *Lectures on QED and QCD*, in *3rd Dubna International Advanced School of Theoretical Physics Dubna, Russia, January 29-February 6, 2005*, pp. 1–156, 2005, [hep-ph/0508242](#).
- [54] L. D. Landau and I. M. Khalatnikov, *The gauge transformation of the Green function for charged particles*, *Sov. Phys. JETP* **2** (1956) 69.
- [55] K. Johnson and B. Zumino, *Gauge Dependence of the Wave-Function Renormalization Constant in Quantum Electrodynamics*, *Phys. Rev. Lett.* **3** (1959) 351.
- [56] T. Fukuda, R. Kubo and K.-i. Yokoyama, *Possible Situation for Gauge Independence of Wave Function Renormalization Constants in Gauge Field Theories*, *Prog. Theor. Phys.* **63** (1980) 1384.
- [57] K. Melnikov and T. van Ritbergen, *The Three loop on-shell renormalization of QCD and QED*, *Nucl. Phys.* **B591** (2000) 515 [[hep-ph/0005131](#)].
- [58] D. J. Broadhurst, N. Gray and K. Schilcher, *Gauge invariant on-shell Z_2 in QED, QCD and the effective field theory of a static quark*, *Z. Phys.* **C52** (1991) 111.
- [59] S. Berman and A. Sirlin, *Some considerations on the radiative corrections to muon and neutron decay*, *Annals of Physics* **20** (1962) 20 .
- [60] M. Fael, L. Mercolli and M. Passera, *W-propagator corrections to μ and τ leptonic decays*, *Phys. Rev.* **D88** (2013) 093011 [[1310.1081](#)].
- [61] E. Gardi and L. Magnea, *Factorization constraints for soft anomalous dimensions in QCD scattering amplitudes*, *JHEP* **03** (2009) 079 [[0901.1091](#)].
- [62] E. Gardi and L. Magnea, *Infrared singularities in QCD amplitudes*, *Nuovo Cim.* **C32N5-6** (2009) 137 [[0908.3273](#)].
- [63] T. Becher and M. Neubert, *Infrared singularities of scattering amplitudes in perturbative QCD*, *Phys. Rev. Lett.* **102** (2009) 162001 [[0901.0722](#)].
- [64] T. Becher and M. Neubert, *On the Structure of Infrared Singularities of Gauge-Theory Amplitudes*, *JHEP* **0906** (2009) 081 [[0903.1126](#)].
- [65] T. Becher and M. Neubert, *Infrared singularities of QCD amplitudes with massive partons*, *Phys. Rev.* **D79** (2009) 125004 [[0904.1021](#)].
- [66] C. W. Bauer, S. Fleming, D. Pirjol and I. W. Stewart, *An Effective field theory for collinear and soft gluons: Heavy to light decays*, *Phys. Rev.* **D63** (2001) 114020 [[hep-ph/0011336](#)].
- [67] C. W. Bauer, D. Pirjol and I. W. Stewart, *Soft collinear factorization in effective field theory*, *Phys. Rev.* **D65** (2002) 054022 [[hep-ph/0109045](#)].
- [68] M. Beneke, A. P. Chapovsky, M. Diehl and T. Feldmann, *Soft collinear effective theory and heavy to light currents beyond leading power*, *Nucl. Phys.* **B643** (2002) 431 [[hep-ph/0206152](#)].

- [69] T. Becher, A. Broggio and A. Ferroglia, *Introduction to Soft-Collinear Effective Theory*, *Lect. Notes Phys.* **896** (2015) pp.1 [[1410.1892](#)].
- [70] A. Broggio, C. Gnendiger, A. Signer, D. Stöckinger and A. Visconti, *SCET approach to regularization-scheme dependence of QCD amplitudes*, *JHEP* **01** (2016) 078 [[1506.05301](#)].
- [71] A. Mitov, G. F. Sterman and I. Sung, *The Massive Soft Anomalous Dimension Matrix at Two Loops*, *Phys. Rev.* **D79** (2009) 094015 [[0903.3241](#)].
- [72] K. G. Chetyrkin, B. A. Kniehl and M. Steinhauser, *Decoupling relations to $\mathcal{O}(\alpha_s^3)$ and their connection to low-energy theorems*, *Nucl. Phys.* **B510** (1998) 61 [[hep-ph/9708255](#)].
- [73] D. R. Yennie, S. C. Frautschi and H. Suura, *The infrared divergence phenomena and high-energy processes*, *Annals Phys.* **13** (1961) 379.
- [74] C. G. Bollini and J. J. Giambiagi, *Dimensional Renormalization: The Number of Dimensions as a Regularizing Parameter*, *Nuovo Cim.* **B12** (1972) 20.
- [75] G. 't Hooft and M. J. G. Veltman, *Regularization and Renormalization of Gauge Fields*, *Nucl.Phys.* **B44** (1972) 189.
- [76] K. G. Wilson, *The Renormalization Group and Strong Interactions*, *Phys. Rev. D* **3** (1971) 1818.
- [77] K. G. Wilson and M. E. Fisher, *Critical exponents in 3.99 dimensions*, *Phys. Rev. Lett.* **28** (1972) 240.
- [78] J. Ashmore, *A Method of Gauge Invariant Regularization*, *Lett. Nuovo Cim.* **4** (1972) 289.
- [79] K. G. Wilson, *Quantum field theory models in less than four-dimensions*, *Phys.Rev.* **D7** (1973) 2911.
- [80] J. C. Collins, *Renormalization, An introduction to renormalization, the renormalization group, and the operator-product expansion*, Cambridge University Press (1984) .
- [81] Z. Bern and D. A. Kosower, *The Computation of loop amplitudes in gauge theories*, *Nucl. Phys.* **B379** (1992) 451.
- [82] A. Signer and D. Stöckinger, *Using Dimensional Reduction for Hadronic Collisions*, *Nucl.Phys.* **B808** (2009) 88 [[0807.4424](#)].
- [83] R. A. Fazio, P. Mastrolia, E. Mirabella and W. J. Torres Bobadilla, *On the Four-Dimensional Formulation of Dimensionally Regulated Amplitudes*, *Eur. Phys. J.* **C74** (2014) 3197 [[1404.4783](#)].
- [84] D. Stöckinger, *Regularization by dimensional reduction: consistency, quantum action principle, and supersymmetry*, *JHEP* **03** (2005) 076 [[hep-ph/0503129](#)].
- [85] C. Gnendiger and A. Signer, *Dimensional schemes for cross sections at NNLO*, *Eur. Phys. J. C* **80** (2020) 215 [[1912.09974](#)].
- [86] F. Jegerlehner, *Facts of life with γ_5* , *Eur. Phys. J.* **C18** (2001) 673 [[hep-th/0005255](#)].
- [87] W. Siegel, *Inconsistency of Supersymmetric Dimensional Regularization*, *Phys. Lett. B* **94** (1980) 37.

- [88] P. Breitenlohner and D. Maison, *Dimensional Renormalization and the Action Principle*, *Commun. Math. Phys.* **52** (1977) 11.
- [89] S. A. Larin, *The Renormalization of the axial anomaly in dimensional regularization*, *Phys. Lett.* **B303** (1993) 113 [[hep-ph/9302240](#)].
- [90] C. Gnendiger and A. Signer, γ_5 in FDH, *Phys. Rev.* **D97** (2018) 096006 [[1710.09231](#)].
- [91] J. G. Korner, D. Kreimer and K. Schilcher, *A Practicable γ_5 scheme in dimensional regularization*, *Z. Phys.* **C54** (1992) 503.
- [92] D. Kreimer, *The Role of γ_5 in dimensional regularization*, [hep-ph/9401354](#).
- [93] S. L. Adler, *Axial vector vertex in spinor electrodynamics*, *Phys. Rev.* **177** (1969) 2426.
- [94] J. S. Bell and R. Jackiw, *A PCAC puzzle: $\pi^0 \rightarrow \gamma\gamma$ in the σ model*, *Nuovo Cim.* **A60** (1969) 47.
- [95] S. L. Adler and W. A. Bardeen, *Absence of higher order corrections in the anomalous axial vector divergence equation*, *Phys. Rev.* **182** (1969) 1517.
- [96] M. Jamin and M. E. Lautenbacher, *TRACER: Version 1.1: A Mathematica package for gamma algebra in arbitrary dimensions*, *Comput. Phys. Commun.* **74** (1993) 265.
- [97] H. H. Patel, *Package-X: A Mathematica package for the analytic calculation of one-loop integrals*, *Comput. Phys. Commun.* **197** (2015) 276 [[1503.01469](#)].
- [98] E. Remiddi and J. A. M. Vermaseren, *Harmonic polylogarithms*, *Int. J. Mod. Phys.* **A15** (2000) 725 [[hep-ph/9905237](#)].
- [99] D. Maitre, *HPL, a mathematica implementation of the harmonic polylogarithms*, *Comput. Phys. Commun.* **174** (2006) 222 [[hep-ph/0507152](#)].
- [100] G. Passarino and M. Veltman, *One Loop Corrections for e^+e^- Annihilation Into $\mu^+\mu^-$ in the Weinberg Model*, *Nucl.Phys.* **B160** (1979) 151.
- [101] R. K. Ellis, Z. Kunszt, K. Melnikov and G. Zanderighi, *One-loop calculations in quantum field theory: from Feynman diagrams to unitarity cuts*, *Physics Reports* **518** (2012) 141 [[1105.4319v4](#)].
- [102] C. Gnendiger, A. Signer and D. Stöckinger, *The infrared structure of QCD amplitudes and $H \rightarrow gg$ in FDH and DRED*, *Phys.Lett.* **B733** (2014) 296 [[1404.2171](#)].
- [103] C. Gnendiger, A. Signer and A. Visconti, *Regularization-scheme dependence of QCD amplitudes in the massive case*, *JHEP* **10** (2016) 034 [[1607.08241](#)].
- [104] I. Jack, D. R. T. Jones, S. P. Martin, M. T. Vaughn and Y. Yamada, *Decoupling of the ϵ -scalar mass in softly broken supersymmetry*, *Phys. Rev.* **D50** (1994) R5481 [[hep-ph/9407291](#)].
- [105] G. Cullen et al., *GoSam-2.0: a tool for automated one-loop calculations within the Standard Model and beyond*, *Eur. Phys. J.* **C74** (2014) 3001 [[1404.7096](#)].
- [106] Z. Bern and A. G. Morgan, *Massive loop amplitudes from unitarity*, *Nucl. Phys.* **B467** (1996) 479 [[hep-ph/9511336](#)].

- [107] Z. Kunszt, A. Signer and Z. Trócsányi, *One-loop helicity amplitudes for all $2 \rightarrow 2$ processes in QCD and $N = 1$ supersymmetric Yang-Mills theory*, *Nuclear Physics B* **441** (1994) 397 [[hep-ph/9305239](#)].
- [108] S. Frixione, Z. Kunszt and A. Signer, *Three-jet cross sections to next-to-leading order*, *Nuclear Physics B* **467** (1996) 399 [[hep-ph/9512328](#)].
- [109] R. Frederix, S. Frixione, F. Maltoni and T. Stelzer, *Automation of next-to-leading order computations in QCD: the FKS subtraction*, *Journal of High Energy Physics* **2009** (2009) [[0908.4272](#)].
- [110] I. Bierenbaum, M. Czakon and A. Mitov, *The singular behavior of one-loop massive QCD amplitudes with one external soft gluon*, *Nucl. Phys.* **B856** (2012) 228 [[1107.4384](#)].
- [111] S. Catani and M. Grazzini, *The soft gluon current at one loop order*, *Nucl. Phys.* **B591** (2000) 435 [[hep-ph/0007142](#)].
- [112] A. Mitov and S. Moch, *The Singular behavior of massive QCD amplitudes*, *JHEP* **05** (2007) 001 [[hep-ph/0612149](#)].
- [113] T. Becher and K. Melnikov, *Two-loop QED corrections to Bhabha scattering*, *JHEP* **06** (2007) 084 [[0704.3582](#)].
- [114] P. Nogueira, *Automatic Feynman graph generation*, *J.Comput.Phys.* **105** (1993) 279.
- [115] M. Sjö Dahl, *ColorMath - A package for color summed calculations in $SU(N_c)$* , *Eur. Phys. J.* **C73** (2013) 2310 [[1211.2099](#)].
- [116] P. Banerjee et al., *Theory for muon-electron scattering @10ppm: A report of the MUonE theory initiative*, *Eur. Phys. J. C* **80** (2020) 591 [[2004.13663](#)].
- [117] M. L. Mangano and S. J. Parke, *Multi-parton amplitudes in gauge theories*, *Physics Reports* **200** (1991) 301 [[hep-th/0509223](#)].
- [118] A. von Manteuffel and C. Studerus, *Reduze 2 - Distributed Feynman Integral Reduction*, [1201.4330](#).
- [119] V. A. Smirnov, *Analytic tools for Feynman integrals*, *Springer Tracts Mod. Phys.* **250** (2012) 1.
- [120] K. G. Chetyrkin and F. V. Tkachov, *Integration by Parts: The Algorithm to Calculate β -functions in 4 Loops*, *Nucl. Phys.* **B192** (1981) 159.
- [121] S. Laporta, *High precision calculation of multiloop Feynman integrals by difference equations*, *Int. J. Mod. Phys.* **A15** (2000) 5087 [[hep-ph/0102033](#)].
- [122] S. Laporta and E. Remiddi, *The Analytical value of the electron ($g - 2$) at order α^3 in QED*, *Phys. Lett.* **B379** (1996) 283 [[hep-ph/9602417](#)].
- [123] R. N. Lee, *Presenting LiteRed: a tool for the Loop InTEgrals REDuction*, [1212.2685](#).
- [124] C. Anastasiou and A. Lazopoulos, *Automatic integral reduction for higher order perturbative calculations*, *JHEP* **07** (2004) 046 [[hep-ph/0404258](#)].
- [125] A. V. Smirnov and F. S. Chuharev, *FIRE6: Feynman Integral REDuction with Modular Arithmetic*, *Comput. Phys. Commun.* **247** (2020) 106877 [[1901.07808](#)].

- [126] P. Maierhöfer, J. Usovitsch and P. Uwer, *Kira – A Feynman integral reduction program*, *Comput. Phys. Commun.* **230** (2018) 99 [[1705.05610](#)].
- [127] A. V. Smirnov, *FIESTA 3: cluster-parallelizable multiloop numerical calculations in physical regions*, *Comput. Phys. Commun.* **185** (2014) 2090 [[1312.3186](#)].
- [128] H. Cheng and T. T. Wu, *Expanding Protons: Scattering at High Energies*. MIT Press, 1987.
- [129] S. Borowka, G. Heinrich, S. P. Jones, M. Kerner, J. Schlenk and T. Zirke, *SecDec-3.0: numerical evaluation of multi-scale integrals beyond one loop*, *Comput. Phys. Commun.* **196** (2015) 470 [[1502.06595](#)].
- [130] T. Huber and D. Maitre, *HypExp: A Mathematica package for expanding hypergeometric functions around integer-valued parameters*, *Comput. Phys. Commun.* **175** (2006) 122 [[hep-ph/0507094](#)].
- [131] M. Beneke and V. A. Smirnov, *Asymptotic expansion of Feynman integrals near threshold*, *Nucl.Phys.* **B522** (1998) 321 [[hep-ph/9711391](#)].
- [132] A. A. Penin, *Two-loop photonic corrections to massive Bhabha scattering*, *Nucl. Phys.* **B734** (2006) 185 [[hep-ph/0508127](#)].
- [133] T. Liu, A. A. Penin and N. Zerf, *Three-loop quark form factor at high energy: the leading mass corrections*, *Phys. Lett.* **B771** (2017) 492 [[1705.07910](#)].
- [134] T. Liu and A. Penin, *High-Energy Limit of Mass-Suppressed Amplitudes in Gauge Theories*, *JHEP* **11** (2018) 158 [[1809.04950](#)].
- [135] J. Blümlein, P. Marquard and N. Rana, *Asymptotic behavior of the heavy quark form factors at higher order*, *Phys. Rev. D* **99** (2019) 016013 [[1810.08943](#)].
- [136] W. Bernreuther, R. Bonciani, T. Gehrmann, R. Heinesch, T. Leineweber et al., *Two-loop QCD corrections to the heavy quark form-factors: The Vector contributions*, *Nucl.Phys.* **B706** (2005) 245 [[hep-ph/0406046](#)].
- [137] T. Becher and M. Neubert, *Drell-Yan Production at Small q_T , Transverse Parton Distributions and the Collinear Anomaly*, *Eur. Phys. J.* **C71** (2011) 1665 [[1007.4005](#)].
- [138] T. Becher, G. Bell and M. Neubert, *Factorization and Resummation for Jet Broadening*, *Phys. Lett.* **B704** (2011) 276 [[1104.4108](#)].
- [139] M. Beneke, *Soft-collinear effective theory*, in *Helmholtz International Summer School: Heavy Quark Physics*, Dubna, 2005.
- [140] J.-y. Chiu, A. Jain, D. Neill and I. Z. Rothstein, *The Rapidity Renormalization Group*, *Phys. Rev. Lett.* **108** (2012) 151601 [[1104.0881](#)].
- [141] V. A. Smirnov, *Asymptotic expansions of two loop Feynman diagrams in the Sudakov limit*, *Phys. Lett.* **B404** (1997) 101 [[hep-ph/9703357](#)].
- [142] M. Fael, *Hadronic corrections to μ -e scattering at NNLO with space-like data*, *JHEP* **02** (2019) 027 [[1808.08233](#)].
- [143] M. Fael and M. Passera, *Muon-Electron Scattering at Next-To-Next-To-Leading Order: The Hadronic Corrections*, *Phys. Rev. Lett.* **122** (2019) 192001 [[1901.03106](#)].

- [144] Y. Ulrich, *The MCMULE manual*, <https://gitlab.psi.ch/mcmule/manual>.
- [145] D. Merkel, *Docker: Lightweight linux containers for consistent development and deployment*, *Linux J.* **2014** (2014) .
- [146] J. Gomes, E. Bagnaschi, I. Campos, M. David, L. Alves, J. a. Martins et al., *Enabling rootless Linux Containers in multi-user environments: the udocker tool*, *Comput. Phys. Commun.* **232** (2018) 84 [[1711.01758](#)].
- [147] A. Denner, S. Dittmaier and L. Hofer, *Collier: a fortran-based Complex One-Loop LIbrary in Extended Regularizations*, *Comput. Phys. Commun.* **212** (2017) 220 [[1604.06792](#)].
- [148] A. Denner and S. Dittmaier, *Scalar one-loop 4-point integrals*, *Nucl. Phys.* **B844** (2011) 199 [[1005.2076](#)].
- [149] A. Denner and S. Dittmaier, *Reduction schemes for one-loop tensor integrals*, *Nucl. Phys.* **B734** (2006) 62 [[hep-ph/0509141](#)].
- [150] A. Denner and S. Dittmaier, *Reduction of one loop tensor five point integrals*, *Nucl. Phys.* **B658** (2003) 175 [[hep-ph/0212259](#)].
- [151] G. P. Lepage, *VEGAS: An adaptive multidimensional integration program*, .
- [152] S. v. d. Walt, S. C. Colbert and G. Varoquaux, *The NumPy Array: A Structure for Efficient Numerical Computation*, *Computing in Science & Engineering* **13** (2011) 22.
- [153] J. D. Hunter, *Matplotlib: A 2D Graphics Environment*, *Computing in Science & Engineering* **9** (2007) 90.
- [154] F. Pérez and B. E. Granger, *IPython: A System for Interactive Scientific Computing*, *Computing in Science & Engineering* **9** (2007) 21.
- [155] A. B. Yoo, M. A. Jette and M. Grondona, *Slurm: Simple linux utility for resource management*, in *Job Scheduling Strategies for Parallel Processing*, (Berlin, Heidelberg), pp. 44–60, Springer Berlin Heidelberg, 2003.
- [156] PARTICLE DATA GROUP collaboration, K. A. Olive et al., *Review of Particle Physics*, *Chin. Phys.* **C38** (2014) 090001.
- [157] E. Gkioulekas, *Using restrictions to accept or reject solutions of radical equations*, *Int. J. of Mathematical Education in Science and Technology* **49** (2018) 1278.
- [158] S. K. Park and K. W. Miller, *Random number generators: Good ones are hard to find*, *Commun. ACM* **31** (1988) 1192.
- [159] G. Marsaglia, *Random numbers fall mainly in the planes*, *Proceedings of the National Academy of Sciences* **61** (1968) 25 [<https://www.pnas.org/content/61/1/25.full.pdf>].
- [160] Y. Ulrich, *Legacy results with MCMULE*, 2020, <https://gitlab.psi.ch/mcmule/user-library>.
- [161] P. Mastrolia, M. Passera, A. Primo and U. Schubert, *Master integrals for the NNLO virtual corrections to μe scattering in QED: the planar graphs*, *JHEP* **11** (2017) 198 [[1709.07435](#)].

- [162] S. Di Vita, S. Laporta, P. Mastrolia, A. Primo and U. Schubert, *Master integrals for the NNLO virtual corrections to μe scattering in QED: the non-planar graphs*, *JHEP* **09** (2018) 016 [[1806.08241](#)].
- [163] P. Mastrolia, M. Passera, A. Primo, U. Schubert and W. J. Torres Bobadilla, *On μe -scattering at NNLO in QED*, *EPJ Web Conf.* **179** (2018) 01014.
- [164] J. Ronca, *NNLO QED Contribution to the $\mu e \rightarrow \mu e$ Elastic Scattering*, *EPJ Web Conf.* **234** (2020) 01015 [[1912.05397](#)].
- [165] A. Masiero, P. Paradisi and M. Passera, *New physics at the MUonE experiment at CERN*, [2002.05418](#).
- [166] P. B. Dev, W. Rodejohann, X.-J. Xu and Y. Zhang, *MUonE sensitivity to new physics explanations of the muon anomalous magnetic moment*, *JHEP* **05** (2020) 053 [[2002.04822](#)].
- [167] C. Carloni Calame, M. Chiesa, S. M. Hasan, G. Montagna, O. Nicrosini and F. Piccinini, *Towards muon-electron scattering at NNLO*, [2007.01586](#).
- [168] L. W. Mo and Y.-S. Tsai, *Radiative Corrections to Elastic and Inelastic ep and μp Scattering*, *Rev. Mod. Phys.* **41** (1969) 205.
- [169] Y.-S. Tsai, *Radiative Corrections to Electron-Proton Scattering*, *Phys. Rev.* **122** (1961) 1898.
- [170] C. de Calan, H. Navelet and J. Picard, *Generalized radiative corrections for hadronic targets*, *Nucl. Phys.* **B348** (1991) 47.
- [171] A. Kwiatkowski, H. Spiesberger and H. J. Mohring, *Heracles: An Event Generator for ep Interactions at HERA Energies Including Radiative Processes: Version 1.0*, *Comput. Phys. Commun.* **69** (1992) 155.
- [172] A. Arbuzov, D. Yu. Bardin, J. Blumlein, L. Kalinovskaya and T. Riemann, *Hector 1.00: A Program for the calculation of QED, QCD and electroweak corrections to ep and $l^\pm N$ deep inelastic neutral and charged current scattering*, *Comput. Phys. Commun.* **94** (1996) 128 [[hep-ph/9511434](#)].
- [173] L. C. Maximon and J. A. Tjon, *Radiative corrections to electron proton scattering*, *Phys. Rev.* **C62** (2000) 054320 [[nucl-th/0002058](#)].
- [174] R. Ent, B. W. Filippone, N. C. R. Makins, R. G. Milner, T. G. O'Neill and D. A. Wasson, *Radiative corrections for $(e, e'p)$ reactions at GeV energies*, *Phys. Rev.* **C64** (2001) 054610.
- [175] A. V. Afanasev, I. Akushevich, A. Ilyichev and N. P. Merenkov, *QED radiative corrections to asymmetries of elastic ep scattering in hadronic variables*, *Phys. Lett.* **B514** (2001) 269 [[hep-ph/0105328](#)].
- [176] F. Weissbach, K. Hencken, D. Rohe, I. Sick and D. Trautmann, *Radiative corrections for $(e, e'p)$ experiments: Going beyond the peaking approximation*, *Eur. Phys. J.* **A30** (2006) 477 [[nucl-th/0411033](#)].
- [177] F. Weissbach, K. Hencken, D. Rohe and D. Trautmann, *Improved radiative corrections to $(e, e'p)$ experiments: Explicit treatment of kinematical corrections in multiphoton bremsstrahlung*, *Phys. Rev.* **C80** (2009) 024602 [[0805.1535](#)].

- [178] I. Akushevich, H. Gao, A. Ilyichev and M. Meziane, *Radiative corrections beyond the ultra relativistic limit in unpolarized ep elastic and Møller scatterings for the PRad Experiment at Jefferson Laboratory*, *Eur. Phys. J. A* **51** (2015) 1.
- [179] G. I. Gakh, M. I. Konchatnij, N. P. Merenkov and E. Tomasi-Gustafsson, *Radiative corrections to elastic proton-electron scattering measured in coincidence*, *Phys. Rev. C* **95** (2017) 055207 [[1612.02139](#)].
- [180] R. D. Bucoveanu and H. Spiesberger, *Second-Order Leptonic Radiative Corrections for Lepton-Proton Scattering*, *Eur. Phys. J. A* **55** (2019) 57 [[1811.04970](#)].
- [181] MEG collaboration, A. Baldini et al., *Muon polarization in the MEG experiment: predictions and measurements*, *Eur. Phys. J. C* **76** (2016) 223 [[1510.04743](#)].
- [182] W. Eichenberger, R. Engfer and A. Van Der Schaaf, *Measurement of the parameter $\bar{\eta}$ in the radiative decay of the muon as a test of the $V - A$ structure of the weak interaction*, *Nucl. Phys. A* **412** (1984) 523.
- [183] D. Pocanic et al., *New results in rare allowed muon and pion decays*, *Int. J. Mod. Phys. Conf. Ser.* **35** (2014) 1460437 [[1403.7416](#)].
- [184] A. B. Arbuzov and T. V. Kopylova, *Michel parameters in radiative muon decay*, *JHEP* **09** (2016) 109 [[1605.06612](#)].
- [185] A. Ferroglia, C. Greub, A. Sirlin and Z. Zhang, *Contributions of the W -boson propagator to μ and τ leptonic decay rates*, *Phys. Rev. D* **88** (2013) 033012 [[1307.6900](#)].
- [186] R. E. Behrends, R. J. Finkelstein and A. Sirlin, *Radiative corrections to decay processes*, *Phys. Rev.* **101** (1956) 866.
- [187] C. Fronsdal and H. Uberall, *μ -Meson Decay with Inner Bremsstrahlung*, *Phys. Rev.* **113** (1959) 654.
- [188] S. Eckstein and R. Pratt, *Radiative muon decay*, *Annals of Physics* **8** (1959) 297 .
- [189] T. Kinoshita and A. Sirlin, *Radiative Decay of the Muon*, *Phys. Rev. Lett.* **2** (1959) 177.
- [190] B. Falk and L. M. Sehgal, *Helicity flip bremsstrahlung: An Equivalent particle description with applications*, *Phys. Lett. B* **325** (1994) 509.
- [191] L. M. Sehgal, *Right-handed electrons in radiative muon decay*, *Phys. Lett. B* **569** (2003) 25 [[hep-ph/0306166](#)].
- [192] V. S. Schulz and L. M. Sehgal, *Wrong helicity electrons in radiative muon decay*, *Phys. Lett. B* **594** (2004) 153 [[hep-ph/0404023](#)].
- [193] E. Gabrielli and L. Trentadue, *Light mesons and muon radiative decays and photon polarization asymmetry*, *Nucl. Phys. B* **792** (2008) 48 [[hep-ph/0507191](#)].
- [194] A. Fischer, T. Kurosu and F. Savatier, *QED one loop correction to radiative muon decay*, *Phys. Rev. D* **49** (1994) 3426.
- [195] A. B. Arbuzov and E. S. Scherbakova, *One loop corrections to radiative muon decay*, *Phys. Lett. B* **597** (2004) 285 [[hep-ph/0404094](#)].

- [196] M. Fael and M. Passera, *Precision tests via radiative μ and τ leptonic decays*, *PoS RADCOR2015* (2016) 091 [[1602.00457](#)].
- [197] B. Oberhof, *Measurement of $\mathcal{B}(\tau \rightarrow l\gamma\nu\bar{\nu}, l = e, \mu)$ at BaBar*, Ph.D. thesis, University of Pisa, Italy, 2015.
- [198] T. Kinoshita and A. Sirlin, *Radiative corrections to Fermi interactions*, *Phys. Rev.* **113** (1959) 1652.
- [199] A. Arbuzov, A. Czarnecki and A. Gaponenko, *Muon decay spectrum: Leading logarithmic approximation*, *Phys.Rev.* **D65** (2002) 113006 [[hep-ph/0202102](#)].
- [200] A. Arbuzov and K. Melnikov, *$\mathcal{O}(\alpha^2 \ln(m_\mu/m_e))$ corrections to electron energy spectrum in muon decay*, *Phys.Rev.* **D66** (2002) 093003 [[hep-ph/0205172](#)].
- [201] C. Anastasiou, K. Melnikov and F. Petriello, *The electron energy spectrum in muon decay through $\mathcal{O}(\alpha^2)$* , *Journal of High Energy Physics* **2007** (2007) 014 [[hep-ph/0505069](#)].
- [202] A. Pak and A. Czarnecki, *Mass effects in muon and semileptonic $b \rightarrow c$ decays*, *Phys. Rev. Lett.* **100** (2008) 241807 [[0803.0960](#)].
- [203] L.-B. Chen, *Two-Loop master integrals for heavy-to-light form factors of two different massive fermions*, *JHEP* **02** (2018) 066 [[1801.01033](#)].
- [204] T. van Ritbergen and R. G. Stuart, *Hadronic contributions to the muon lifetime*, *Phys. Lett.* **B437** (1998) 201 [[hep-ph/9802341](#)].
- [205] A. I. Davydychev, K. Schilcher and H. Spiesberger, *Hadronic corrections at $\mathcal{O}(\alpha^2)$ to the energy spectrum of muon decay*, *Eur. Phys. J.* **C19** (2001) 99 [[hep-ph/0011221](#)].
- [206] L. Naterop, A. Signer and Y. Ulrich, *handyG – rapid numerical evaluation of generalised polylogarithms in Fortran*, *Comput. Phys. Commun.* **253** (2020) 107165 [[1909.01656](#)].
- [207] A. Gurgone, *Search for the $\mu \rightarrow e X$ decay with the MEG II apparatus: radiative corrections and sensitivity*, Tesi di Laurea Magistrale, "University of Pisa", 2020.
- [208] S. Dittmaier, *A General approach to photon radiation off fermions*, *Nucl. Phys.* **B565** (2000) 69 [[hep-ph/9904440](#)].
- [209] R. J. Hernandez-Pinto, G. F. R. Sborlini and G. Rodrigo, *Towards gauge theories in four dimensions*, *JHEP* **02** (2016) 044 [[1506.04617](#)].
- [210] G. F. R. Sborlini, F. Driencourt-Mangin, R. Hernandez-Pinto and G. Rodrigo, *Four-dimensional unsubtraction from the loop-tree duality*, *JHEP* **08** (2016) 160 [[1604.06699](#)].
- [211] G. F. R. Sborlini, F. Driencourt-Mangin and G. Rodrigo, *Four-dimensional unsubtraction with massive particles*, *JHEP* **10** (2016) 162 [[1608.01584](#)].
- [212] G. Rodrigo, F. Driencourt-Mangin, G. F. R. Sborlini and R. J. Hernandez-Pinto, *Applications of the loop-tree duality*, *PoS LL2016* (2016) 037 [[1608.01800](#)].
- [213] T. Gehrmann and E. Remiddi, *Two loop master integrals for $\gamma^* \rightarrow 3$ jets: The Planar topologies*, *Nucl. Phys.* **B601** (2001) 248 [[hep-ph/0008287](#)].

- [214] T. Gehrmann and E. Remiddi, *Two loop master integrals for $\gamma^* \rightarrow 3$ jets: The Nonplanar topologies*, *Nucl. Phys.* **B601** (2001) 287 [[hep-ph/0101124](#)].
- [215] G. Bell, *Higher order QCD corrections in exclusive charmless B decays*, Ph.D. thesis, Munich U., 2006. [0705.3133](#).